**Politecnico di Torino**

Department of Mechanical and Aerospace Engineering

Master's Thesis in Mechanical Engineering

# DESIGN AND OPTIMIZATION THROUGH FINITE ELEMENT ANALYSES

# OF A RECUMBENT RACING BICYCLE

# FOR THE WORLD HUMAN POWERED SPEED CHALLENGE

Supervisors:                                                        Author:

**Prof. Cristiana Delprete**                              **Alessandro Basile**

**Engr. Paolo Baldissera**

A.Y. 2022-2023

*To Gianna and my family*

# CONTENTS

# INTRODUCTION

The following paper deals with the design of a recumbent racing-bike frame. The design of the new frame makes use of the aid of various optimization analyses, which are performed with models created using the Finite Element method. In particular, this bike is designed to compete in the World Human-Powered Speed Challenge.

The WHPSC is held in Battle Mountain in Nevada, and teams from all over the world, including the Policumbent team, compete in it with the goal of setting a new land speed record for vehicles that rely on human power alone. The current world speed record belongs to Todd Reichart of the AeroVelo team, whose bike reached the speed of 144.17 km/h (89.59 MPH) in 2016 [1]. The Policumbent team reached the maximum speed of 136.49 km/h in 2019, with the Taurus prototype ridden by Andrea Gallo [2].

The frame proposed in this thesis will be completely new and will have the objective of halving the mass and increasing the stiffness compared to the Taurus frame, yet using the same type of carbon fibers and the same fiber volume fraction of the composite material as in that prototype. The new frame proposal has been designed to satisfy manufacturing constraints and also to be compatible with an already existing aerodynamic fairing, for which new attaching elements have been created. Moreover, an upgrade for the transmission has been developed, which improves the stability of the bicycle.

First, to find out the rigidity of the Taurus frame, an FE model of it was created and then subjected to various static analyses. All the analyses performed and reported in this paper were done using Altair's software HyperMesh, HyperView, and HyperGraph, and the solver Optistruct. The new frame was designed with the help of a topology optimization, a free-size optimization, a size optimization and a shuffle optimization analysis, which are implemented within Optistruct. The optimization analyses are to be intended as calculation tools and do not replace the role of the designer, who still has the task of creating the FE models, setting up the analyses and, at the end of each optimization, having to interpret and to re-elaborate the results obtained. Finally, the achievement of the objectives stated above was verified by subjecting the new frame to the same static analyses used to calculate the stiffness of the Taurus frame.

This thesis will begin by presenting, in the first chapter, the technical aspects to conduct a finite element analysis with Optistruct. The second chapter will follow, and it will be dedicated to the analysis of the Taurus frame in order to define the targets of the new frame. The third chapter will describe the design process of the new frame, which will then be re-analyzed and compared with Taurus in the fourth chapter. At the end of the thesis, conclusions and possible developments will be proposed.

# 1. PRACTICAL ASPECTS OF FEA WITH OPTISTRUCT

The aim of this chapter is to present the basic aspects of performing a finite element analysis (FEA) with the solver Optistruct. The finite element method is a numerical method, which is implemented inside Optistruct. As Bathe states,

> 'the finite element method is used to solve physical problems in engineering analysis and design. […] The idealization of the physical problem to a mathematical problem requires certain assumptions that together lead to differential equations governing the mathematical model. The finite element analysis solves this mathematical model' [3, Chapt. 1, Par.1.2].

The topics presented are going to be useful to introduce the work done, which, however, has required a more in-depth study of Optistruct and of the Altair's programs so as to be able to acquire all the necessary knowledge.

## 1.1 Phases of FEA

A finite element analysis (FEA) consists of three main phases:

1) Pre-processing

In the first phase the FE model is created, and the type of analysis and the boundary conditions are defined. To create an FE model, the components are meshed and the elements are assigned some properties. With the Optistruct solver it is possible to perform different types of analyses, such as linear and non-linear static, modal, frequency response, optimization, thermal, and other analyses [4]. These operations can be performed through the Graphical User Interface (GUI) of the pre-processing software, but some operations can also be performed through text files. In fact, the pre-processing software can produce a text file that will be the input file of the solver to carry out the analysis. The input files are readable by users as text documents, have a precise structure, and describe the FEA through the solver cards. In this thesis the pre-processing software Hypermesh has been used, while some operations have been performed by writing the cards directly in the text of the input file; this is why knowing the structure of the input files has been fundamental.

2) Solving

In the solving phase, the solver performs the calculations to solve the problem. In this thesis the Optistruct solver was used. If there are errors in the model, the solving phase might end immediately and produce an output file describing the errors or part of them. In fact, before starting the solving phase, it is advisable to carry out a complete check of the model.

3) Post-processing

At the end of the solving phase, the solver outputs all the data requested in the pre-processing phase. In

fact, if some data were not requested at the start of the analysis, they will not be present among the outputs. The outputs can be produced as text files or in other formats readable by post-processing software. In this thesis the post-processing software HyperView and HyperGraph were used. In the post-processing phase, the output data are analyzed considering both the real physical phenomenon and the FE model. The user must interpret the output data and verify that they are representative of the physical phenomenon to be simulated.

## 1.2 Structure of the input file

The preparation of the analyses presented in this paper have been done by both GUI and text editor. Knowing the structure of the input file allows a better management of the models and of the analyses. In particular, a structure with many include files has been used, as described below.

As Figure 1.1 shows, an input file for performing an analysis in Optistruct is composed of three parts [5]:

1) the I/O Options Section controls all the subcases that are defined in the input file. In this part we can define the type, the format and the frequency of the outputs, and the title;

2) the Subcase Information Section contains all the information for defining the subcases. Each subcase is defined specifying the analysis type and which of the boundary conditions (defined in the Bull Data Section) are applied. For example, for a linear static analysis, it contains the text 'ANALYSIS STATICS'; the SPC ID, which indicates the constraints; and the LOAD ID. In case of an optimization analysis, it also contains the information about the objective function;

3) the Bulk Data Section is the longest part of the input file and starts with the BEGIN BULK statement. It contains the definition of the elements, properties, materials, coordinate systems, boundary conditions. In case of optimizations, it contains also the definition of the design variables and of the response functions. When an include structure is used, the Bulk Data Section contains the command 'INCLUDE', which recalls the model that has been defined in another separate file.

When an include structure is used, it is possible to use the same model for different analyses. Therefore, we can have many input files with different I/O Options and Subcase sections that recall the same include file. In this document, each optimization analysis has a dedicated model, while the modal analysis and the static analysis use a different set of includes [Appendix]. Therefore, the include structure has been used to:

- create the desired frame assembly excluding or including the fairing, the transmission and the cyclist mass;

- have a shorter input file, in which to write the I/O Options and Subcase sections via text editor;

- use the same include file of the frame for both the static and the modal analyses;

- avoid accidental errors caused by exporting and importing the same model several times.

```
 1  STRAIN(H3D) = ALL
 2  STRESS(H3D) = ALL
 3  DISPLACEMENT(H3D) = ALL
 4  DISPLACEMENT(OPTI) = 10000
 5  GPFORCE(OPTI) = 1000
 6  SPCFORCE(OPTI) = ALL
 7  CFAILURE(H3D,NDIV=1) = ALL
 8  CSTRAIN(H3D,NDIV=1) = ALL
 9  CSTRESS(H3D,NDIV=1) = ALL
10  $
11  SUBCASE        1
12    LABEL Forza peso ciclista
13  ANALYSIS STATICS
14    SPC =         3
15    LOAD =        4
16  $
17  $
18  SUBCASE        2
19    LABEL Pedalata DX
20  ANALYSIS STATICS
21    SPC =         3
22    LOAD =        7
23  $
24  $
25  SUBCASE        3
26    LABEL Pedalata SX
27  ANALYSIS STATICS
28    SPC =         3
29    LOAD =        8
30  $$
31  $$
32  BEGIN BULK
33  $$
34  INCLUDE 'include/INC_TELAIO_TAURUS.fem'
35  INCLUDE 'include/INC_TRASMISSIONE_SIMULACRO.fem'
36  $
37  SPCADD         3         1         2
38  $
39  SPC            1     20059     12356      0.0
40  SPC            1     20060     12356      0.0
41  SPC            1         1         3      0.0
42  SPC            2         4         6      0.0
43  $
44  LOADADD        7       1.0       1.0         4       1.0         5
45  LOADADD        8       1.0       1.0         4       1.0         6
46  $
47  FORCE          4         9     01.0       0.0       0.0    -687.0
48  FORCE          5        10     01.0    55.188       0.0       0.0
49  FORCE          5        10     01.0       0.0   694.435       0.0
50  FORCE          5        10     01.0       0.0       0.0   -68.665
51  FORCE          6        10     01.0   -55.186       0.0       0.0
52  FORCE          6        10     01.0       0.0   694.435       0.0
53  FORCE          6        10     01.0       0.0       0.0   -68.665
54  FORCE          5         2     01.0   -55.188       0.0       0.0
55  FORCE          5         2     01.0       0.0-694.435       0.0
56  FORCE          5         2     01.0       0.0       0.0    68.665
57  FORCE          6         3     01.0    55.186       0.0       0.0
58  FORCE          6         3     01.0       0.0-694.435       0.0
59  FORCE          6         3     01.0       0.0       0.0    68.665
60  $
61  ENDDATA
```

I/O Options Section

Subcase Information Section

Bulk Data Section

**Figure 1.1**: Sections of an input file with an include structure.

To create an input file with multiple include files that must join together, rules in numbering are needed. Furthermore, it is not possible to define the same node several times. In fact, when a node is the junction between multiple components that are situated in different includes, it is written in both includes. In this

case, the redundant definitions of the node need to be commented out using the symbol $ via text editor. Without this trick and without numbering rules it is not possible to create includes that join together.

Each include has to use a defined numbering range, otherwise there could be the possibility that any entity contained within the include file is rewritten, inevitably generating errors. Moreover, the loaded nodes and the constrained nodes have a fixed numbering so as to be able to define the loads and constraints for multiple input files.

In this paper we have used the following rules:

- the numbering of each frame entity is between 20000000 and 29999999;
- the numbering of each fairing entity is between 50000000 and 59999999;
- the numbering of each transmission entity is between 10000000 and 19999999;
- the numbering of the nodes used to calculate the internal forces of the transmission is between 5000 and 5999;
- the numbering of the nodes of the plotel elements used to calculate the displacements is between 10000 and 19999;
- the numbering of the interface nodes between Frame-Transmission and Frame-Fairing is between 20000 and 29999;
- the nodes where the forces and constraints are applied have a fixed number and are listed in Tables 2.3 and 2.4.

## 1.3 Models with Optistruct

### 1.3.1 Optistruct elements

The user has to decide which kind of elements to use to create an FE model. The choice of the type of element and of the mesh size is justified by the shape of the component and by the degree of detail required. We could use 3D elements and a fine mesh for any structure but this would lead to a model with high number of DOFs that could cause an unjustifiably high computational cost. 1D elements are suitable for modeling beams or bolts, 2D elements for plate-type components, and 3D elements for bulky components, or for those with any shape when a detailed analysis is required [6, Chapt. 11].

All the elements, except for RBE2, RBE3 and for Plotel elements, need a property. Due to their formulation, different elements have different properties. For example, 1D elements need information about the cross-sectional area; 2D elements about the thickness of the plate, or thicknesses in case of multi-layers; while 3D elements do not need any geometrical information. All 1D, 2D and 3D elements need information about the material. Usually, all the above information is contained in the respective properties.

An Optistruct-element card contains the IDs of the nodes and of the property that define the element, as well as other card fields that depend on the element type. A node is defined by the card GRID, which

contains the coordinates of the node with reference to the coordinate system specified in the third field. In the seventh field of the GRID card, we can specify the coordinate reference system associated to the node; this is useful for defining forces or constraints that are not aligned to the axes of the global reference system. A property card contains the information mentioned above and the material card ID. The card MAT1 is used to define isotropic materials and the card MAT8 is used to define orthotropic materials for shell elements.

Below, a CQUAD4-element card has been used as an example to show the relationships between element, nodes, property and material. The third and seventh fields of the GRID cards in this case are blank since they refer to the global reference system.



**Figure 1.2**: A CQUAD4-element card and the cards related to it. (Green) ID of the CQUAD4 element. (Yellow) IDs of the GRID cards. (Red) ID of the PSHELL-property card. (Blue) ID of the MAT1-material card.

All the elements and properties supported by Optistruct are described in its manual [7]. Therefore, the table below shows only the elements used in this paper.

| Type of element | | No. of nodes | Optistruct card element | Optistruct card property | Info to specify in the property |
|---|---|---|---|---|---|
| 0D | Rigid | one independent node, one or multi dependent nodes | RBE2 | No property | |
| | Interpolation rigid | multi independent nodes, one dependent node | RBE3 | No property | |
| 1D | Plotel | 2 | PLOTEL | No property | |
| | Beam | 2 | CBEAM | PBEAM | Material and cross-sectional area |
| 2D | Shell | 3 | CTRIA3 | PSHELL for one-layer components. PCOMPP for multi-layer components | PSHELL: material and thickness. PCOMPP: allowable interlaminar shear stress and failure theory. |
| | | 4 | CQUAD4 | | |
| 3D | Solid | 4 | CTETRA | PSOLID | Material |
| | | 8 | CHEXA | | |

**Table 1.1**: List of elements used in this paper.

The PCOMPP property has been used to model the laminates and it is different from other properties. It can contain the information about the allowable interlaminar shear stress, about the failure theory, and other, but it cannot contain any information about the plies and their materials. The PCOMPP property is used in ply-based shell modeling, a quite recent method for building composites. This is different from the previous properties PCOMP and PCOMPG, which are used in zone-base modeling. The ply-based modeling

method is more efficient to design and update, so there are considerable advantages in using it for composite design optimizations [8]. The following section shows how to define a laminate with the PCOMPP property.

### 1.3.2 Defining a laminate

To define a laminate through the PCOMPP property, we have to follow the steps below.

1) Defining the shape of the ply through a set of elements with the SET card.

2) Defining the 0° orientation of all the elements by modifying the 8th field of the CQUAD4 cards and the 7th field of the CTRIA3 cards. It is possible to orient all the elements quickly and easily thanks to the GUI present in Hypermesh (2D panel/composites/material orientation). The orientation of a ply is defined with reference to the local reference system of the element, which is different from element to element. In order to define a single material direction, the orientation of all the elements must be changed.

3) Defining the ply-material characteristic. The ply material is homogeneous and has the same mechanical characteristics of the composite material, which is heterogeneous. Composite materials are heterogeneous by definition because they are made up of a reinforcing phase and a matrix, which have different characteristics from each other. The ply material is defined by the MAT8 card because a lamina with a long-fiber reinforcement is an orthotropic material. Inside the MAT8 card, we have to insert the mechanical characteristics of the composite material, which depend on: those of the fibers and of the matrix; the orientation of the fibers; and $V_f$ or $W_f$.

    $W_f$ is the fiber mass (or weight) fraction and $W_m$ is the matrix mass fraction, which are defined as follows:

    $$W_f = \frac{fiber\ mass}{total\ mass} \quad ; \quad W_m = \frac{matrix\ mass}{total\ mass} \quad ; \quad \text{So } W_f + W_m = 1$$

    Instead, $V_f$ is the fiber volume fraction and $V_m$ is the matrix volume fraction, which are defined as follows:

    $$V_f = \frac{fiber\ volume}{total\ volume} \quad ; \quad V_m = \frac{matrix\ volume}{total\ volume} \quad ; \quad \text{So } V_f + V_m = 1$$

    If these data are not provided by the suppliers, they must be estimated using the Classical Laminate Theory (CLT) [9].

4) Defining the ply through the card PLY, by doing the following.

    a. Specifying the thickness of the ply according to the material data.

        Usually long-fiber fabrics are produced with standard densities per unit area and we can derive their thickness using the following formula:

        $$t_{fiber} = \frac{\rho_{A,fiber}}{\rho_{V,fiber}}$$

where $\rho_{A,fiber}$ is the fiber mass per unit area and $\rho_{V,fiber}$ is the fiber mass per unit volume. Since we have a composite material, we must also consider the thickness of the matrix. Referring to the Classical Laminate Theory we know that the matrix and the fibers extend over the same area. So we can use the following formula:

$$t_{matrix} = \frac{\rho_{A,matrix}}{\rho_{V,matrix}} = \frac{\rho_{A,fiber} \cdot \left(\frac{1}{W_f} - 1\right)}{\rho_{V,matrix}}$$

where $\rho_{A,matrix}$ is the matrix mass per unit area and $\rho_{V,matrix}$ is the matrix mass per unit volume. In case of a hand lay-up process, the mass of the fabric is calculated before the lamination process and the mass of the matrix is obtained by subtracting the mass of the fabric from the mass of the final component so as to calculate the right value of $W_f$. The value of $\rho_{A,fiber}$ ; $\rho_{V,fiber}$ and $\rho_{V,matrix}$ are given by the suppliers.

To conclude, the total thickness of the ply is [10]:

$$t_{ply} = t_{fiber} + t_{matrix}$$

    b.  Specifying the ply material from the ones defined in step 3.

    c.  Specifying the orientation of the fibers that compose the material.

    d.  Indicating the shape of the ply from the ones defined in step 1.

5) Assigning the PCOMPP property to the elements used to define the plies. In the PCOMPP property we have to indicate the maximum allowable interlaminar shear stress and the failure criterion.

6) Defining the laminate through the card STACK by indicating the sequence of the defined plies.

# 2. FE MODEL AND ANALYSES OF THE TAURUS PROTOTYPE

This chapter is dedicated to the analysis of the frame of the Taurus prototype. This will be preceded by the description of both the existing frame and of its FE model. The aim of the analyses of the Taurus' frame is to learn its structural behavior and to measure the stiffness and the frequencies of global modes in order to define the targets for the new frame.

FEAs have been run by writing an input file which contains references to several include files. The input file varies according to which analysis is carried out, whereas the include files remain unvaried as they refer to the existing prototype, which will not be modified.

The include files generated for Taurus are the following:

- ' INC_TELAIO_TAURUS.fem ', which includes the frame and the fork;
- ' INC_TRASMISSIONE_SIMULACRO.fem ', for the bicycle transmission;
- ' INC_CARENA_TAURUS.fem ', for the removable aerodynamic fairing;
- ' INC_MASSA_CICLISTA.fem', for the lumped mass, which stands for the cyclist.

In order to avoid conflicts between the include files, while performing the analyses the procedure described in Chapter 1 has been followed. Each include file has a pre-established numeration and has a set of nodes which will be taken into account in the post-processing phase. The input files are reported in Appendix A; the include files, however, could not be provided due to their large dimension.

The following section is dedicated to the description of the existing components and of their relative FE models for each include file.

## 2.1 Frame include file

### 2.1.1 Description of the existing frame

The main structure of the frame consists of:

- Five sandwich panels: four of those are parallel to the YZ-plane (*c* in Fig. 2.1) and one is perpendicular to it (backrest, *a* in Fig. 2.1). The former are joined together by bolts, spacers and other reinforcing elements (*m* in Fig. 2.1).
- A Rollbar (*b* in Fig. 2.1): it protects the cyclist in the event of a fall and contributes to the stiffness of the frame. A sleeve coupling allows the rollbar to be opened on one side, so as to facilitate the cyclist's entrance. The sleeve coupling can be closed for better frame stiffness.
- The Lower crossbeam (*l* in Fig. 2.1): it closes the C-shaped section created by the front panels and it is glued to them with some section bars (*i* in Fig. 2.1). The lower crossbeam also hosts the fork rail guide, which limits the transversal deformation of the fork.

- A partial aerodynamic fairing (*j* in Fig. 2.1): it is glued to the frame, contributes to the frame's stiffness and constitutes part of the full aerodynamic fairing.

The remaining components of the bicycle are, front to rear:

- The pentagon-shaped plate (*e* in Fig. 2.1): it is connected to the frame by bolts. The bottom bracket is mounted on it. In case the position of the bottom bracket needs to be moved to accommodate the cyclist's position, the pentagon plate can be dismantled and replaced with a modified one.

- A sprocket set shaft support (*d* in Fig. 2.1): besides hosting the sprocket set shaft, it contributes to the stiffness of the frame.

- Fork assembly components (*h* in Fig. 2.1): it is connected to the frame by the headset plate-support and the fork rail guide. The headset-support plates are bolted to the section bar placed between the panels. The fork rail guide is curve-shaped to allow the handlebar to rotate, limiting the transversal deformation of the fork.

- A seat (*g* in Fig. 2.1): it is where the cyclist will lay down.

- Rear dropouts (*f* in Fig. 2.1): they accommodate the rear wheel and the two disc brake calipers.

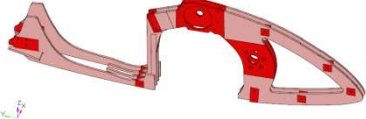The structure of the frame and its exploded view are shown below.
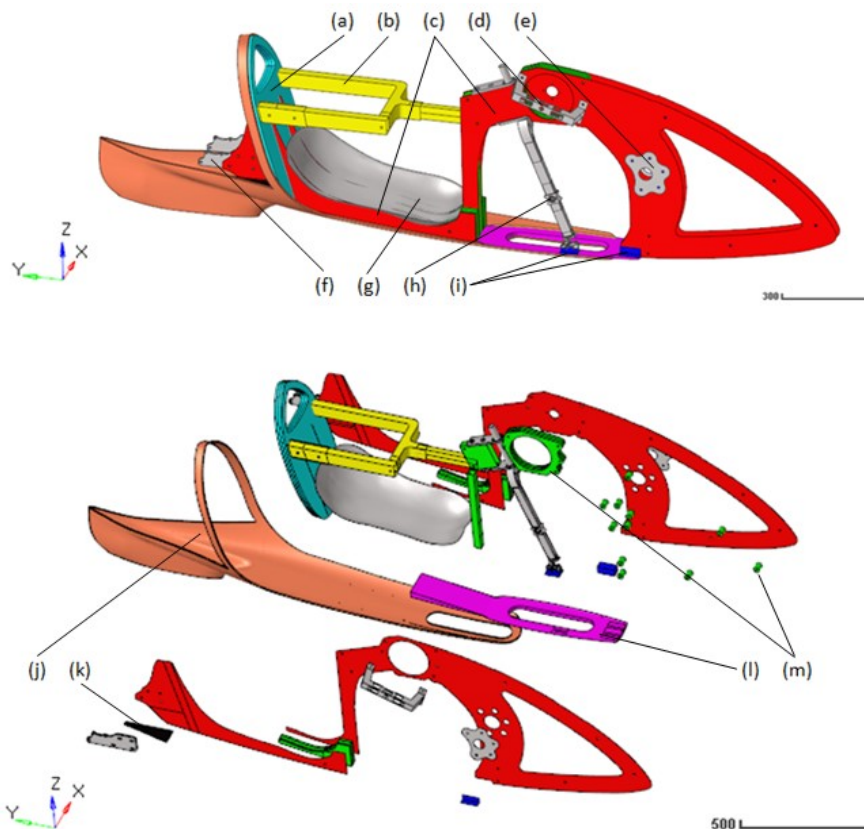


(a) backrest panel, (b) rollbar, (c) lengthwise panels, (d) sprocket set shaft support, (e) pentagon-shaped plate, (f) rear dropouts, (g) seat, (h) fork, (i) connection elements: lower crossbeam-panels, and lower crossbeam-fork rail guide, (j) partial aerodynamic fairing composing the frame, (k) connection elements: lengthwise panels-partial aerodynamic fairing, (l) lower crossbeam, (m) spacers and reinforcing elements.

**Figure 2.1**: Frame of the Taurus prototype (above) and exploded view (below).

To complete the description of the frame, we have reported below the thickness, the materials used, and the orientation of the carbon-fiber fabrics. Most of the frame's components have been made from carbon-fiber composites, while only some from aluminum. All the fibers with a 0-degree orientation are p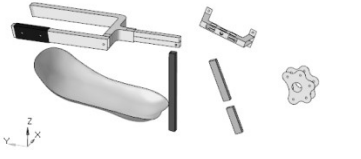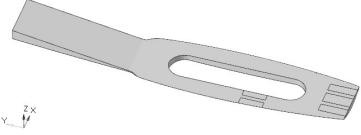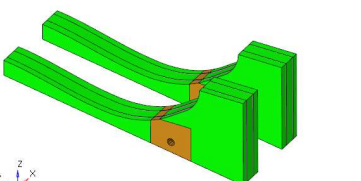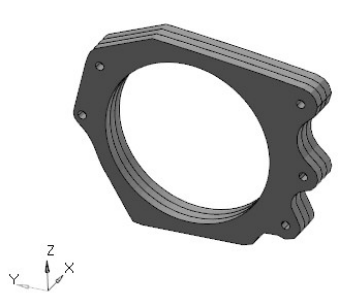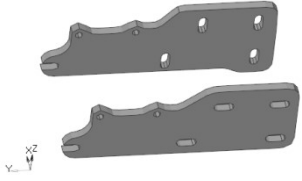arallel to the global Y-axis (Fig. 2.1), with the exception of the fork tubes, where the fibers are parallel to the fork's local Z-axis (Fig. 2.11).

The lengthwise panels have a sandwich structure, with two different cores. A PVC core has mostly been used, with the exception of those areas with bolts, which feature a plywood core. This is because plywood has a higher Young's modulus than PVC, therefore allowing to carry the compressive load due to the bolt tensile load.

The BOM and the ply book for the Taurus prototype are shown below (Tab. 2.1). The matrix material is the Epoxy resin and its volume fraction is equal to 0.6.

| View | Components | Description of layers |
|---|---|---|
|  | Lengthwise panels and frame-fairing connecting panels | - 2 layers of plain-wave carbon-fiber fabric 280 g/m$^2$<br>- Core: plywood 10 mm (in red) and PVC 10 mm (in pink)<br>- 2 layers of plain-wave carbon-fiber fabric 280 g/m$^2$ |
|  | Backrest | - 2 layers of plain-wave carbon-fiber fabric 280 g/m$^2$<br>- Plywood 10 mm<br>- 2 layers of plain-wave carbon-fiber fabric 280 g/m$^2$<br>- Plywood 10 mm<br>- 2 layers of plain-wave carbon-fiber fabric 280 g/m$^2$<br>- Plywood 10 mm<br>- 2 layers of plain-wave carbon-fiber fabric 280 g/m$^2$ |
|  | Partial aerodynamic fairing composing the frame | - Carbon-fiber fabric 200 g/m$^2$<br>- PVC 6 mm<br>- Carbon-fiber fabric 200 g/m$^2$ |

| | Rollbar, seat, vertical reinforcing bar, sprocket set shaft support, fork tubes, pentagon plate | Carbon-fiber components with a thickness of 2.5 mm |
|---|---|---|
| | Lower crossbeam | Carbon-fiber fabric 200 g/m$^2$ |
| | Connection elements (Lower crossbeam-panels and lower crossbeam-fork rail guide) | Carbon-fiber components with a thickness of 2.0 mm |
| | Spacers between the lengthwise panels | - PVC 10 mm (in green) <br> Plywood 10 mm (in brown) <br> - 2 layers of plain-wave carbon-fiber fabric 280 g/m$^2$ <br> - PVC 10 mm (in green) <br> Plywood 10 mm (in brown) <br> - 2 layer of plain-wave carbon-fiber fabric 280 g/m$^2$ <br> - PVC 10 mm (in green) <br> Plywood 10 mm (in brown) |
| | Spacers between the lengthwise panels | - 2 layers of plain-wave carbon-fiber fabric 280 g/m$^2$ <br> - PVC 10 mm <br> - 2 layers of plain-wave carbon-fiber fabric 280 g/m$^2$ <br> - PVC 10 mm <br> - 2 layers of plain-wave carbon-fiber fabric 280 g/m$^2$ <br> - PVC 10 mm <br> - 2 layers of plain-wave carbon-fiber fabric 280 g/m$^2$ |

| | Rear dropouts | Carbon-fiber components with a thickness of 8.0 mm |
|---|---|---|
| | Reinforcing section bar | Aluminum 2.5 mm |
| | Headset-support plates, fork elements, fork rail guide | Aluminum, solid section |

**Table 2.1**: Bill Of Materials (BOM) and ply book for the Taurus prototype.

### 2.1.2 Mesh of the frame

Now that all the data regarding the geometry and the materials of the frame have been collected, it is possible to create the correspondent FE model.

To proceed with the mesh generation, we have different types of elements and their respective properties. It follows a description of how the frame has been modeled, whereas the description of the type of finite elements can be found back in Chapter 1.

The Taurus model is made from first-order elements:

- All the bolts are modeled with 1D elements (CBEAM). The bolt connections follow a Rigid-Beam-Rigid arrangement (Fig. 2.2). The bolt extremities (CBEAM) are connected to the master nodes of the rigid elements (rigids with locked DOF 1 to 6). The bolt holes, designated for rigid connection, feature a washer (Fig. 2.3). A washer is composed of one or two rows of quad elements of

increasing height, this is because a more regular mesh with a higher density allows it to calculate the stress gradient more accurately [3, Chapt.4].

The aim of the analyses presented in this paper is that of conducting an evaluation of the prototype's overall behavior and this is why a modeling of this kind has been chosen. If the aim were to assess the bolt connections more specifically, a non-linear analysis would be needed, together with a more-detailed model and a higher mesh density. In the non-linear analysis it would then be possible to consider the stress gradients within the bolts and within the connected components, and the contact forces.
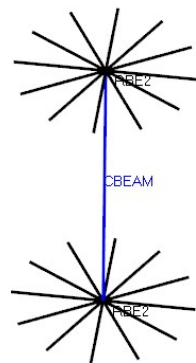


**Figure 2.2**: Rigid-Beam-Rigid bolt modeling
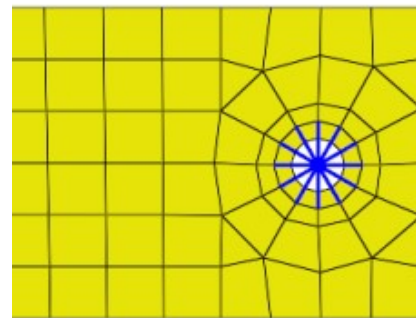


**Figure 2.3**: Washer.

- The main panels and the tubes are modeled with 2D elements (CQUAD4 and CTRIA3) as their thickness is significantly lower than their length (Fig. 2.4). The mesh of the panels follows the lines that separate those areas with a PVC core from those with a plywood core, so as to assign properties accordingly. As well as this, the mesh follows the lines that define the gluing area between the panels and the internal reinforcements, so as to create the right connections between surfaces.
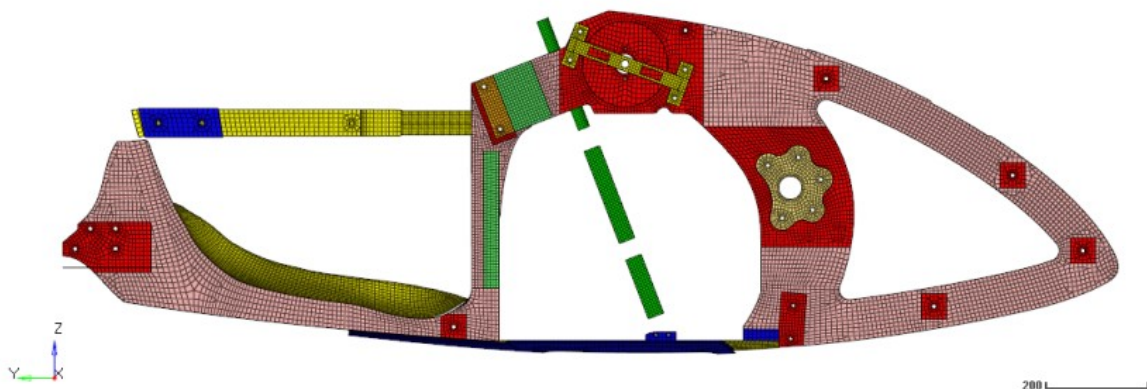


**Figure 2.4**: Components with a 2D mesh.

- The spacers, part of the fork and the rear dropouts are modeled with 3D elements (CHEXA, CPENTA, CTETRA) as they present a solid section (Fig. 2.5).
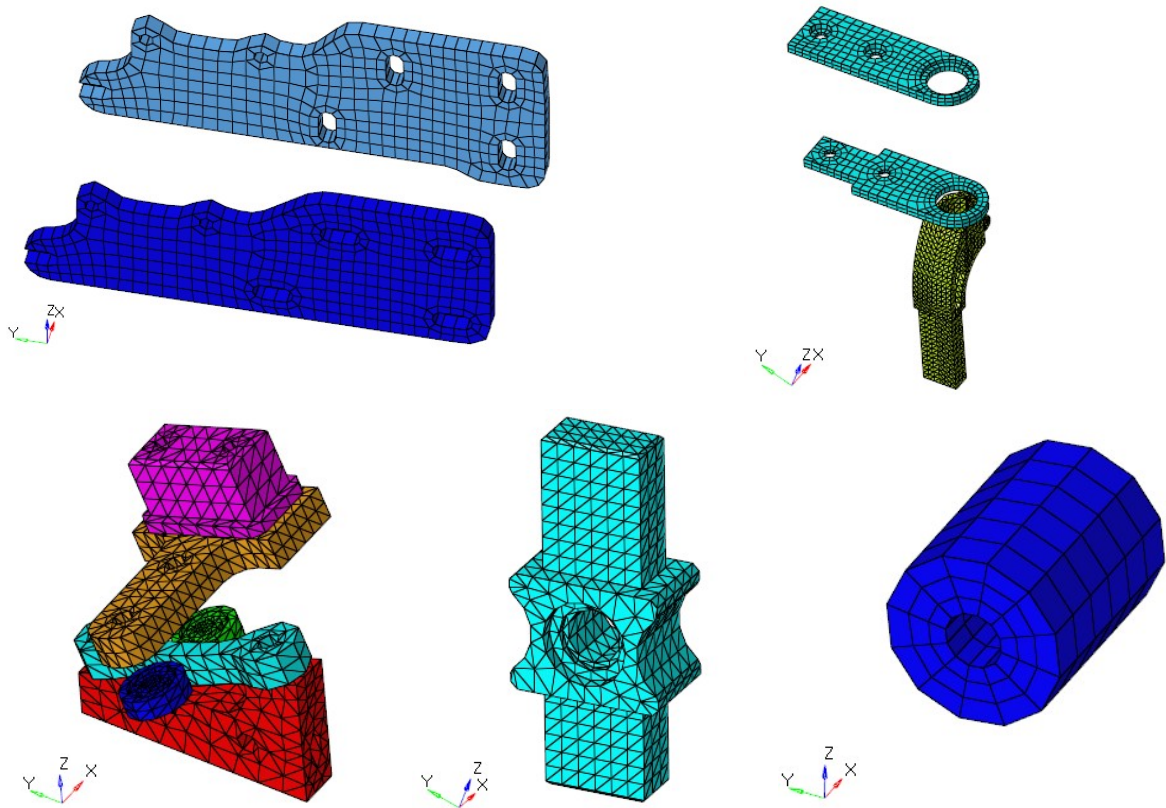


**Figure 2.5**: Components with a 3D mesh.

- The sandwich-structure panels that act as spacers and the backseat panel are modeled by combining 3D and 2D elements (Fig. 2.6). This choice is due to the significant thickness of the components and to the fact that the stress condition along Axis-3 cannot be simply overlooked (Fig. 2.7). In this case the sandwich structure follows a Shell-Solid-Shell arrangement, in which the shells are defined by the same nodes that define the hexa. It follows that the 2D elements that make up the skin of the sandwich panels have been made on the 3D elements that make up the core (Fig. 2.7). The same technique is used to shape the partial aerodynamic fairing glued to the frame, hereinafter referred to as 'fixed fairing' (in orange in Fig. 2.6). The latter could also be modeled with only 2D elements but the Shell-Solid-Shell arrangement has been chosen here to allow the insertion of a contact surface between the edge of the fixed fairing (orange in Fig. 2.17) and that of the removable fairing (green in Fig. 2.17). In this way, the faces of the hexa are useful to define the contact between the edges of the fixed and removable fairing. Figure 2.17 shows that the rear edge of the tail has been made shorter than the existing prototype's one because by being very thin it would have produced degenerate hexa elements. The edge shown is very thin so as to reduce the drag coefficient and it does not affect the stiffness of the frame significantly.
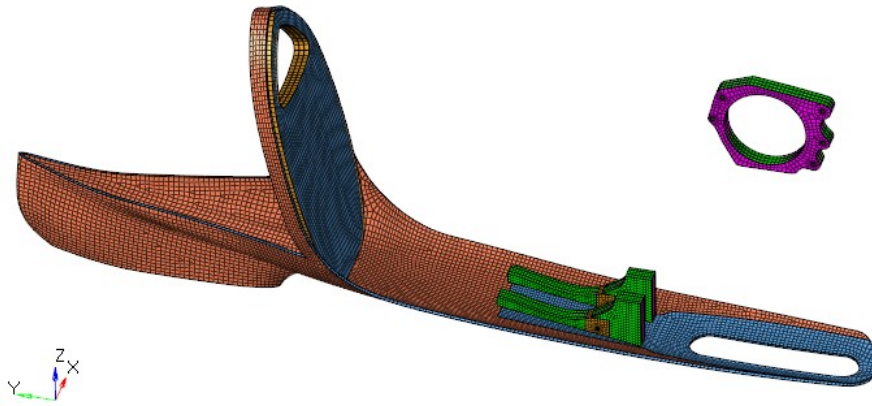
**Figure 2.6**: Components with a combined 2D and 3D mesh.



| (a) | (b) |
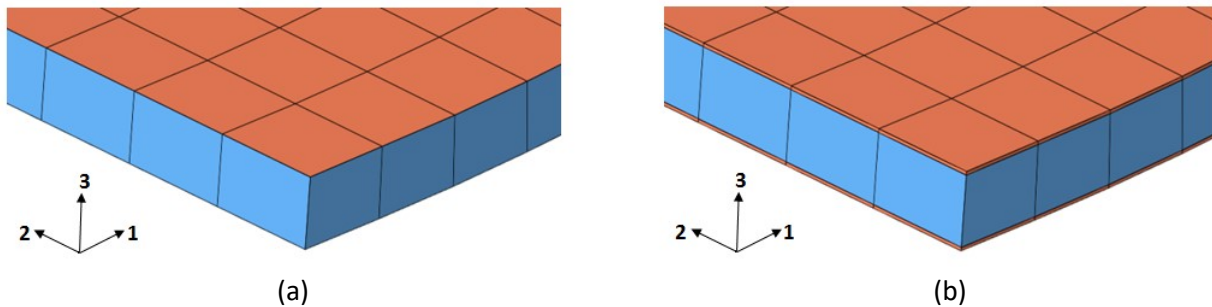
**Figure 2.7**: (a) Shell-Solid-Shell without the thickness view of the shell elements. (b) Shell-Solid-Shell with the thickness view of the shell elements.

- To highlight the reading-nodes set, elements of the PLOTEL type have been created (Fig. 2.8). Plotels are one-dimensional elements without properties and are used only to facilitate visualization [7].
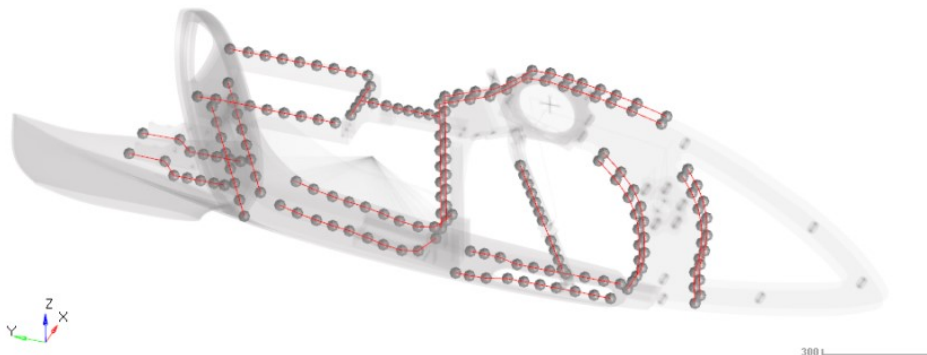


**Figure 2.8**: Plotel elements.

### 2.1.3 Modeling of the frame's ply

After meshing the frame, the next step is to assign properties to the different elements. Through properties we can attribute specific materials, thicknesses, and layers of the fabric that make up the composite materials.

In our model we have chosen to design a fabric with two ply layers, one for the fibers that form the warp yarn and another for those fibers that form the fill or weft yarn. For this reason, the two are perpendicular

to each other. Thanks to this choice, in the post-processing phase, it will be possible to view the stresses and the failure index for each lamina. The term 'lamina' indicates a set of fibers, parallel to each other, immersed in the matrix. Laminae are orthotropic and, depending on how they are oriented, present very different strength and stiffness values; this is why adjacent laminae that have different orientations present similar strain but different stress and failure index values [9]. One alternative is to design a fabric with one ply layer, which will provide the same results for stiffness, but in that case information about the stress condition of each lamina would be lost. Whichever the case, it is important that the modeling choice is consistent with the values of thickness and with the Young's moduli assigned to the ply.

As described in Chapter 1, the ply thickness depends on the fabric's density per area and on the amount of resin. The Young's moduli and ultimate strengths depend not only on the areal weight of the fabric and on the amount of resin, but also on the orientation of the fibers.

Since the two ply layers of the fabric are equally balanced, they each have an area density equal to half that of the whole fabric. The description of the properties and the procedure for defining the lay-up process can be found in Chapter 1, together with how the Young's moduli and ultimate strengths of the composite materials have been defined.

### 2.1.4 Connections and kinematics within the frame

The frame of the Taurus prototype was assembled using bolts, bearings and glue.

Glue was used for the connections between (Fig. 2.9):

- the internal reinforcement elements and the panels;
- the lower crossbeam and the panels;
- the partial aerodynamic fairing and the frame;
- the rollbar and the frame;
- the fork tubes and the metal elements.

The adhesive bonding has been simulated through TIE contacts in which the connected parts have, by definition, the same displacements. This type of contacts can be used both for Linear Static Analyses (STATICS) and for Small Displacement Nonlinear Analyses (NLSTAT) [7].
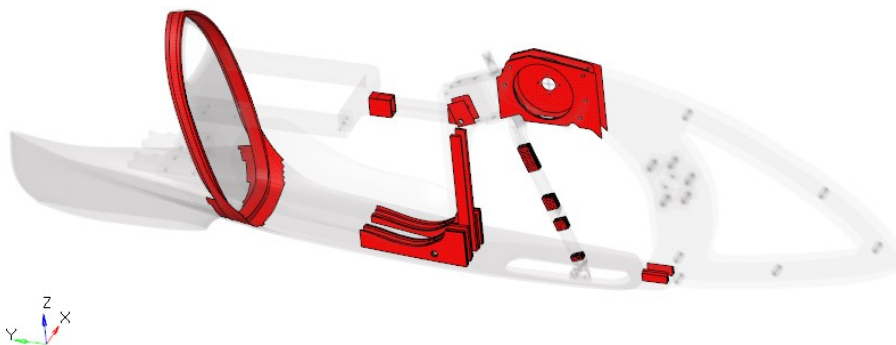


**Figure 2.9**: Areas where adhesive bonding has been simulated through TIE contacts.

A description of bolt modeling can be found in Section 2.1.2, so we will now proceed with addressing the modeling of the internal and external constraints.

The constraints are applied through rigid elements (RBE2 elements in Optistruct). Rigid elements have a master node and can have one or more slave nodes, the displacements of which depend on the master node. In the RBE2 card it is possible to define which displacements of the master node to impose on the slave nodes, so as to determine kinematics. In particular, the locked DOFs are indicated in field 4 of the RBE2 card and they are in the global reference system [7]. When there is a rotation or movement along an axis that does not coincide with any of the global axes, a new coordinate system must be defined and associated with the rigid master node (field 7 of the master node GRID card). This is the case of the fork in this model, which we will consider later.

For what concerns internal constraints (e.g. bearings of headset), two modeling arrangements are used so as to leave some DOF free between two components. The first arrangement is more convenient for connecting separate include files while the second is for components within the same include file:

- Type 1: Rigid (with locked DOF 1 to 6) linked to component A – Rigid with one slave node with modified DOF (the rigid with a modified DOF has one slave node with the same position as the master node) – Rigid (with locked DOF 1 to 6) linked to component B (Fig. 2.10 a);
- Type 2: Beam – Rigid with modified DOF linked to component C (Fig. 2.10 b).
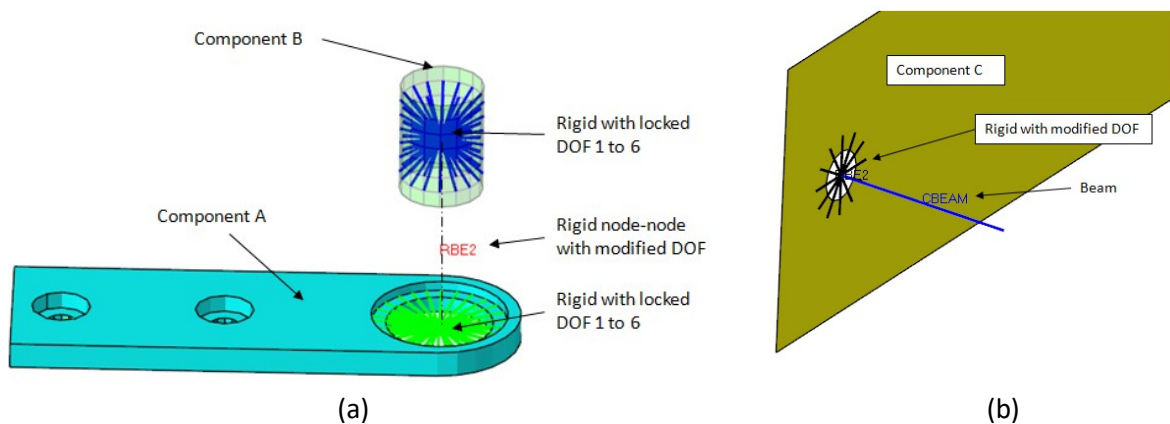


**Figure 2.10**: (a) Exploded view of Type-1 connecting modeling. (b) Type-2 connecting modeling.

The following kinematics are implemented in the include files of the frame and fork:

- Rotation of the fork around its own axis: the kinematics has been achieved through a Type-1 modeling. Rigids with a modified DOF have a locked DOF 1, 2 for the upper plate and a locked DOF 1, 2, 3 for the lower plate, with their nodes lying on the rotation axis of the fork. On the fork tube there is also another rigid (locked DOF 1 to 6) to which a local coordinate system has been assigned; this will prove useful in Section 2.4. The Z-axis of the local system coincides with the rotation axis of the fork (Fig. 2.11 b).
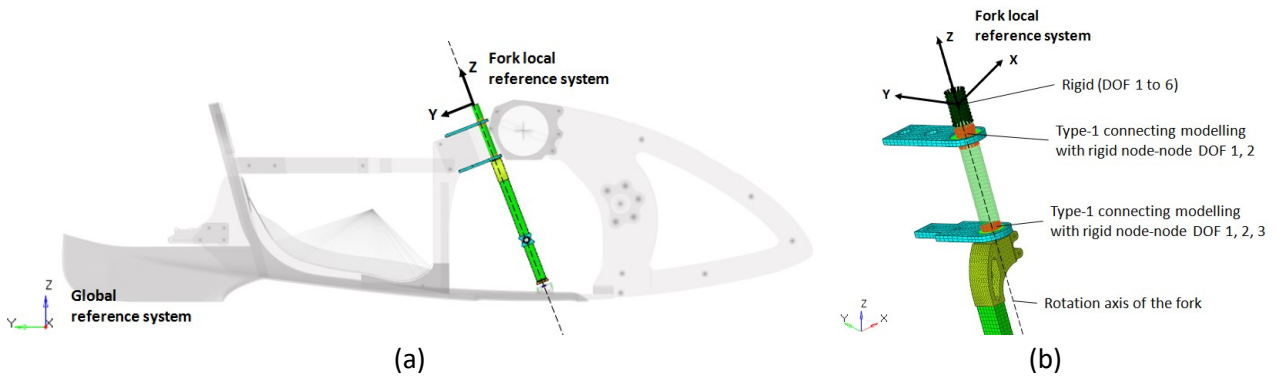
**Figure 2.11**: (a) Fork local reference system and global reference system. (b) Headset kinematics modeling.

- Sliding of the bearings along the rail guide of the fork. The function of the rail guide is to limit lateral deformations of the fork without hindering the rotation of the handlebar. This is why the curved surface of the rail guide is generated by the arc belonging to the circle that lies on the local XY-plane and that has its center on the local Z-axis (Fig. 2.12.b). In the existing prototype there are some little clearances between the bearings and the rail guide, which allow small deformations of the fork without causing rotations. Therefore, by considering small linear displacements, it is only relevant to lock the relative movements between the bearings and rail guide in the X-direction (rigid with locked DOF 1 in local system). The conducted debug analyses have showed that applying further constraints would cause unrealistic stresses and deformations. To lock only the relative movements in the X-direction and to allow the rotation of the fork, the master nodes of the rigids lie on the axis of rotation of the fork (Fig. 2.12.a). The rotation of the fork is verified in the seventh rigid mode in the free-free modal analysis presented in Section 2.5. A modeling of this kind is also effective for conducting modal analyses in which, because linear, it is not possible to define the slide or friction contacts. Given the type of modeling, the stresses of the components in Figure 2.12.b will not be evaluated in the post-processing phase.

-
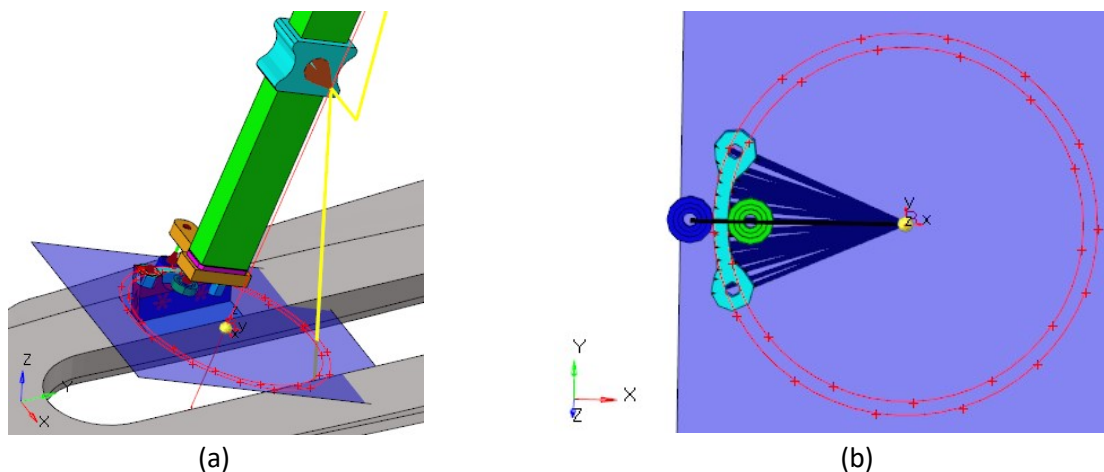


**Figure 2.12**: (a) XY-plane of the fork local reference system. (b) Fork guide rail with circles used to generate its contact surface with the guide bearings.

- Rotation of the rollbar arm: the rollbar has a pin at point A with a local axis parallel to the global X-axis (Fig. 2.13). The right arm of the rollbar can rotate around the pin to allow the cyclist to enter and it can be closed again with a sleeve coupling (in blue in Fig. 2.13). The kinematics follows a Type-2 modeling, with a rigid with a locked DOF 1,2,3,5,6 (only DOF 4 is free). Therefore, the transmission of the moment around the X-axis will not be possible between the tubes connected by the pin.
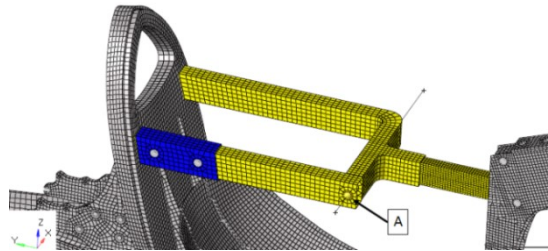


**Figure 2.13**: Point A shows the pin of the right arm of the rollbar. In blue, the sleeve coupling.

## 2.2 Transmission include file

The transmission has been included in the FE model so as to evaluate the forces and moments transmitted on the frame.

### 2.2.1 Description of transmission and substitute transmission

The transmission consists of a 108-tooth chainring, which a chain connects to a floating sprocket-set with 13 to 40 teeth (Fig. 2.15.a). The floating sprocket-set mechanism is patented and allows the chain to keep straight, which increases the efficiency of the transmission [11].

A 34-tooth chainring is mounted on the same shaft of sprocket set and, by means of a second chain, it is connected to the 18-tooth sprocket mounted on the front-wheel hub (Fig. 2.15.c). The overrunning clutch is embedded in the 18-tooth sprocket.

In order to conduct a static test, a substitute transmission has been modeled. It is similar to the one used in the test *'4.8.4 Frame – fatigue test with pedalling forces'* of the European Standard EN14781, which does not feature a sprocket mounted on the wheel axle (Fig. 2.14) and in which the chain is replaced by a tie rod with a ball-joint at each end [12]. In this way, the chainring substitute will be able to perform small rotation angles about its axis only in the event of frame deformation.
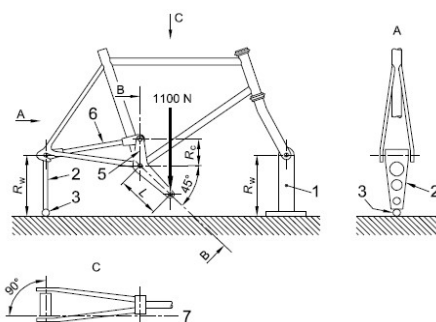


**Figure 2.14**: '*4.8.4 Frame – fatigue test with pedalling forces'* test method from EN14781 [12, Figure 27]

### 2.2.2 Transmission FE modeling

The pedals, sprockets and tie rods are modeled using RBE2 and CBEAM elements with a fictitious material, the Young's modulus of which is 100 times higher than that of steel. The elements of the transmission are very rigid in order to evaluate only the rigidity of the frame and not to introduce other deformable elements. Inserting CBEAMs has been preferred to having solely rigids. In an all-rigid modeling, due to the needed connections, there would have been slave nodes dependent on more master nodes. CBEAMs prevent these errors to occur.

The bottom-bracket bearings, sprocket-set-shaft bearings and the ball-joint at the end of the tie rods follow a Type-1 modeling with Rigid Node-Node with a locked DOF 1, 2, 3 (Fig. 2.15.e). The existing transmission and its FE model are shown below.



| (a) | (b) |
| --- | --- |



| (c) | (d) | (e) |
| --- | --- | --- |
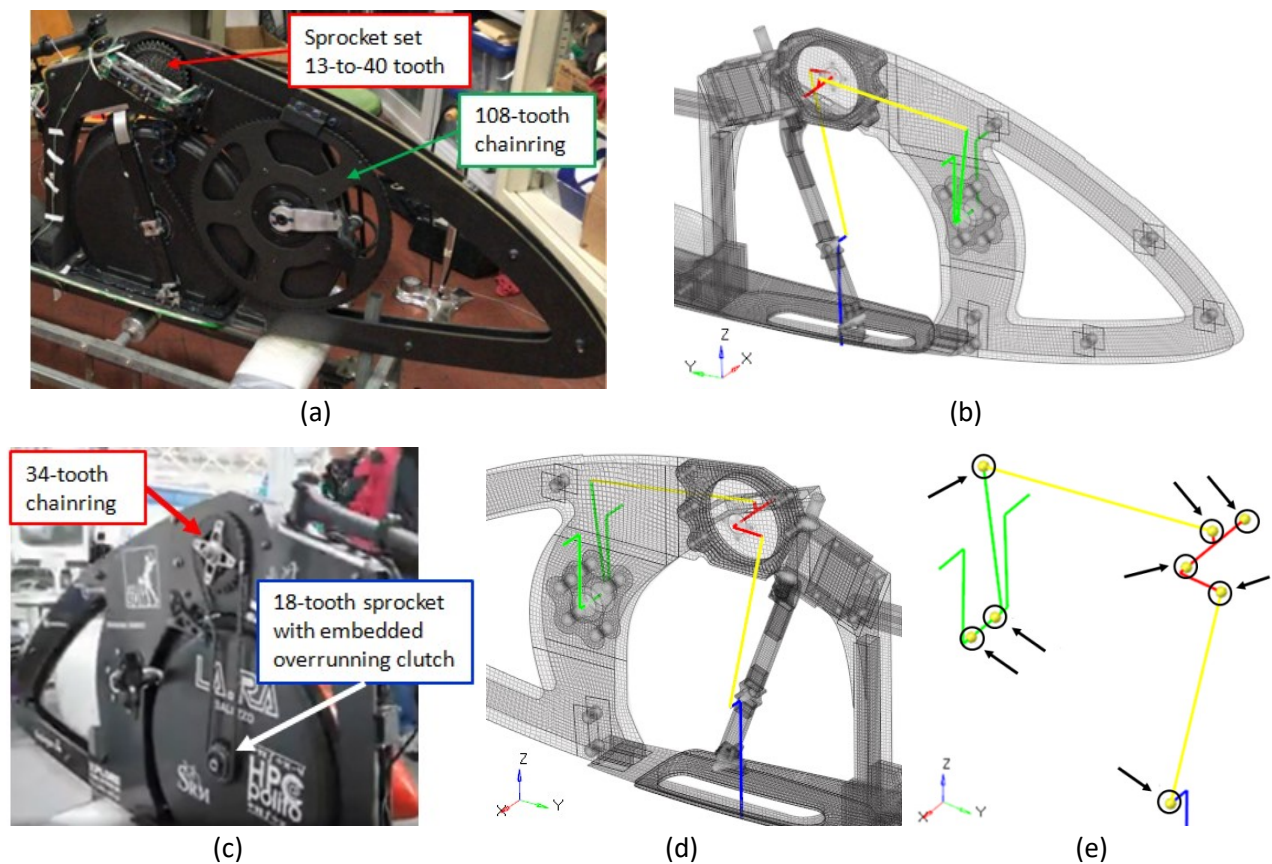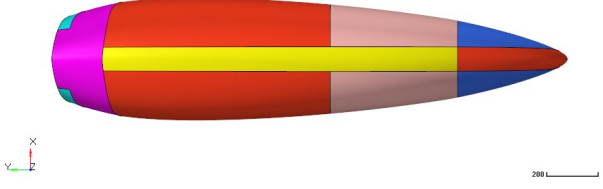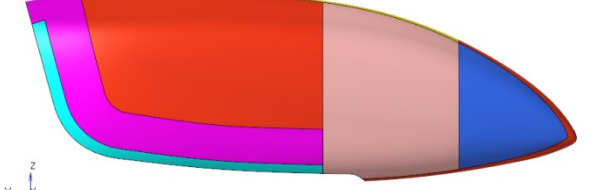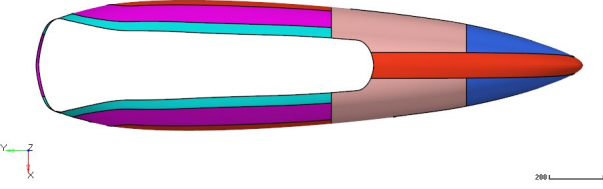
**Figure 2.15**: (a) Real main chainring and sprocket set, (b) FE modeling of substitute transmission. (c) Real chainring and spocket, (d) FE modeling of the substitute transmission without the final sprocket, as for the European Standard EN14781, (e) Transmission Type-1 connections are indicated by arrows.

## 2.3 Removable aerodynamic fairing include file

In the modal analyses, the include file of the removable aerodynamic fairing was used in order to evaluate the resonance frequencies of the frame-cyclist-fairing system, in which the connections between the frame and the removable aerodynamic fairing are particularly important.

## 2.3.1 Description of removable aerodynamic fairing

The full aerodynamic fairing has the task of reducing aerodynamic drag and of protecting the cyclist in the event of a fall. This is why the most critical areas have higher thicknesses. Below, the ply book of the removable aerodynamic fairing.



| | |
|---|---|
|  | Yellow: Carbon-fiber fabric, 180 g/m$^2$ *(external layer)* <br> PVC, 6 mm <br> Kevlar-fiber fabric, 115 g/m$^2$ *(internal layer)* <br> Red: Carbon-fiber fabric, 180 g/m$^2$ *(external layer)* <br> PVC, 3 mm <br> Kevlar-fiber fabric, 115 g/m$^2$ *(internal layer)* <br> Fuchsia: Kevlar-fiber fabric, 115 g/m$^2$ *(external layer)* <br> Carbon-fiber fabric, 180 g/m$^2$ <br> PVC, 3 mm <br> Kevlar-fiber fabric, 115 g/m$^2$ *(internal layer)* <br> Pink: Carbon-fiber fabric, 180 g/m$^2$ *(external layer)* <br> Nomex honeycomb, 3 mm <br> Kevlar-fiber fabric, 115 g/m$^2$ *(internal layer)* <br> Cyan: Kevlar-fiber fabric, 115 g/m$^2$ *(external layer)* <br> Carbon-fiber fabric, 180 g/m$^2$ <br> PVC, 6 mm <br> Kevlar-fiber fabric, 115 g/m$^2$ *(internal layer)* <br> Blue: Carbon-fiber fabric 180 g/m$^2$ *(external layer)* <br> Kevlar fiber fabric 115 g/m$^2$ *(internal layer)* |

**Table 2.2**: Removable aerodynamic fairing ply book.

The removable fairing is connected to the frame by means of support surfaces, belts, and a block guide that blocks vertical and transverse displacements as well as rotations around the Y and Z-Axes. When the belts are pulled, the edges of the removable fairing come into contact with the fairing fixed to the frame, and the front block guide reaches its housing. For safety reasons it is possible to detach the belts and remove the fairing from the outside of the vehicle [1], accessing it by the rear tail, which is fixed with adhesive tape. The rear tail is not included in the FE model as it is attached in place with adhesive tape, has a low mass, and does not perform a structural function (blue in Fig. 2.17).

### 2.3.2 Removable aerodynamic fairing mesh

The removable fairing is modeled using shell elements on which ply layers have been defined, following the same method as for the frame. The fairing has different thicknesses and a smooth outer surface, which is why there are small steps inside the fairing. To reproduce the same geometry, the shell elements have associated a PCOMPP card with thickness offset (Fig. 2.16).
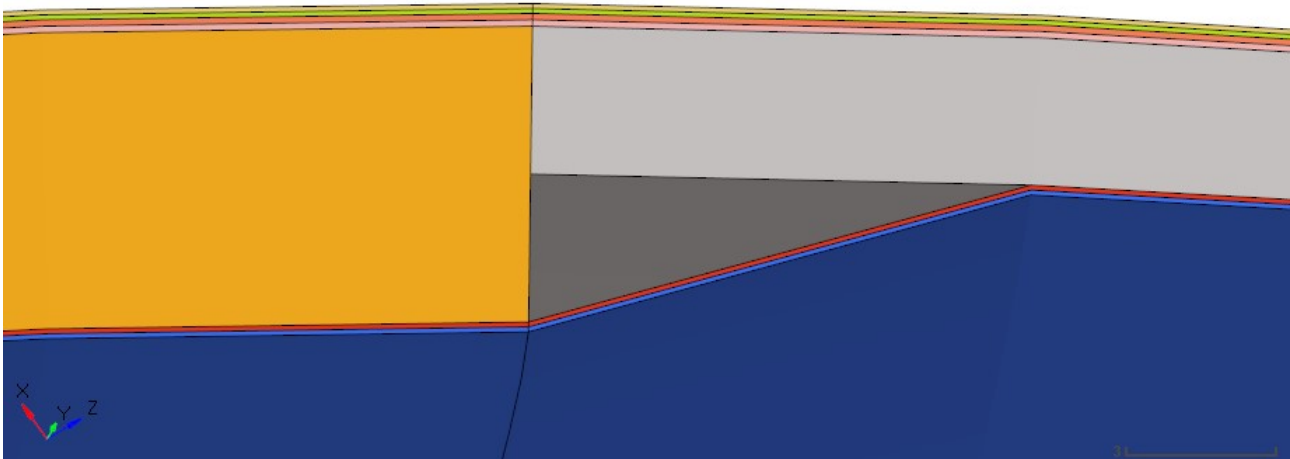


**Figure 2.16**: Picture produced with the thickness view of shell elements of the removable aerodynamic fairing. The outer surface is smooth whereas the step is on the inner surface.

### 2.3.3 Removable fairing FE Connections

The belts are modeled using rigid elements that follow a Type-1 modeling, in which the Rigid Node-Node have a locked DOF 1, 2, 3. In this way, the end of the belt can rotate freely (Fig. 2.18).

The front guide block allows the sliding of the removable fairing along the Y-axis for its insertion and removal, but it blocks the transverse and vertical relative movements between the fairing and the frame along the X and Z-axis respectively, as well as their relative rotations around the Y and Z-axis. The front guide block is modeled by means of two rigid elements that have the same master node (with locked DOF 1, 3, 5, 6 in the local system) to which a local reference system has been associated, with the Z-axis perpendicular to the surface of the fairing (Fig. 2.18).

The removable fairing include file is used in the modal analysis for which it is not possible to define slide or fiction-type contacts. For this reason, the contacts between the fairing fixed to the frame and the edge of the removable fairing have been modeled by means of TIE-type contacts, which can also be used in linear analyses [7]. This represents an obligatory choice to be able to conduct the modal analysis, and even though it is not perfectly compliant to reality, it allows us to evaluate the frequencies of the prototype natural modes with satisfying accuracy. Another modeling practice consists in creating a series of CBUSH elements in which the stiffness values are calibrated through experiments conducted on real components.
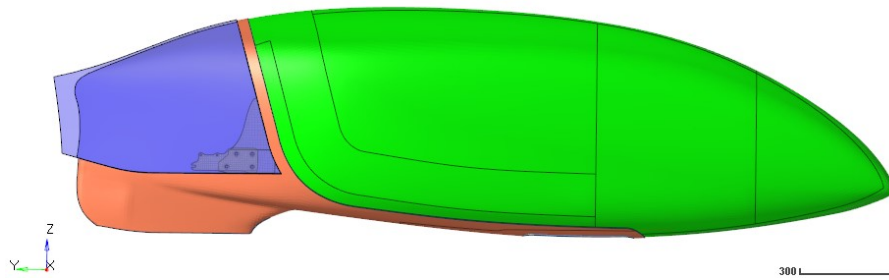
**Figure 2.17**: Rear tail (blue), removable aerodynamic fairing (green), partial aerodynamic fairing composing the frame (orange).
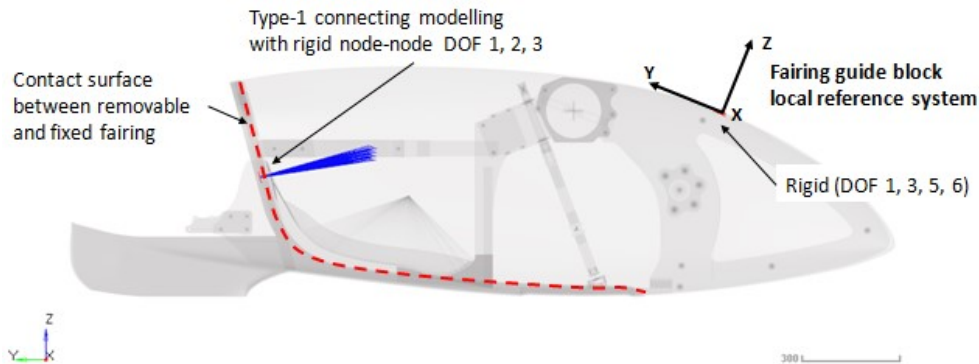


**Figure 2.18**: Connections between removable and fixed aerodynamic fairing.

## 2.4 Static tests

In this part we will conduct three static tests on the frame of the Taurus prototype. There will be a first part dedicated to the pre-processing phase and a second one dedicated to the post-processing phase and evaluations. The pre-processing phase will include a description of the constraints and of the forces applied for each subcase, while the post-processing phase will cover the appraisal of the outputs, on which subsequent evaluations of the frame structure will be based. In particular, the static tests on the Taurus frame are useful to obtain the stiffness targets for the design of the new frame.

*Pre-Processing*

The static analysis is divided into three subcases, in which the constraint conditions remain unvaried while the applied forces change. The constraint conditions are similar to those used in the test *'4.8.4 Frame – fatigue test with pedalling forces'* of the European Standard EN14781 [12].

The constraint conditions are as follows:

- The rear dropouts are constrained in all directions, except for the rotation around the global X-axis, as in the non-driving wheel of the standard.
- The rotation of the handlebar around its axis is blocked. It results that the rotation of the fork around its own axis is blocked, as it happens in a race when the cyclists blocks it with their arm. We have to highlight that the headset bearings are free to rotate. In this way, the deformations of the frame may cause relative rotations between the fork and the frame. To lock the handlebar rotation,

a rigid with a newly-assigned local system has been used. In the local system, the Z-axis coincides with the rotation axis of the fork (Fig. 2.11).

- The substitute of the front wheel is simply supported by the ground. Therefore, the contact point between the driving wheel and the ground is constrained only in the global-Z direction, as in the standard.

It follows a description of the forces applied in each of the three subcases.

- Subcase 1:

In the first subcase the aim is to evaluate the effect of the sole weight force due to the mass of the cyclist. Assuming a cyclist mass of 70 kg, a force of -687 N is applied in Z, in the central node of a RBE3 which is positioned in the COG (center of gravity) of the cyclist's body (Fig. 2.19). The RBE3 distributes the force without adding stiffness to the structure.



(a)



(b)
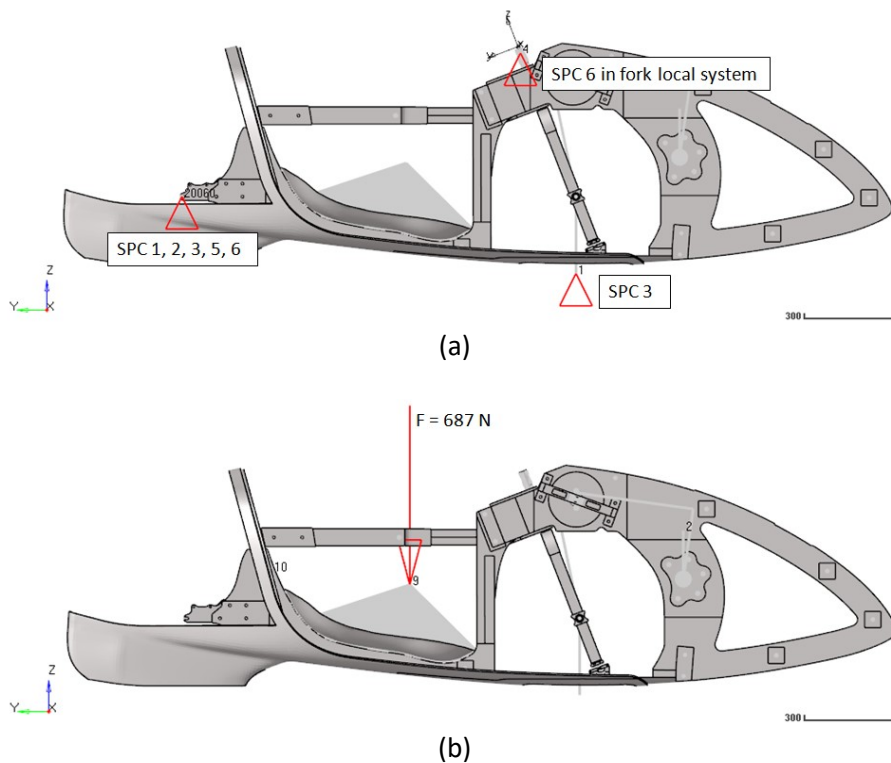
**Figure 2.19**: (a) Constraints used in Subcases 1, 2 and 3. (b) Force applied in Subcase 1.

- Subcase 2:

The second subcase evaluates the maximum force applied to the right pedal when the latter reaches the highest Z-coordinate (Fig. 2.20). The magnitude of the forces varies during the pedaling phase [13, Chapt. 2] and, in this case, the maximum force occurs when the pedal reaches the highest Z-coordinate. In this phase, it is assumed that the cyclist leans on the backrest to be able to push the pedal. The forces described have a magnitude equal to 700 N, have opposite directions, and lie on the straight line between the right pedal

and the central point of the backrest (Fig. 2.20). The force on the backrest is applied by means of an RBE3 element. Furthermore, the force applied in Subcase 1 is added to this subcase.



(a)



(b)
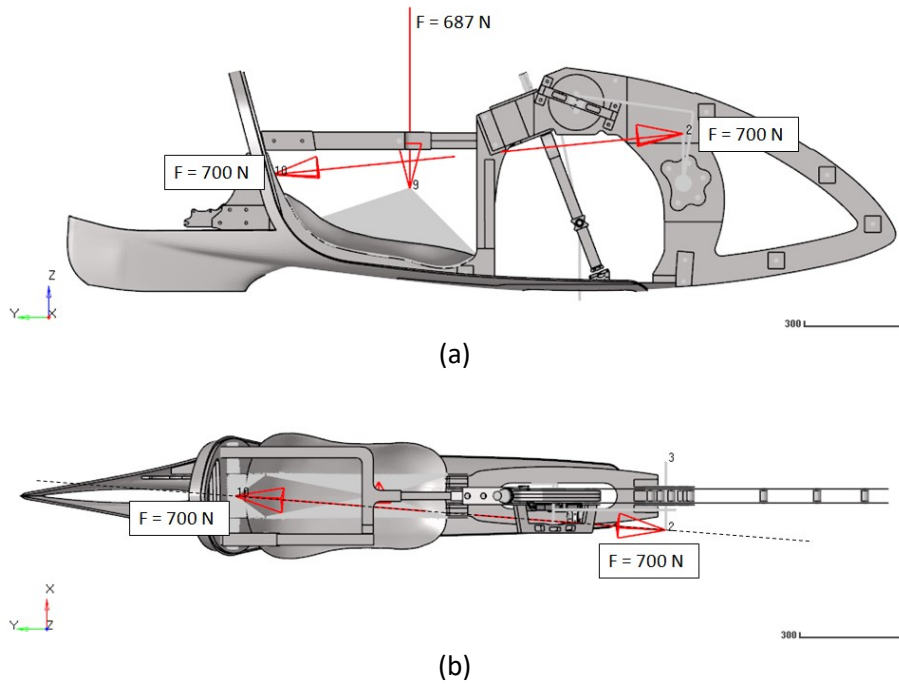
**Figure 2.20**: Forces applied in Subcase 2. (a) Right view, (b) top view.

- Subcase 3:

The third subcase is the same as Subcase 2, but this time the maximum force is applied to the left pedal. The straight line on which the two forces lie passes between the left pedal and the centre of the backrest (Fig. 2.21).



(a)



(b)
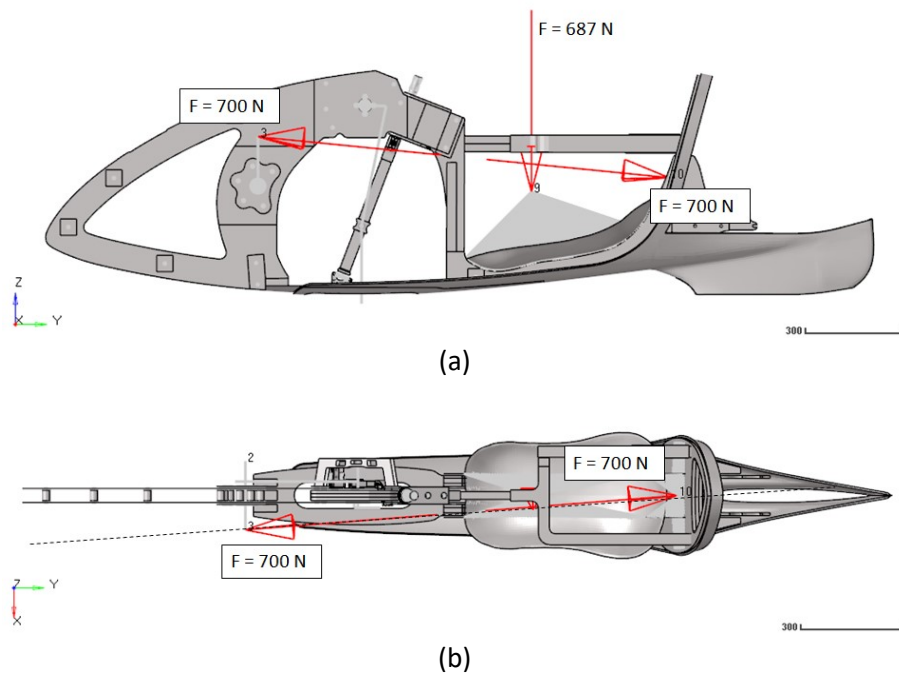
**Figure 2.21**: Forces applied in Subcase 3. (a) Left view, (b) top view.

The three subcases are executed through an input file that contains references to the include files 'INC_TELAIO_TAURUS.fem' and 'INC_TRASMISSIONE_SIMULACRO.fem'. The include files have been created and edited as text so that they are assembled when referred to in the input file (see Chapter 1). The input file has been written with cards and with the syntax used by the Optistruct solver, and it is reported in Appendix A.

In the first lines of the input file, the following files are requested in output for each subcase:

- *.spcf, with the reactions forces and reactions moments due to applied constraints;
- *.gpf, with the interaction forces within the transmission;
- *.disp, with the displacements for a set of nodes;
- *.h3d, with the results for producing the contour plot of the strains, stresses, displacements and failure indexes.

The files *.spcf, *.gpf, and *.disp are readable by text editor while *.h3d files are readable by post-processing software.

*Post-Processing*

In the post-processing phase, for each subcase we will evaluate:

- Reaction forces: the first check consists in verifying that the reaction forces corresponding to free DOF are null. After that, we have to verify that the sum of the applied forces and reaction forces of the entire model are null. The reaction forces reported in the *.spcf file refer to the global reference system, unless a node has been associated to a local reference system. The latter case occurs in the handlebar constraint. To verify the global equilibrium, the handlebar reaction force has been transferred into the global reference system.

- Interacting forces inside the transmission, and forces transmitted from the transmission to the frame.

- Displacements due to deformations: the work done to deform the frame represents a loss of energy, indeed we can notice that the frame deformation causes a displacement of the pedals, which does not produce the rotation of the wheel. It is important to evaluate how the deformations distribute along the frame so as to verify there are no abrupt changes. Similarly, global stiffness tests are conducted on the automotive chassis because deformation discontinuities represent potential rupture points under operating conditions [14, Chapt. 7]. The relative displacement between the right pedal and the backrest in Subcase 1, and the relative displacements between the left pedal and the backrest in Subcase 2, will be used to calculate the target stiffness for the new frame.

- Stress, strain and failure index distributions: to check the reliability of the frame, we will analyze all ply and interlaminar stresses, strains and failure indexes. The ply failure index has been computed

according to Hoffman's Theory. Hoffman's Theory takes into account the orientation of the material and also different strength values for tensile and for compressive stress conditions [7]. In this way, we have more realistic results than if using Hill's Theory, which does not distinguish between tensile and compressive strength. The rupture of the material occurs when the failure index is equal or higher than 1 [9].

The results obtained for each subcase are shown below.

### 2.4.1 Subcase 1

*Constraint reactions and global equilibrium check*

| | | SUBCASE 1: Applied forces (in global system) | | |
|---|---|---|---|---|
| | Node id | Fx [N] | Fy [N] | Fz [N] |
| Right pedal | 2 | 0,0 | 0,0 | 0,0 |
| Left pedal | 3 | 0,0 | 0,0 | 0,0 |
| Seat | 9 | 0,0 | 0,0 | -687,0 |
| Backrest | 10 | 0,0 | 0,0 | 0,0 |
| TOT | | 0,0 | 0,0 | -687,0 |

**Table 2.3**: Applied forces in global system for Subcase 1.

| | | SUBCASE 1: Reaction forces (in global system) | | | | | |
|---|---|---|---|---|---|---|---|
| | Node id | RFx [N] | RFy [N] | RFz [N] | RMx [Nm] | RMy [Nm] | RMz [Nm] |
| Front wheel | 1 | 0,0 | 0,0 | 390,9 | 0,0 | 0,0 | 0,0 |
| Fork | 4 | 0,0 | 0,0 | 0,0 | 0,0 | 0,0 | 0,0 |
| Left bike dropout | 20059 | -4,8 | 0,0 | 148,2 | 0,0 | 0,0 | -0,1 |
| Right bike dropout | 20060 | 4,8 | 0,0 | 148,0 | 0,0 | 0,0 | 0,1 |
| TOT | | 0,0 | 0,0 | 687,0 | 0,0 | 0,0 | 0,0 |

**Table 2.4**: Reaction forces in global system for Subcase 1.

The equilibrium along the X, Y and Z-axes is verified since the constraint reactions are equal and opposite to the applied forces in every direction. We do not have constraint reactions on the fork as no force is applied on the pedals. The equilibrium of the moments is calculated for convenience with respect to Node 1, which has coordinates 0,0,0, in order to use the coordinates of the nodes to obtain the arms. For example, with $coord_{x,k}$ we want to indicate the x-coordinate of Node *k*, while with $F_{x,k}$ we want to indicate the force in x-direction in Node *k*. Also the equilibrium of the moments is verified because the results of the following summations are zero.

Equilibrium check of moments around the X-axis passing through Node 1:

$$\sum_{k \in \{1,2,3,4,9,10,20059,20060\}} \left( -F_{y,k} \cdot coord_{z,k} + F_{z,k} \cdot coord_{y,k} + RM_{x,k} \right) = 0 \; Nm \tag{2.1}$$

Equilibrium check of moments around the Y-axis passing through Node 1:

$$\sum_{k \in \{1,2,3,4,9,10,20059,20060\}} \left( F_{x,k} \cdot coord_{z,k} - F_{z,k} \cdot coord_{x,k} + RM_{y,k} \right) = 0 \; Nm \tag{2.2}$$

Equilibrium check of moments around the Z-axis passing through Node 1:

$$\sum_{k\in\{1,2,3,4,9,10,20059,20060\}} \left(-F_{x,k} \cdot coord_{y,k} + F_{y,k} \cdot coord_{x,k} + RM_{z,k}\right) = 0 \ Nm \qquad (2.3)$$

*Transmission forces*

In this subcase there are no applied forces on the pedals, so there are no internal forces in the transmission.

*Deformations*

In this subcase the frame bends downwards and rotates around the rear bike dropouts (*C* in Fig. 2.22), while the fork bends moving forward (*D* in Fig. 2.22). As a first approach, the following image shows the plotel elements (Fig. 2.8) in red for the initial condition, and in blue for the final condition, with deformation view amplified by 100 times so as to see the global behavior.
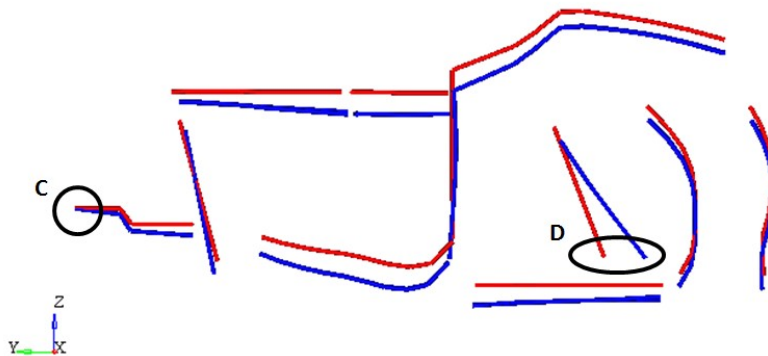


**Figure 2.22**: Plotel elements before (red) and after (blue) load application for Subcase 1.

Z-displacements are higher in point *A* than in point *B* because in point *A* there is the pin of the rollbar (Fig. 2.23) that does not lock the rotation between Tube 01 and Tube 02, meanwhile in point *B* the section is not interrupted. The presence of the pin and of the asymmetrical fork causes deformations that are not perfectly symmetrical between the left and the right side. Therefore, from the graphs in Figure 2.25, we can see that the Z-displacements on the right and left side are not equal. The aforementioned graphs show the Z-displacements of the nodes belonging to the plotel elements (Fig. 2.24), and each node ID is listed in the key. The elements and their relative graph have the same color to simplify viewing (Fig. 2.24-2.25).
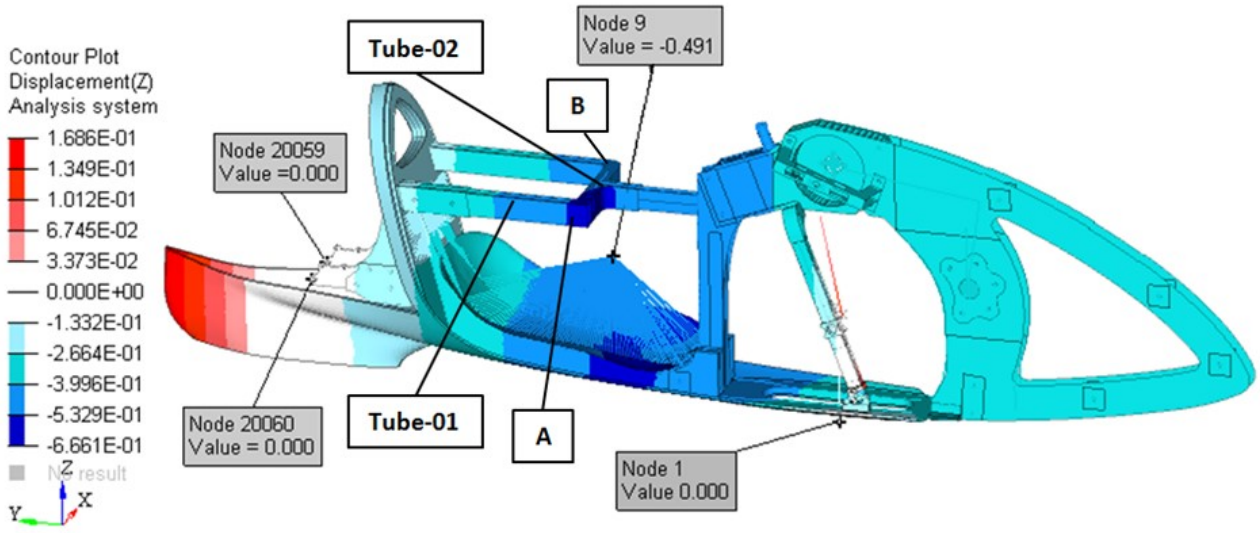
**Figure 2.23**: Z-displacements in global system for Subcase 1. Scale in mm.



(a)



(b)
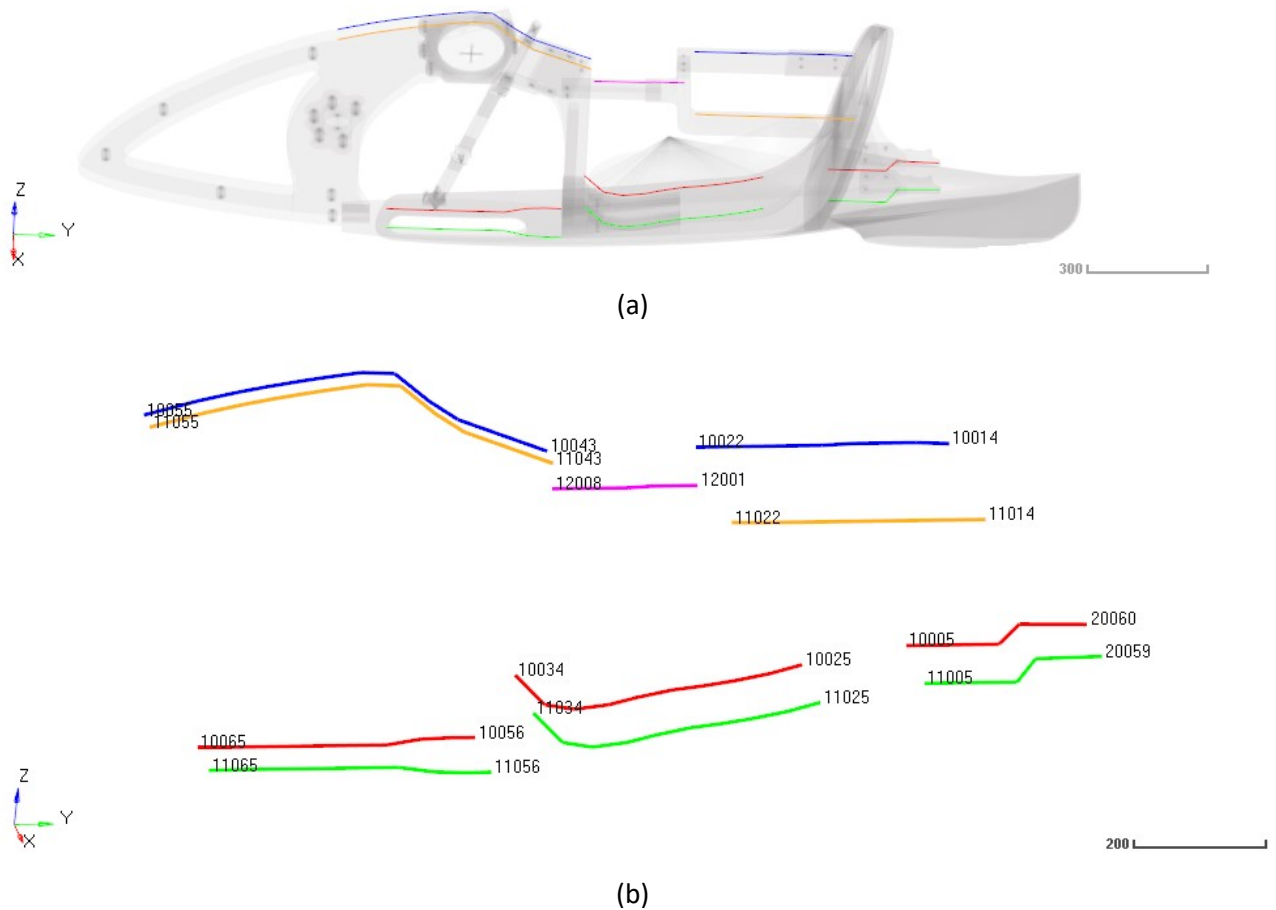
**Figure 2.24**: (a) Position of the plotel elements on the frame. (b) Plotel elements. Only the ID of the first and of the last node of the series are shown.

(a)



(b)
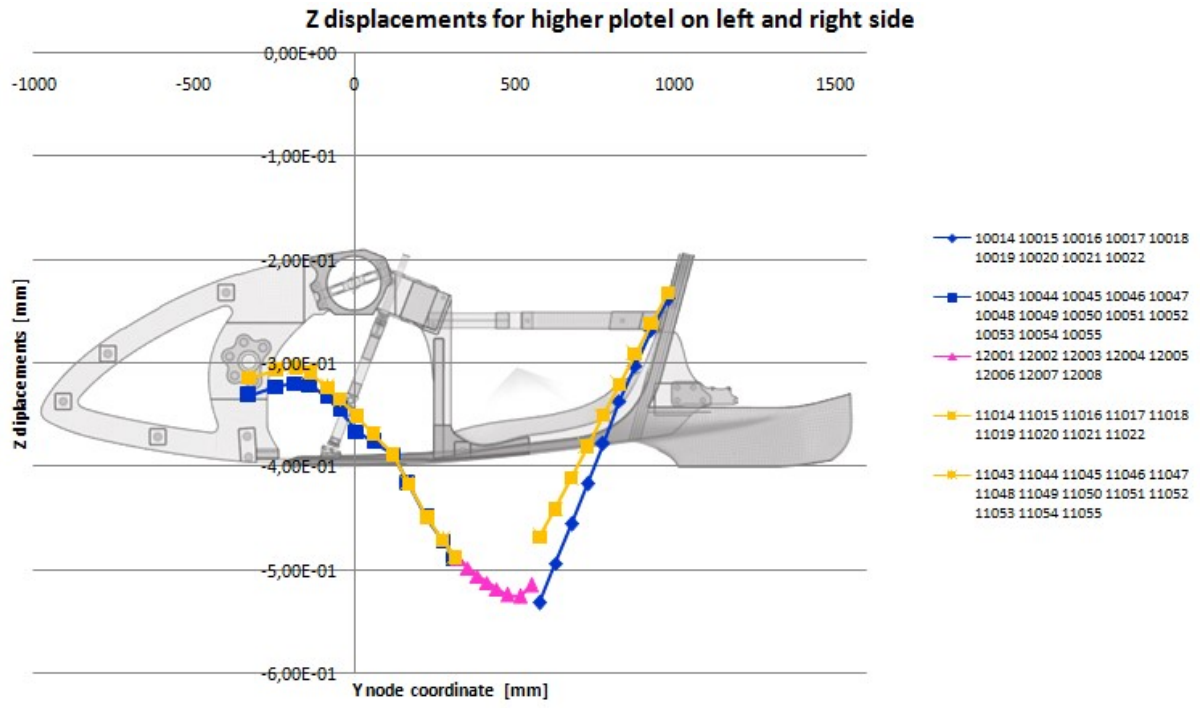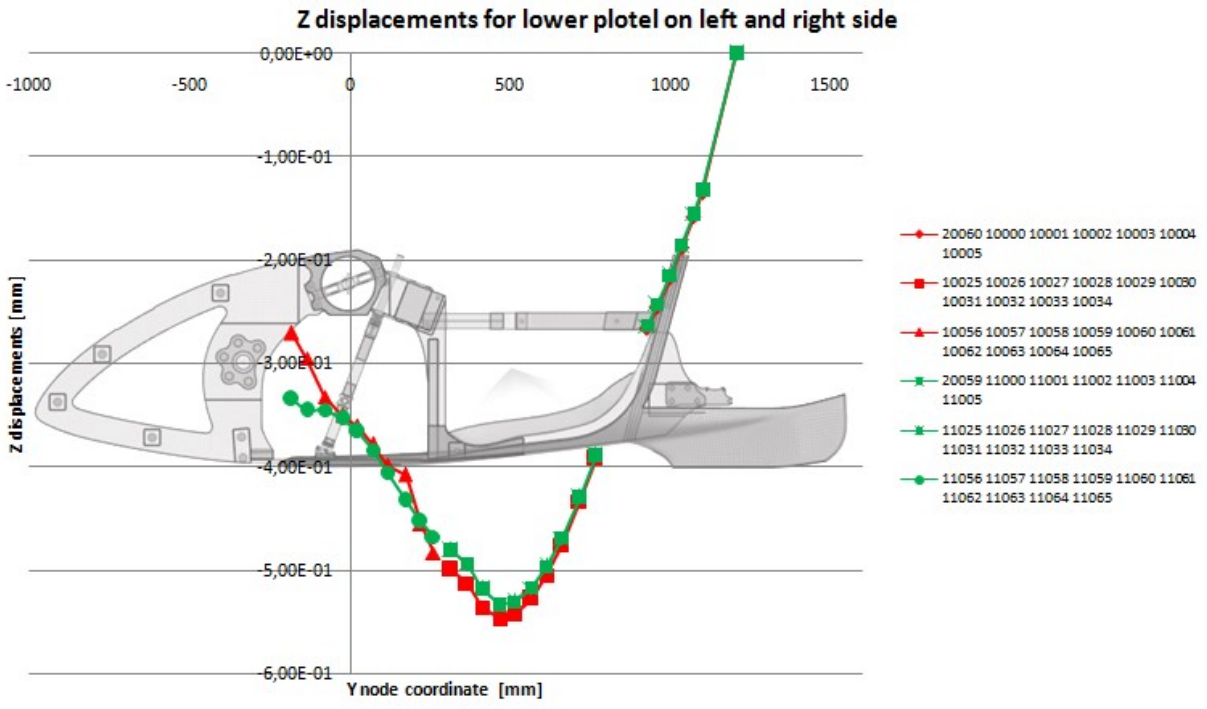
**Figure 2.25**: Z-displacements in global system of plotel nodes for Subcase 1.

This asymmetrical condition between the left and right side causes a rotation around the Y-axis. The rotation around the Y-axis is visible from the deformation in X-direction, in which the upper part has negative values (blue in Fig. 2.26) and the bottom of the fork has positive values (red in Fig. 2.26).
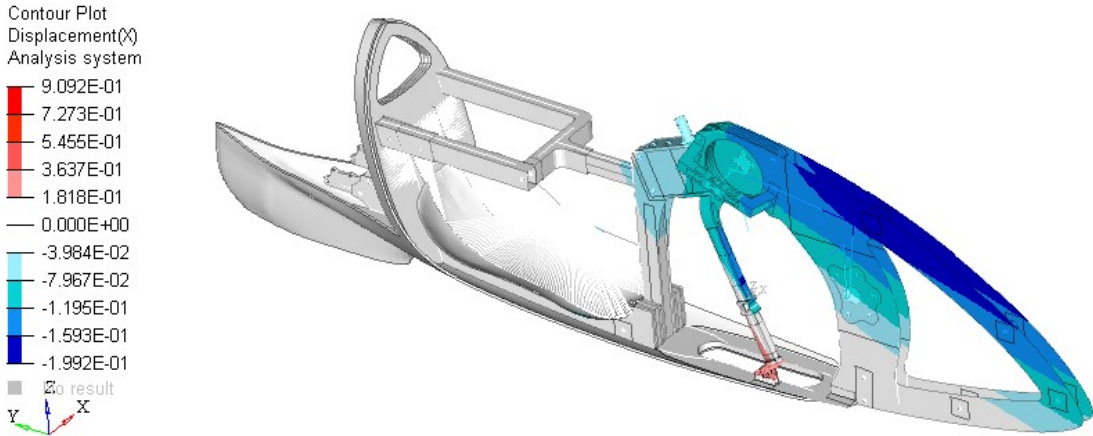
**Figure 2.26**: X-displacements in global system for Subcase 1. Scale in mm.

From the Y-displacements we can notice that the fork bends moving forward, but the rear part of the frame bends moving backward (the bottom part of the frame is red and the bottom part of the fork is blue in Fig. 2.27).
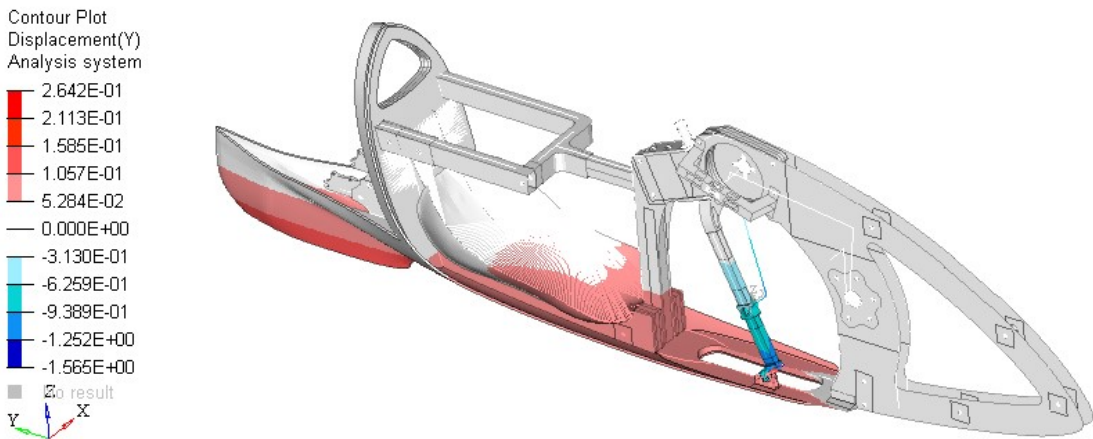


**Figure 2.27**: Y-displacements in global system for Subcase 1. Scale in mm.

The relative displacements between the bottom of the fork and the frame are so small that the guide bearings of the fork do not leave the rail that is attached to the frame (Fig. 2.28). In Figure 2.28 there is no view amplification factor, and the red lines represent the condition of the unloaded frame.
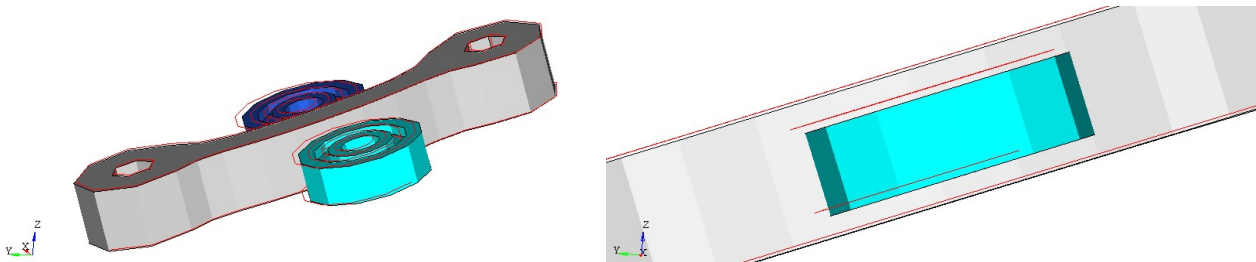


**Figure 2.28**: Guide bearings and rail of the fork during load application for Subcase 1. The red lines are for when unloaded.

*Stiffness and displacement of seat loading point*

In the loading point there is a displacement of -0.491 mm in Z (Fig. 2.23) and the loading force is -687 N in Z (Tab. 2.3), so the local static stiffness of the loading point is:

$$K_{z,9} = \frac{F_{z,9}}{displ_{z,9}} = 1399 \, N/mm$$

*Stress, strain and failure index*

In this subcase the most stressed area is between the front and rear wheel axes because we have only a force in minus-Z on the seat, and the constraints are on the wheels. The bottom bracket is not loaded and is outside that area, therefore it does not present relevant stresses. The attaching point between the frame and the guide rail of the fork is a stressed area because there is a rotation around the Y-axis, which is due to asymmetries, as explained before (Fig. 2.26). The panels of the frame have strong discontinuities in strain, stress and failure index distribution due to different core materials and to the internal reinforcements that carry the load.

Moreover, the left and right parts show different values due to the asymmetry of the frame and fork.

To understand the distribution of stress and strain in the ply layers, we have to remember their properties.

In Figure 2.29 and 2.30 there are plotted strains and stresses for:

- Ply ID 20000000 (Sandwich_sup1_carbonio_280_ply1di2), which has fibers oriented at 0°
- Ply ID 20000001 (Sandwich_sup1_carbonio_280_ply2di2), which has fibers oriented at 90°.

Those ply layers are adjacent and have different orientation. From Figure 2.29 and 2.30 we can see that they have similar strain distribution but different stress distribution. Stresses are higher when the lamina is loaded along the fibers' direction due to the higher modulus in that same direction. This is why the ply at 0° is more stressed in zone-A and the ply at 90° is more stressed in zone-B (Fig. 2.30).
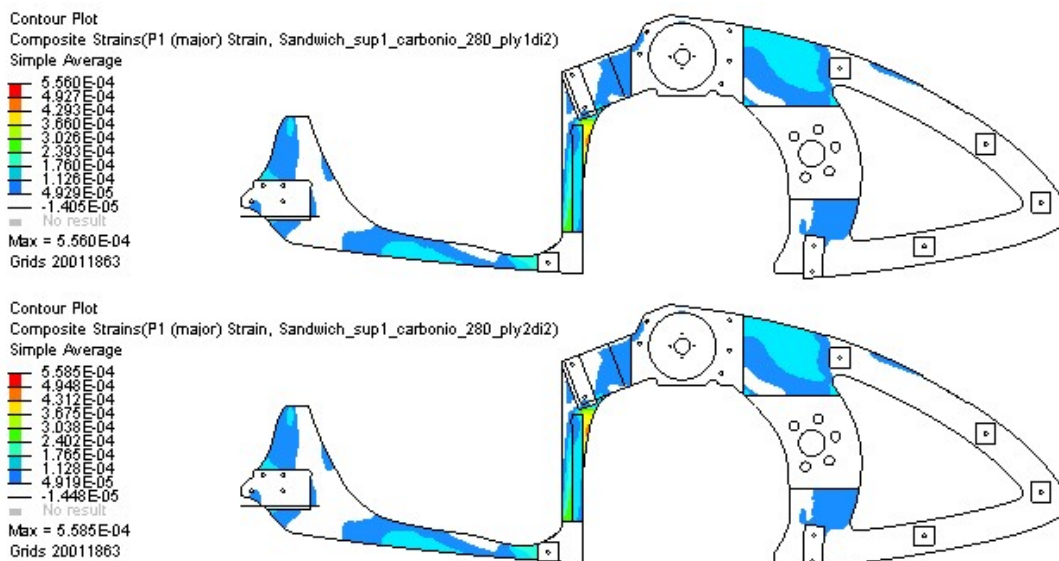


**Figure 2.29**: Strains for Subcase 1. (above) Strains for the 0°-oriented lamina with ID 20000000. (below) Strains for the 90°-oriented lamina with ID 20000001.
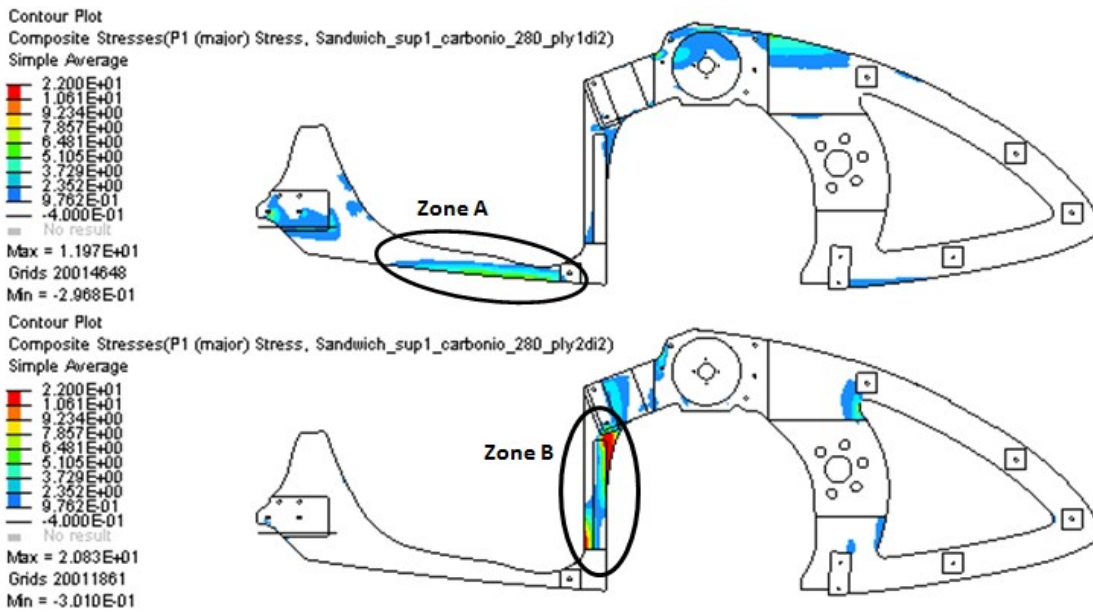
**Figure 2.30**: Stresses for Subcase 1. (above) Stresses for the 0°-oriented lamina with ID 20000000. (below) Stresses for the 90°-oriented lamina with ID 20000001.

In the frame model there are 28 ply layers, and all the information for each ply layer is useful to analyze the frame. Plotting the contour plots of stress, strain and failure-index for each ply layer could be too lengthy for the purpose of this document. To summarize the overall results we will show the distribution of the maximum values in the laminate (therefore only the maximum value of all ply layers will be reported), and we will indicate the ply ID with the highest failure index.
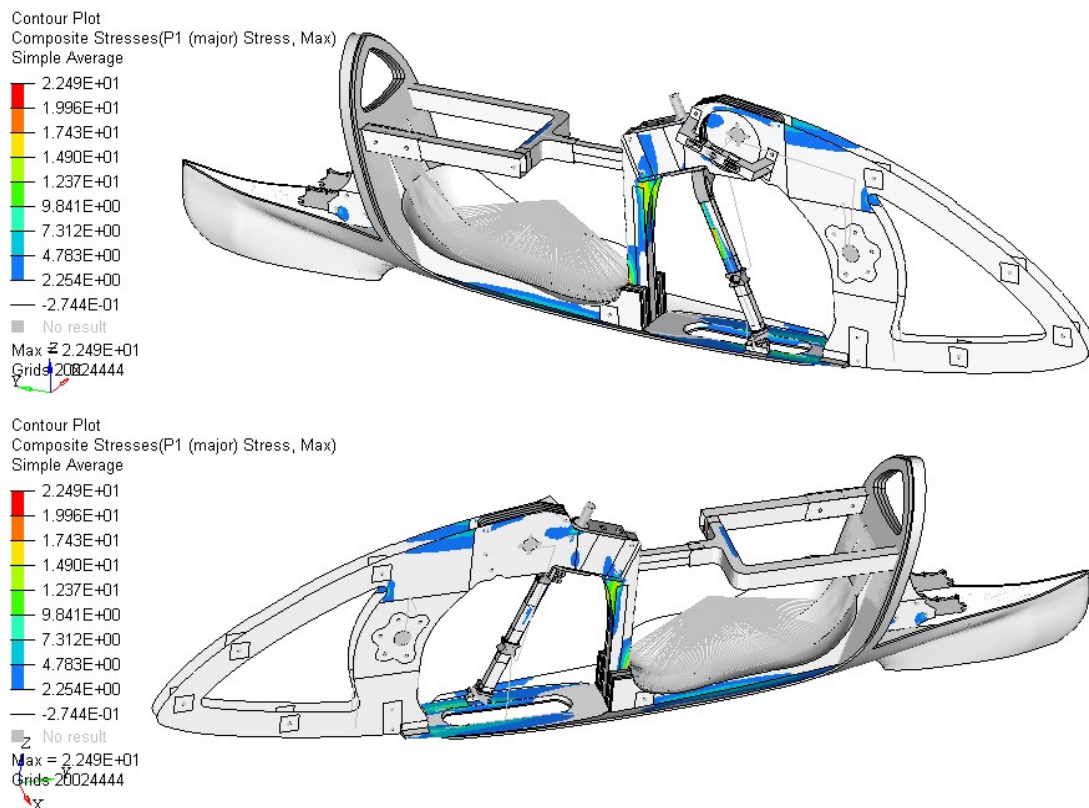


**Figure 2.31**: P1 max stresses for Subcase 1. Scale in MPa. (above) Right view, (below) left view.
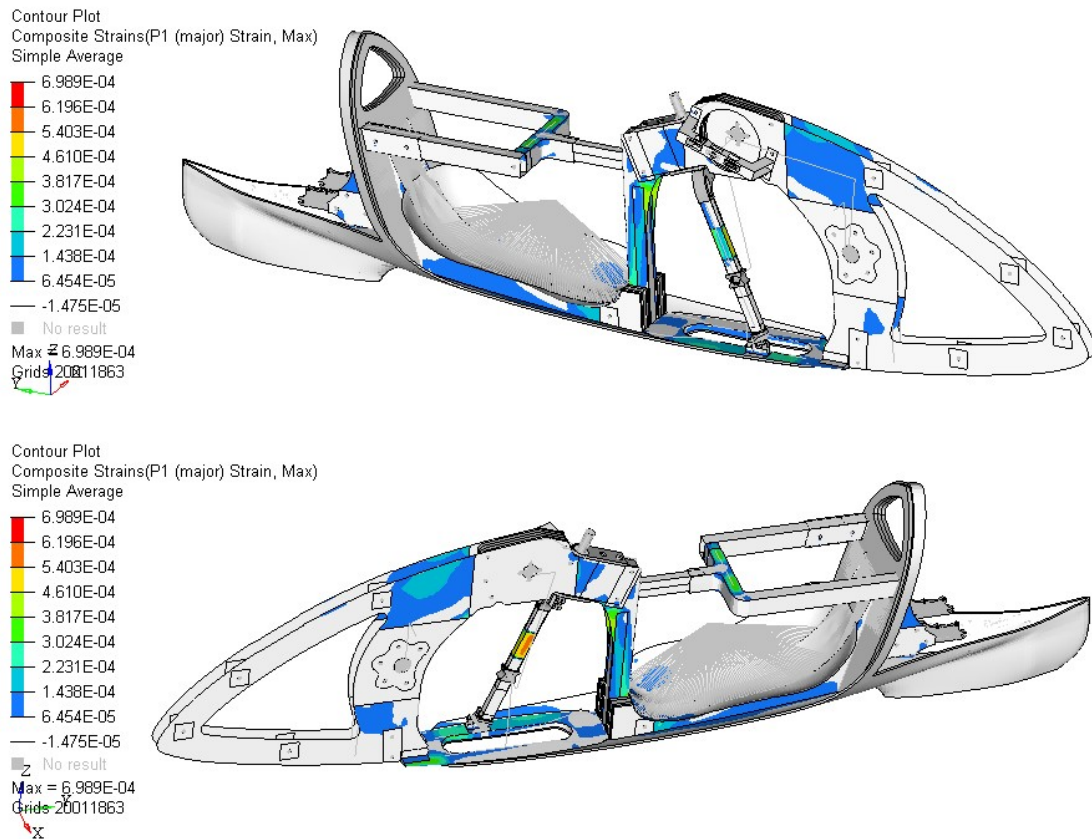
**Figure 2.32**: P1 max strains for Subcase 1. (above) Right view, (below) left view.

In Figure 2.31 and 2.32 there are the contour plots of max stresses and max strains of all ply layers. Those contour plots are useful to indentify the working area, but not to predict the composite failure since the information about orientation is lost.

To predict the rupture of the frame, in Figure 2.33 there is the contour plot of the maximum values of composite failure indexes of all ply layers. The composite failure index takes into account the strength of the ply layer according to Hoffman's Theory, and the bonding strength between the ply layers. The highest value between the ply failure index and the bonding failure index determines the laminate composite failure index. Moreover, the failure of only one ply layer determines the laminate failure. In Figure 2.34 there is the contour plot that indicates the ply layer (through its ID number) with the highest failure index.

In this subcase, the maximum failure index is on the fork and it is equal to 0.020. The maximum failure index on the frame (ply ID = 20000028) is equal to 0.016.
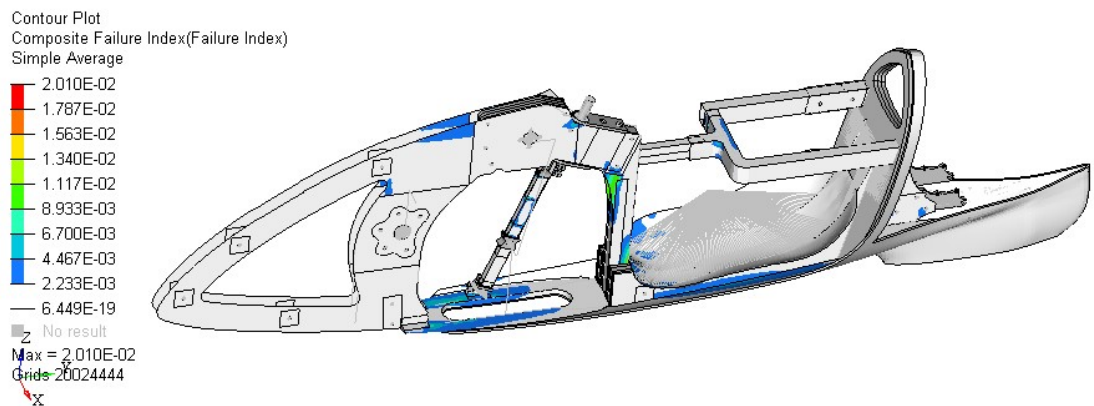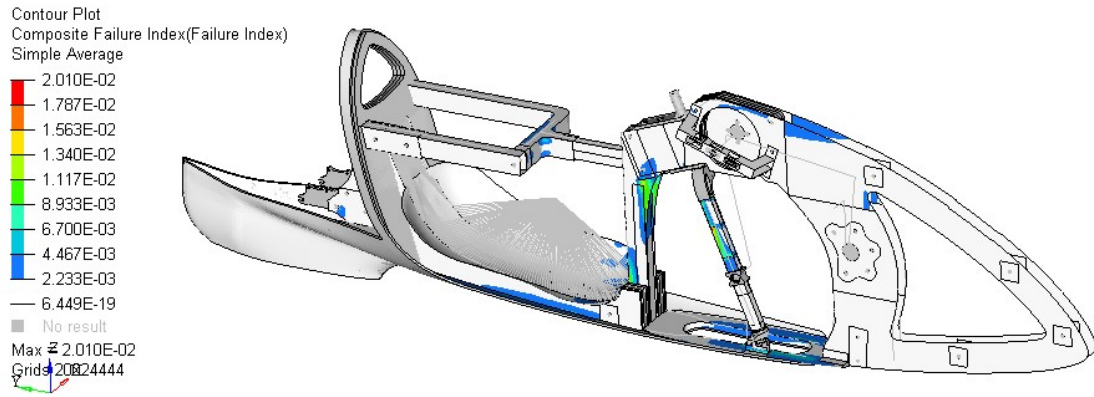
**Figure 2.33**: Maximum composite failure indexes for Subcase 1. (above) Right view, (below) left view.
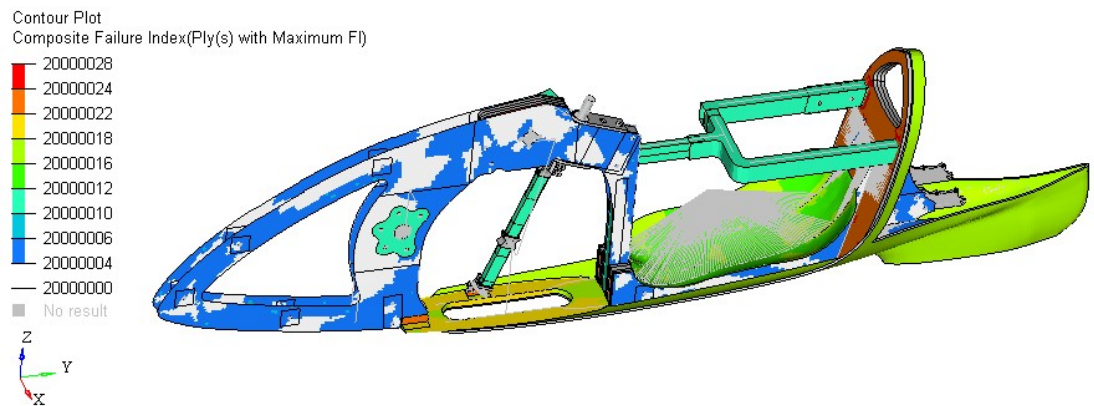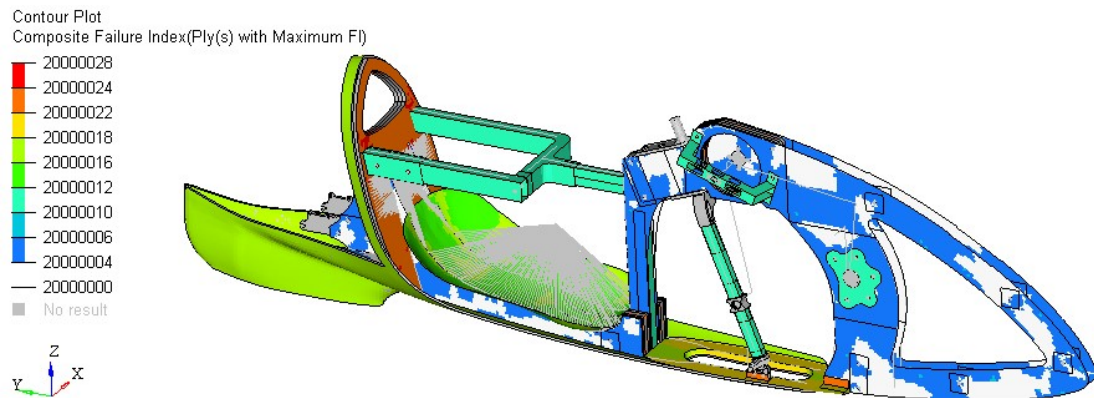


**Figure 2.34**: Ply ID in which there is the maximum failure index for Subcase 1. (above) Right view, (below) left view.

### 2.4.2 Subcase 2

*Constraint reactions and global equilibrium check*

| | Node id | SUBCASE 2: Applied forces (in global system) | | |
|---|---|---|---|---|
| | | Fx [N] | Fy [N] | Fz [N] |
| Right pedal | 2 | -55,2 | -694,4 | 68,7 |
| Left pedal | 3 | 0,0 | 0,0 | 0,0 |
| Seat | 9 | 0,0 | 0,0 | -687,0 |
| Backrest | 10 | 55,2 | 694,4 | -68,7 |
| TOT | | 0,0 | 0,0 | -687,0 |

**Table 2.5**: Applied forces in global system for Subcase 2.

| | Node id | SUBCASE 2: Reaction forces (in global system) | | | | | |
|---|---|---|---|---|---|---|---|
| | | RFx [N] | RFy [N] | RFz [N] | RMx [Nm] | RMy [Nm] | RMz [Nm] |
| Front wheel | 1 | 0,0 | 0,0 | 390,9 | 0,0 | 0,0 | 0,0 |
| Fork | 4 | 0,0 | 0,0 | 0,0 | 0,0 | 0,3 | 0,8 |
| Left bike dropout | 20059 | -5,1 | -7,4 | 150,5 | 0,0 | -0,1 | -0,1 |
| Right bike dropout | 20060 | 5,1 | 7,4 | 145,7 | 0,0 | 0,0 | 0,1 |
| TOT | | 0,0 | 0,0 | 687,0 | 0,0 | 0,3 | 0,8 |

**Table 2.6**: Reaction forces in global system for Subcase 2.

| | Node id | SUBCASE 2: Reaction forces (in local system) | | | | | |
|---|---|---|---|---|---|---|---|
| | | RFx [N] | RFy [N] | RFz [N] | RMx [Nm] | RMy [Nm] | RMz [Nm] |
| Fork | 4 | 0,0 | 0,0 | 0,0 | 0,0 | 0,0 | 0,87 |

**Table 2.7**: Reaction forces in fork local system for Subcase 2.

The equilibrium of forces is verified because the applied forces are equal to the reaction forces. The forces applied on the right pedal and on the backrest are aligned and are directed opposite to each other. The torque equilibrium is verified by Equations 2.1, 2.2 and 2.3, which are equal to zero. The torque reaction at Node 4 is due to $F_{y\ local,5009}$, which is the Y-component of force at Node 5009 in the fork local reference system. Force at Node 5009 is aligned to the tie rod and we have $F_{y\ local,5009}$ because the tie rod and the rotation axis of the fork make the angle $\theta$ = 9.341° on the YZ-plane (Fig. 2.35.a).

Knowing that the magnitude of the force at Node 5009 is $F_{5009}$ = 151.1 N (Tab. 2.8), knowing the value of angle $\theta$ and of the lever arm of $F_{y\ local,5009}$ respect to the fork rotational axis, which is equal to $R$=35.5 mm (Fig. 2.35.b), we can check the torque reaction around the fork rotational axis:

$$RM_{z\ local,4} = F_{5009} \cdot \sin\theta \cdot R = 0.87\ Nm$$



(a)                                                                 (b)
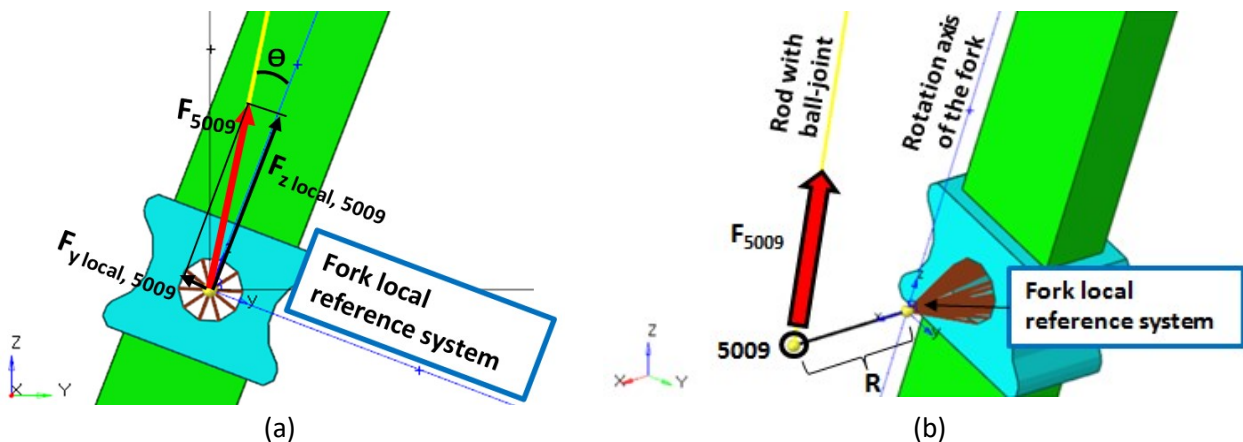
**Figure 2.35**: (a) Force at Node 5009 in global and local reference system. (b) Arm $R$ of $F_{y\ local,\ 5009}$ around the rotation axis of the fork.

*Transmission forces*

In this subcase we apply a force on the right pedal (node ID = 2), so we have forces inside the transmission. The forces transmitted to the frame play an important role in the global deformation of the frame. In Figure 2.36 there is the free body diagram of some parts of the transmission, and their numerical values are listed in Table 2.8.

| SUBCASE 2 | | | |
|---|---|---|---|
| Node Id | Fx [N] | Fy [N] | Fz [N] |
| 2 | -55,2 | -694,4 | 68,7 |
| 3 | 0,0 | 0,0 | 0,0 |
| 5002 | 0,5 | 472,6 | 65,6 |
| 5003 | 0,0 | -30,5 | -148,0 |
| 5005 | -0,5 | -472,6 | -65,6 |
| 5009 | 0,0 | 30,5 | 148,0 |
| 5014 | 27,1 | 1059,0 | -93,0 |
| 5015 | 27,5 | -836,7 | -41,2 |
| 5017 | -6,2 | 283,1 | 199,7 |
| 5018 | 6,8 | 220,1 | 13,8 |



**Table 2.8**: Forces inside transmission for Subcase 2.  **Figure 2.36**: Free body diagram of transmission elements for Subcase 2.
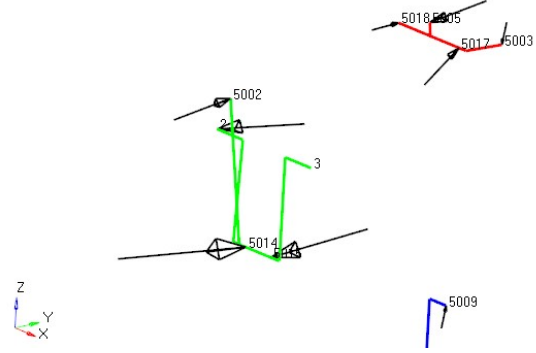
We have verified that the green and red elements in Figure 2.36 are in equilibrium, so we have:

$$F_2 + F_3 + F_{5002} + F_{5014} + F_{5015} = 0 \ N \tag{2.4}$$

$$F_{5003} + F_{5005} + F_{5017} + F_{5018} = 0 \ N \tag{2.5}$$

Equilibrium check of moments around X-axis passing through Node 1:

$$\sum_{k \in \{2,3,5002,5014,5015\}} \left(-F_{y,k} \cdot coord_{z,k} + F_{z,k} \cdot coord_{y,k}\right) = 0 \ Nm \tag{2.6}$$

$$\sum_{k \in \{5003,5005,5017,5018\}} \left(-F_{y,k} \cdot coord_{z,k} + F_{z,k} \cdot coord_{y,k}\right) = 0 \ Nm \tag{2.7}$$

Equilibrium check of moments around Y-axis passing through Node 1:

$$\sum_{k \in \{2,3,5002,5014,5015\}} \left(F_{x,k} \cdot coord_{z,k} - F_{z,k} \cdot coord_{x,k}\right) = 0 \ Nm \tag{2.8}$$

$$\sum_{k \in \{5003,5005,5017,5018\}} \left(F_{x,k} \cdot coord_{z,k} - F_{z,k} \cdot coord_{x,k}\right) = 0 \ Nm \tag{2.9}$$

Equilibrium check of moments around Z-axis passing through Node 1:

$$\sum_{k \in \{2,3,5002,5014,5015\}} \left(-F_{x,k} \cdot coord_{y,k} + F_{y,k} \cdot coord_{x,k}\right) = 0 \ Nm \tag{2.10}$$

$$\sum_{k \in \{5003,5005,5017,5018\}} \left(-F_{x,k} \cdot coord_{y,k} + F_{y,k} \cdot coord_{x,k}\right) = 0 \ Nm \tag{2.11}$$

As described previously, Node 5002 is linked to Node 5005 with a tie rod, and Node 5003 is linked to Node 5009 through a tie rod as well. For this reason we have:

$$F_{5002} = -F_{5005} \tag{2.12}$$

$$F_{5003} = -F_{5009} \tag{2.13}$$

Forces seen by the tie rod are opposite to $F_{5002}$, $F_{5005}$, $F_{5003}$, $F_{5009}$, so the tie rods are in traction as the real chain. In Figure 2.37 we can see the forces transmitted from the transmission to the frame, so we observe forces at the nodes of the frame. As described previously, the connections between the frame and the transmission are made by special rigid elements. For this reason we have that:

$$F_{5014} = -F_{20000} \tag{2.14}$$

$$F_{5015} = -F_{20001} \tag{2.15}$$

$$F_{5017} = -F_{20056} \tag{2.16}$$

$$F_{5018} = -F_{20058} \tag{2.17}$$
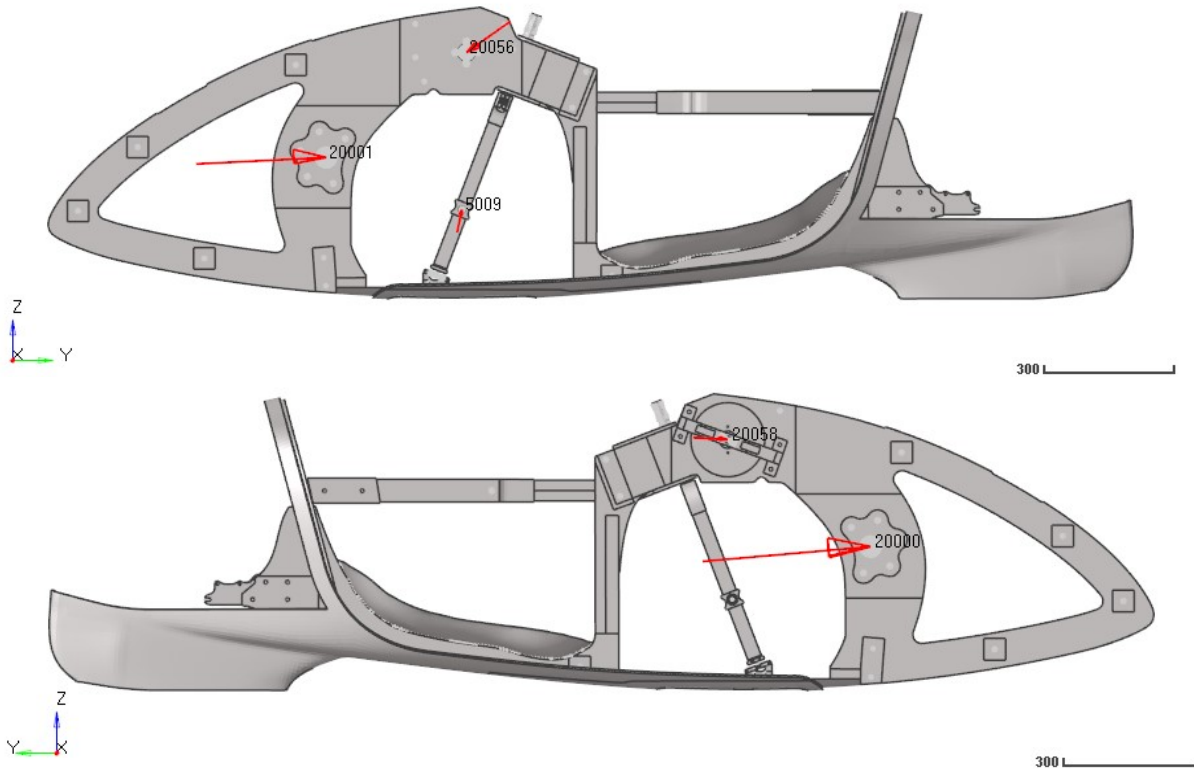


**Figure 2.37**: Forces transmitted from the transmission to the frame for Subcase 2. (above) Left view. (below) Right view.

Looking at Table 2.8, at Equations 2.14 and 2.15, and at Figure 2.37, we can notice that the forces on the frame at the attaching points of the bottom bracket (Nodes 20000 and 20001) and of the sprocket-set-shaft bearings (Nodes 20056 and 20058) induce a reaction torque on the frame. To evaluate their value we use the following formula.

Moment around Z-axis (passing through Node 1) from bottom bracket to frame:

$$M_{z,bottom\ bracket} = \sum_{k \in \{20000,20001\}} \left( -F_{x,k} \cdot coord_{y,k} + F_{y,k} \cdot coord_{x,k} \right) \tag{2.18}$$

Moment around Z-axis (passing through Node 1) from sprocket-set shaft to frame:

$$M_{z,gears\ shaft} = \sum_{k \in \{20056,20058\}} \left(-F_{x,k} \cdot coord_{y,k} + F_{y,k} \cdot coord_{x,k}\right) \tag{2.19}$$

$$M_{z,bottom\ bracket} = 32.9\ Nm$$
$$M_{z,gears\ shaft} = 18.0\ Nm$$

Another effect induced by the second tie-rod forces is the bending of the fork around Y-axis. Indeed, forces at Nodes 5009 and 50056 tend to decrease the distance between the front-wheel axis and the gear-shaft axis. Moreover, the force at Node 5009 tends to move the fork forward and to make it rotate around its axis as highlighted in the previous part.

These observations will help us understand the global deformations presented in the next section.

*Deformations*

Subcase-2 loading forces are equal to those in Subcase 1, plus a force on the right pedal and a force on the backrest. Therefore, the frame bends downwards as in Subcase 1, and it also bends with positive sign around Y and Z-axes. As a first approach, Figure 2.38 shows the plotel elements (Fig. 2.8) in red for the initial condition, and in blue for the final condition, with deformation view amplified by 100 times so as to see the global behavior.
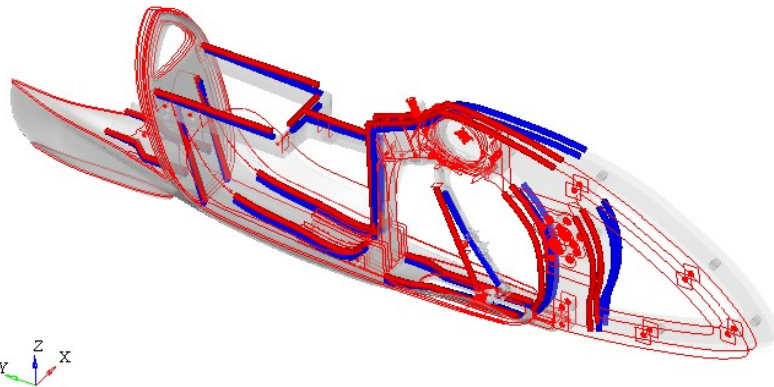


**Figure 2.38**: Plotel elements before (red) and after (blue) load application for Subcase 2.

The frame bends with positive sign around Z-axis because the applied forces on the right pedal and the backrest increase their distance; and it also bends with positive sign around Y-axis because the lower part of the frame is stiffer than the upper part (Fig. 2.38). Moreover, the forces at Node 5009 tend to move the fork forward, increasing the bending downwards.

The result is a complex deformed shape, which is described more in detail in the following images.

X-displacements present positive and negative values, so there is an area in which the curvature is higher. To identify that area we use a graph which shows the X-displacements of nodes belonging to plotel elements (Fig. 2.40).
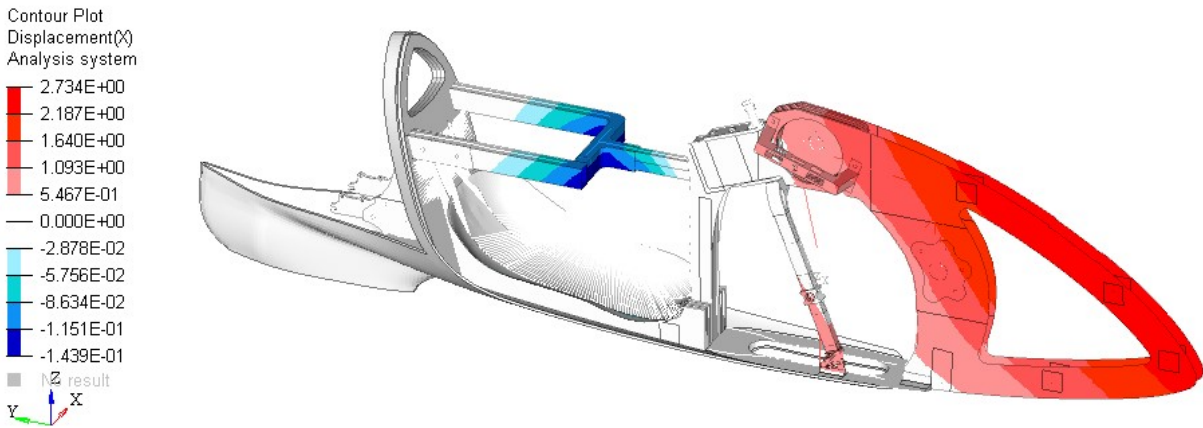
**Figure 2.39**: X-displacements in global system for Subcase 2. Scale in mm.
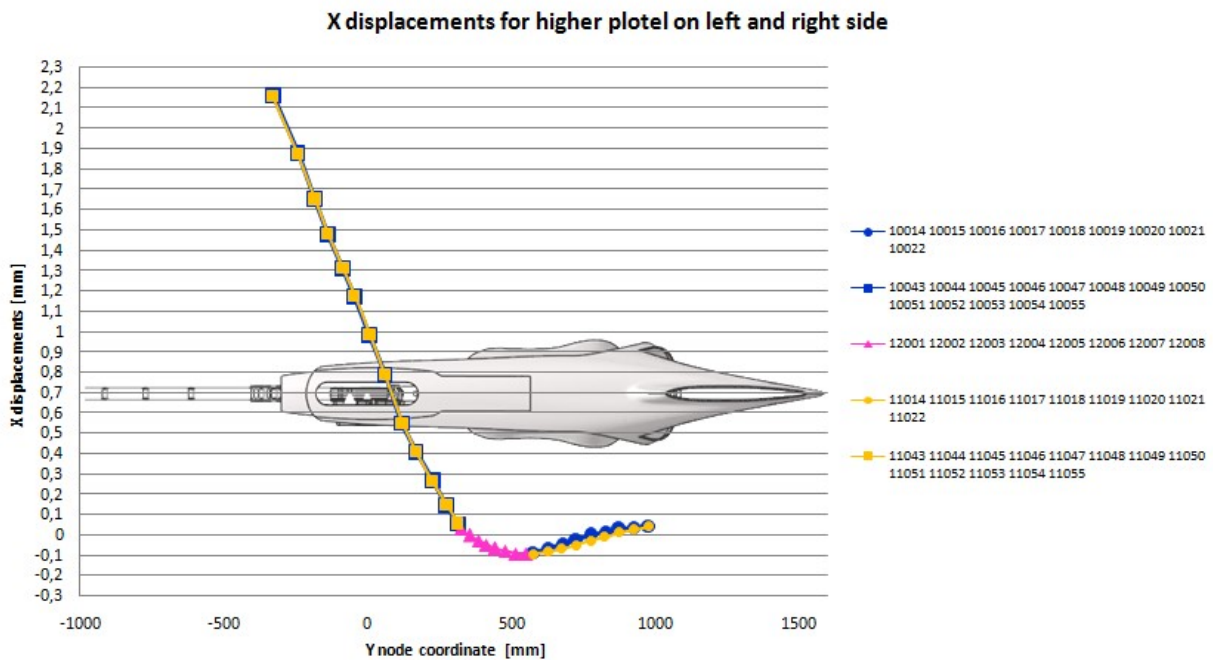


**Figure 2.40**: X-displacements in global system of plotel nodes for Subcase 2.

The bottom of the fork has negative Y-displacements (blue in Fig. 2.41) and the bottom of the frame has positive Y-displacements (red in Fig. 2.41) due to the cyclist weight force, as in Subcase 1. The attaching points of the bottom bracket and of the sprocket-set shaft have negative Y-displacements on the right side (above in Fig. 2.41), and almost zero on the left side (below in Fig. 2.41) due to the rotation around Z-axis. Z-displacements are zero in the constrained points of the rear dropouts and in that of the front wheel due to the global constraints. Z-displacements are mainly negative due to the downward bending induced by the cyclist's weight force. Looking more accurately, the left part of the frame has higher displacements in absolute value respect to right part (Fig. 2.42) due to the rotation around Y-axis.
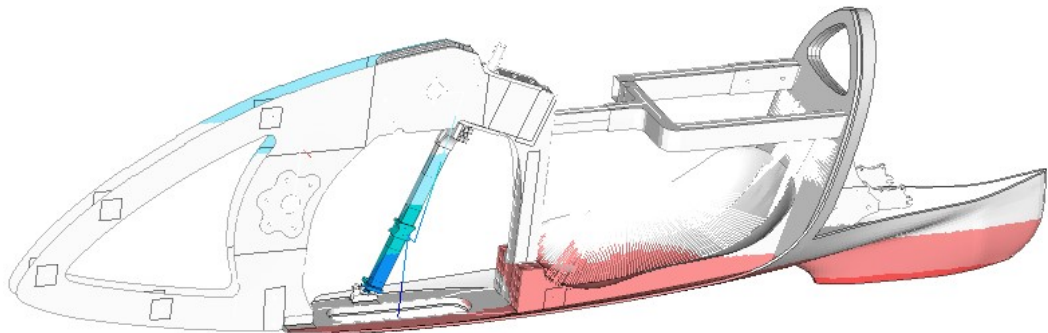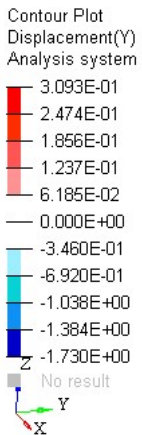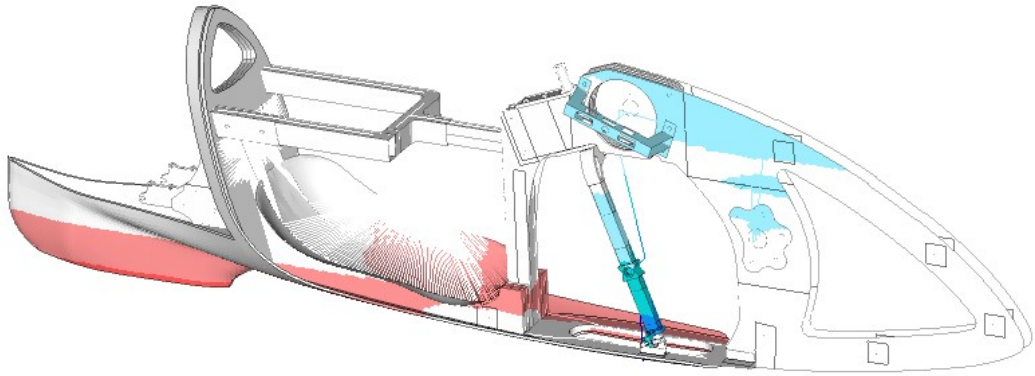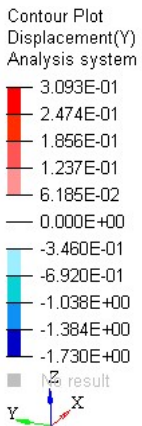
**Figure 2.41**: Y-displacements in global system for Subcase 2. Scale in mm. (above) Right view. (below) Left view.
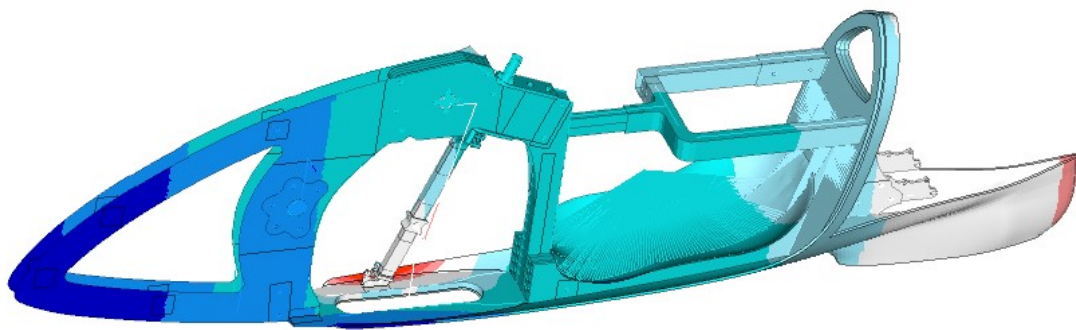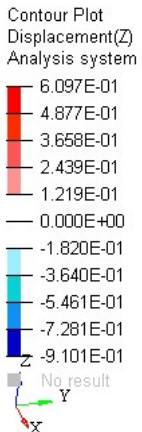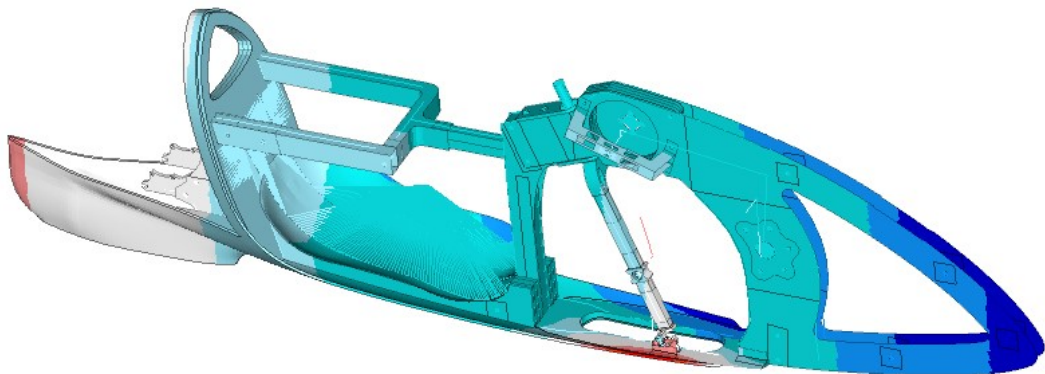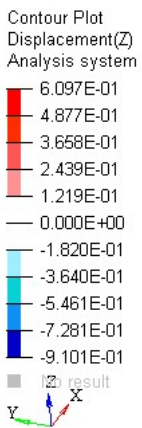


**Figure 2.42**: Z-displacements in global system for Subcase 2. Scale in mm. (above) Right view. (below) Left view.

In the following figure we can check that in Subcase 2 the bearings that guide the fork do not leave the rail. In Figure 2.43 there is no view amplification factor and the red lines represent the condition of the unloaded frame.
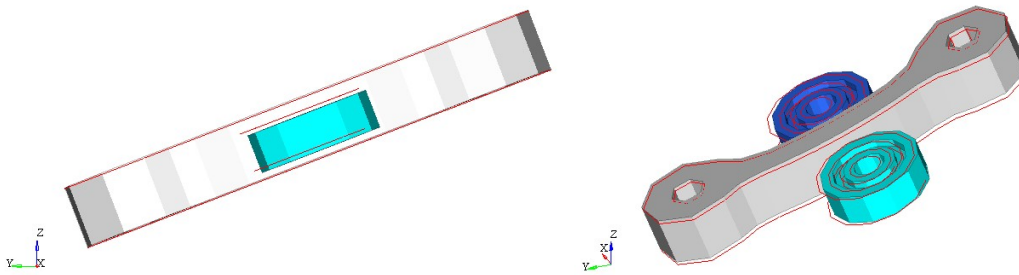


**Figure 2.43**: Guide bearings and rail of the fork during load application for Subcase 2. The red lines are for when unloaded.

*Stiffness and displacement between right pedal and backrest*

An important parameter to evaluate the frame is the deformation measured from the right pedal to the backrest, because the work done by the cyclist to produce that deformation is a loss of energy.

In Subcase 1 there were little negative displacements of the pedals due to the frame deformation, while in Subcase 2 there is a positive displacement of the right pedal. Therefore, the deformation caused by the force on the right pedal is the sum of the two contributions.

The relative displacement between Node 2 and Node 10 is:

- -0.040 mm at the end of Subcase 1
- 0.588 mm at the end of Subcase 2.

Therefore, the total deformation between Node 2 and Node 10 is $d_{2,10}$ = 0.628 mm. Recalling the applied force of *F*=700 N, we have a local stiffness of:

$$K_{2,10} = \frac{F}{d_{2,10}} = 1115 \; N/mm$$

*Stress, strain and failure index*

As for Subcase 1, the contour plots in Figure 2.44 and 2.45 show the maximum stress and strain values in the laminate. These are useful to see that the right side is more stressed than the left side, but they cannot show us where the material could break. So, Figures 2.46 show the maximum failure indexes of the laminate, and Figures 2.47 show the ply in which these maximum failure indexes are present, by means of the ply ID number. The highest composite failure index is on the frame (ply ID = 20000028), and it is equal to 0.026.
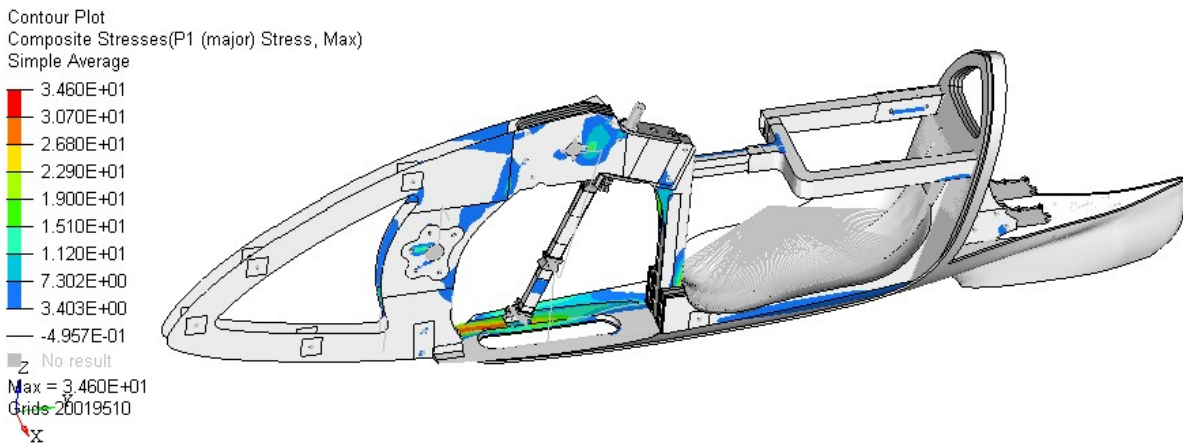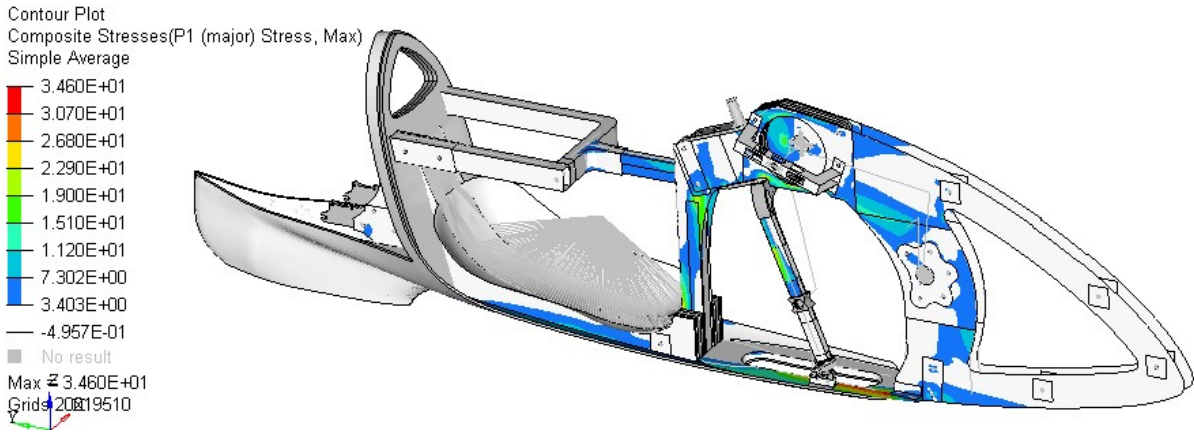
**Figure 2.44**: P1 max stress for Subcase 2. Scale in MPa. (above) Right view, (below) left view.
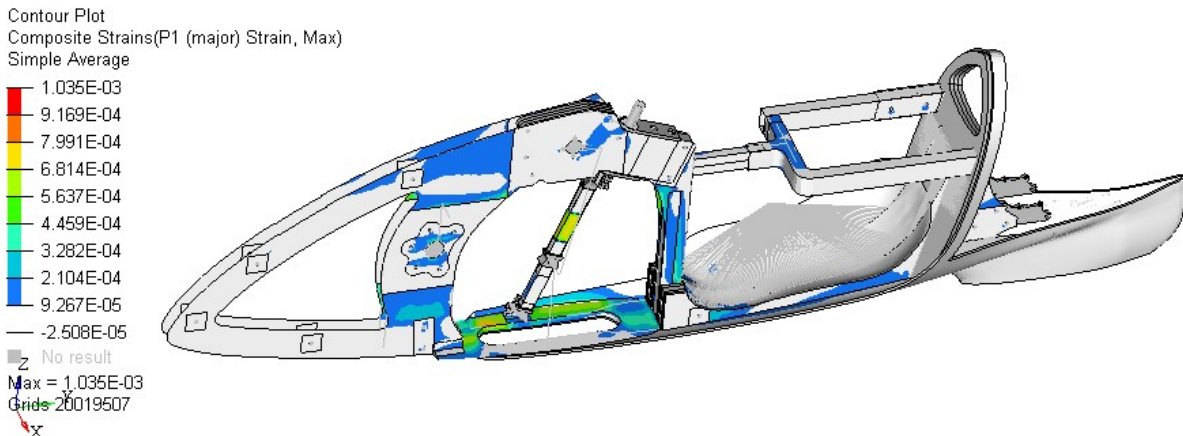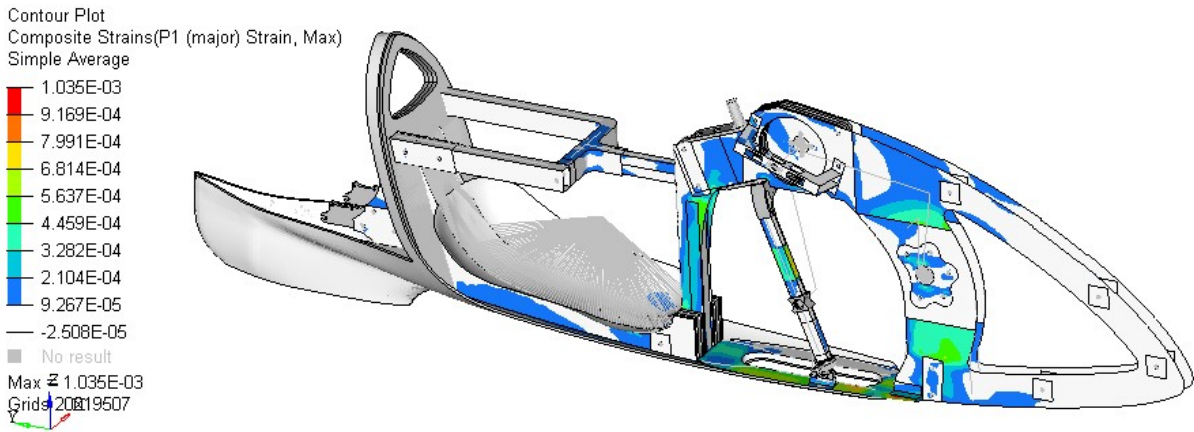


**Figure 2.45**: P1 max strain for Subcase 2. (above) Right view, (below) left view.
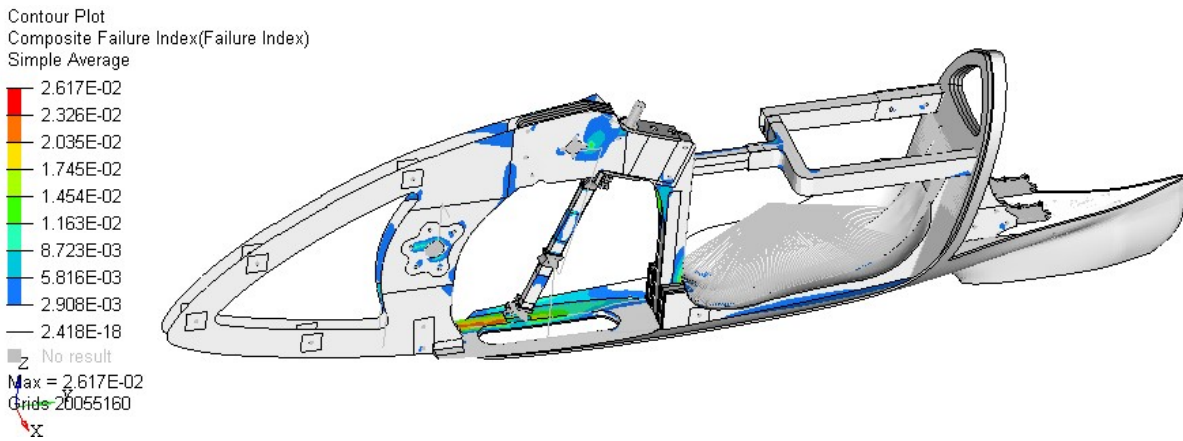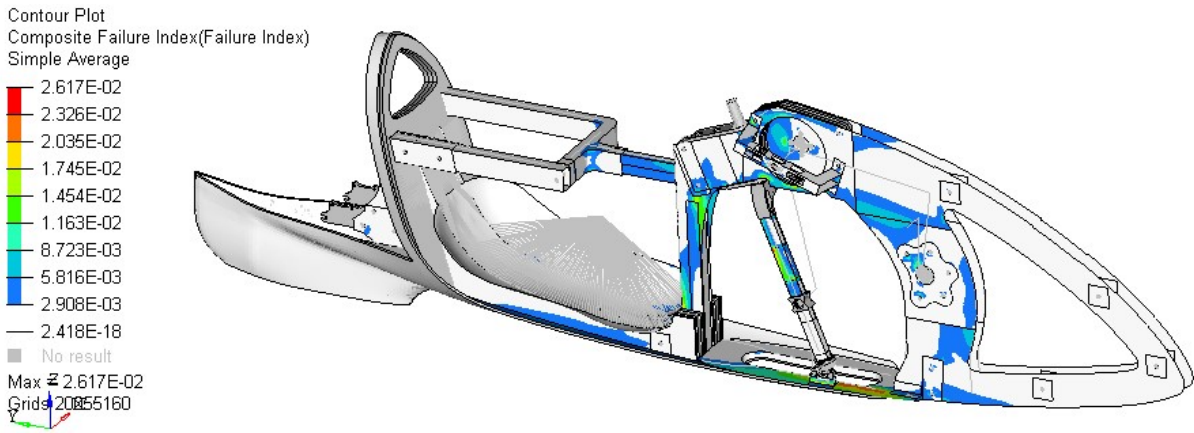
**Figure 2.46**: Maximum composite failure index for Subcase 2. (above) Right view, (below) left view.
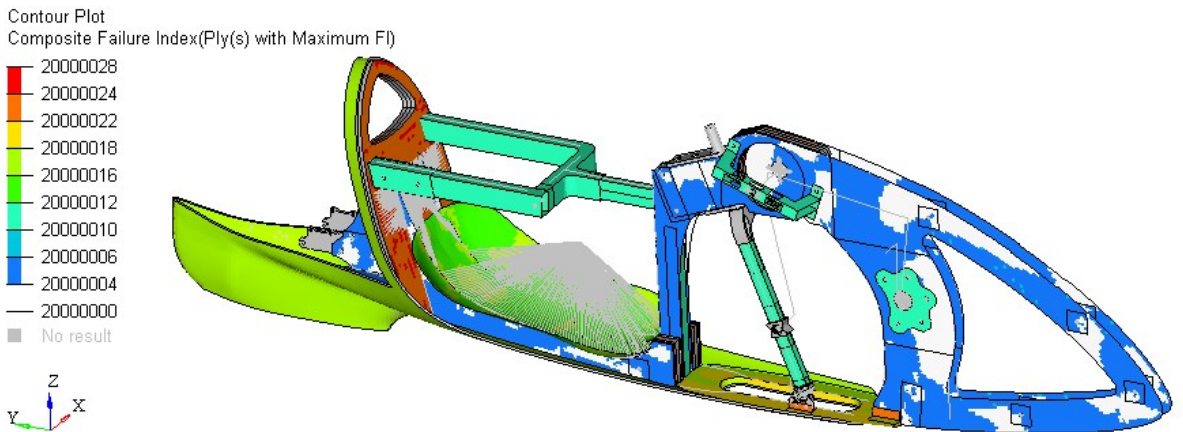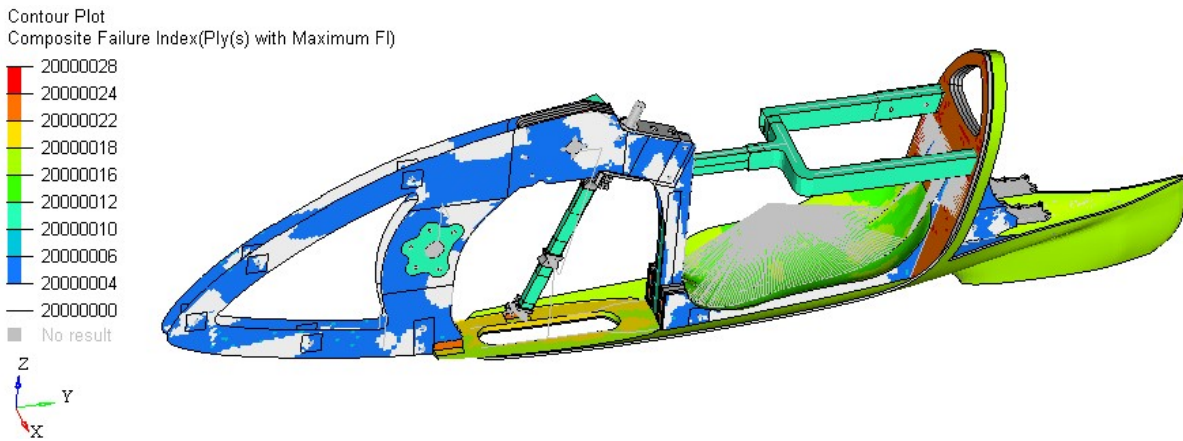


**Figure 2.47**: Ply ID in which there is the maximum failure index for Subcase 2. (above) Right view, (below) left view.

### 2.4.3 Subcase 3

*Constraint reactions and global equilibrium check*

| | Node id | SUBCASE 3: Applied forces (in global system) | | |
|---|---|---|---|---|
| | | Fx [N] | Fy [N] | Fz [N] |
| Right pedal | 2 | 0,0 | 0,0 | 0,0 |
| Left pedal | 3 | 55,2 | -694,4 | 68,7 |
| Seat | 9 | 0,0 | 0,0 | -687,0 |
| Backrest | 10 | -55,2 | 694,4 | -68,7 |
| TOT | | 0,0 | 0,0 | -687,0 |

**Table 2.9**: Applied forces in global system for Subcase 3.

| | Node id | SUBCASE 3: Reaction forces (in global system) | | | | | |
|---|---|---|---|---|---|---|---|
| | | RFx [N] | RFy [N] | RFz [N] | RMx [Nm] | RMy [Nm] | RMz [Nm] |
| Front wheel | 1 | 0,0 | 0,0 | 390,9 | 0,0 | 0,0 | 0,0 |
| Fork | 4 | 0,0 | 0,0 | 0,0 | 0,0 | 0,3 | 0,8 |
| Left bike dropout | 20059 | -5,1 | -7,4 | 151,6 | 0,0 | 0,0 | -0,1 |
| Right bike dropout | 20060 | 5,1 | 7,4 | 144,6 | 0,0 | 0,1 | 0,1 |
| TOT | | 0,0 | 0,0 | 687,0 | 0,0 | 0,4 | 0,8 |

**Table 2.10**: Reaction forces in global system for Subcase 3.

| | Node id | SUBCASE 3: Reaction forces (in local system) | | | | | |
|---|---|---|---|---|---|---|---|
| | | RFx [N] | RFy [N] | RFz [N] | RMx [Nm] | RMy [Nm] | RMz [Nm] |
| Fork | 4 | 0,0 | 0,0 | 0,0 | 0,0 | 0,0 | 0,87 |

**Table 2.11**: Reaction forces in fork local system for Subcase 3.

The equilibrium of forces is verified because the applied forces are equal to reaction forces. Forces applied on the left pedal and backrest are aligned and have opposite direction to each other. The torque equilibrium is verified by Equations 2.1, 2.2 and 2.3, which are equal to zero. The torque reaction at Node 4 (due to fork rotation constraint) is equal to that of Subcase 2 because it depends on the forces transmitted by the second tie rod, which do not change magnitude and direction.

*Transmission forces*

In this subcase we apply a force on the left pedal (node ID = 3), so we have forces inside the transmission. The forces transmitted to the frame play an important role in the global deformation of the frame. In Figure 2.48 there is the free-body diagram of some parts of the transmission and their numerical values are listed in Table 2.12.

| SUBCASE 3 | | | |
|---|---|---|---|
| Node Id | Fx [N] | Fy [N] | Fz [N] |
| 2 | 0,0 | 0,0 | 0,0 |
| 3 | 55,2 | -694,4 | 68,7 |
| 5002 | 0,5 | 472,6 | 65,6 |
| 5003 | 0,0 | -30,5 | -148,0 |
| 5005 | -0,5 | -472,6 | -65,6 |
| 5009 | 0,0 | 30,5 | 148,0 |
| 5014 | -28,0 | -1562,0 | -146,3 |
| 5015 | -27,7 | 1784,0 | 12,0 |
| 5017 | 3,2 | 283,1 | 199,7 |
| 5018 | -2,7 | 220,1 | 13,8 |

**Table 2.12**: Forces inside transmission for Subcase 3.
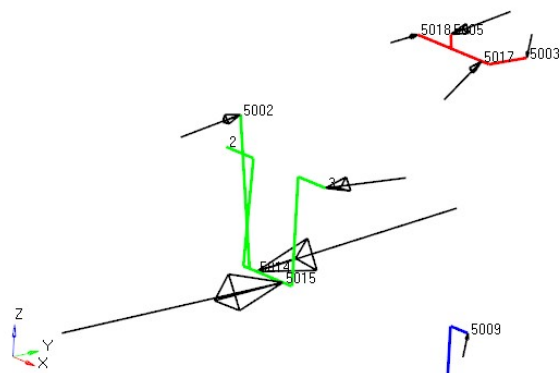


**Figure 2.48**: Free-body diagram of transmission elements for Subcase 3.

As for the previous subcases, also in Subcase 3 we have verified the equilibrium of green and red parts through the Equations 2.4-2.11. Moreover, the Equations 2.12 and 2.13 are verified and the tie rods are in traction condition. We can notice that the drive torque produced by the left pedal does not change compared to the previous subcase. Indeed, forces at the tie rods extremities (Nodes 5002, 5005, 5003 and 5009) do not change. The distance between Node 3 and Node 5002 is greater than the distance between Node 2 and Node 5002 (Fig. 2.48). Therefore, to satisfy the equilibrium of the green parts, the forces at the bottom bracket (Nodes 5014 and 5015) have to increase.

Remembering Equations 2.14-2.17, we can evaluate the forces transmitted to the frame.
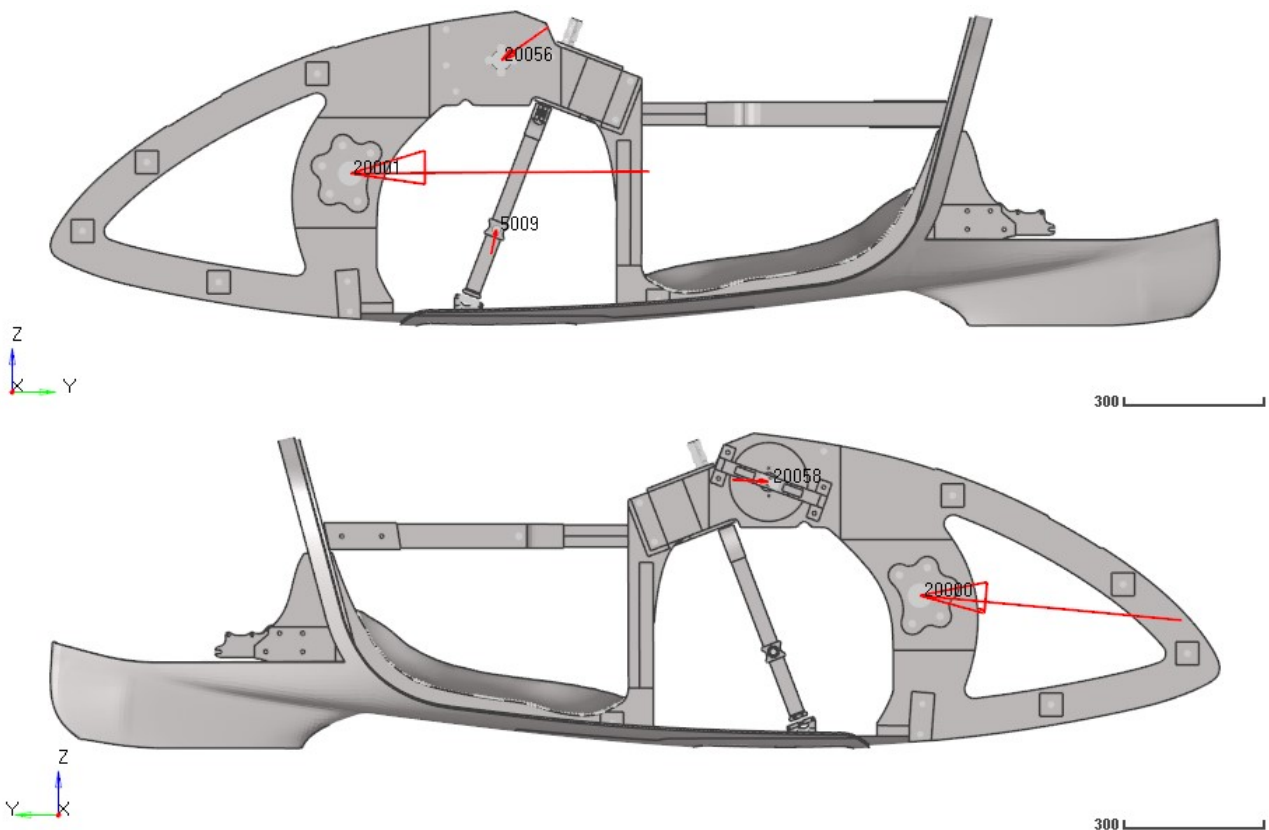


**Figure 2.49**: Forces transmitted from the transmission to the frame for Subcase 3. (above) Left view, (below) right view.

The torques transmitted from the bottom bracket and from the sprocket-set shaft have been evaluated through Equations 2.18 and 2.19.

$$M_{z,bottom\ bracket} = -71.0\ Nm$$

$$M_{z,gears\ shaft} = 18.0\ Nm$$

The torque transmitted from the sprocket-set shaft does not change. Compared to the previous subcase, the change of reaction force at the bottom bracket causes a higher torque with an opposite direction.

As opposed to what happens in Subcase 2, $M_{z,bottom\ bracket}$ and $M_{z,gears\ shaft}$ have opposite directions. This condition produces different deformations on the frame (Fig. 2.52).

Forces on the second tie rod (Nodes 5003 and 5009) do not change, so they have the same effect on the fork as in the previous subcase.

*Deformations*

In Subcase 3, the loading forces are equal to those of Subcase 1, plus a force on the left pedal, and a force on the backrest. Except for the fact that we load the opposite pedal, the loading forces are equal to those in Subcase 2.

As a first approach, Figure 2.50 shows the plotel elements (Fig. 2.8), in red for the initial condition and in blue for the final condition, with deformation view amplified by 100 times so as to see the global behavior. The frame bends with negative sign around Z-axis and Y-axis (Fig. 2.50) because the applied forces on the left pedal and on the backrest increase their distance, and the lower part of the frame is stiffer than the upper part. Moreover, the forces at Node 5009 tend to move the fork forward, increasing the bending downwards.
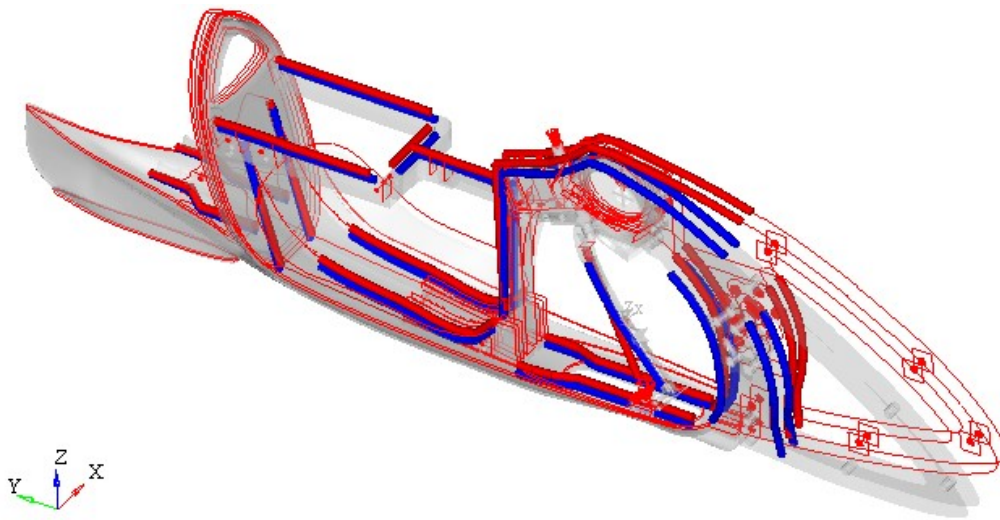


**Figure 2.50**: Plotel elements before (red) and after (blue) load application for Subcase 3.

The result is a complex deformed shape, which is described more in detail in the following images.

In Subcase 3, the X-displacements present positive and negative values but in this case the curvature is higher compared to that in Subcase 2 (Fig. 2.51). The higher curvature that we see in Fig. 2.52 is due to the fact that the torques transmitted from the bottom bracket and from the sprocket-set shaft have opposite sign.
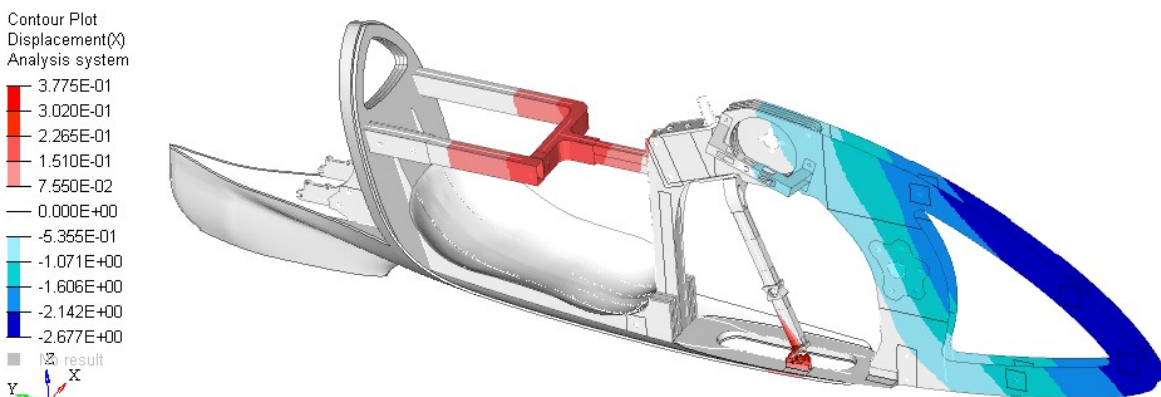


**Figure 2.51**: X-displacements in global system for Subcase 3. Scale in mm.
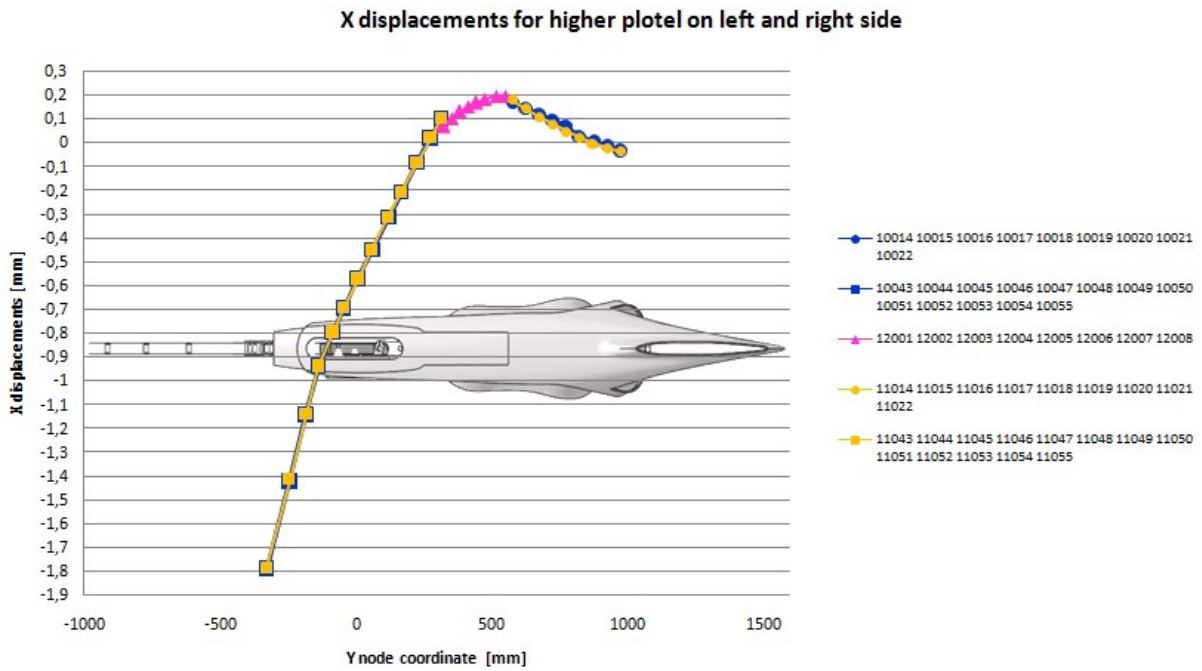
**Figure 2.52**: X-displacements in global system of plotel nodes for Subcase 3.

For Y and Z-displacements we can refer back to the same observations done for Subcase 2, but now we have negative rotations around Z-axis and Y-axis because we load the opposite pedal. Therefore Y-displacements are higher in modulus on the left side and Z-displacements are higher in modulus on the right side.
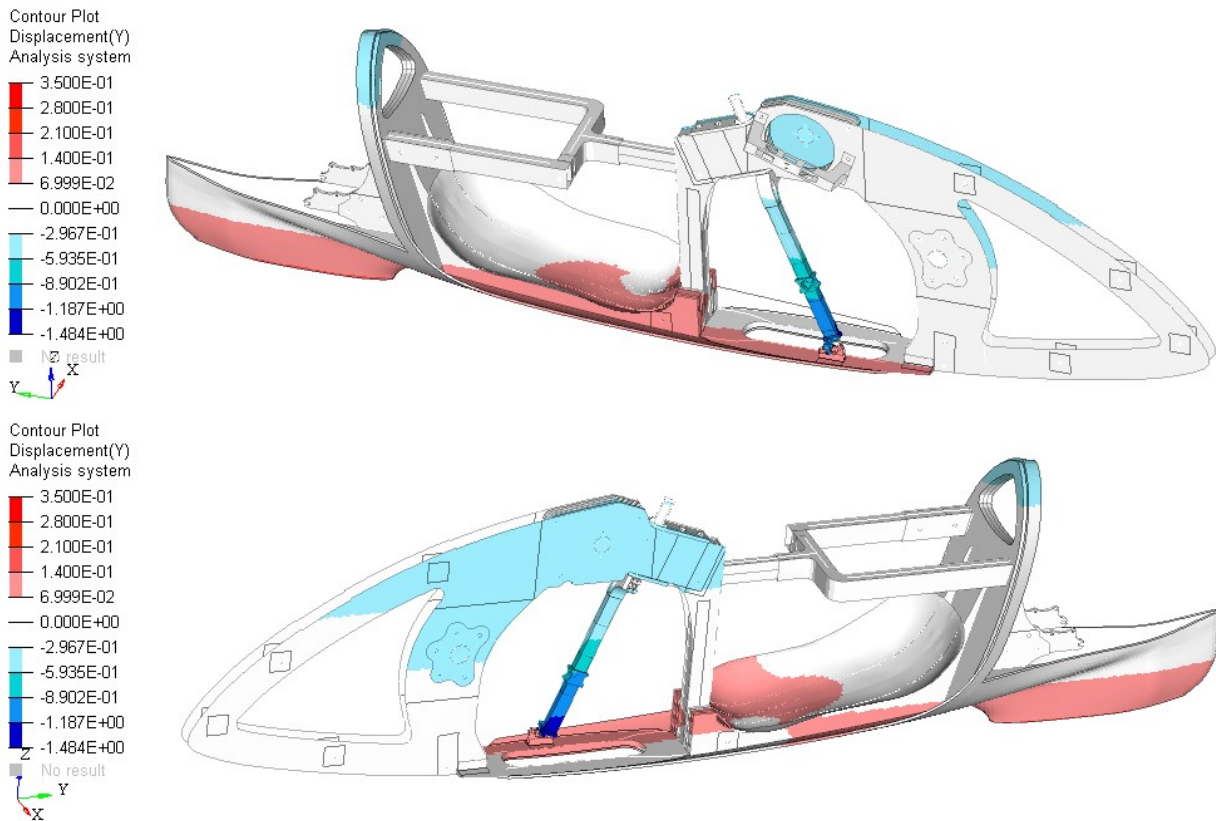


**Figure 2.53**: Y-displacements in global system for Subcase 3. Scale in mm. (above) Right view. (below) Left view.
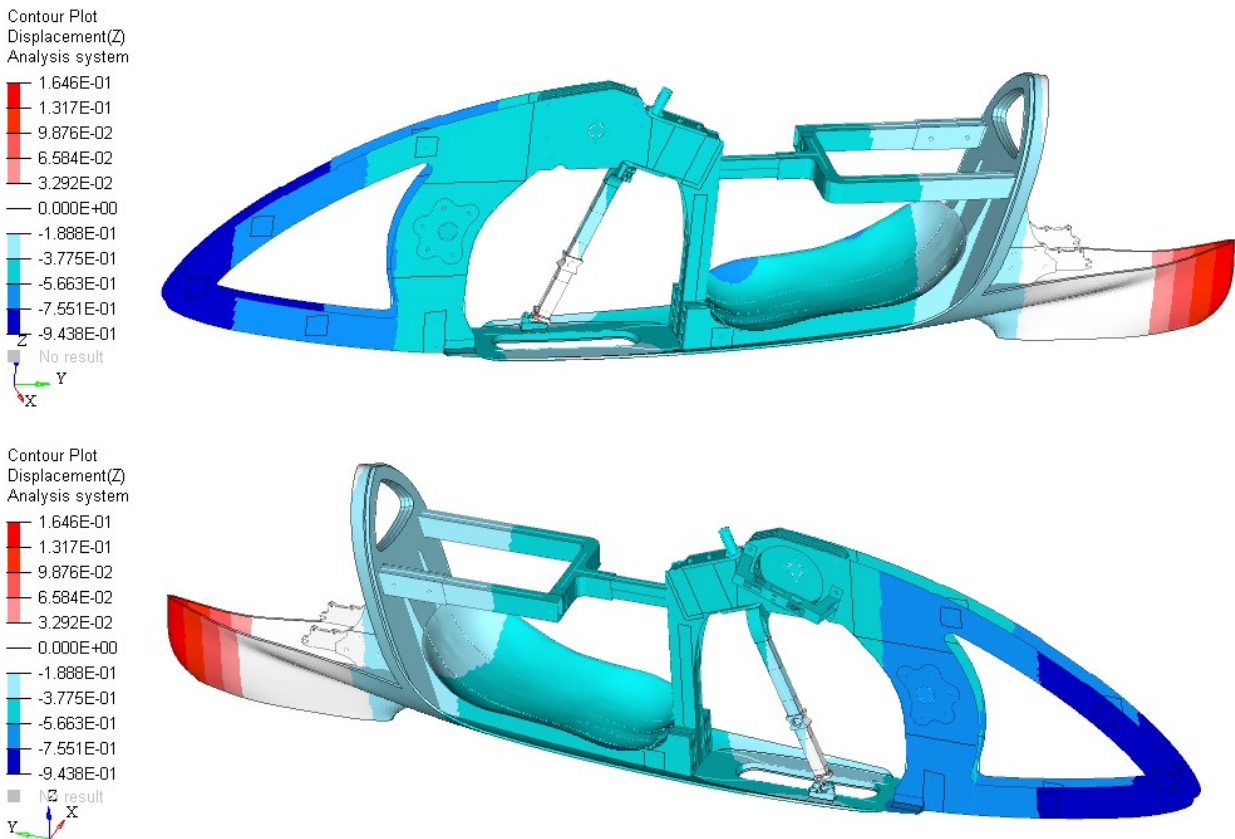
**Figure 2.54**: Z-displacements in global system for Subcase 3. Scale in mm. (above) Right view. (below) Left view.

In the following image we can check that also in Subcase 3 the bearings that guide the fork do not leave the rail. In Fig. 2.55 there is no view amplification factor and the red lines represent the condition of the unloaded frame.
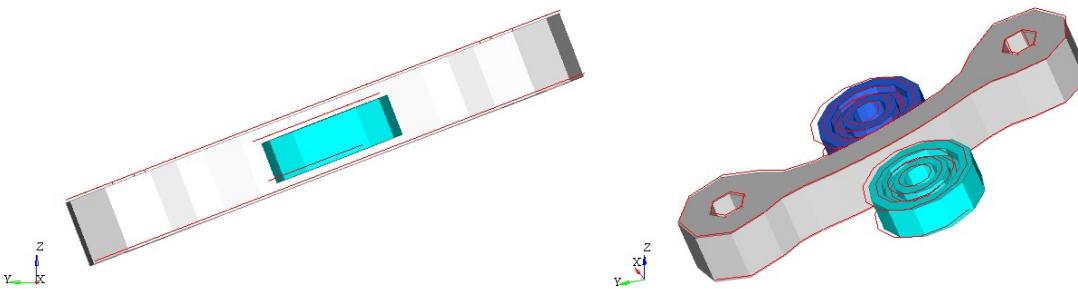


**Figure 2.55**: Guide bearings and rail of the fork during load application for Subcase 3. The red lines are for when unloaded.

*Stiffness and displacement between left pedal and backrest*

As in the previous subcase, we have evaluated the relative displacement between the loaded pedal and the backrest. In this subcase we load the left pedal that has node ID equal to 3, so we have that the relative displacement between Node 3 and Node 10 is:

- -0.011 mm at the end of Subcase 1
- 0.981 mm at the end of Subcase 3.

The total deformation between Node 3 and Node 10 is $d_{3,10}$ = 0.992 mm. Recalling the applied force of F=700 N we have a local stiffness of:

$$K_{3,10} = \frac{F}{d_{3,10}} = 706 \; N/mm$$

As expected, $K_{3,10}$ is lower than $K_{2,10}$, which has been measured in the previous subcase. This is because in Subcase 3 we load the pedal opposite to the first chainring, which causes a higher reaction torque on the bottom-bracket attaching points of the frame.

*Stress, strain and failure index*

The contour plots in Figure 2.56 and 2.57 indicate the maximum stress and strain values present in the laminate. Unlike in Subcase 2, in Subcase 3 it is the left side that is most stressed. Figures 2.58 show the maximum failure indexes of the laminate, and Figures 2.59 show the ply in which these maximum failure indexes are present, by means of the ply ID number. The highest composite failure index is on the frame (ply ID = 20000028) and is equal to 0.029.
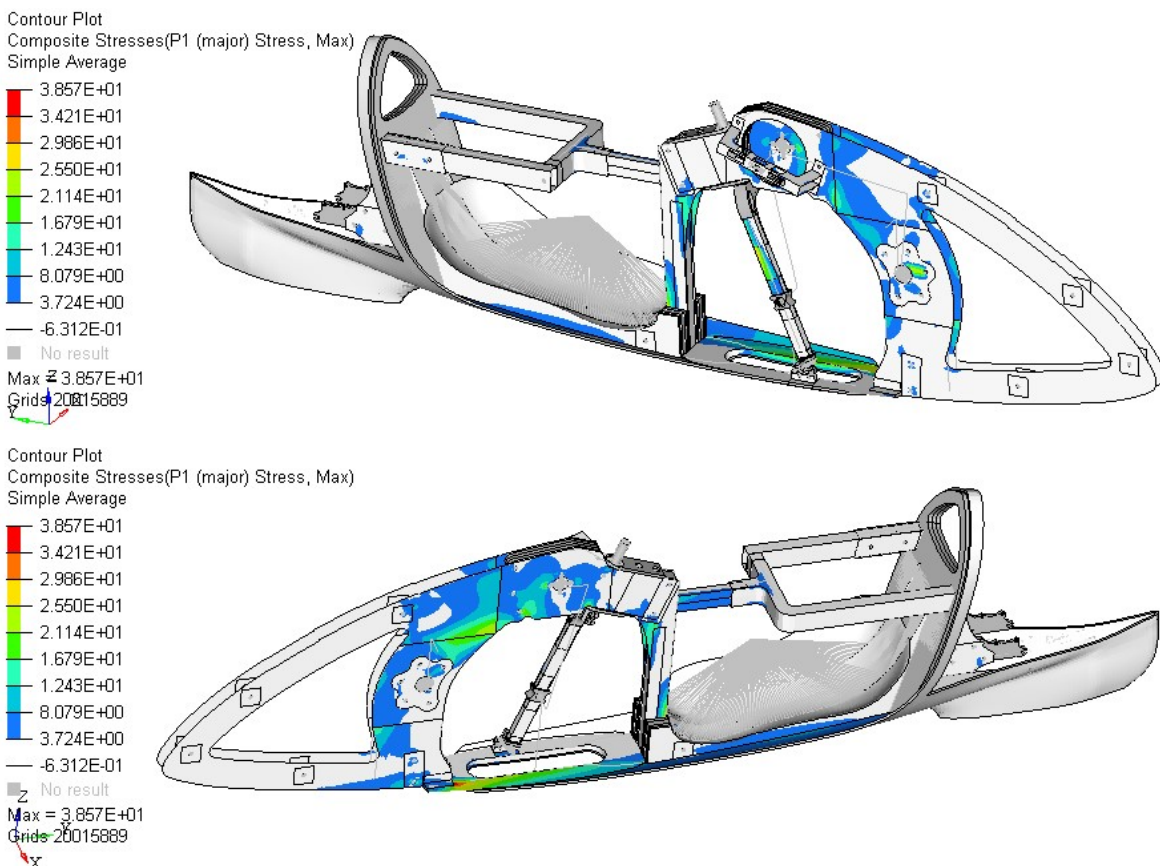


**Figure 2.56**: P1 max stress for Subcase 3. Scale in MPa. (above) Right view, (below) left view.
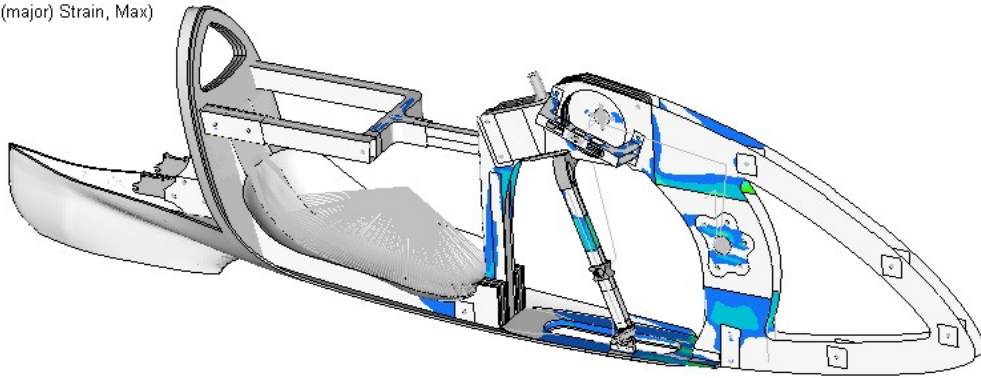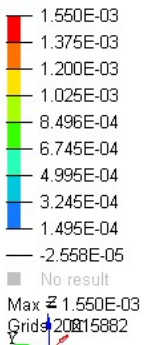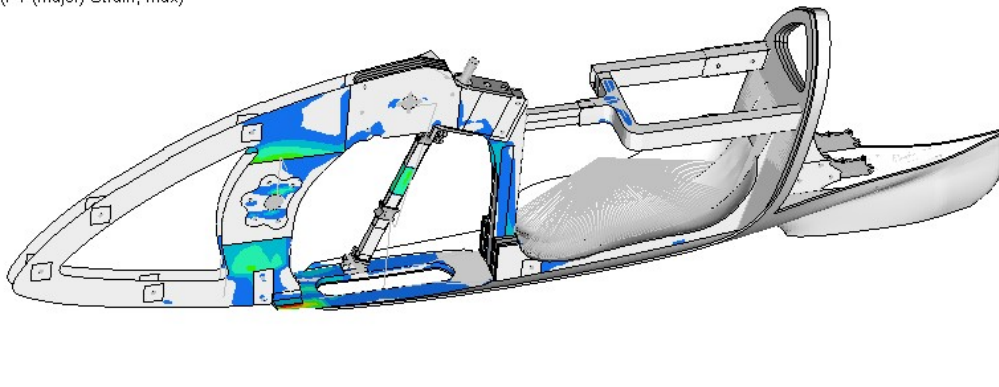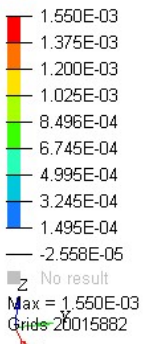
**Figure 2.57**: P1 max strain for Subcase 3. (above) Right view, (below) left view.
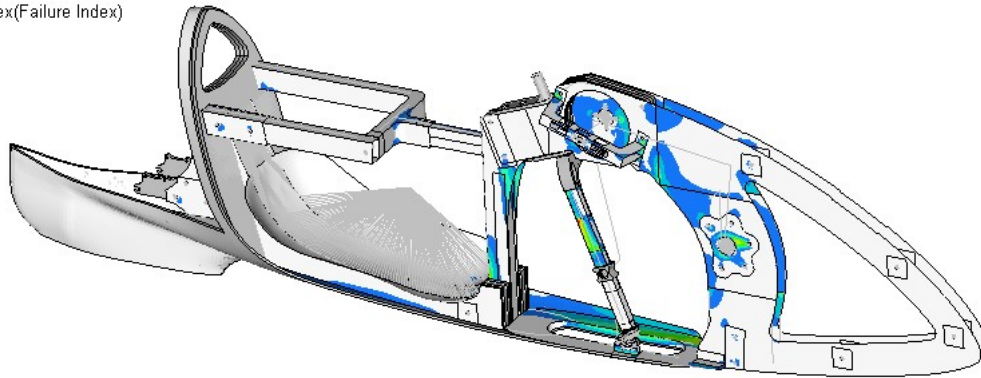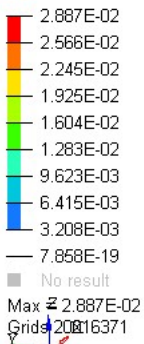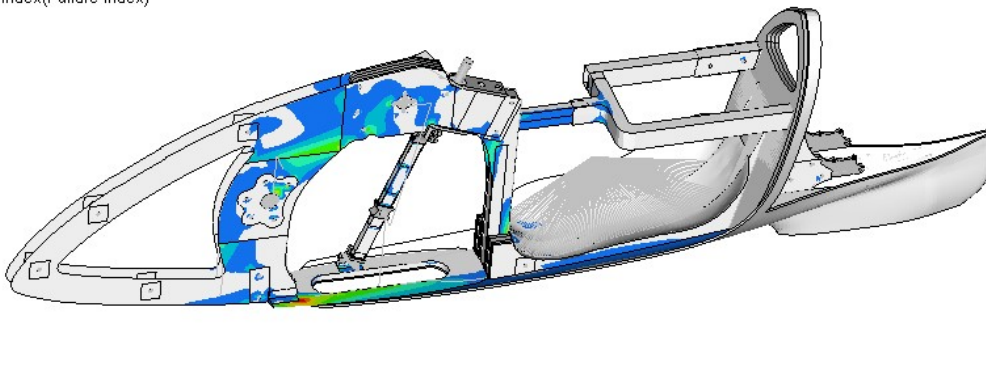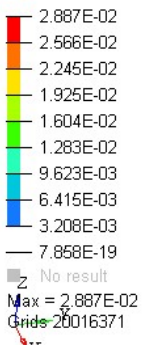


**Figure 2.58**: Maximum composite failure index for Subcase 3. (above) Right view, (below) left view.
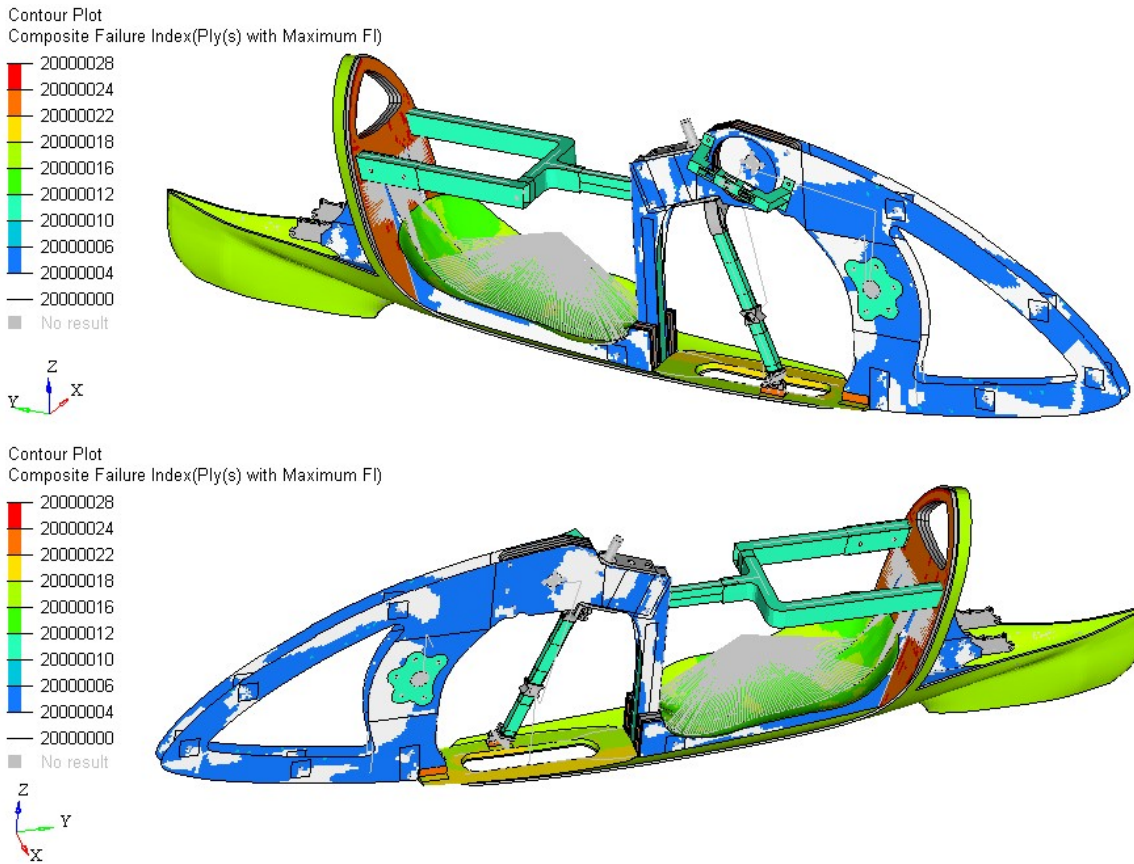
**Figure 2.59**: Ply ID in which there is the maximum failure index for Subcase 3. (above) Right view, (below) left view.

## 2.5 Modal analyses

Modal analyses have been performed with two different models. The first model is composed of the frame and cyclist mass, whereas the second one is composed of the frame, cyclist mass and removable aerodynamic fairing. By introducing the removable fairing, we also want to evaluate the frequency in which there is a relative motion between it and the frame. The relative motion between the frame and the fairing is possible due to the clearance. In the second model, the connections between the frame and the fairing are important.
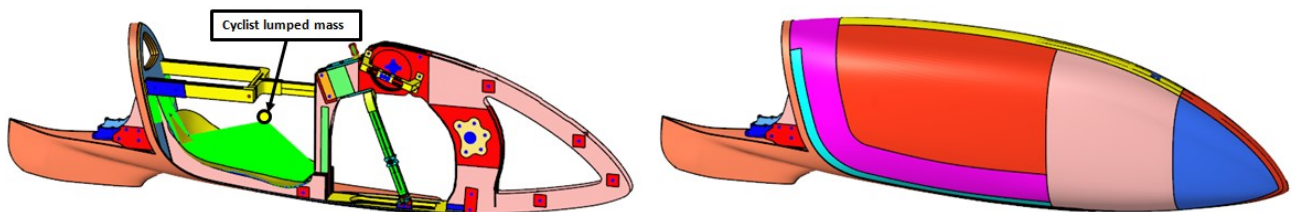


**Figure 2.60**: (left) Model composed of frame and cyclist lumped mass. (right) Model composed of frame, aerodynamic fairing and cyclist lumped mass.

Under operating conditions there are many excitation inputs, and the complete study of the dynamic response of the frame is not the purpose of this paper because that would require different kinds of analyses and a dedicated discussion.

In this part we want to evaluate the natural frequencies and first global modes of the frame. In particular, we want to check that the first torsion mode and the first bending mode do not fall into the range of the pedaling frequency and the rotating frequency of the wheel. It follows a description of the excitation inputs taken into account.

- Cadence or pedaling rate: it is the number of revolutions done by a pedal in a period of time. The maximum cadence recorded by the cyclist Andrea Gallo on the Taurus prototype is about 115 rpm. Therefore, both the right and left pedal forces have a maximum frequency of 1.9 Hz and they are 180° out of phase. The forces on the pedals flex the frame around the global Z-axis. In particular, the force on the right pedal flexes the frame towards the left and the force on left pedal flexes the frame towards the right. It results a bending moment on the frame that changes direction every 180° made by a pedal, so the bending moment changes direction with a frequency that is double the cadence frequency.

- Mass of the rotating parts: the residual imbalance of wheels and sprockets exerts forces on their supports with a frequency equal to the rotational speed. [15, Chapt. 26]. Assuming a max speed of 136.5 km/h of the vehicle and given that the wheels have a diameter of 20'' (the effective diameter $D_{eff}$ is almost 490 mm), the exciting-force frequency from the wheels is almost 24.6 Hz.

$$Circumference\ of\ the\ wheel = \pi \cdot D_{eff} = 1.54\ m$$

$$Vehicle\ speed = 136.5\frac{km}{h} = 37.9\ \frac{m}{sec}$$

$$RPS\ of\ the\ wheel = \frac{Vehicle\ speed}{Circumference} = 24.6$$

The handlebar rotations can also induce vibrations on the frame because the front wheel undergoes greater lateral displacements than the rear wheel [13, Chapt. 8]. The rotation of the fork is necessary to keep the trajectory straight and the bicycle balanced. We assume that the rotations of the fork have a lower frequency than the cadence, so we will not take those into account.

In the following modal analyses a free-free condition has been used, so there are no boundary conditions. For this reason we have seven rigid modes at zero frequency, six of which are frame rigid-body modes and one is the mode in which the fork rotates around its axis. This result also constitutes a check on the validity of the fork kinematics. The input files used for these analyses are reported in Appendix A and the results are presented in the following section.

## 2.5.1 Modal analysis of the model with frame and cyclist mass

The following images show the seven rigid modes for the first model with the frame and the lumped mass of the cyclist. The red lines indicate the non-deformed condition.
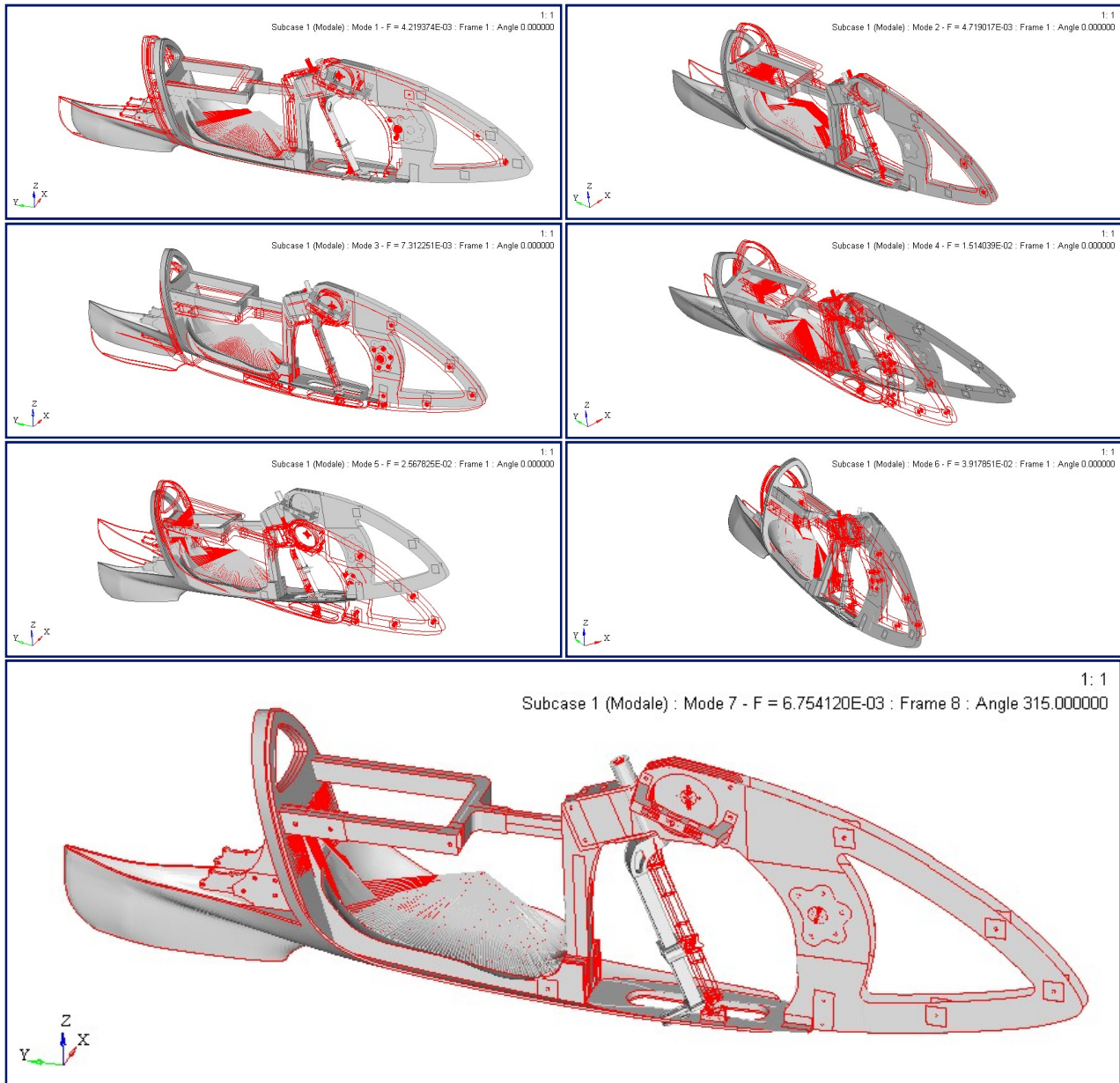


**Figure 2.61**: Modes 1 to 6 are the rigid modes of the frame. Mode 7 is the rigid mode due to the rotation of the fork around its axis.

The first bending mode around Z-axis is at 27.2 Hz (Fig. 2.62).
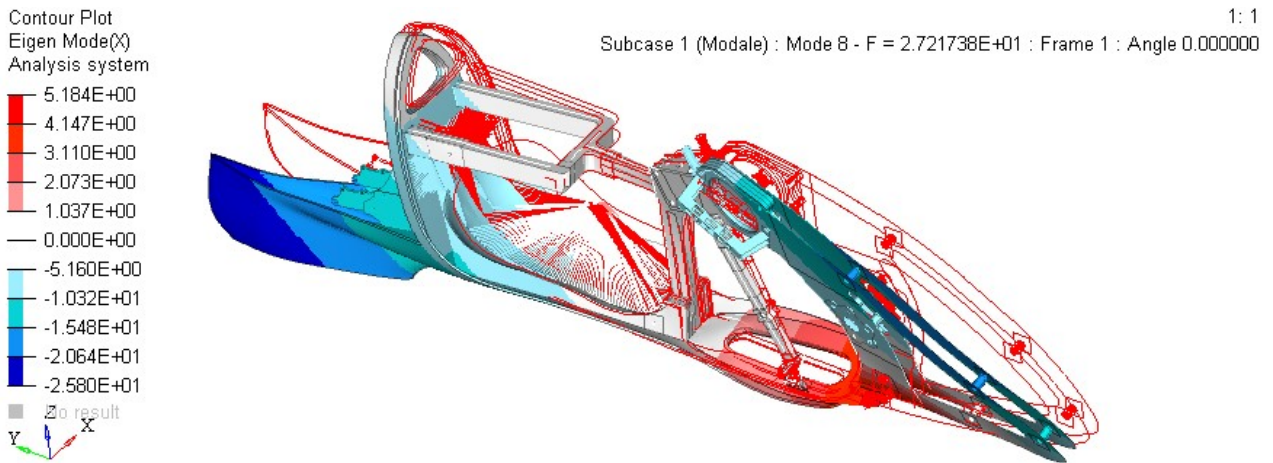


**Figure 2.62**: (Mode 8) First bending mode around Z-axis.

The first torsion mode around Y-axis is at 63.6 Hz (Fig. 2.63).
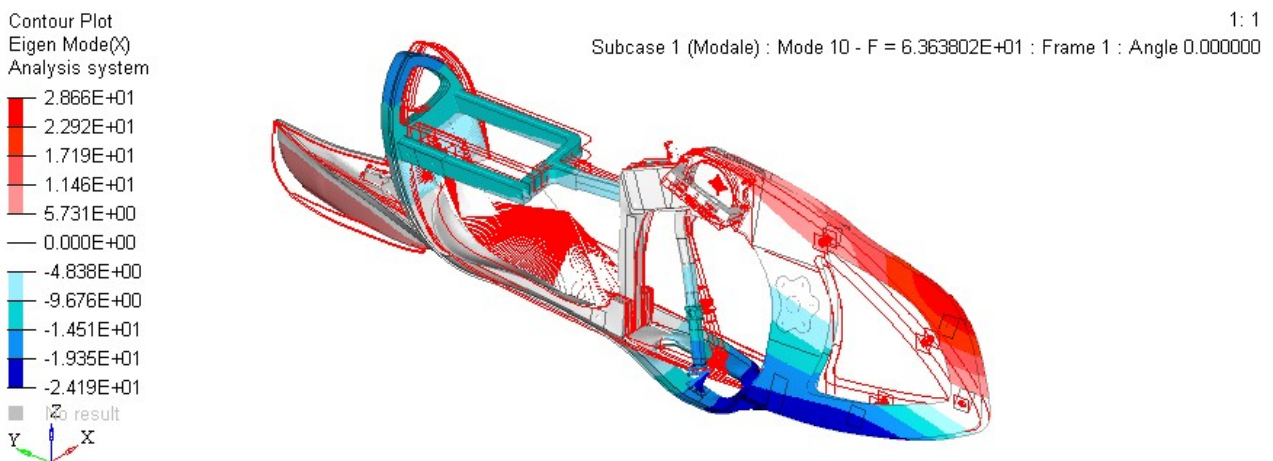


**Figure 2.63**: (Mode 10) First torsion mode around Y-axis

The first bending mode around X-axis is at 66.8 Hz (Fig. 2.64).
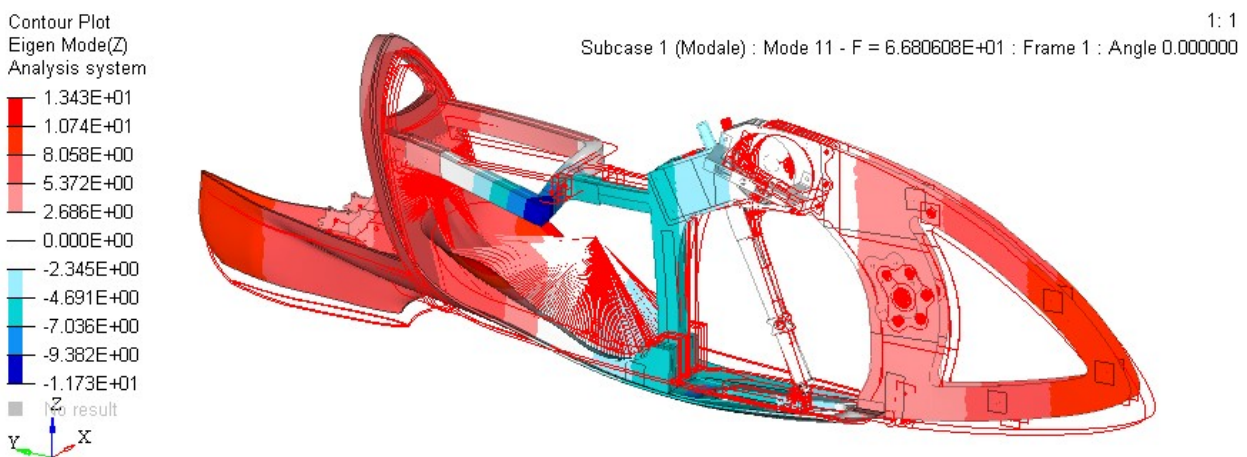


**Figure 2.64**: (Mode 11) First bending mode around X-axis.

The first bending mode is at 27.2 Hz, which is higher than the cadence frequency and than the RPS (round per second) of the wheel. Moreover, without the fairing, the speed of the vehicle is considerably lower than the record speed, so there is no resonance under operating conditions.

## 2.5.2 Modal analysis of the model with frame, cyclist mass and removable aerodynamic fairing

The following images show the seven rigid modes for the second model with the frame, aerodynamic fairing and lumped mass of the cyclist. The red lines indicate the non-deformed condition.
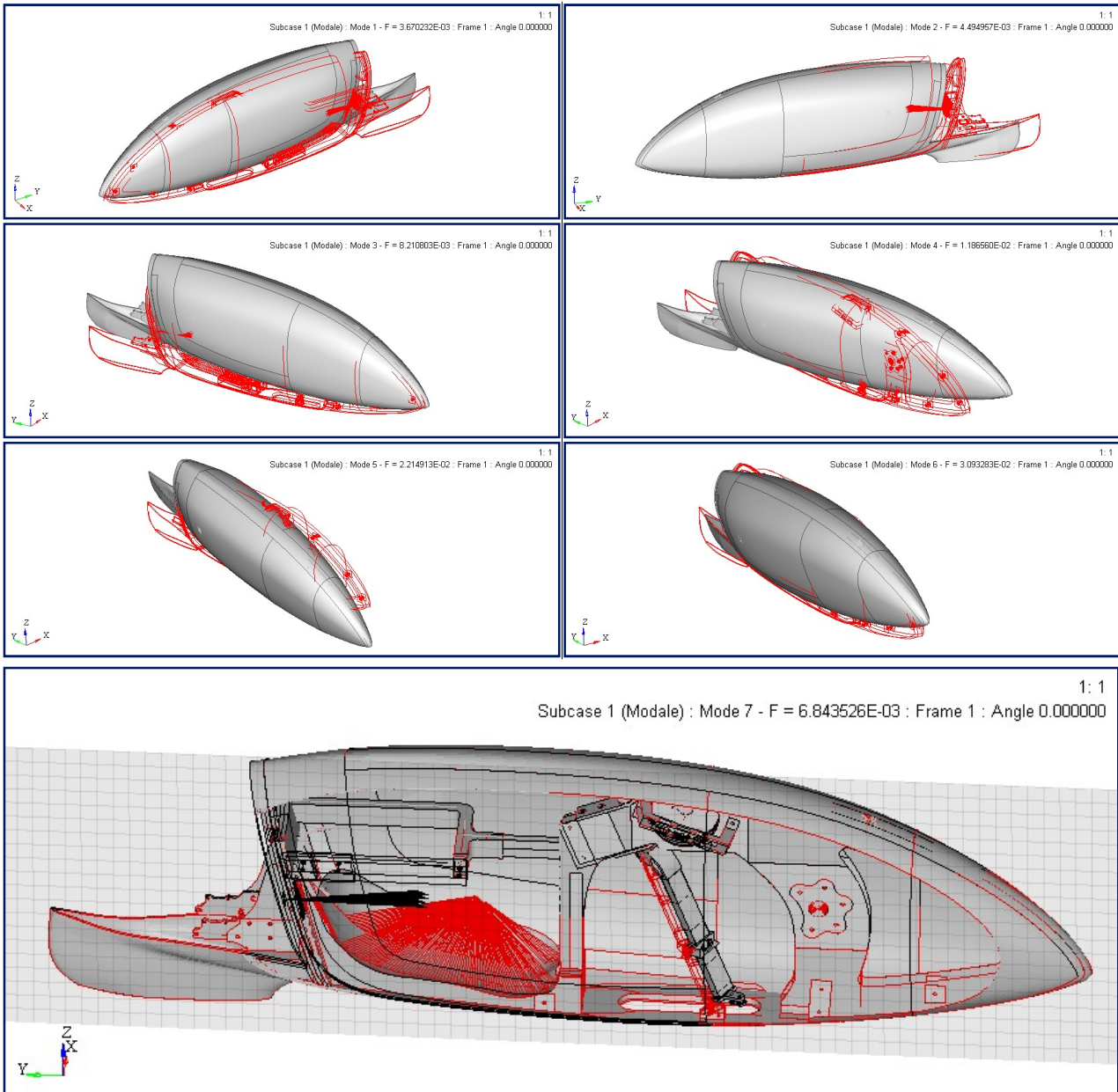


**Figure 2.65**: Modes 1 to 6 are the rigid modes of the frame and of the fairing. Mode 7 is the rigid mode due to the rotation of the fork around its axis (image with section cut to visualize the fork).

The first bending mode around Z-axis is at 40.2 Hz (Fig. 2.66). The aerodynamic fairing adds mass, but to a greater extent it adds stiffness to the structure, so we have an increase of the natural frequencies. We can notice a relative movement between the frame and the fairing in the front part of the vehicle, in which there is clearance. The connections between the fairing and the frame are important in order to limit their reciprocal displacement. If we eliminated the guide block, the first non-rigid mode would be at 24.2 Hz,

which would be very close to the max rotation frequency of the wheels. In particular, in this mode we would have a bending mode around Z-axis with higher reciprocal displacements between the frame and the fairing (Fig. 2.67). To avoid resonance at the maximum speed of the vehicle, a guide block has been introduced.
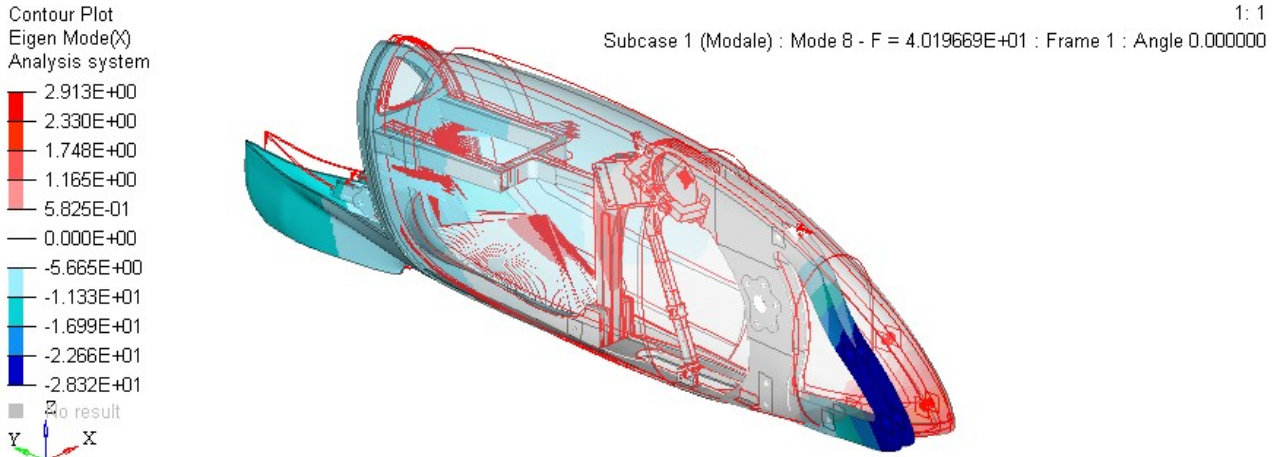


**Figure 2.66**: (Mode 8) First bending mode around Z-axis.
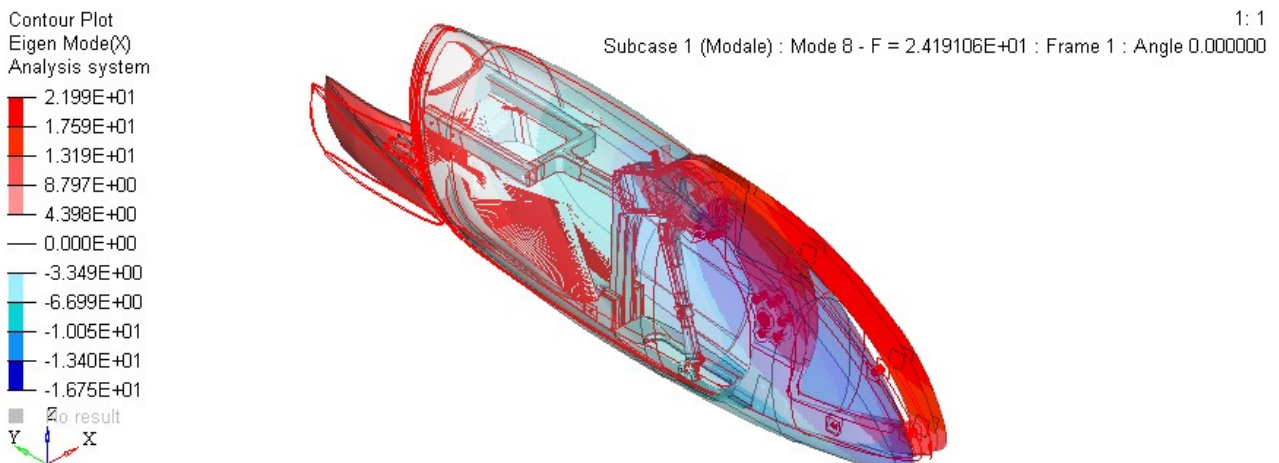


**Figure 2.67**: Additional analysis without the guide block of the fairing. (Mode 8) Bending mode around Z-axis.

The first bending mode around X-axis is at 75.4 Hz (Fig. 2.68).
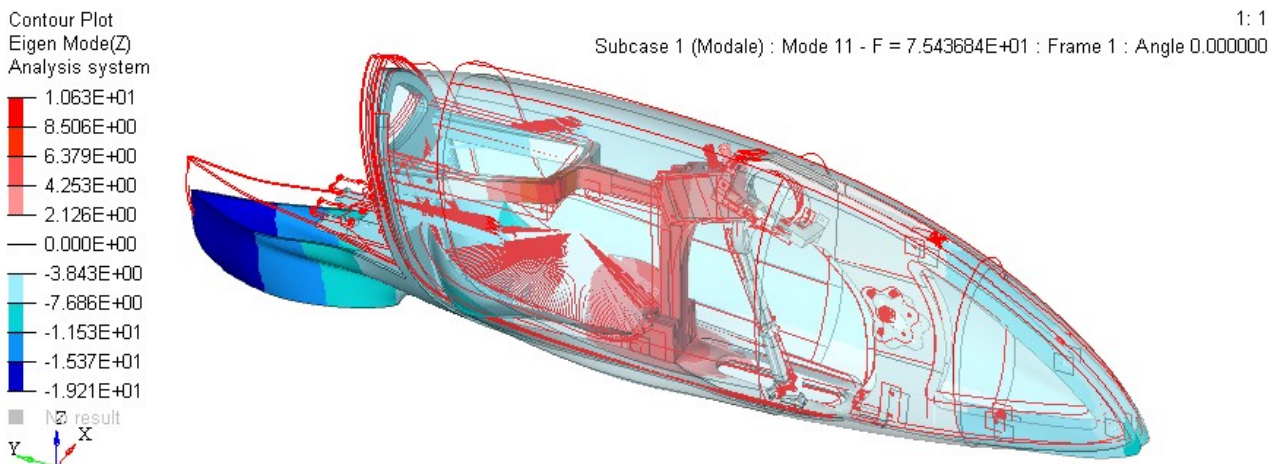


**Figure 2.68**: (Mode 11) First bending mode around X-axis.

The first torsion mode around Y-axis is at 94.1 Hz (Fig. 2.69).
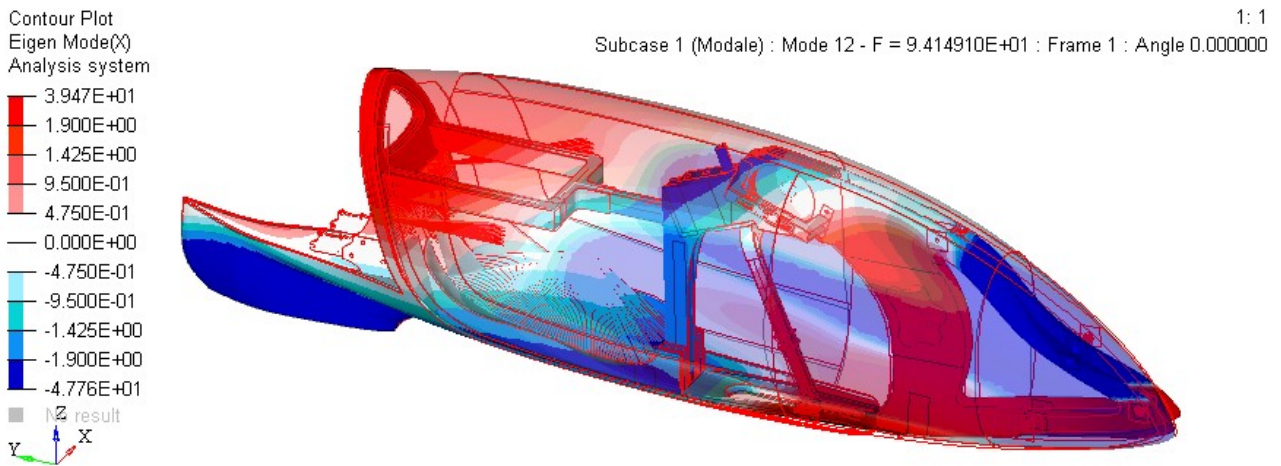


**Figure 2.69**: (Mode 12) First torsion mode around Y-axis.

With the current configuration, the global natural frequencies are higher than the cadence and than the RPS of the wheel, so there is no resonance due to internal excitations.

# 3. DESIGN AND OPTIMIZATION OF THE NEW FRAME PROPOSAL

In this chapter we will proceed with the design of a new frame with the aid of optimization analyses. The design process is divided into several successive stages:

1) Defining the optimal shape of the frame (with the help of the topology optimization analysis);

2) Calculating the ideal thickness distribution (with the help of the free-size optimization analysis);

3) Defining the shapes, orientations and thicknesses of the plies, in agreement with the suppliers available on the market (with the help of the size optimization analysis);

4) Defining the ply stacking sequence (with the help of the shuffle optimization analysis).

The first two phases can be defined as Concept Design while the last two as Design Fine-Tuning [16].

Each phase, in turn, presents: a first part of pre-processing, in which the model for the specific analysis is created; this is followed by the solving part, which is performed by the solver; and finally the post-processing part and re-elaboration of the results. The pre-processing, post-processing and re-processing of the results are done by the designer and are essential to achieve the right results. The optimization analyses, which are implemented within Optistruct, are powerful tools but the use of the software is intended as a calculation tool and does not replace the role of the designer.

The objectives of the new project are to increase the stiffness of the frame and to reduce the mass, compared with the Taurus prototype. These two goals are in conflict with each other, so we can never have a single solution to the problem. Many optimized solutions would be possible where a mass increase would cause an increase in the stiffness, or where a mass decrease would cause a decrease in stiffness. Multi-Objective Optimizations (or Pareto optimizations), in which goals are in conflict with each other, produce multiple solutions and are very expensive in computational terms [17]. This has led to the decision to increase the stiffness as much as possible and to set a target mass of 6 kg. Considering that the frame of the Taurus prototype is 12 kg in weight, the mass of the frame will be halved.

In the next chapter, the new frame will be subjected to the same subcases as the Taurus prototype's in order to allow a final comparison.

## 3.1 Basics of optimization

This section is dedicated to the optimization fundamentals that are useful to set up and to discuss the optimization analyses. *'The basic principle of optimization is to find the best possible solution under given circumstances'* [18]. There are many optimization methods and algorithms, but the DRCO approach defines an optimization problem to its fundamentals, and it is also used to set up an optimization problem in Optistruct. The DRCO approach consists in defining the Design variables, the Responses functions, the Constraint functions and the Objective function [19], which are described as follows [16, Chapt.2].

- **Design variables:** these are the variables that define the design space of the optimization problem. They can be modified by the optimizer during the calculation. The areas of the model excluded from the design space constitute the non-design space, and will not be modified by the software. The kind of design variable defines the type of optimization problem. Examples of the type of optimization problems are: Topology, Topography, Free-size, Shape, Size, Free-Shape, and Composite Shuffle.

- **Response functions:** these can be a value or a function that measures the changing performance of the system. Responses can be subcase dependent or subcase independent.

- **Constraint functions:** these are the upper or lower limit applied on responses that are linked to the design variable.

- **Objective function:** this is the response of the system that we want to maximize or minimize.

The aim of the optimization analysis is to minimize (or maximize) the objective function by changing the design variables and, at the same time, by not violating the constraints. Optistruct solves the optimization problem through the local approximation method, an iterative process that consists of the following steps:

1) **Finite elements analysis**

2) **Convergence test:**

   The optimization ends with a feasible design, if for two consecutive iterations the constraints violations are less than 1% and the objective-function changes are smaller than the objective tolerances.

   The optimization ends with an infeasible design, if for three consecutive iterations the constraints violations are more than 1%, the constraints-violations changes are less than 0.2%, and the objective-function changes are smaller than the objective tolerances.

   If we have neither a feasible nor an infeasible design, the iterations continue.

3) **Response screening:**

   In order to speed-up the computation, the optimization model reduces the amount of variables and stores only the most significant responses.

4) **Design-sensitivity analysis for retained responses:**

   It calculates derivatives of structural responses with respect to the design variables.

5) **Optimization of the approximate problem formulated using the sensitivity information:**

   The optimizer builds an approximate model on which most of the optimization work is done. The optimizer asks to perform an FE analysis only when necessary. The approximate model has been built using the sensitivity analysis, which in turn uses a reduced set of responses. Therefore, we have an approximate solution, which has to be verified by a final analysis.

6) **Back to 1)**

At each iteration, the design variables change within a narrow range to achieve a stable convergence. In particular, the bigger changes are in the first iterations in order to conduct fewer FE analyses. The local-approximation method is more susceptible to finding the local optimum instead of the global optimum. Global-approximation methods and explorative techniques have more probability to find the global optimum. No method can guarantee to reach the global optimum, unless the objective function is convex. For this reason, the solution proposed by the optimization analysis can be influenced by the starting model [19]. This observation highlights the importance of the role of the software user.

## 3.2 Defining the new frame shape

The first step of the new frame design is to define a new shape of the frame. The new geometry has to fit in the new aerodynamic fairing and leave room for the wheels, transmission, fork, and for the cyclist's body and movement. Knowing the available volume for the frame, we have conducted a topology optimization from which we have extracted a first frame shape. The topology optimization produced a raw geometry that has been reshaped in order to satisfy manufactory constraints.

### 3.2.1 Topology optimization fundamentals

Topology optimizations have the aim of optimizing the shape of a structure that is defined within the design space, according to the imposed constraints and objectives [16].

Optistruct solves topological optimizations using the SIMP method (Solid Isotropic Material with Penalization), which consists of using the density method together with a penalization technique. The problem is addressed by defining for each element an equivalent density, which is the design variable. The elastic modulus of the element's material will be directly proportional to its equivalent density. If the equivalent density is equal to 1 it means that the element has 100% density, while if the equivalent density is equal to 0 it means that the element is eliminated, i.e. a vacuum is created. In fact, obtaining equivalent densities of only 0s and 1s is computationally very expensive, so the solver will create equivalent densities in between 0 and 1. Equivalent densities in between 0 and 1 make no sense in physical terms, and it will be a task for the designer to interpret and re-analyse the obtained structure.

A penalization technique is used to penalize the creation of elements with intermediate equivalent density between 0 and 1. The penalization technique used is the 'power law representation of elasticity properties', which is defined as follows:

$$\underline{K}(\rho) = \rho^p \cdot K \tag{3.1}$$

Where $\underline{K}$ is the penalized stiffness matrix of an element,

K is the real stiffness matrix of an element,

ρ is the equivalent density of an element,

and p is the penalization factor, which is always greater than 1 [17].

### 3.2.2 Model creation for the topology optimization

The design variable of a topology optimization is the equivalent density of the finite elements. The topology analysis cannot create new elements. Therefore, if we want to evaluate all the possible frame shapes, we have to generate a mesh for the whole available volume. The available volume for the frame has been obtained using a Boolean subtraction. Starting from the total volume of the new aerodynamic fairing (Fig. 3.1), we have subtracted the volume of the wheels, transmission, fork, and that for the cyclist's body and movement (Fig. 3.2).
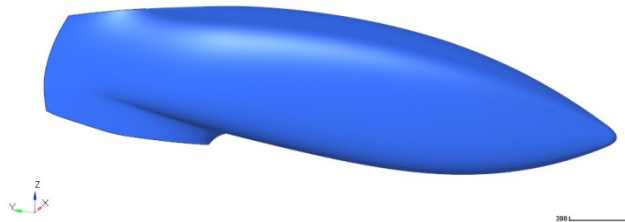


**Figure 3.1**: Volume of the new aerodynamic fairing
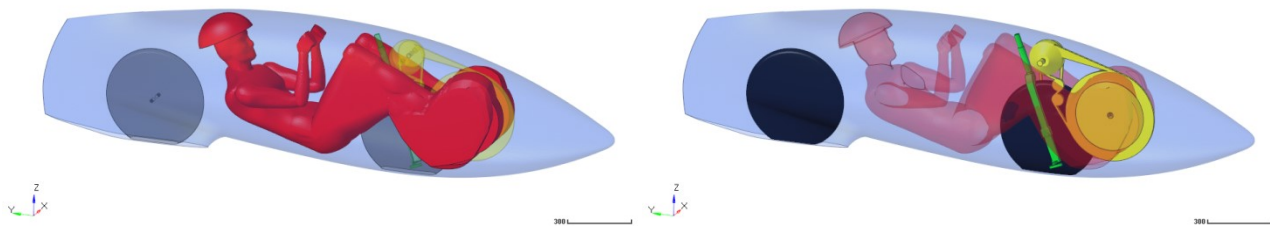


**Figure 3.2**: (Left) Volume needed for the cyclist' body and movement in red. (Right) Volume needed for the wheels in black, for the fork in green and for the transmission in yellow. The volume necessary for the movements of the sprocket set and of the chain has also been considered.

The resulting volume (pink in Fig. 3.3) has been discretized through tetra elements, which create the design space of the topology analysis. During pedaling, there is a small clearance (<2 mm) between the feet and the fairing. In those areas we can only have degenerate tetra elements, unless we reduce drastically the mesh size. Those few elements are not relevant for the structure, so they have been deleted to satisfy the quality of the mesh (*A* in Fig. 3.4).
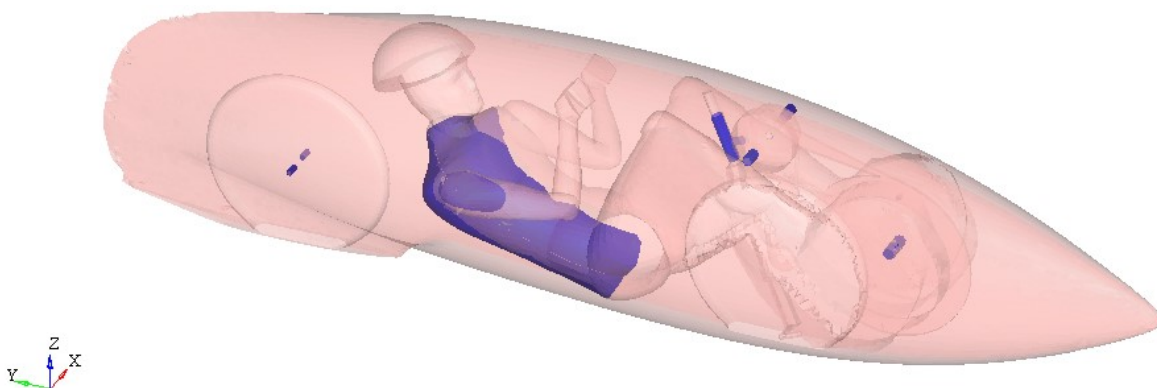


**Figure 3.3**: Design space (pink) and the non-design space (blue) of the topology optimization.
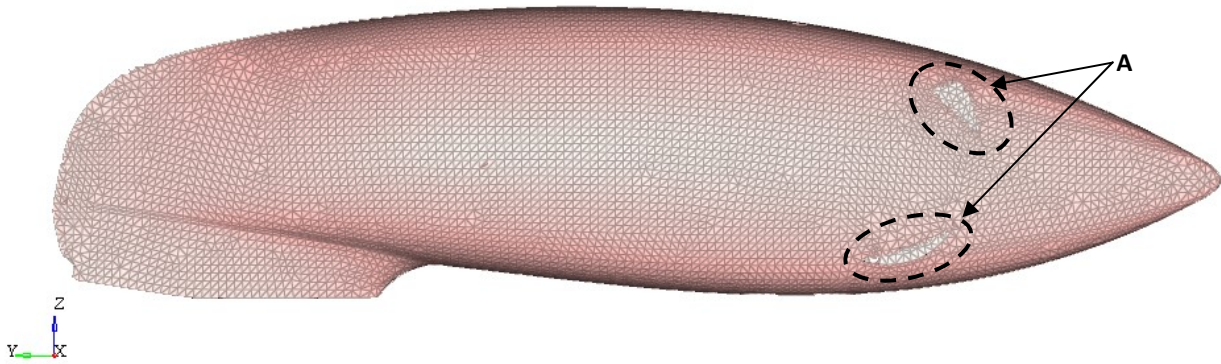
**Figure 3.4**: Tetra elements that make the design space for the topology optimization. *A* indicates the holes needed to avoid degenerate tetra elements.

The material assigned to the design space is homogeneous and has the same density of the carbon-fibre composite (with carbon-fibre volume fraction equal to 0.4) and the Young's modulus of a cross-ply laminate at 0°. In Optistruct, It is possible to define the anisotropic material for solid elements through the card MAT9 [7], but at this phase of design concept we do not know the shape of the frame and it is better not to define arbitrary directions with a higher Young's modulus. The non-design spaces are the head tube, the bottom bracket tube, the transmission supports, the rear wheel supports, the seat, and the fork (blue in Fig. 3.3). The transmission supports have been modified to assemble the new transmission, as described in the next section.

### 3.2.3 New transmission design

The Taurus transmission has been modified to delete the moment reaction around the fork axis, which occurs on the fork during pedaling. The transmission has an added sprocket that makes the chain parallel to the fork axis (Fig. 3.5.a). In this way, the force transmitted from the chain does not have components on the XY-plane of the fork local system, and cannot generate a moment around the fork axis (Fig. 3.5.b). To allow the alignment of the chain with different sizes of front-wheel sprocket, or with forks that have a different fork rake or offset, the housing of the added sprocket has been thought as an oval slot in which to insert a dedicated and interchangeable support (Fig. 3.5.a and Fig. 3.6.a). A similar solution is adopted in racing motorcycles to allow swingarm adjustments (*A* in Fig. 3.6.b) [20].

Other solutions are possible: we could think of mounting the added sprocket onto the end of an arm that can be locked in different positions, or onto a rail with an adjustment screw, as in some bicycles with sliding dropouts (Fig. 3.7.a) [21], or as in the motorcycle swingarm (*B* in Fig. 3.6.b). Alternatively, we could design a simpler and less flexible solution, with the added sprocket mounted onto a fixed axis and having the same size as the final sprocket, and a fork with a fixed offset (Fig. 3.7.b).

(a)



(b)
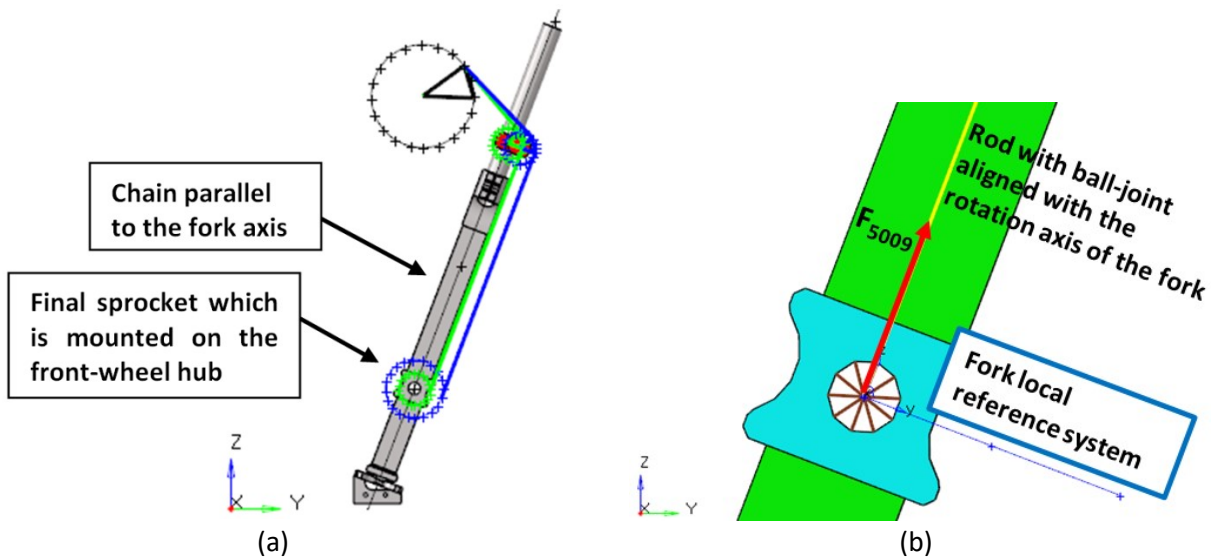
**Figure 3.5**: (a) Transmission update to delete the steering moment due to pedaling. In blue and green are two configurations of the transmission, with different sizes of the final sprocket. The chain is parallel to the fork axis in both configurations due to the dedicated support of the added sprocket. (b) FE model of the new substitute transmission.



(a)



(b)
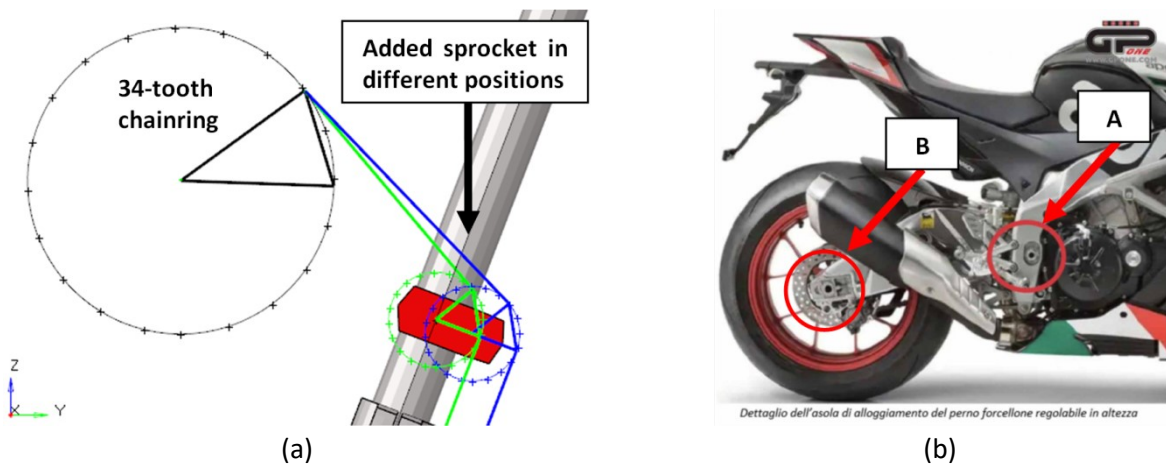
**Figure 3.6**: (a) Zoom of Figure 3.5.a on the added sprocket and its support of the new transmission. (b) *A* indicates the oval slot with its interchangeable support of a motorcycle swingarm. *B* indicates the rail with its adjustment screw [20].



(a)



(b)
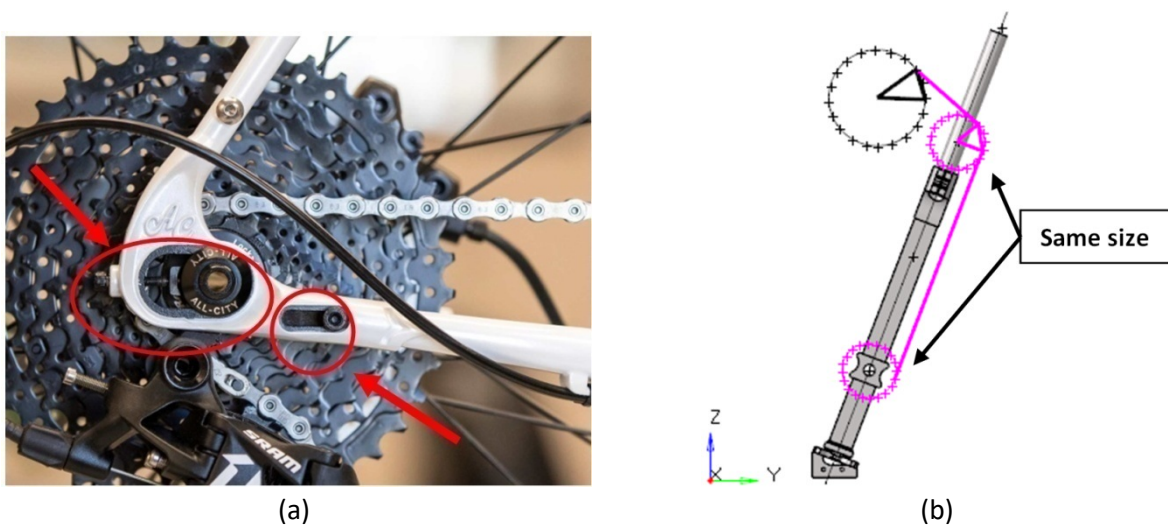
**Figure 3.7**: (a) Sliding dropouts of a bicycle [21]. (b) Solution with the added sprocket mounted onto a fixed axis and having the same size as the final sprocket, and a fork with a fixed offset.

### 3.2.4 Topology optimization

*Pre-Processing*

The conducted topology optimization has the objective of minimizing the weighted compliance computed in three different subcases, and has a maximum total-mass constraint of 6 kg. The three subcases mentioned before are equal to those used in Chapter 2 for the Taurus prototype. The input file used to run the analysis is in Appendix B and recalls the model described in Section 3.2.2 and the transmission described in the previous section. In the following part there are the details about the DRCO used in the topology optimization:

- Design variable: this is the equivalent density of each element belonging to the design space. It is defined trough the card DTPL. It is possible to introduce many manufacturing constraints that are useful for casting processes, for extrusion processes or to introduce specified pattern geometries [22]. Forces transmitted from the bottom bracket to the frame have different magnitude during the right and the left pedaling. For this reason, we expect a frame with a non-symmetrical geometry and we want to evaluate this aspect by not imposing a geometry pattern. Instead, we have imposed a constraint on the member size. The member-size constraint (MEMBSIZ option) acts on the penalization technique and allows limiting the upper and the lower thickness of the structure (respectively MAXDIM and MINDIM value). The member-size constraint has to be compatible with the mesh size, even if in Optistruct it works as qualitative control more than quantity control [22]. We impose a MINDIM equal to 50 mm so as to avoid too many branches and a complex shape. MAXDIM was not necessary because of the limited available space.
- Mass response: this computes the total mass of the model.
- Weighted compliance response: since we can have only one response function to minimize, and due to the fact that we want to consider more compliance values (one per each subcase), the weighted compliance has been used. The weighted compliance $C_w$ is the sum of more compliances, each multiplied by a scale factor [16, Chapt.1]. The compliance computed in Subcase 2 and Subcase 3 is multiplied by a scale factor equal to 1, whereas the compliance computed in Subcase 1 is multiplied by a scale factor equal to 0.5.

$$C_w = \sum w_i \cdot C_i \tag{3.2}$$

The compliance is the inverse of the stiffness. The definition of the compliance is *'measure of the ability of a body or structure to exhibit a deformation due to the action of external forces'* [23]. The deformation of a structure depends on the load and constraint conditions, as well as on the geometry and the materials. Therefore, we have different compliance values for different subcases even in the same structure. If we consider a single degree of freedom (SDOF) spring, the compliance can be defined as the displacement divided by the force along the force direction (units

mm/N). In more complex structures, we have more local deformations, and the choice of the reading point and the choice of the reference system can lead to different values.

In Optistruct *'The compliance is the strain energy of the structure and can be considered a reciprocal measure for the stiffness of the structure'* [16, Chapt. 1, Par. 1.2]. This results as a different definition of the compliance, but due to the fact that the forces are constant, the compliance is proportional to the inverse of the stiffness (Eq. 3.3). For this reason, in Figure 3.12 we have joule instead of mm/N.

$$C = \frac{1}{2} \cdot u \cdot f = \frac{1}{2} \cdot \frac{f^2}{K} \propto const \cdot \frac{1}{K} \tag{3.3}$$

$$\text{where } f = K \cdot u$$

$$C = \frac{1}{2} \cdot K \cdot u^2 = \frac{1}{2} \int_0^V (\varepsilon \cdot \sigma) dv \tag{3.4}$$

Where $C$ is the compliance, $f$ is the force, $u$ is the displacement due to deformation, $K$ is the stiffness, $\varepsilon$ is the strain, $\sigma$ the stress, and $V$ is the volume.

During the optimization, the forces are constant while the optimizer changes the shape of the structure in order to increase the stiffness ($K$) therefore reducing the compliance ($C$).

- Constraint function: it is possible to impose an upper and a lower limit to a chosen response, but in this case we have imposed only an upper limit of 6 kg on the mass response function.

- Objective function: this is to minimize the weighted-compliance response function, in order to maximize the stiffness of the frame.

The response functions have been defined through the card DRESP1, and the constraint function through the card DCONSTR [7].

*Post-Processing*

At the end of the topology optimization analysis, we have a new density distribution of the elements belonging to the design space (Fig. 3.8). As already mentioned in Section 3.2.1, the Young's modulus is proportional to the equivalent density, and the intermediate equivalent density does not have physical correspondence. To visualize the new shape, we have deleted the elements with lower equivalent densities (Fig. 3.9). After that, we have used the new outer surface to generate a geometry file (*.step) that will be useful in the next step (Fig. 3.10).
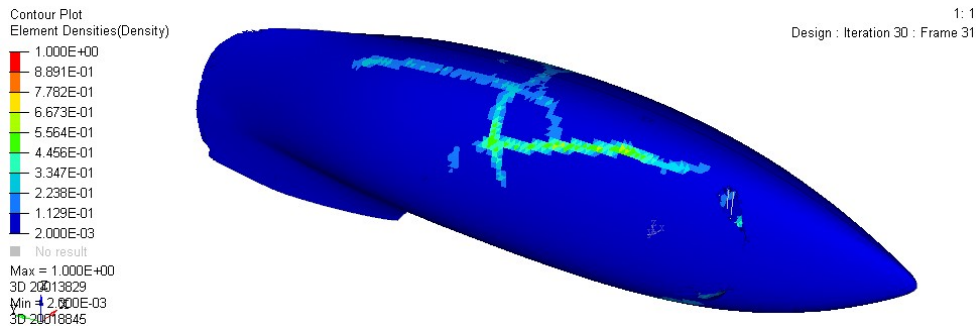
**Figure 3.8**: Equivalent density distribution at the end of the topology optimization.
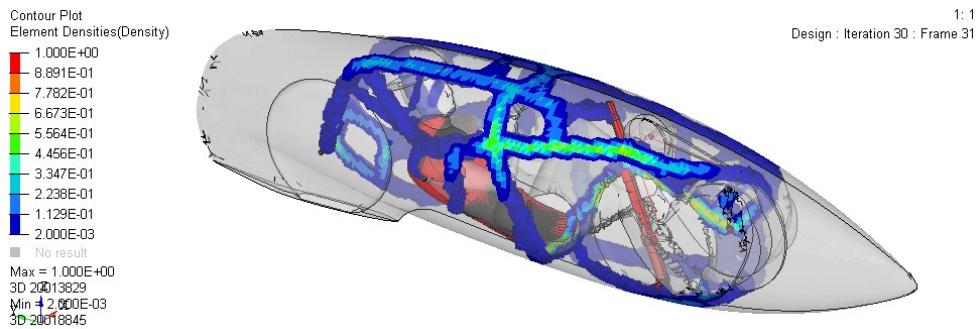


**Figure 3.9**: Equivalent density distribution at the end of the topology optimization (contour plot obtained hiding the less dense elements).
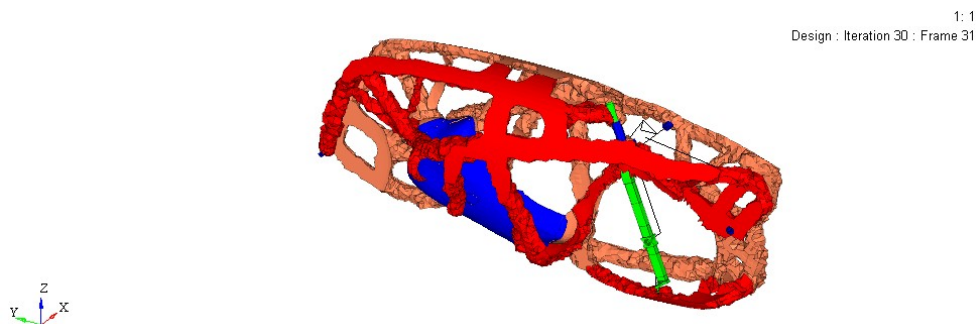


**Figure 3.10**: Surfaces obtained deleting the less dense elements.

The topology optimization finished with a feasible design, so the constraint has been satisfied. In particular, the optimization reached the maximum iteration number, which had been set equal to 31 (through the option DESMAX in card DOPTPRM). The major changes are achieved in the first iterations and, given the purpose of this phase, we have restricted the maximum iteration number to save computation time. The following pictures show the trend of the constraint function (Fig. 3.11) and the objective function (Fig. 3.12).
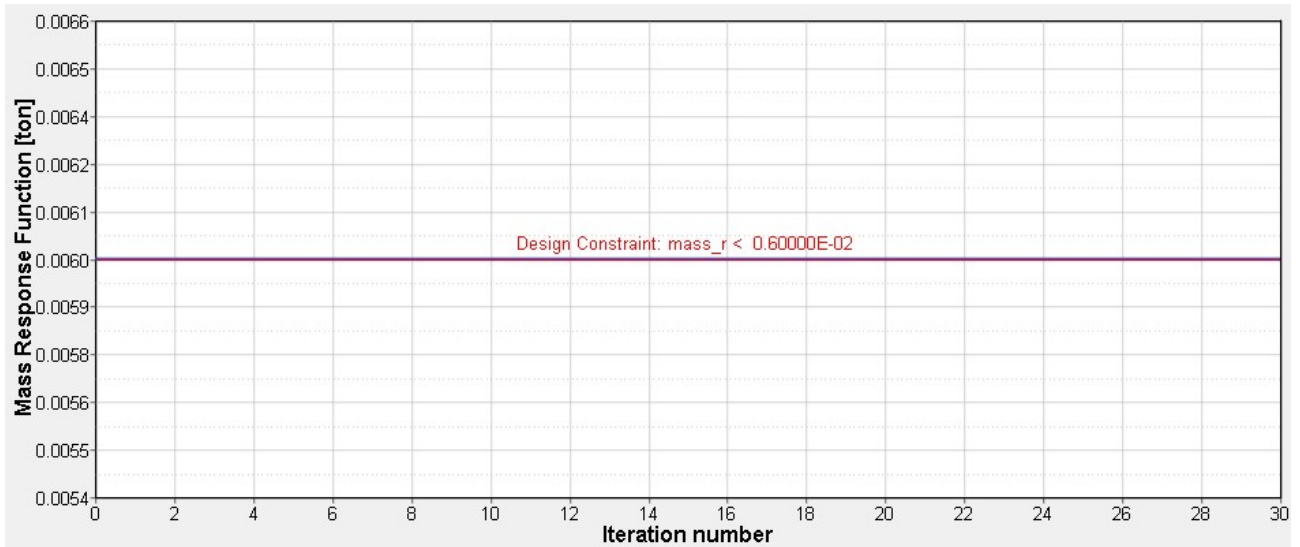
**Figure 3.11**: Mass response function, which is the constraint function of the current topology optimization.
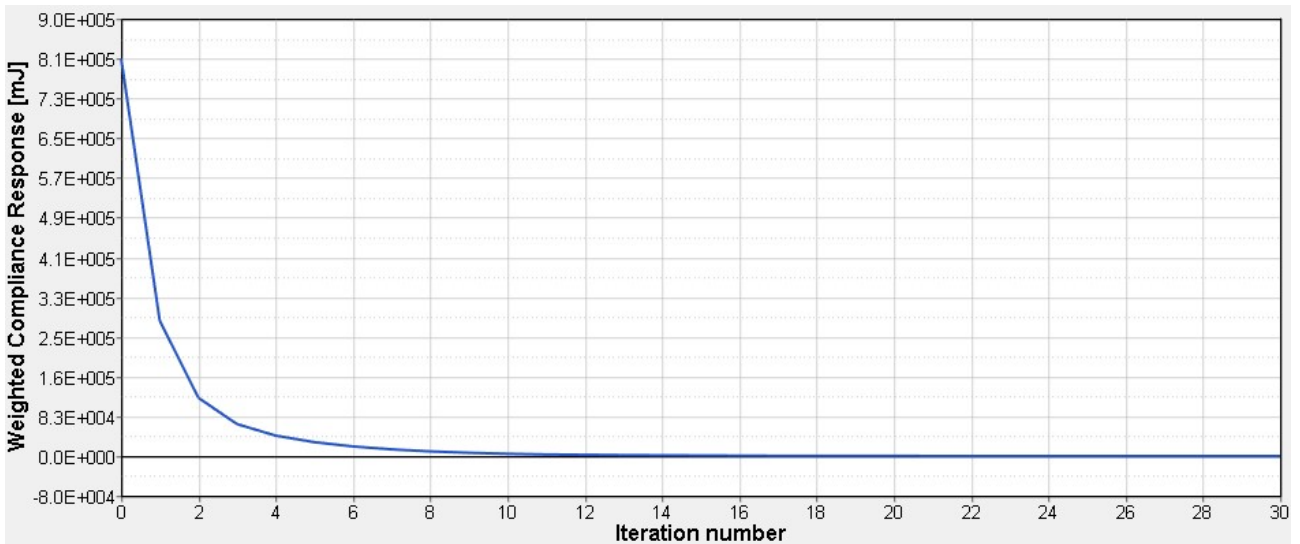


**Figure 3.12**: Weighted-compliance function, which is the objective function of the current topology optimization.

In Optistruct, the iteration number zero is the first iteration. As a matter of fact, the total mass of the starting model was equal to 43 kg and at Iteration Zero it was already equal to 6 kg (Fig. 3.11). The objective to minimize the weighted compliance has been satisfied because it decreases during the optimization iterations (Fig. 3.12).

In the following part there are going to be some observations about the geometry obtained after deleting the elements with the lower equivalent densities (Fig. 3.10). The result of a topology analysis strongly depends on the definition of the loadcases, which in this case are equal to those used for the Taurus prototype.

Summarizing the main stiffness requirements, the new geometry should be optimized to limit:

- downward bending;
- bending leftward and rightward;

69

- the rotation of the bottom bracket around Z-axis.

These main requirements have been satisfied by the optimizer, as explained in the following points:

- The triangulation between the rear dropouts and the headset resists to the downward bending (Fig. 3.13.a). In particular, the optimizer has generated additional beams in the higher part of the frame (*A* in Fig. 3.13.a).

- The presence of two main lateral tubes, which are positioned in the most lateral points inside the fairing, limit the bending leftward and rightward of the frame during pedaling. These tubes extend from the backrest to the bottom bracket because it is in those points that the forces are applied (*F* in Fig. 3.14.a).

- The bottom-bracket area has many attaching points that limit its deformations. In the upper part, it is connected with the main lateral tubes and to the central tube (*H* in Fig. 3.13.a). The central tube houses the headset. In the lower part, the bottom-bracket area is connected with two lateral tubes (*D* in Fig. 3.13.a). The latter tubes are connected to the seat, and one of them houses the fork rail.

To limit specific deformations more effectively, the optimizer has acted upon the areas above, which have a higher impact on them. However, all the beams that compose the frame work together during pedaling, and each zone influences the adjacent one and the global behavior.

### 3.2.5 Reshape

The geometry that was extracted during the post-processing phase has rough surfaces, and reproducing it would be complicated. Therefore, we need to reshape the geometry of the frame in order to make it feasible and with smooth surfaces. The reshaping has been done manually and, although the main features have been kept, some beams have been deleted and others have been added, based on other aspects that the topology optimization could not take into account. In fact, the geometry that has been produced by the topology analysis is based only on the static subcases.



(a)                                                                   (b)
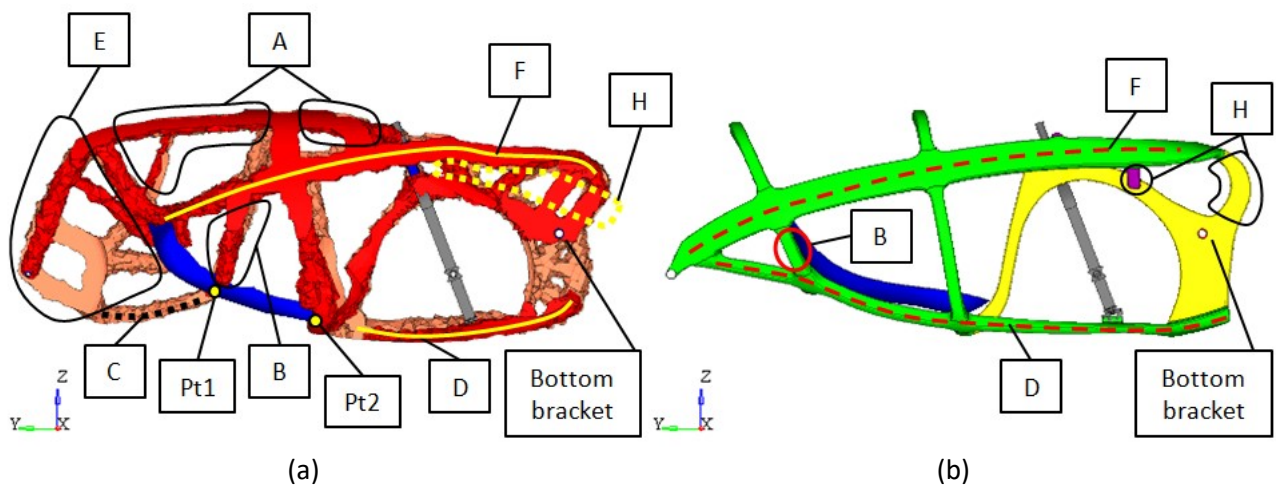
**Figure 3.13**: (a) Left view of the surfaces extracted from the topology optimization. (b) Left view of the surfaces after manual reshaping.
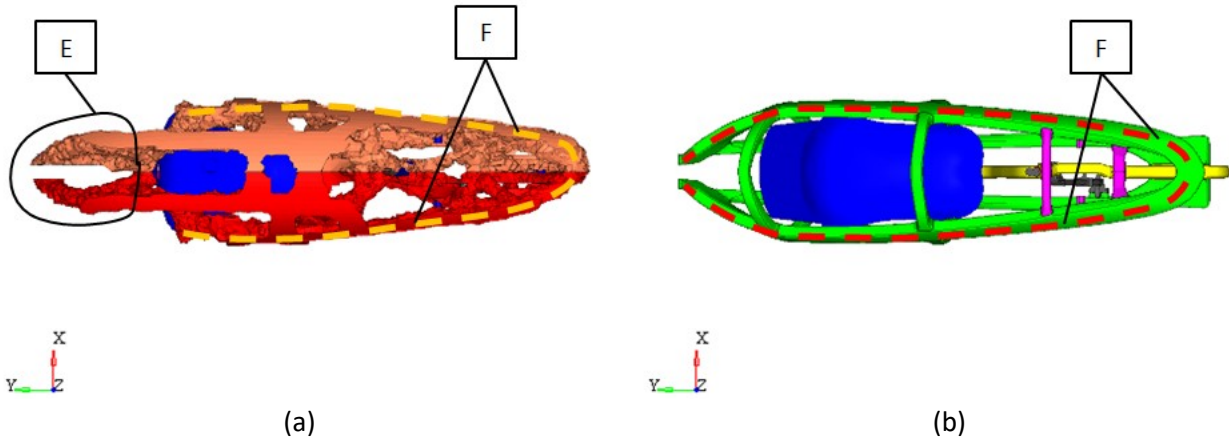
**Figure 3.14**: (a) Top view of the surfaces extracted from the topology optimization. (b) Top view of the surfaces after manual reshaping.
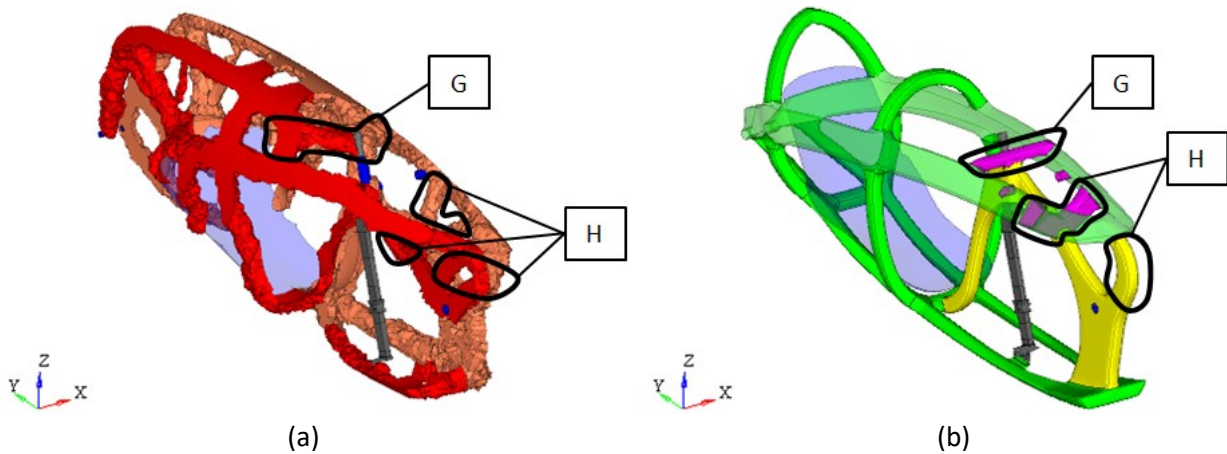


**Figure 3.15**: (a) View of the surfaces extracted from the topology optimization. (b) View of the surfaces after manual reshaping.

Figures 3.13, 3.14 and 3.15 show the geometry of the frame before and after the reshaping process. The following points explain which main changes have been made in the reshaping process:

- Beams indicated with letter *A* in Figure 3.13.a have been deleted to simplify the entrance end the exit of the cyclist. For the same reason, Beams *B* have been moved backward (Fig. 3.13). Beams *B* and *C* (Fig 3.13.a) pass trough point *Pt1* to sustain the weight force of the cyclist. As a matter of fact, point *Pt1* and point *Pt2* are the extremities of the Rbe3 element used to apply the weight force of the cyclist (Fig. 3.13.a).

- The topology optimization could not delete the seat because it had been defined as part of the non-design space, therefore the seat has been used as a structural component (blue in Fig. 3.13.a). The undesired aspects are that, if we removed the seat, the frame would not have structural integrity and that is why the seat should not be removable. For this reason, Beams *D* have been elongated to the rear dropouts, and Beam *C* has been deleted (Fig. 3.13).

- In the rear zone, Beams *E* (Fig. 3.14.a) are in a more central position because in that zone there are no forces that induce the bending of the frame around the Z-axis. Beams *E* have been deleted and Beams *F* have been elongated to the rear dropouts (Fig. 3.14.b). In this way, we have:
  o simplified the geometry and bypassed the structural function of the seat;
  o given more structural stiffness under lateral forces, which are not accounted in the subcases. During the run, the cyclist has to make some adjustments to the handlebars to maintain the equilibrium of the bicycle [13]. These movements cause lateral oscillations of the frame.
- The connections between the central beams and the lateral beams in zone *G* and zone *H* have been simplified (Fig. 3.15)
- The bottom-bracket zone has been simplified with a continuous section with no holes (Fig. 3.13). Instead of holes, we are going to develop a zone with more thickness values.

## 3.3 Compute the ideal composite thickness

After defining the shape of the frame, we need to compute the ideal thickness of the carbon fiber composite for each direction. This phase is crucial for knowing the best thickness and orientation distributions, and for defining the first shapes of the fabrics. The final result of this phase is still conceptual, but some fabric constraints have to be imposed in this phase. In the next steps, we will edit the ideal solution to make it feasible.

### 3.3.1 Free-size optimization fundamentals

A free-size optimization is a per-element optimization which allows to independently modify the thickness of every single shell that belongs to the design space. A free-size optimization presents differences depending on whether the material is composite or homogeneous. We need to remember that, in the case of composite materials, the thickness of the shell is the sum of the thicknesses of the plies present inside it. As a result, the design variable of a free-size optimization:
- for homogeneous materials, is the thickness of the single shell. Thus, there is an independent variation of the thickness of each shell.
- for composite materials, is the thickness of the single ply contained in the single shell. Therefore, for each element, there is an independent variation of the thickness of each single ply that is present inside it.

The thickness of each ply can vary freely between T and T0 (Fig. 3.16), where T is the initial thickness and T0 is the final thickness. The final thickness T0 can never be greater than the initial thickness T. For this reason, oversized plies must be created in the starting model, i.e. a superlaminate.
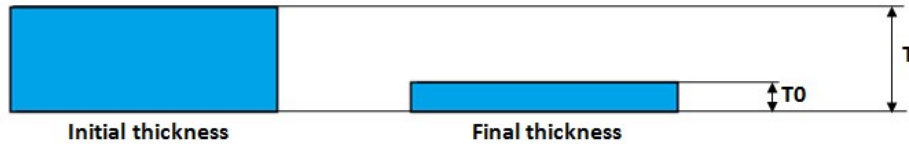
**Figure 3.16**: Initial thickness T and a final thickness T0 of a shell element during a free-size optimization.

In this type of analysis we can introduce different types of constraints on the ply and on the laminate. Furthermore, we can cancel the effects of the stacking sequence using the SMEAR option on the STACK card [16]. The effects of the stacking sequence will be explored in the shuffle optimization, which is the last optimization. It is advantageous to insert some constraints already in this conceptual phase, since it would be more difficult to insert them in the next phase of Size. The imposition of constraints on the thickness and distribution of the ply prevents unwanted deformations during the curing phase of the laminate and also during the operation of the final component. The free-size optimization manufacturing constraints are defined in the design variable, which is defined by the DSIZE card [7].

In the DSIZE card it is possible to define the following:

- Member size control (MEMBSIZE);
- Laminate thickness range (LAMTHICK);
- Ply thickness range (PLYTHICK) or the thickness percentage (PLYPCT). It is also possible to exclude some ply layers from constraints (PTEXC);
- Ply with constant thickness (CONST);
- Ply balance (BALANCE);
- Ply drop-off (PLYDRP).

Moreover, during the laminate definition (card STACK) it is possible to define the laminate as symmetric or non-symmetric [7].

At the end of the optimization, in the output we will have a new thickness distribution for each ply. If we use a free-size optimization within a 3-phase composite optimization we can ask the solver to prepare for the size phase by creating ply bundles. Ply bundles are a continuous distribution of shells having a unique thickness and orientation, and they represent the fabric shapes suggested by the solver. They are obtained through an algorithm that reworks the new thickness distribution. Ply bundles usually have very irregular shapes that are difficult to make, and thicknesses that are difficult to find on the market. For these reasons, a user-managed re-analysis phase will be necessary. The preparation card for the size phase is OUTPUT,FSTOSZ,YES, which creates a file of the *.fem type that contains the ply bundles suggested by the optimizer, and some cards that will be useful in the size phase. By default, the OUTPUT,FSTOSZ,YES card creates 4 ply bundles per orientation, while if we want more ply bundles we have to specify it in the first option field (for example OUTPUT,FSTOSZ,YES,8 generates 8 ply bundles per orientation) [24].

### 3.3.2 Model creation for the free-size optimization

The model for the free-size optimization has a superlaminate, which has oversized ply layers. The zero-degree direction of the laminate follows the longitudinal direction of the beams (Fig. 3.17). Each ply contains only fibers, parallel to each other, that are immersed in the matrix.
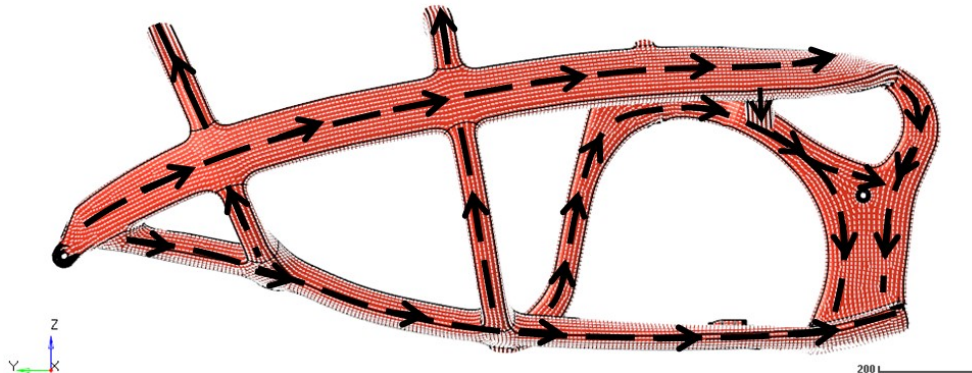


**Figure 3.17**: The arrows indicate the 0° direction of all the plies.

The superlaminate of the model is defined through the card STACK with Symmetric-Smear option. All the ply layers are oversized and are 2.0 mm thick (Fig. 3.18), while the orientations used are 0°, +45°, -45° and 90°. The option Smear has been introduced to cancel the effect of the stacking sequence in this conceptual phase. A laminate is symmetric if all the plies are symmetric to the middle surface of the laminate. Therefore, symmetric ply layers have the same material, thickness and orientation. The symmetric laminate does not warp or bend after the curing process because symmetric laminates do not have bending-extension coupling. This last property is important to preserve the initial geometry after the thermal process because we cannot avoid the residual forces that are due to the thermal process [25].
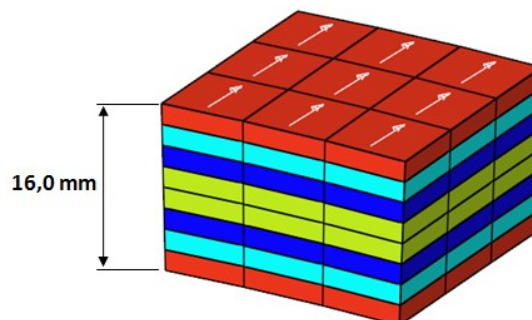


**Figure 3.18**: Symmetric superlaminate used for the frame in the free-size optimization.

### 3.3.3 Free-size optimization

*Pre-Processing*

The conducted free-size optimization has the objective of minimizing the weighed compliance and has the constraint on the maximum value of the total mass, as in the topology optimization. The input file used to run the analysis is in Appendix B and recalls the model described in the previous section and the transmission described in Section 3.2.3. The weighted compliance has been computed using the same static

74

subcases that have been used for the topology optimization, while the maximum total mass constraint has been set equal to 5 kg. The design variable of this optimization is the superlaminate described in the previous section, which has oversized plies because the optimizer can only reduce the initial thickness, as already explained in Section 3.3.1. The manufacturing constraints are defined inside the design variable. In this conceptual phase, we have introduced some constraints that are not too strict so as to give more freedom to the optimizer and to avoid extreme values. The applied manufacturing constraints are the:

- Member size control of 50 mm, used to limit the complexity of the thickness distribution. Therefore the function of this parameter is similar to that used in the topology optimization;

- Laminate thickness between 0.5 mm and 2.5 mm and minimum ply thickness of 0.01 mm, to avoid areas that are too thin and too thick;

- Balanced plies at +45° and -45°, to reduce coupling between in-plane normal strains and in-plane shear strains [25] ;

- Maximum ply drop-off of 1.25 mm. This limit is high because we are in a conceptual phase and it will be lower in the next steps. The maximum ply drop-off is useful to have a smooth thickness transition in order to avoid stress concentration factors.



**Figure 3.19**: Ply drop-off

In the free-size optimization we have introduced the card OUTPUT,FSTOSZ,YES, which will produce 4 ply bundles per orientation, useful for the next step.

*Post-Processing*

The Free-size optimization has produced a new ply-thickness distribution and finished with a feasible design since the new total mass is equal to 5 kg and all the manufacturing constraints have been satisfied. Figures from 3.20 to 3.22 show the new laminate thickness distribution, and we can notice that the laminate thickness constraints have been satisfied since the higher laminate thickness is 2.5 mm and the lower laminate thickness is 0.5 mm. Figures 3.23 and 3.24 show the ply thickness per fiber orientation. The thickness distribution of the ply at +45° is equal to that at -45° because the balance constraint has been observed by the optimizer (Fig. 3.24).
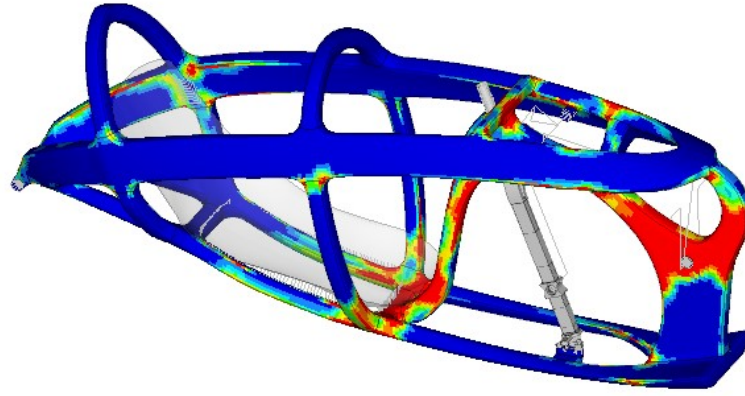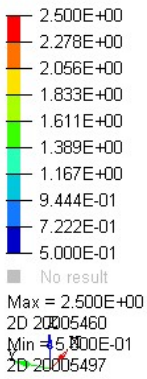
**Figure 3.20**: Final laminate thickness distribution of the free-size optimization.
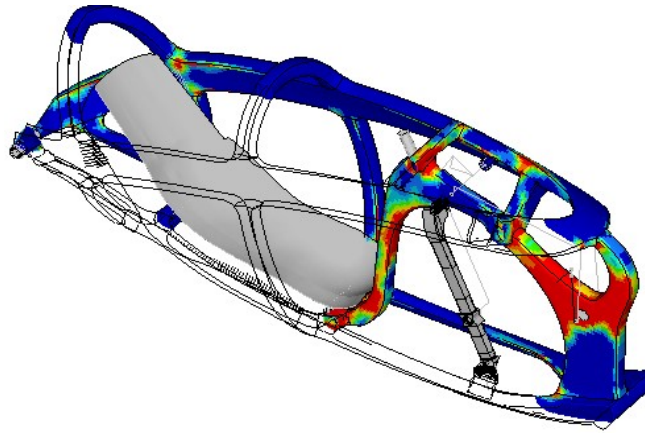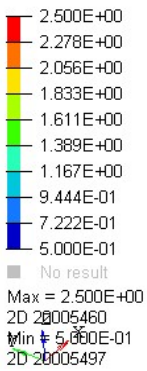


**Figure 3.21**: Final laminate thickness distribution of the free-size optimization. Right section to visualize the central tubes.
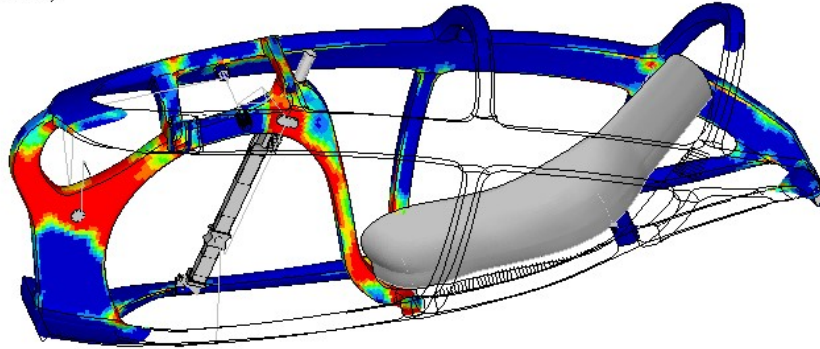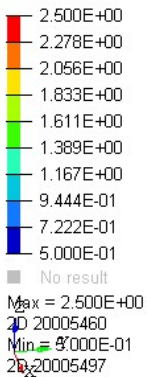


**Figure 3.22**: Final laminate thickness distribution of the free-size optimization. Left section to visualize the central tubes.
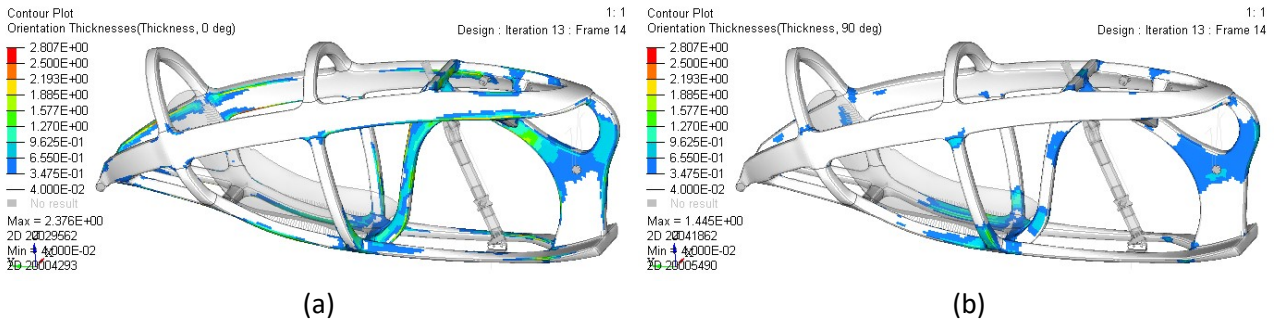
**Figure 3.23**: Sum of the thicknesses of all plies at 0° (a) and 90° (b) in the last iteration of the free-size optimization.
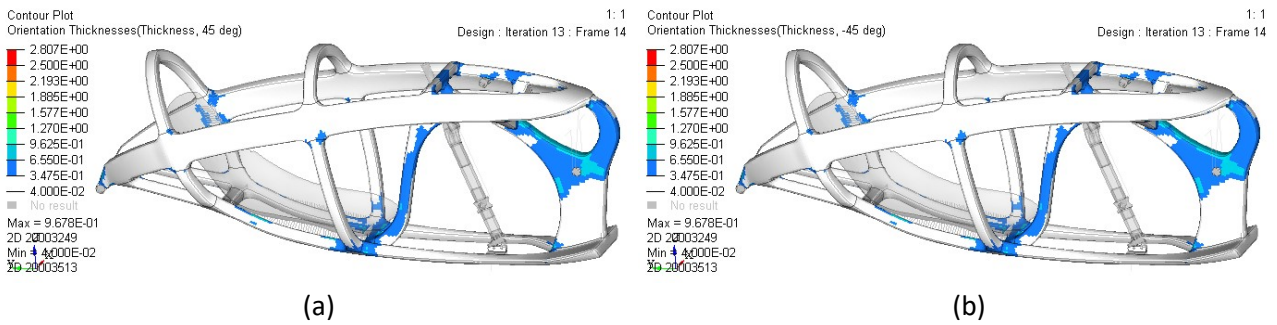


**Figure 3.24**: Sum of the thicknesses of all plies at +45° (a) and -45° (b) in the last iteration of the free-size optimization.

Figure 3.25 shows the total-mass response function, and Figure 3.26 shows the weighted-compliance response function. The total-mass response function decreases at each iteration, whereas the weighted-compliance response increases until the third iteration, and then it decreases. The trends of the two functions depend on the trend of the thicknesses of the frame. Until the third iteration, the thickness decreases uniformly (Fig. 3.27); consequently, the weighted compliance increases (Fig. 3.26) and the total mass decreases (Fig. 3.25). From the fourth iteration, the thickness of the most crucial areas starts to increase, while the thickness of the other areas continues to decrease (Fig. 3.28). This is why the total mass at the fourth iteration is lower than the total mass at the third iteration, and for the same reason the frame at the fourth iteration is stiffer than the frame at the third iteration. As the graph in Figure 3.26 shows, the weighted compliance at the fourth iteration is lower than in the third iteration. Looking at the final iteration, we can notice that the higher thicknesses are placed in the bottom bracket zone, in the new sprocket support, and in the vertical tube (Fig. 3.20-3.22).

In addition to the results already presented, the optimizer produced 4 ply bundles per orientation, which are stored in the file 'RUN_FREESIZE_sizing.13.fem', and which will be presented in the next step.
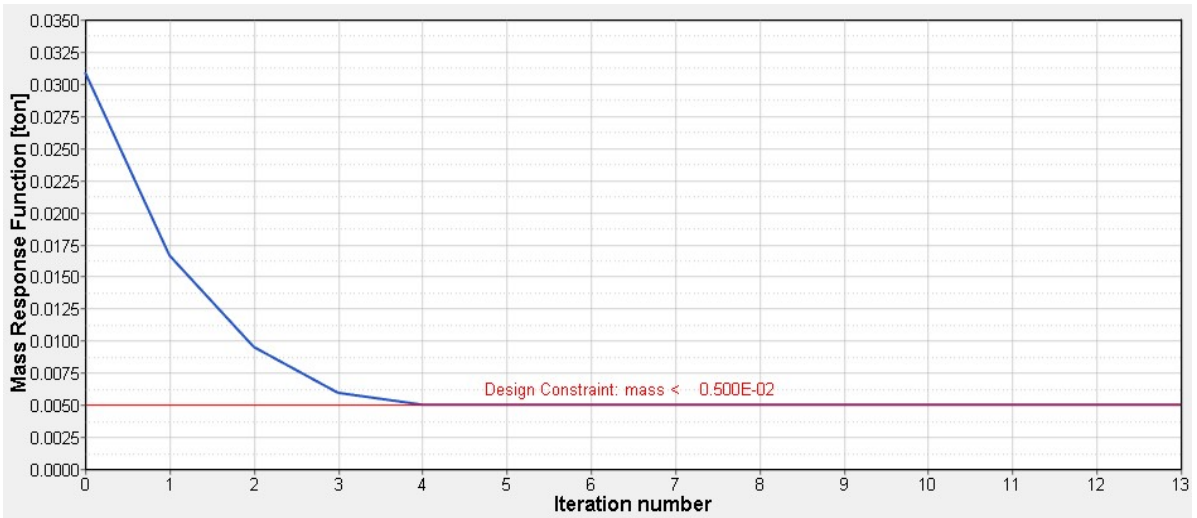
**Figure 3.25**: Mass response function, which is the constraint function of the current free-size optimization.
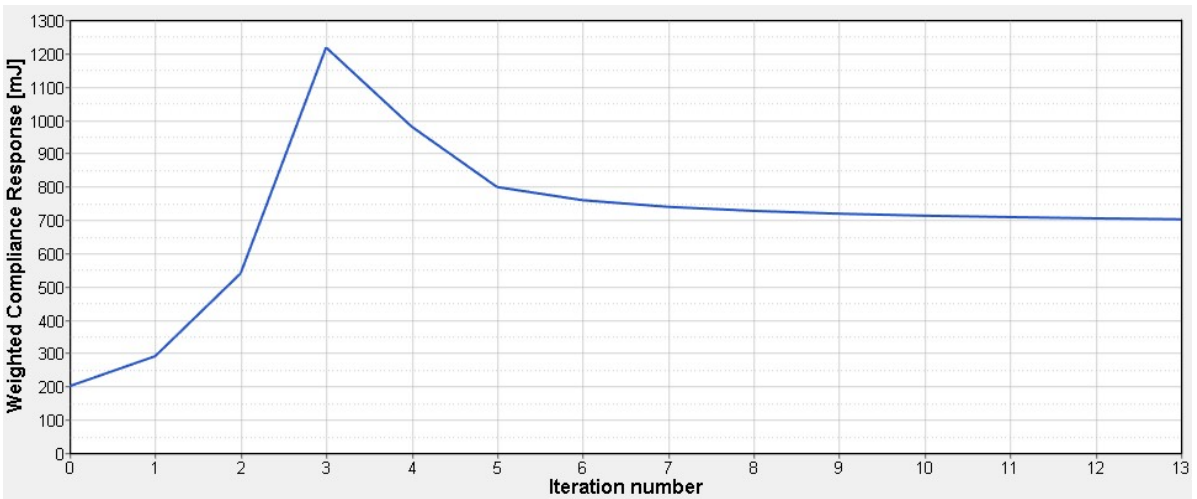


**Figure 3.26**: Weighted compliance, which is the objective function of the current free-size optimization.



(a)                                                              (b)
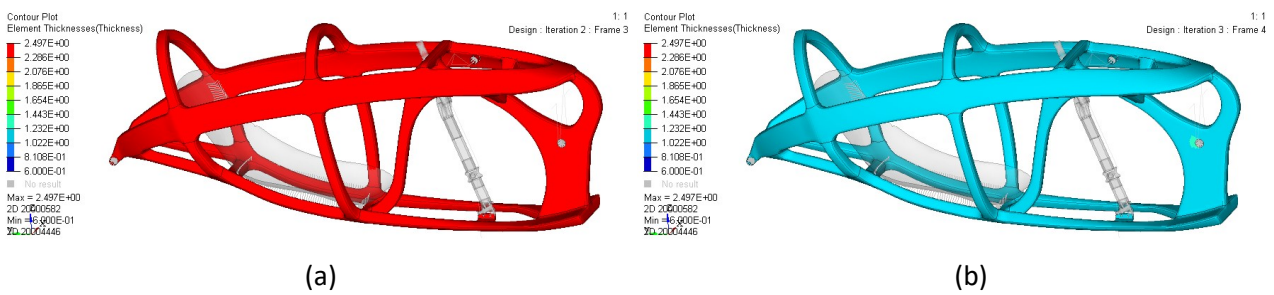
**Figure 3.27**: Total thickness at iteration 2 (a) and 3 (b) of the free-size optimization.



(a)                                                              (b)
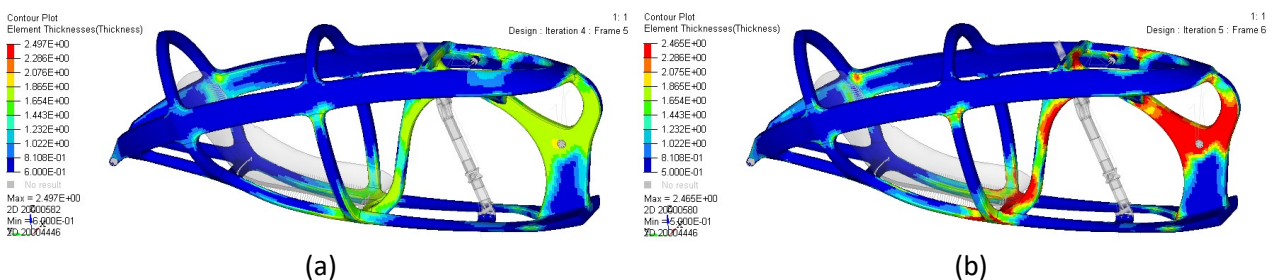
**Figure 3.28**: Total thickness at iteration 4 (a) and 5 (b) of the free-size optimization.

## 3.4 Defining the shape and thickness of the ply layers

The aim of this phase is to define the shape, the orientation and the density per area of all ply layers, according to the fabrics' availability on the market and to the manufacturing constraints. The starting point of this phase is based on the ideal thickness distribution computed in the previous step.

### 3.4.1 Size optimization fundamentals

Contrary to the topology and the free-size optimization, the design variables in the size optimization are not defined. As we have seen previously, the design variables of a topology optimization are the densities of the elements, and the design variables of a free-size optimization are the thicknesses of the elements. The size optimization runs by modifying the parameters of the properties. For example, during a size optimization we could change the thickness of the shells, or the cross-section of a beam, or the stiffness of a spring, or any parameter of many properties. In the size optimization, we have the independent design variables, as in every optimization analysis, but these have to be related to their respective properties. The parameter of a property is defined as a function of a design variable by the design-variable-to-property relationship card DVPREL1 or DVPREL2. The card DVPREL1 defines the simplest relationship, which is expressed by Equation 3.5, while through the card DVPREL2 it is possible to define more complex equations [16].

$$P_i = C_0 + \sum_i COEFF_i \cdot DDVI_i \tag{3.5}$$

Where:

$C_0$ is a constant and its default value is equal to zero,

$COEFF_i$ is the coefficient of the design variable and its default value is equal to one,

$DDVI_i$ is the design variable.

A design variable in the size optimization is defined through the card DESVAR. In the card DESVAR we can specify the initial value of the design variable, the upper and lower bond of the design variable, and we can allow specific discrete values by recalling the card DDVAL. The latter option is useful when the choice of materials is limited. We can observe that the size optimization is a property-based optimization and the topology and the free-size optimization are element-based optimizations. Therefore, in the size optimization, all elements having the same property are going to undergo the same changes.

### 3.4.2 Model creation for the size optimization

In this phase we create the model that will be used for the size optimization. We have to define the shapes and the orientations of the fabrics because the size optimization can only find the optimal ply thickness. The shapes of the plies have been made taking into account:

- the ideal thickness distribution computed in the free-size optimization;

- the ply bundles suggested by the optimizer;
- laminate manufacturing constraints (drop-off, balance of plies at +45° and at -45°, sym. laminate);
- fabric thicknesses available on the market;
- the joints between the tubes of the frame.

The ply bundles suggested by the optimizer are placed in the file 'RUN_FREESIZE_sizing.13.fem' made in the previous analysis. The plies are identified by a five-digit ID in which each number position corresponds to a different meaning:

- the first digit indicates the design variable defined in the free-size optimization;
- the second digit indicates the orientation of the ply. The number 1 indicates plies at 0°, the number 2 indicates plies at +45°, the number 3 indicates plies at -45° and the number 4 indicates plies at 90°;
- the last three digits are a progressive ID to distinguish the different plies with the same design variable and orientation. All plies with ID 'xx100' cover the complete surface available.

The laminate produced in the file 'RUN_FREESIZE_sizing.13.fem' has 32 plies, but since the laminate is symmetric we need the description of half of them. The thicknesses and orientation of those plies are listed in the following table and their covering areas are shown from Figure 3.29 to 3.32. The figures of all the plies with ID xx100 are omitted because they do not add information about the covering area.

| PLY ID | Thickness [mm] | Orientation [°] | PLY ID | Thickness [mm] | Orientation [°] |
|--------|----------------|-----------------|--------|----------------|-----------------|
| 11100  | 0.08           | 0               | 13100  | 0.06           | -45             |
| 11200  | 0.09           | 0               | 13200  | 0.04           | -45             |
| 11300  | 0.22           | 0               | 13300  | 0.11           | -45             |
| 11400  | 0.79           | 0               | 13400  | 0.28           | -45             |
| 12100  | 0.06           | +45             | 14100  | 0.05           | 90              |
| 12200  | 0.04           | +45             | 14200  | 0.04           | 90              |
| 12300  | 0.11           | +45             | 14300  | 0.14           | 90              |
| 12400  | 0.28           | +45             | 14400  | 0.49           | 90              |

**Table 3.1**: Thicknesses and orientation of the ply bundles suggested by the optimizer.
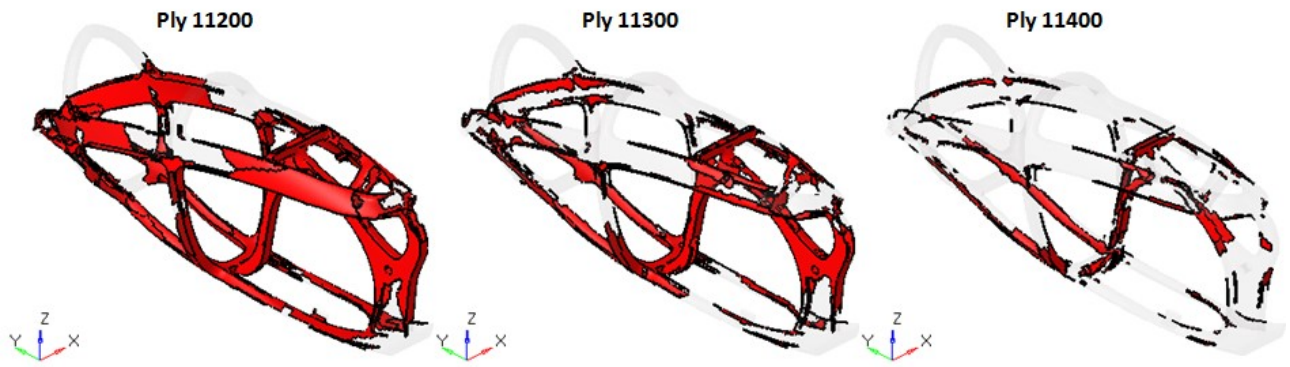
**Figure 3.29**: Ply bundles at 0° suggested by the optimizer (Ply 11100 is omitted because it covers the complete surface).
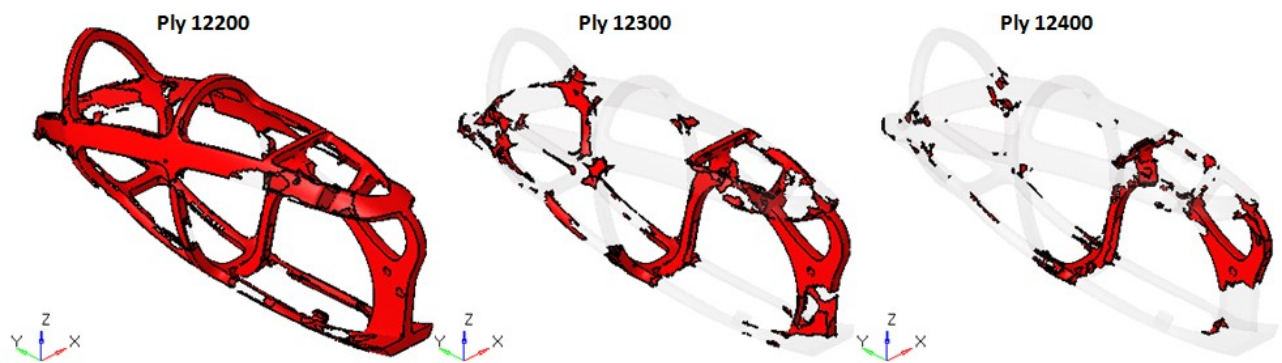


**Figure 3.30**: Ply bundles at +45° suggested by the optimizer (Ply 12100 is omitted because it covers the complete surface).
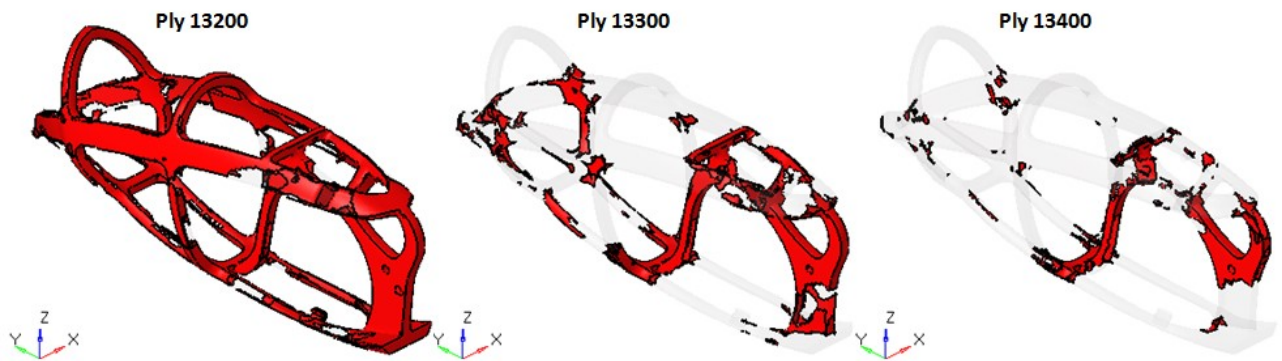


**Figure 3.31**: Ply bundles at -45° suggested by the optimizer (Ply 13100 is omitted because it covers the complete surface).
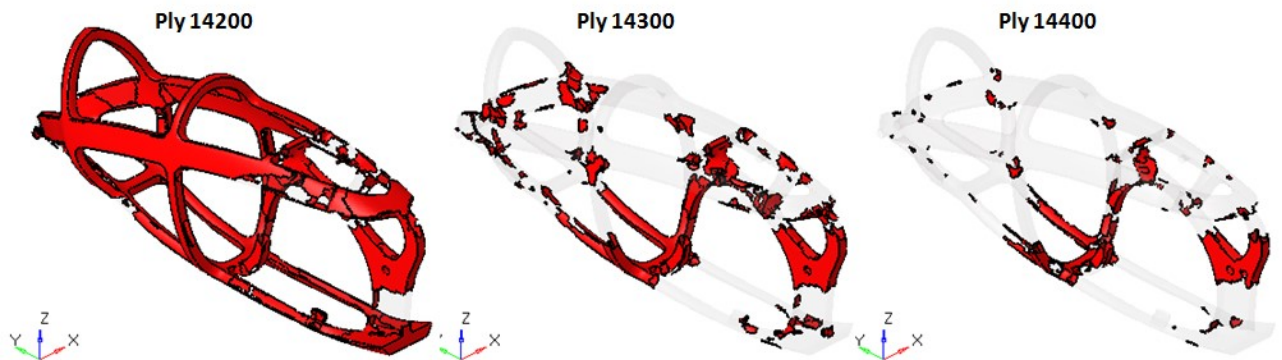


**Figure 3.32**: Ply bundles at 90° suggested by the optimizer (Ply 14100 is omitted because it covers the complete surface).

We can notice that the ply layers at +45° and -45° have the same thicknesses and the same covering areas due to the constraint introduced in the input file. The ply bundles suggested by the optimizer have irregular edges that are difficult to manufacture, and some plies are very thin and are not available on the market. Moreover, the ply bundles produced by the optimizer do not consider the subdivision of the frame into several tubes and the joints between them. For all these reasons, the ply bundles have been reshaped manually.
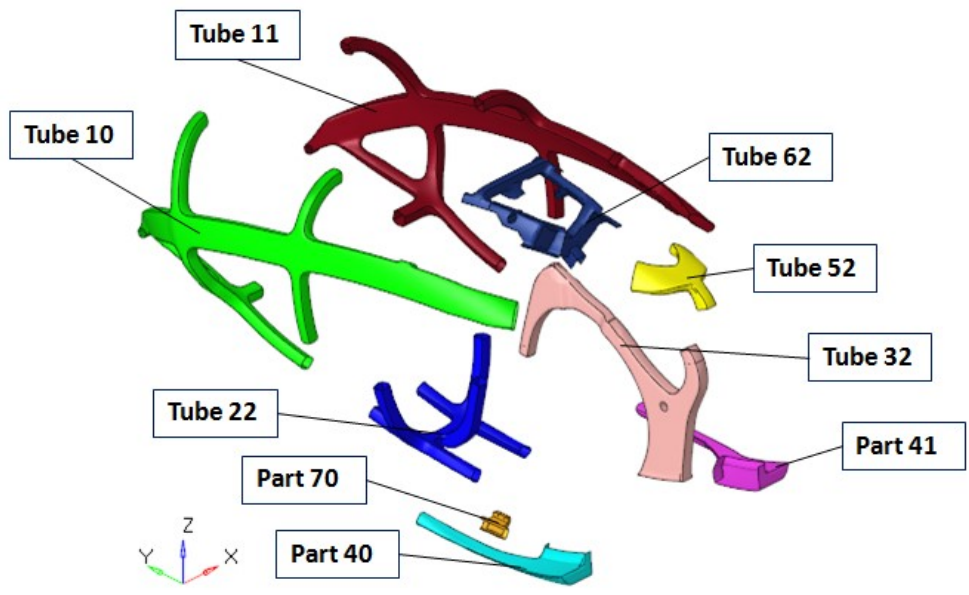


**Figure 3.33**: Components that make the frame.

The frame is not a monocoque but is made up of many tubes joined together (Fig. 3.33). The extension of the tubes also depends on the position of the junction points. The joints must guarantee stiffness continuity and we have to consider that they add weight to the frame. For these reasons, the joints are positioned, as far as possible, in the least critical zones, which coincide with the thinner areas computed by the free-size optimization (Fig. 3.20). The tubes fit inside each other and their contact surfaces are joined together by structural glue (Fig. 3.43). After the gluing process, the outer surface of the joint is reinforced by external carbon fiber fabrics (Fig. 3.37 and 3.38). Only tubes at Junction 9 do not fit inside each other; otherwise, the assembly of the frame would not be possible (Fig. 3.36 and 3.37). The main assembling phases are illustrated in the following figures, with the close red lines delimiting the overlaps between the tubes.



(a)                                             (b)

**Figure 3.34**: (a) Sub-assembly 1. (b) Sub-assembly 2.
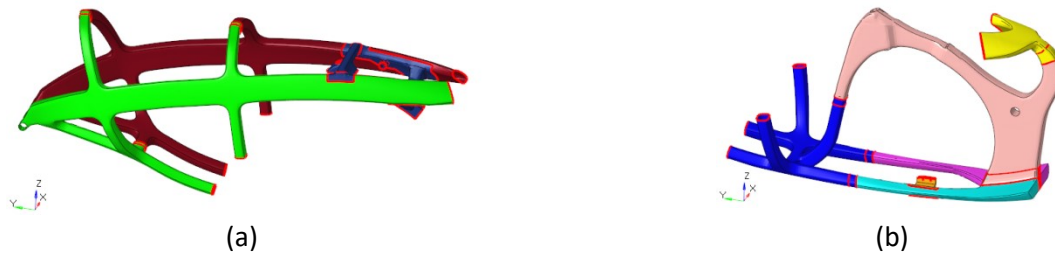
**Figure 3.35**: (a) Sub-assembly 4. (b) Sub-assembly 3, obtained composing the sub-assembly 1 and 2.
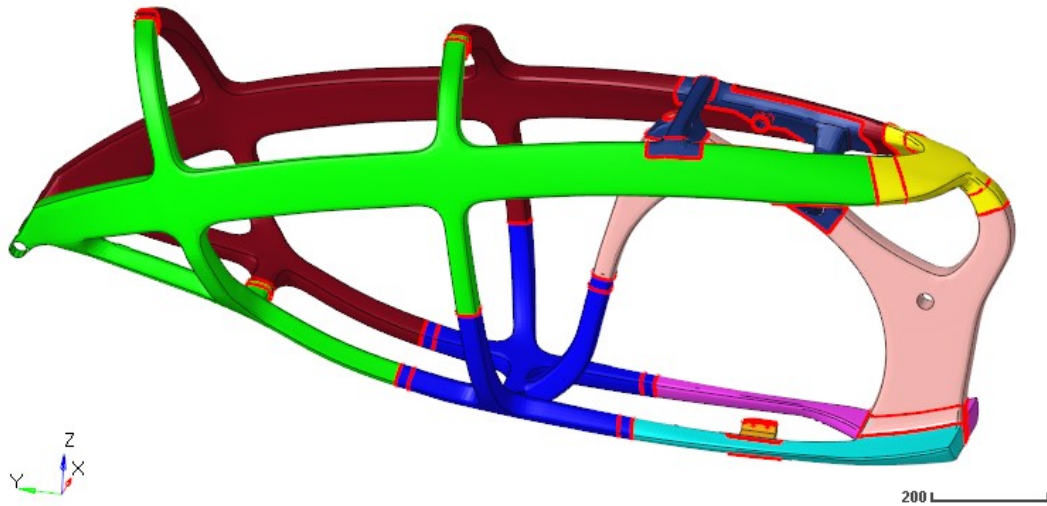


**Figure 3.36**: Frame after gluing all the components together. The close red lines delimit the overlaps between the tubes.
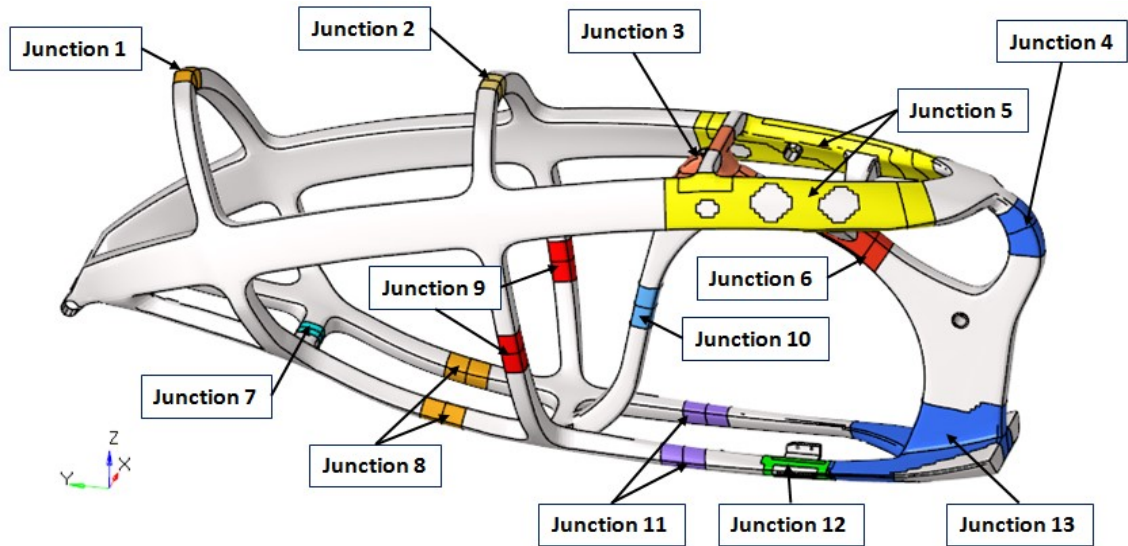


**Figure 3.37**: Reinforcements of the joints, applied after gluing all the components of the frame.
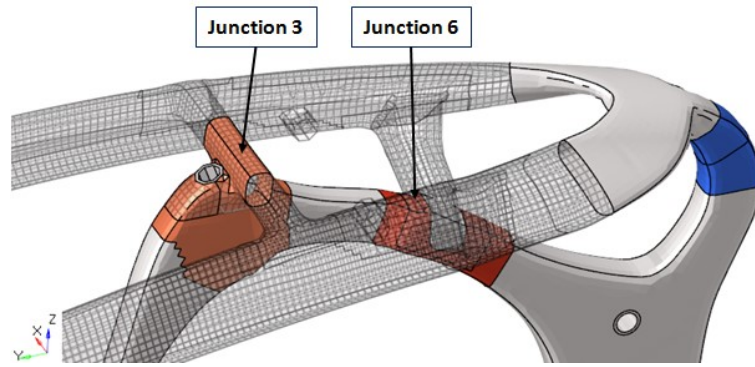
**Figure 3.38**: Reinforcements of the joints, applied after gluing all the components of the frame.

Following all the above observations, the ply bundles have been reshaped manually. Each component of the frame has base plies plus reinforcement plies. The base plies cover the complete surface of the related component. The reinforcement plies cover a reduced area of the related component. The following figures show only the sets of elements that define the covering areas of the reinforcement plies.
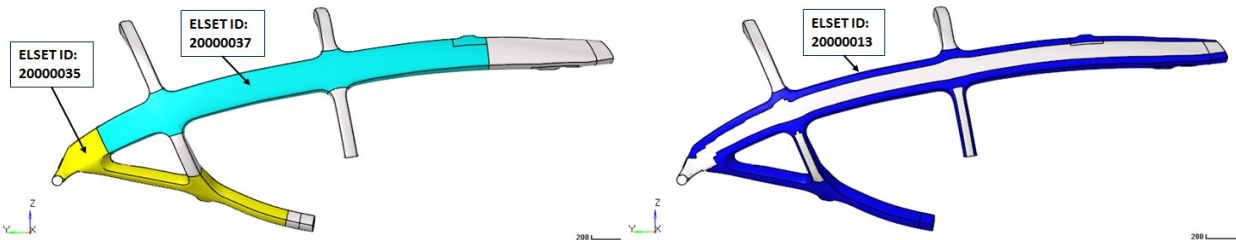


**Figure 3.39**: Sets of elements that define the covering areas of some plies of Tube 10.
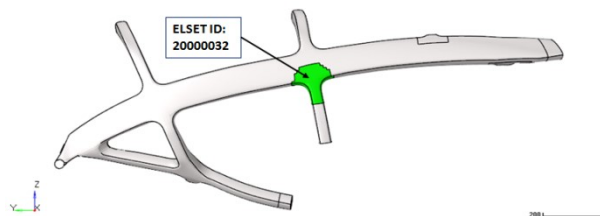


**Figure 3.40**: Set of elements that define the covering area of some plies of Tube 10.

The sets of elements with ID 20000036, 20000038, 20000015, and 20000033 are respectively symmetrical to 20000035, 20000037, 20000013, 20000032.



(a)                                                                                                              (b)
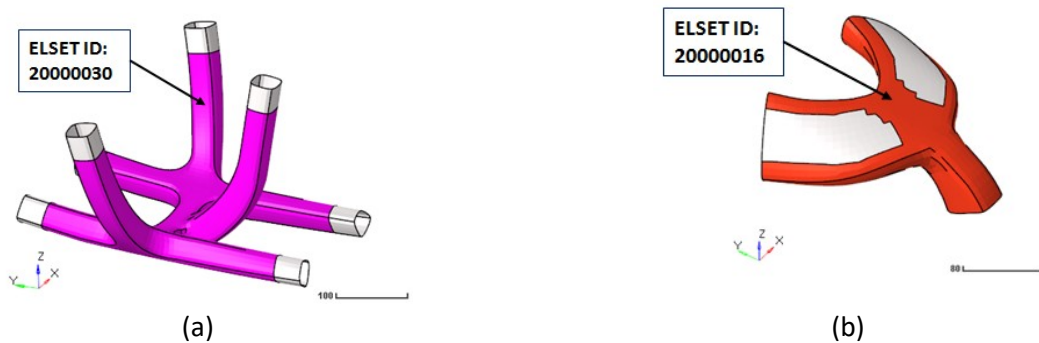
**Figure 3.41**: Sets of elements that define the covering areas of some plies of Tube 22 (a) and Tube 52 (b).
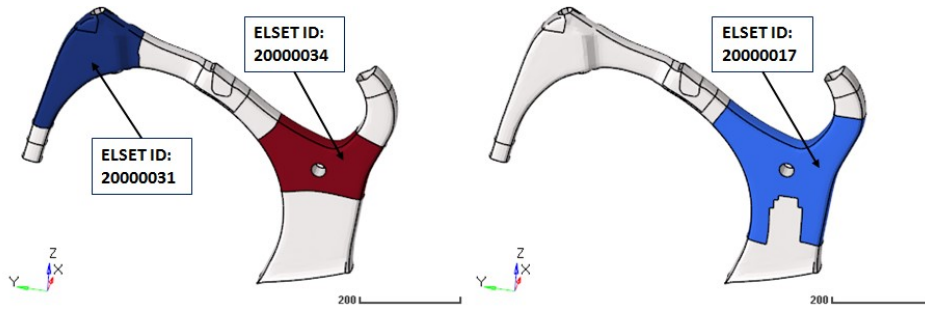
**Figure 3.42**: Sets of elements that define the covering areas of some plies of Tube 32.

At the end of the reshaping process, we have 189 plies that make 10 components and 13 junction reinforcements (Tab. 3.4). To handle many plies, additional rules have been introduced to generate the ply IDs. The new ply ID has additional numbers before the previous ID. In particular:

- the plies that compose the tubes start with the ID number of the corresponding tube;
- the plies that compose the external junction reinforcements always start with the number 9 followed by the ID number of the corresponding junction;
- if the ply is symmetrical to one already defined, the first number in absolute is the number 5.

This organization is further clarified in Table 3.4, which reports the description of the final laminate.

### 3.4.3 Size optimization

*Pre-Processing*

The size optimization has the objective of minimizing the weighted compliance with the maximum mass constraint, by assigning to each ply the thicknesses available on the market (Tab. 3.2 and 3.3). The total-mass constraint is 7.1 kg, which is equivalent to a maximum frame mass of 6 kg, considering that the non-design space weighs 1.1 kg. The weighted compliance has been computed using the same static subcases that have been used for the previous optimization. The shapes of the plies have been defined in the model described in the previous section and cannot be changed by the size optimization. The input file used to run the analysis [Appendix B] recalls the model described in the previous section and the transmission described in Section 3.2.3.

| Areal weight of the CF reinforcement [g/m²] | Thickness of the CF reinforcement [mm] | Thickness due to the matrix [mm] | Thickness of the ply lamina [mm] |
|---|---|---|---|
| 50 | 0.03 | 0.04 | 0.07 |
| 100 | 0.06 | 0.08 | 0.14 |
| 125 | 0.07 | 0.10 | 0.18 |
| 150 | 0.09 | 0.13 | 0.21 |
| 200 | 0.11 | 0.17 | 0.28 |
| 250 | 0.14 | 0.21 | 0.35 |
| 300 | 0.17 | 0.25 | 0.42 |
| 400 | 0.23 | 0.33 | 0.56 |
| 600 | 0.34 | 0.50 | 0.84 |

**Table 3.2**: Unidirectional carbon-fiber fabrics available on the market.

| Thickness of PVC layer [mm] |
| --- |
| 3 |
| 6 |
| 10 |

**Table 3.3**: PVC layers available on the market.

In the design space of this optimization we have 189 plies but we have to remember that the laminates are symmetric with the exception of the laminates that make the joints. For this reason we have to define the thickness of only 122 plies. Therefore, we need 122 DVPREL1 cards and 122 design variables. Each design variable recalls its DDVAL card to assign only the discrete thicknesses available on the market. Each DVPREL1 card links the design variable with the corresponding ply. Although it is possible to define the cards through the GUI of Hypermesh, it is more efficient to write them via text editor because the ply, the design variable and the DVPREL1 cards can have the same ID number. To do this it is essential to know the structure of all the cards used.

The laminate constraints used in this size optimization are the balancing of the plies at +45° and -45° and the ply drop-off, as in the free-size optimization. At the junction between the tubes we have steps (Fig. 3.43) but inside each tube a ply drop-off lower than 1.0 mm is preferable.
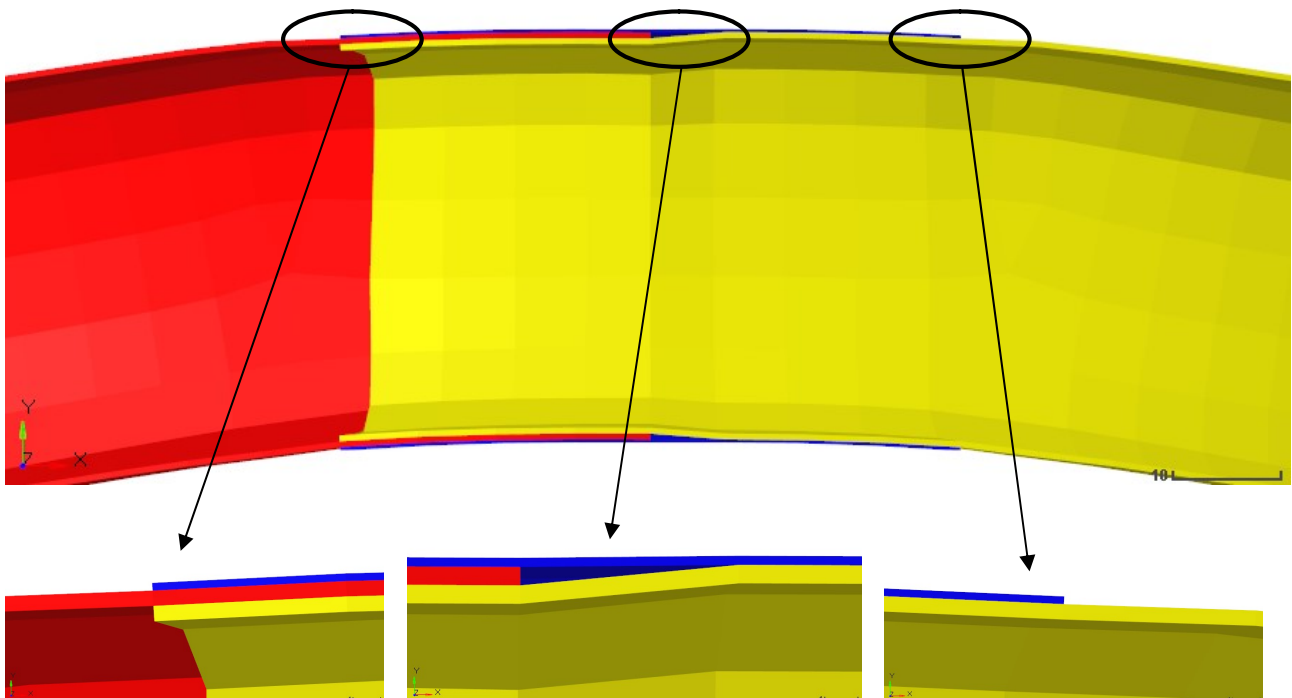


**Figure 3.43**: Tube 10 (red) and 11 (yellow) at the junction. Junction 2 reinforcement (blue). Zoom of the steps.

In the Size optimization we have introduced the card OUTPUT,SZTOSH,YES which introduces the input file for the stacking optimization.

*Post-Processing*

The size optimization has chosen the optimal thicknesses values among those available in order to have the stiffest frame with 6 kg. The final thickness value of each ply is listed in Table 3.4. Figure 3.44 shows the new laminate-thickness distribution, which is more feasible than the previous one (Fig. 3.20). Figures 3.45 and 3.46 show the thickness distribution per orientation, and we can notice that the thickness distribution of the ply at +45° is equal to that at -45° because the balance constraint has been observed by the optimizer.
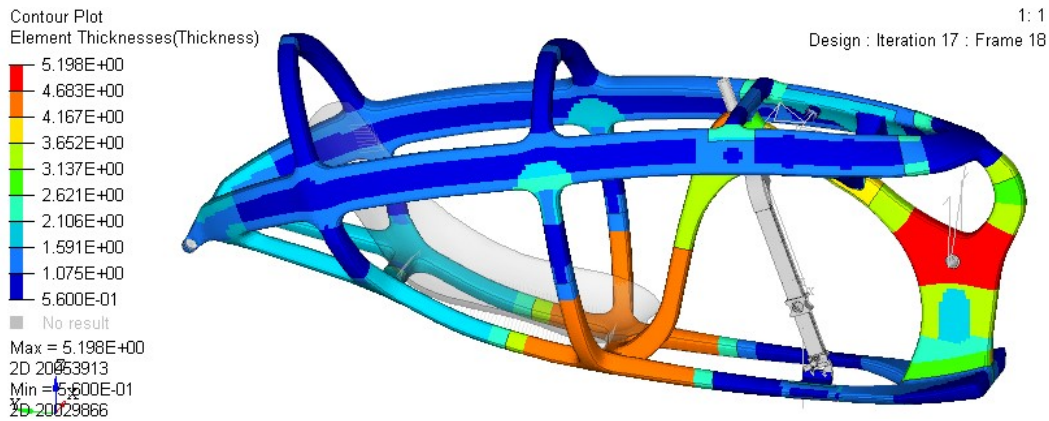


**Figure 3.44**: Final laminate-thickness distribution of the size optimization.



(a)                                                                                          (b)
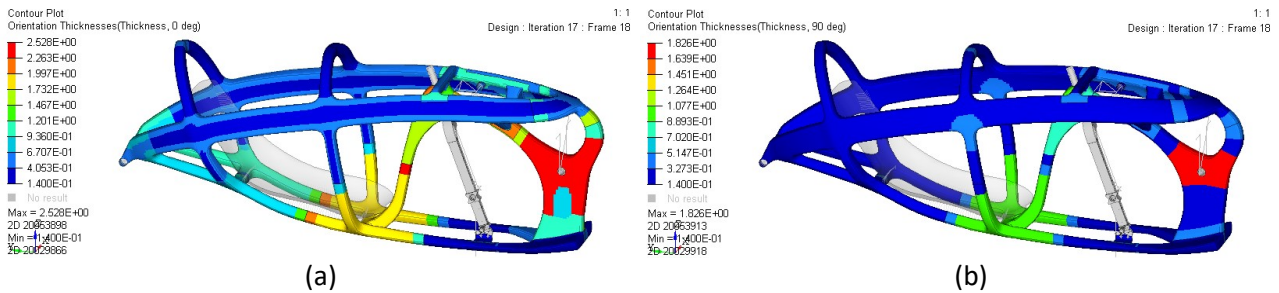
**Figure 3.45**: Sum of the thicknesses of all plies at 0° (a) and 90° (b) in the last iteration of the size optimization.



(a)                                                                                          (b)
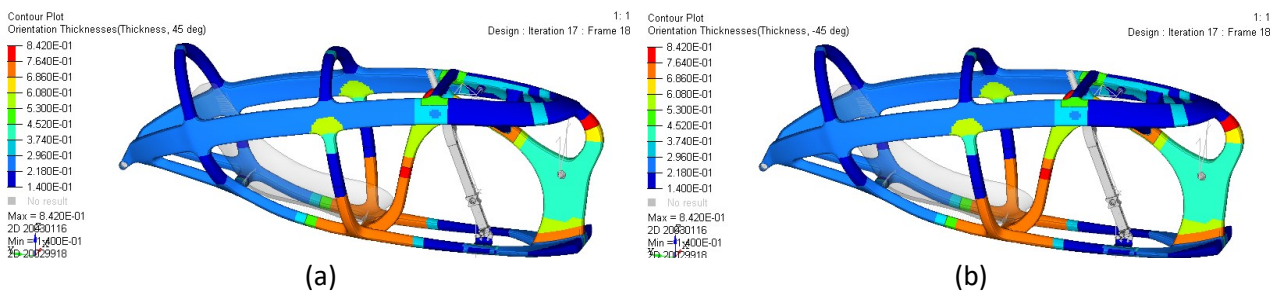
**Figure 3.46**: Sum of the thicknesses of all plies at +45° (a) and -45° (b) in the last iteration of the size optimization.

Figure 3.47 shows the total-mass response function and Figure 3.48 shows the weighted-compliance response function. The derivate of the current mass response function oscillates between positive and negative values, as opposed to the one obtained by the free-size optimization; this is because in this case the optimizer is forced to use discrete values. Therefore, the optimum point cannot be reached with a continuum increase or decrease in thickness.
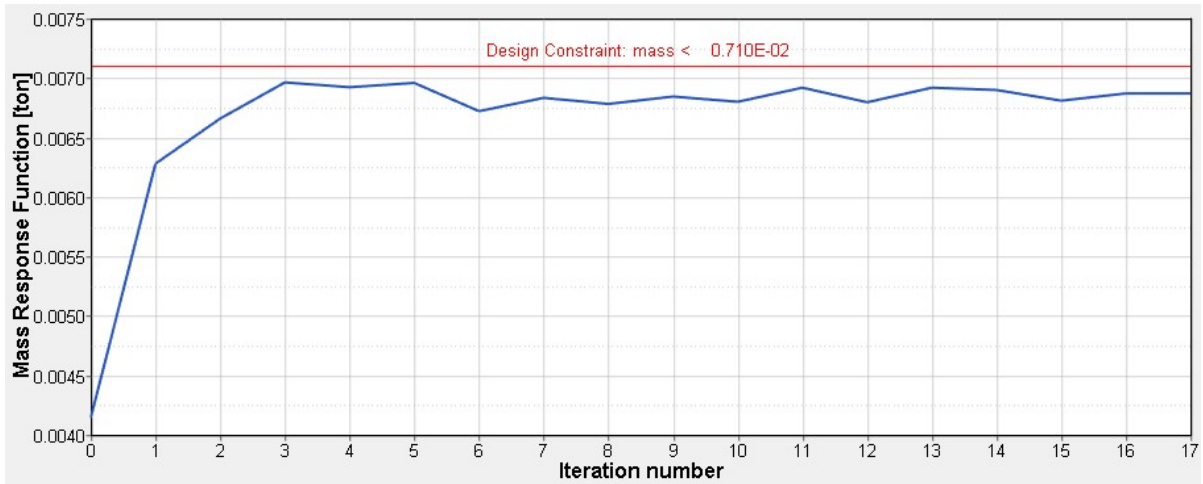
**Figure 3.47**: Mass response function, which is the constraint function of the current size optimization.
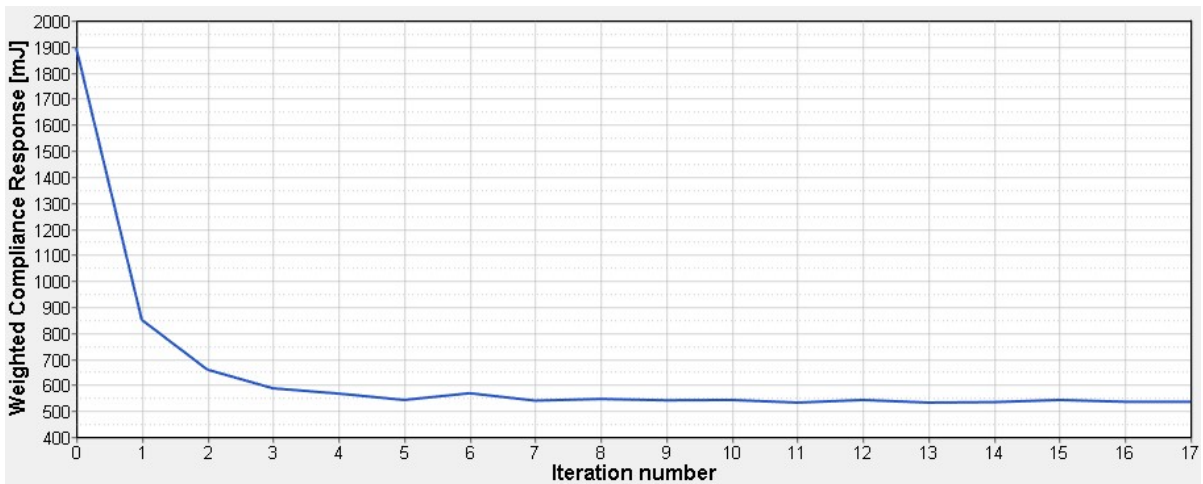

**Figure 3.48**: Weighted compliance, which is the objective function of the current size optimization.

## 3.5 Defining the stacking sequence of the ply layers

This is the last phase of the composite optimization process. In this phase we will define the stacking sequence of the ply layers according to the ply-book rules. The stacking sequence is the last aspect to completely define the laminates. The final analysis aimed to verify the achievements of the objectives will be presented in the next chapter.

### 3.5.1 Shuffle optimization fundamentals

The aim of the shuffle optimization is to define the optimal layup or stacking sequence of the ply layers. The stacking sequence influences the interlaminar stresses and the strength of the laminate [26]. We can stack the plies in order to limit the interlaminar stresses, since the interlaminar shear strength (ILSS) is an aspect to consider during the design process. The interlaminar stresses can be calculated within the assumptions of the classical lamination theory [9, Chapt. 6]. Instead, if we want to evaluate the interlaminar stress at the edges, we can use the analytical approach of Pipe and Pagano [9, Chapt. 8], or use FE models.

These observations lead to the ply-book rules that we want to observe in the shuffle optimization analysis. The most important rules are listed below [27] [28]:

- gradual ply drop-off to avoid stress concentration, and covering the ply drop-off with the more extended ply (Fig. 3.49);



**Figure 3.49**: Suggested gradual ply drop-off.

- minimizing the angle change between plies to limit the interlaminar stress due to Poisson's mismatch. For example, using the [0/+45/90/-45] stacking sequence;
- not stacking many plies with the same orientation to avoid the delamination between two groups of plies with different orientations. Instead, spacing ply angles as much as possible;
- reinforcing free edges with additional ply (Fig. 3.50).



**Figure 3.50**: Free edge reinforcement ply (red)

Other useful rules can be:

- making sure to stack plies with a thickness of at least 10% of that of the laminate in each direction to account for unexpected loads;
- in case of junctions between carbon fibers and metal parts, stacking a glass-fibre ply between them to avoid Galvanic Corrosion [10].

The design variable of the shuffle optimization is defined by the card DSHUFFLE. Inside the card DSHUFFLE it is possible to define the following stacking constraints [24]:

- MAXSUCC defines the maximum number of plies with the same orientation;
- PAIR allows to pair plies at +45° with plies at -45°;
- CORE and COVER options define the stacking sequence of the core and of the cover respectively. Therefore, the user can impose an arbitrary stacking sequence (for example 0°/+45°/90°/-45°). In case of non-symmetric laminates, the option CORE cannot define the actual core but defines the bottom ply layer.

### 3.5.2 Model creation for the shuffle optimization

To create the model for the shuffle optimization, we start from the model obtained after the size optimization. For the reasons that will be explained in the next part, the elements that make the Tube 10 and the Tube 11 cannot also define the other parts. This is because the elements positioned where the

tubes overlap define the plies belonging to many tubes of the frame. To achieve this result, there are duplicate elements in the mesh. The duplicate elements are defined by the same nodes, therefore the connection between the parts is ensured.

After this observations, we have defined three different laminates as follows:

- we have removed the option 'Smear' from all the laminates to consider the stacking sequence effects;

- we have created a laminate for Tube 10 and a laminate for Tube 11. Both laminates have been defined as 'symmetric' because each of them contains only a single part. This aspect is important to correctly define the sequences of the plies at the junctions.

- we have created another laminate for all the other parts. In order to properly define the junctions of the tubes, inside the card STACK we have swapped the option 'symmetric' with option 'total' and subsequently we have defined the symmetric plies. The laminate of each component is symmetric, but the card STACK that defines many tubes cannot be defined with the option 'symmetric'.

The last two points are important at this phase because we are removing the option 'Smear' and we want to evaluate the stacking sequences of the plies. We have created duplicate elements because, according to Optistruct, one ply cannot belong to many laminates. The need for many laminates will be explained in the following section.

### 3.5.3 Shuffle optimization

The shuffle optimization has the same constraint function and the same objective function as the previous optimization, but has different design variables. The manufacturing constraints that we want to introduce in the design variables are:

1) each part has to have a symmetric laminate;

2) stacking consequently no more than 4 plies with the same orientation (through option MAXSUCC in cad DSHUFFLE);

3) $[0°/+45°/90°/-45°]_S$ stacking sequence is preferred (through option COVER and CORE in card DSHUFFLE);

4) all the plies that make the same tube have to be adjacent to each other. Although a command to make a group of plies adjacent does not exist, we can use many DSHUFFLE cards that act on different laminates. For this reason, we have created more laminates inside the model dedicated to this optimization;

5) all the plies that make the reinforcement junctions are the most external;

6) The tubes fit inside each other at the junctions. In particular:

   o Tube 41 fits inside Tube 22, and Tube 32;

   o Tube 40 fits inside Tube 22, Tube 32, and Part 70;

- o Tube 32 fits inside Tube 22, Tube 52, and Tube 62;
- o Tube 11 fits inside Tube 10, Tube 22, Tube 52, and Tube 62;
- o Tube 10 fits inside Tube 22.

We have created a laminate for each DSHUFFLE card to satisfy the constraints 4), 5) and 6). Optistruct cannot distinguish which tube a ply belongs to. Moreover, at the junctions, the cover ply of a tube becomes the core ply of the next tube. Therefore, the current solution is to modify the dedicated model and assign a component to a laminate, and then a laminate to a DSHUFFLE card.

We can observe that the frame has a relatively small number of plies and except for Tubes 10 and 11, the solution of the optimization is simple. For this reason, we have created a design variable for Tube 10 and a design variable for Tube 11. Each design variable acts on the corresponding laminate.

For all the parts, except for Tubes 10 and 11, we can take advantage of the ply's ID rules and fulfill the shuffle requirements by reordering the ply IDs inside the card STACK (through a text editor). The input file to perform the shuffle optimization is in Appendix B.

Figure 3.51 shows the total-mass response function and Figure 3.52 shows the weighted-compliance response function.
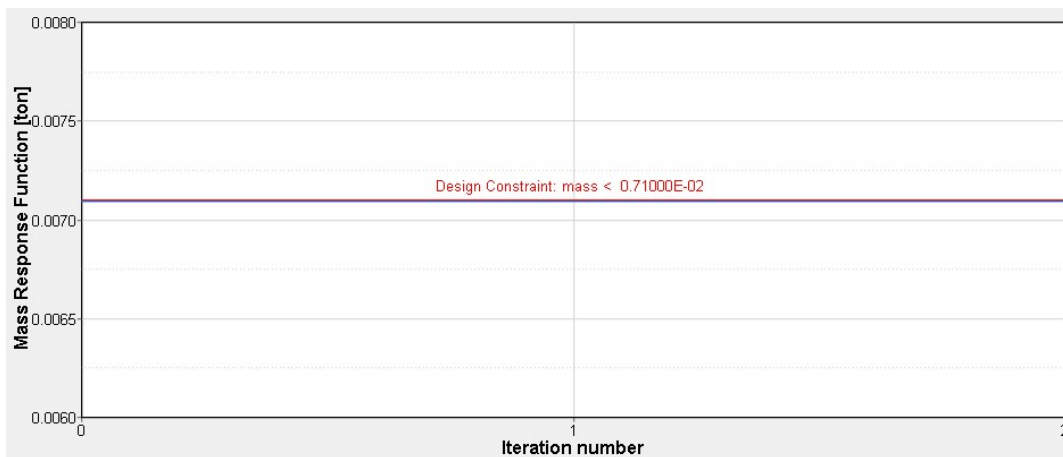


**Figure 3.51**: Mass response function, which is the constraint function of the current shuffle optimization.
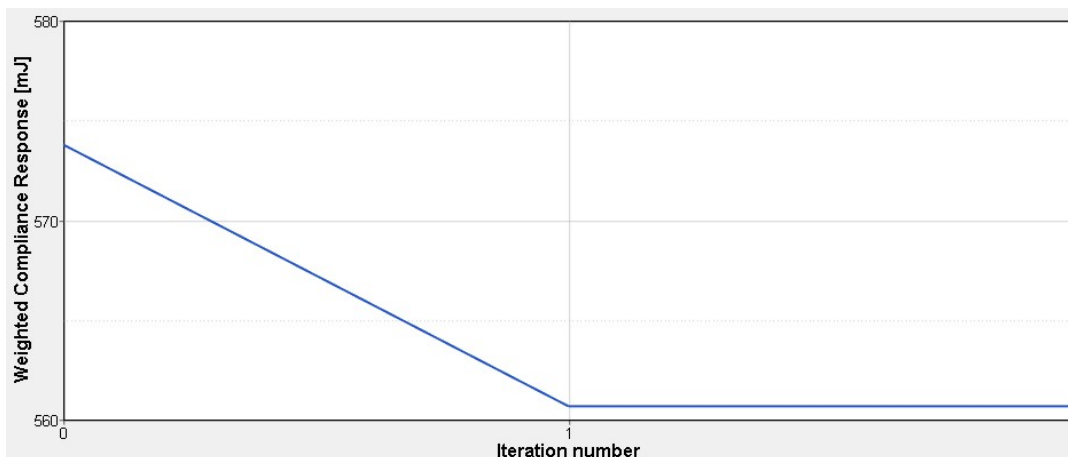


**Figure 3.52**: Weighted compliance, which is the objective function of the current shuffle optimization.

91

The mass response function is constant because the shuffle optimization changes only the stacking sequence of the plies. The weighted-compliance response function shows a little increase in the stiffness, compared with the previous optimizations.

The final stacking sequence scheme is specified in the following table, where the first plies of each part are the most external:

| | Ply Name | Ply ID | Density per area [g/m^2] | Orientation [°] | Property | Covering area ID | |
|---|---|---|---|---|---|---|---|
| Junction 1 | G1__Ply11100 | 9111100 | 50 | 0 | UD CFRP | 20000022 | row 1 |
| | G1__Ply12100 | 9112100 | 50 | 45 | UD CFRP | 20000022 | row 2 |
| | G1__Ply14100 | 9114100 | 50 | 90 | UD CFRP | 20000022 | row 3 |
| | G1__Ply13100 | 9113100 | 50 | -45 | UD CFRP | 20000022 | row 4 |
| Junction 2 | G2__Ply11100 | 9211100 | 50 | 0 | UD CFRP | 20000023 | row 5 |
| | G2__Ply12100 | 9212100 | 50 | 45 | UD CFRP | 20000023 | row 6 |
| | G2__Ply14100 | 9214100 | 50 | 90 | UD CFRP | 20000023 | row 7 |
| | G2__Ply13100 | 9213100 | 50 | -45 | UD CFRP | 20000023 | row 8 |
| Junction 3 | G3__Ply11100 | 9311100 | 50 | 0 | UD CFRP | 20000028 | row 9 |
| | G3__Ply12100 | 9312100 | 50 | 45 | UD CFRP | 20000028 | row 10 |
| | G3__Ply14100 | 9314100 | 50 | 90 | UD CFRP | 20000028 | row 11 |
| | G3__Ply13100 | 9313100 | 50 | -45 | UD CFRP | 20000028 | row 12 |
| Junction 4 | G4__Ply11100 | 9411100 | 150 | 0 | UD CFRP | 20000024 | row 13 |
| | G4__Ply12100 | 9412100 | 150 | 45 | UD CFRP | 20000024 | row 14 |
| | G4__Ply14100 | 9414100 | 150 | 90 | UD CFRP | 20000024 | row 15 |
| | G4__Ply13100 | 9413100 | 150 | -45 | UD CFRP | 20000024 | row 16 |
| Junction 5 | G5__Ply11100 | 9511100 | 50 | 0 | UD CFRP | 20000029 | row 17 |
| | G5__Ply12100 | 9512100 | 50 | 45 | UD CFRP | 20000029 | row 18 |
| | G5__Ply14100 | 9514100 | 50 | 90 | UD CFRP | 20000029 | row 19 |
| | G5__Ply13100 | 9513100 | 50 | -45 | UD CFRP | 20000029 | row 20 |
| Junction 6 | G6__Ply11100 | 9611100 | 600 | 0 | UD CFRP | 20000025 | row 21 |
| | G6__Ply12100 | 9612100 | 125 | 45 | UD CFRP | 20000025 | row 22 |
| | G6__Ply14100 | 9614100 | 125 | 90 | UD CFRP | 20000025 | row 23 |
| | G6__Ply13100 | 9613100 | 125 | -45 | UD CFRP | 20000025 | row 24 |
| Junction 7 | G7__Ply11100 | 9711100 | 50 | 0 | UD CFRP | 20000026 | row 25 |
| | G7__Ply12100 | 9712100 | 50 | 45 | UD CFRP | 20000026 | row 26 |
| | G7__Ply14100 | 9714100 | 50 | 90 | UD CFRP | 20000026 | row 27 |
| | G7__Ply13100 | 9713100 | 50 | -45 | UD CFRP | 20000026 | row 28 |
| Junction 8 | G8__Ply11100 | 9811100 | 600 | 0 | UD CFRP | 20000021 | row 29 |
| | G8__Ply12100 | 9812100 | 125 | 45 | UD CFRP | 20000021 | row 30 |
| | G8__Ply14100 | 9814100 | 125 | 90 | UD CFRP | 20000021 | row 31 |
| | G8__Ply13100 | 9813100 | 125 | -45 | UD CFRP | 20000021 | row 32 |
| Junction 9 | G9__Ply11100 | 9911100 | 50 | 0 | UD CFRP | 20000018 | row 33 |
| | G9__Ply12100 | 9912100 | 50 | 45 | UD CFRP | 20000018 | row 34 |
| | G9__Ply14100 | 9914100 | 50 | 90 | UD CFRP | 20000018 | row 35 |
| | G9__Ply13100 | 9913100 | 50 | -45 | UD CFRP | 20000018 | row 36 |
| Junction 10 | G10__Ply11100 | 9101110 | 600 | 0 | UD CFRP | 20000019 | row 37 |
| | G10__Ply12100 | 9101210 | 200 | 45 | UD CFRP | 20000019 | row 38 |
| | G10__Ply14100 | 9101410 | 100 | 90 | UD CFRP | 20000019 | row 39 |
| | G10__Ply13100 | 9101310 | 200 | -45 | UD CFRP | 20000019 | row 40 |

| | | | | | | |
|---|---|---|---|---|---|---|
| **Junction 11** | G11__Ply11100 | 9111110 | 100 | 0 | UD CFRP | 20000020 row 41 |
| | G11__Ply12100 | 9111210 | 50 | 45 | UD CFRP | 20000020 row 42 |
| | G11__Ply14100 | 9111410 | 50 | 90 | UD CFRP | 20000020 row 43 |
| | G11__Ply13100 | 9111310 | 50 | -45 | UD CFRP | 20000020 row 44 |
| **Junction 12** | G12__Ply11100 | 9121110 | 100 | 0 | UD CFRP | 20000027 row 45 |
| | G12__Ply12100 | 9121210 | 100 | 45 | UD CFRP | 20000027 row 46 |
| | G12__Ply14100 | 9121410 | 100 | 90 | UD CFRP | 20000027 row 47 |
| | G12__Ply13100 | 9121310 | 100 | -45 | UD CFRP | 20000027 row 48 |
| **Junction 13** | G13__Ply11100 | 9131110 | 100 | 0 | UD CFRP | 20000014 row 49 |
| | G13__Ply12100 | 9131210 | 100 | 45 | UD CFRP | 20000014 row 50 |
| | G13__Ply14100 | 9131410 | 100 | 90 | UD CFRP | 20000014 row 51 |
| | G13__Ply13100 | 9131310 | 100 | -45 | UD CFRP | 20000014 row 52 |
| **Tube 22** | T22__Ply11100 | 2211100 | 300 | 0 | UD CFRP | 20000006 row 53 |
| | T22__Ply11200 | 2211200 | 400 | 0 | UD CFRP | 20000030 row 54 |
| | T22__Ply12100 | 2212100 | 50 | 45 | UD CFRP | 20000006 row 55 |
| | T22__Ply12200 | 2212200 | 200 | 45 | UD CFRP | 20000030 row 56 |
| | T22__Ply14100 | 2214100 | 50 | 90 | UD CFRP | 20000006 row 57 |
| | T22__Ply14200 | 2214200 | 300 | 90 | UD CFRP | 20000030 row 58 |
| | T22__Ply13100 | 2213100 | 50 | -45 | UD CFRP | 20000006 row 59 |
| | T22__Ply13200 | 2213200 | 200 | -45 | UD CFRP | 20000030 row 60 |
| | TS22__Ply13200 | 52213200 | 200 | -45 | UD CFRP | 20000030 row 61 |
| | TS22__Ply13100 | 52213100 | 50 | -45 | UD CFRP | 20000006 row 62 |
| | TS22__Ply14200 | 52214200 | 300 | 90 | UD CFRP | 20000030 row 63 |
| | TS22__Ply14100 | 52214100 | 50 | 90 | UD CFRP | 20000006 row 64 |
| | TS22__Ply12200 | 52212200 | 200 | 45 | UD CFRP | 20000030 row 65 |
| | TS22__Ply12100 | 52212100 | 50 | 45 | UD CFRP | 20000006 row 66 |
| | TS22__Ply11200 | 52211200 | 400 | 0 | UD CFRP | 20000030 row 67 |
| | TS22__Ply11100 | 52211100 | 300 | 0 | UD CFRP | 20000006 row 68 |
| **Tube 52** | T52__Ply11100 | 5211100 | 50 | 0 | UD CFRP | 20000008 row 69 |
| | T52__Ply11200 | 5211200 | 150 | 0 | UD CFRP | 20000016 row 70 |
| | T52__Ply12100 | 5212100 | 50 | 45 | UD CFRP | 20000008 row 71 |
| | T52__Ply14100 | 5214100 | 50 | 90 | UD CFRP | 20000008 row 72 |
| | T52__Ply13100 | 5213100 | 50 | -45 | UD CFRP | 20000008 row 73 |
| | TS52__Ply13100 | 55213100 | 50 | -45 | UD CFRP | 20000008 row 74 |
| | TS52__Ply14100 | 55214100 | 50 | 90 | UD CFRP | 20000008 row 75 |
| | TS52__Ply12100 | 55212100 | 50 | 45 | UD CFRP | 20000008 row 76 |
| | TS52__Ply11200 | 55211200 | 150 | 0 | UD CFRP | 20000016 row 77 |
| | TS52__Ply11100 | 55211100 | 50 | 0 | UD CFRP | 20000008 row 78 |
| **Tube 62** | T62__Ply11100 | 6211100 | 150 | 0 | UD CFRP | 20000007 row 79 |
| | T62__Ply12100 | 6212100 | 50 | 45 | UD CFRP | 20000007 row 80 |
| | T62__Ply14100 | 6214100 | 50 | 90 | UD CFRP | 20000007 row 81 |
| | T62__Ply13100 | 6213100 | 50 | -45 | UD CFRP | 20000007 row 82 |
| | TS62__Ply13100 | 56213100 | 50 | -45 | UD CFRP | 20000007 row 83 |
| | TS62__Ply14100 | 56214100 | 50 | 90 | UD CFRP | 20000007 row 84 |
| | TS62__Ply12100 | 56212100 | 50 | 45 | UD CFRP | 20000007 row 85 |
| | TS62__Ply11100 | 56211100 | 150 | 0 | UD CFRP | 20000007 row 86 |

| | | | | | | | |
|---|---|---|---|---|---|---|---|
| | T10__Ply11100 | 1011100 | 50 | 0 | UD CFRP | 20000004 | row 87 |
| | T10__Ply12100 | 1012100 | 50 | 45 | UD CFRP | 20000004 | row 88 |
| | T10__Ply14100 | 1014100 | 50 | 90 | UD CFRP | 20000004 | row 89 |
| | T10__Ply13100 | 1013100 | 50 | -45 | UD CFRP | 20000004 | row 90 |
| | T10__Ply12200 | 1012200 | 100 | 45 | UD CFRP | 20000032 | row 91 |
| | T10__Ply13200 | 1013200 | 100 | -45 | UD CFRP | 20000032 | row 92 |
| | T10__Ply11200 | 1011200 | 150 | 0 | UD CFRP | 20000013 | row 93 |
| | T10__Ply14200 | 1014200 | 125 | 90 | UD CFRP | 20000032 | row 94 |
| | T10__Ply12300 | 1012300 | 50 | 45 | UD CFRP | 20000035 | row 95 |
| | T10__Ply13300 | 1013300 | 50 | -45 | UD CFRP | 20000035 | row 96 |
| | T10__Ply11300 | 1011300 | 100 | 0 | UD CFRP | 20000035 | row 97 |
| | T10__Ply12400 | 1012400 | 50 | 45 | UD CFRP | 20000037 | row 98 |
| | T10__Ply13400 | 1013400 | 50 | -45 | UD CFRP | 20000037 | row 99 |
| Tube 10 | T10__Ply14300 | 1014300 | 50 | 90 | UD CFRP | 20000035 | row 100 |
| | TS10__Ply14300 | 51014300 | 50 | 90 | UD CFRP | 20000035 | row 101 |
| | TS10__Ply13400 | 51013400 | 50 | -45 | UD CFRP | 20000037 | row 102 |
| | TS10__Ply12400 | 51012400 | 50 | 45 | UD CFRP | 20000037 | row 103 |
| | TS10__Ply11300 | 51011300 | 100 | 0 | UD CFRP | 20000035 | row 104 |
| | TS10__Ply13300 | 51013300 | 50 | -45 | UD CFRP | 20000035 | row 105 |
| | TS10__Ply12300 | 51012300 | 50 | 45 | UD CFRP | 20000035 | row 106 |
| | TS10__Ply14200 | 51014200 | 125 | 90 | UD CFRP | 20000032 | row 107 |
| | TS10__Ply11200 | 51011200 | 150 | 0 | UD CFRP | 20000013 | row 108 |
| | TS10__Ply13200 | 51013200 | 100 | -45 | UD CFRP | 20000032 | row 109 |
| | TS10__Ply12200 | 51012200 | 100 | 45 | UD CFRP | 20000032 | row 110 |
| | TS10__Ply13100 | 51013100 | 50 | -45 | UD CFRP | 20000004 | row 111 |
| | TS10__Ply14100 | 51014100 | 50 | 90 | UD CFRP | 20000004 | row 112 |
| | TS10__Ply12100 | 51012100 | 50 | 45 | UD CFRP | 20000004 | row 113 |
| | TS10__Ply11100 | 51011100 | 50 | 0 | UD CFRP | 20000004 | row 114 |
| | T11__Ply11100 | 1111100 | 50 | 0 | UD CFRP | 20000005 | row 115 |
| | T11__Ply12100 | 1112100 | 50 | 45 | UD CFRP | 20000005 | row 116 |
| | T11__Ply14100 | 1114100 | 50 | 90 | UD CFRP | 20000005 | row 117 |
| | T11__Ply13100 | 1113100 | 50 | -45 | UD CFRP | 20000005 | row 118 |
| | T11__Ply12200 | 1112200 | 100 | 45 | UD CFRP | 20000033 | row 119 |
| | T11__Ply13200 | 1113200 | 100 | -45 | UD CFRP | 20000033 | row 120 |
| | T11__Ply11200 | 1111200 | 150 | 0 | UD CFRP | 20000015 | row 121 |
| | T11__Ply14200 | 1114200 | 100 | 90 | UD CFRP | 20000033 | row 122 |
| | T11__Ply12300 | 1112300 | 50 | 45 | UD CFRP | 20000036 | row 123 |
| | T11__Ply13300 | 1113300 | 50 | -45 | UD CFRP | 20000036 | row 124 |
| | T11__Ply11300 | 1111300 | 200 | 0 | UD CFRP | 20000036 | row 125 |
| | T11__Ply12400 | 1112400 | 50 | 45 | UD CFRP | 20000038 | row 126 |
| | T11__Ply13400 | 1113400 | 50 | -45 | UD CFRP | 20000038 | row 127 |
| Tube 11 | T11__Ply14300 | 1114300 | 50 | 90 | UD CFRP | 20000036 | row 128 |
| | TS11__Ply14300 | 51114300 | 50 | 90 | UD CFRP | 20000036 | row 129 |
| | TS11__Ply13400 | 51113400 | 50 | -45 | UD CFRP | 20000038 | row 130 |
| | TS11__Ply12400 | 51112400 | 50 | 45 | UD CFRP | 20000038 | row 131 |
| | TS11__Ply11300 | 51111300 | 200 | 0 | UD CFRP | 20000036 | row 132 |
| | TS11__Ply13300 | 51113300 | 50 | -45 | UD CFRP | 20000036 | row 133 |
| | TS11__Ply12300 | 51112300 | 50 | 45 | UD CFRP | 20000036 | row 134 |
| | TS11__Ply14200 | 51114200 | 100 | 90 | UD CFRP | 20000033 | row 135 |
| | TS11__Ply11200 | 51111200 | 150 | 0 | UD CFRP | 20000015 | row 136 |
| | TS11__Ply13200 | 51113200 | 100 | -45 | UD CFRP | 20000033 | row 137 |
| | TS11__Ply12200 | 51112200 | 100 | 45 | UD CFRP | 20000033 | row 138 |
| | TS11__Ply13100 | 51113100 | 50 | -45 | UD CFRP | 20000005 | row 139 |
| | TS11__Ply14100 | 51114100 | 50 | 90 | UD CFRP | 20000005 | row 140 |
| | TS11__Ply12100 | 51112100 | 50 | 45 | UD CFRP | 20000005 | row 141 |
| | TS11__Ply11100 | 51111100 | 50 | 0 | UD CFRP | 20000005 | row 142 |

| | | | | | | | |
|---|---|---|---|---|---|---|---|
| | T32__Ply11100 | 3211100 | 300 | 0 | UD CFRP | 20000009 | row 143 |
| | T32__Ply11200 | 3211200 | 600 | 0 | UD CFRP | 20000017 | row 144 |
| | T32__Ply11300 | 3211300 | 300 | 0 | UD CFRP | 20000031 | row 145 |
| | T32__Ply12100 | 3212100 | 150 | 45 | UD CFRP | 20000009 | row 146 |
| | T32__Ply12300 | 3212300 | 50 | 45 | UD CFRP | 20000031 | row 147 |
| | T32__Ply14100 | 3214100 | 50 | 90 | UD CFRP | 20000009 | row 148 |
| | T32__Ply14200 | 3214200 | 600 | 90 | UD CFRP | 20000034 | row 149 |
| | T32__Ply14300 | 3214300 | 200 | 90 | UD CFRP | 20000031 | row 150 |
| | T32__Ply13100 | 3213100 | 150 | -45 | UD CFRP | 20000009 | row 151 |
| Tube 32 | T32__Ply13300 | 3213300 | 50 | -45 | UD CFRP | 20000031 | row 152 |
| | TS32__Ply13300 | 53213300 | 50 | -45 | UD CFRP | 20000031 | row 153 |
| | TS32__Ply13100 | 53213100 | 150 | -45 | UD CFRP | 20000009 | row 154 |
| | TS32__Ply14300 | 53214300 | 200 | 90 | UD CFRP | 20000031 | row 155 |
| | TS32__Ply14200 | 53214200 | 600 | 90 | UD CFRP | 20000034 | row 156 |
| | TS32__Ply14100 | 53214100 | 50 | 90 | UD CFRP | 20000009 | row 157 |
| | TS32__Ply12300 | 53212300 | 50 | 45 | UD CFRP | 20000031 | row 158 |
| | TS32__Ply12100 | 53212100 | 150 | 45 | UD CFRP | 20000009 | row 159 |
| | TS32__Ply11300 | 53211300 | 300 | 0 | UD CFRP | 20000031 | row 160 |
| | TS32__Ply11200 | 53211200 | 600 | 0 | UD CFRP | 20000017 | row 161 |
| | TS32__Ply11100 | 53211100 | 300 | 0 | UD CFRP | 20000009 | row 162 |
| | T70__Ply11100 | 7011100 | 50 | 0 | UD CFRP | 20000012 | row 163 |
| | T70__Ply12100 | 7012100 | 50 | 45 | UD CFRP | 20000012 | row 164 |
| | T70__Ply14100 | 7014100 | 50 | 90 | UD CFRP | 20000012 | row 165 |
| Part 70 | T70__Ply13100 | 7013100 | 50 | -45 | UD CFRP | 20000012 | row 166 |
| | TS70__Ply13100 | 57013100 | 50 | -45 | UD CFRP | 20000012 | row 167 |
| | TS70__Ply14100 | 57014100 | 50 | 90 | UD CFRP | 20000012 | row 168 |
| | TS70__Ply12100 | 57012100 | 50 | 45 | UD CFRP | 20000012 | row 169 |
| | TS70__Ply11100 | 57011100 | 50 | 0 | UD CFRP | 20000012 | row 170 |
| | T40__Ply11100 | 4011100 | 50 | 0 | UD CFRP | 20000011 | row 171 |
| | T40__Ply12100 | 4012100 | 50 | 45 | UD CFRP | 20000011 | row 172 |
| | T40__Ply14100 | 4014100 | 50 | 90 | UD CFRP | 20000011 | row 173 |
| Tube 40 | T40__Ply13100 | 4013100 | 50 | -45 | UD CFRP | 20000011 | row 174 |
| | TS40__Ply13100 | 54013100 | 50 | -45 | UD CFRP | 20000011 | row 175 |
| | TS40__Ply14100 | 54014100 | 50 | 90 | UD CFRP | 20000011 | row 176 |
| | TS40__Ply12100 | 54012100 | 50 | 45 | UD CFRP | 20000011 | row 177 |
| | TS40__Ply11100 | 54011100 | 50 | 0 | UD CFRP | 20000011 | row 178 |
| | T41__Ply11100 | 4111100 | 125 | 0 | UD CFRP | 20000010 | row 179 |
| | T41__Ply12100 | 4112100 | 50 | 45 | UD CFRP | 20000010 | row 180 |
| | T41__Ply14100 | 4114100 | 50 | 90 | UD CFRP | 20000010 | row 181 |
| Tube 41 | T41__Ply13100 | 4113100 | 50 | -45 | UD CFRP | 20000010 | row 182 |
| | TS41__Ply13100 | 54113100 | 50 | -45 | UD CFRP | 20000010 | row 183 |
| | TS41__Ply14100 | 54114100 | 50 | 90 | UD CFRP | 20000010 | row 184 |
| | TS41__Ply12100 | 54112100 | 50 | 45 | UD CFRP | 20000010 | row 185 |
| | TS41__Ply11100 | 54111100 | 125 | 0 | UD CFRP | 20000010 | row 186 |
| | Seat_skin1of2 | 2000001 | 150 | 0/90 | Fabric CFRP | 20000003 | row 187 |
| Seat | Seat_core | 2000003 | | | 6mm PVC | 20000003 | row 188 |
| | Seat_skin2of2 | 2000002 | 150 | 0/90 | Fabric CFRP | 20000003 | row 189 |

**Table 3.4**: Description of the final laminate.

Some of the plies that make the same tube and that are one after the other in the table above are not always adjacent because they can cover different areas. The ply covering area is specified by the covering area ID. The same consideration is valid for the tubes that are one after the other in the table above. For example, all the junctions are never adjacent to each other.

# 4. FINAL TESTS OF THE NEW FRAME PROPOSAL AND COMPARISON WITH TAURUS

This chapter is dedicated to the final tests of the new frame proposal designed in the previous chapter. This part is crucial to verify the achievement of the objectives. The objectives that had been imposed on the new frame are the halving of the mass and the increase of the stiffness compared to the Taurus frame. In order to perform a fair comparison, the final tests have been conducted using the same subcases used to analyze Taurus.

## 4.1 Static tests

The static tests conducted in this section are identical to those used in Chapter 2. The loaded nodes have the same ID numbers and the same position of those used for Taurus. For this reason, also the applied forces have the same directions and magnitudes of those used for Taurus. Moreover, the constrained nodes have the same ID numbers and the same positions, except for the dropouts that have only a change in position (Fig. 4.1).
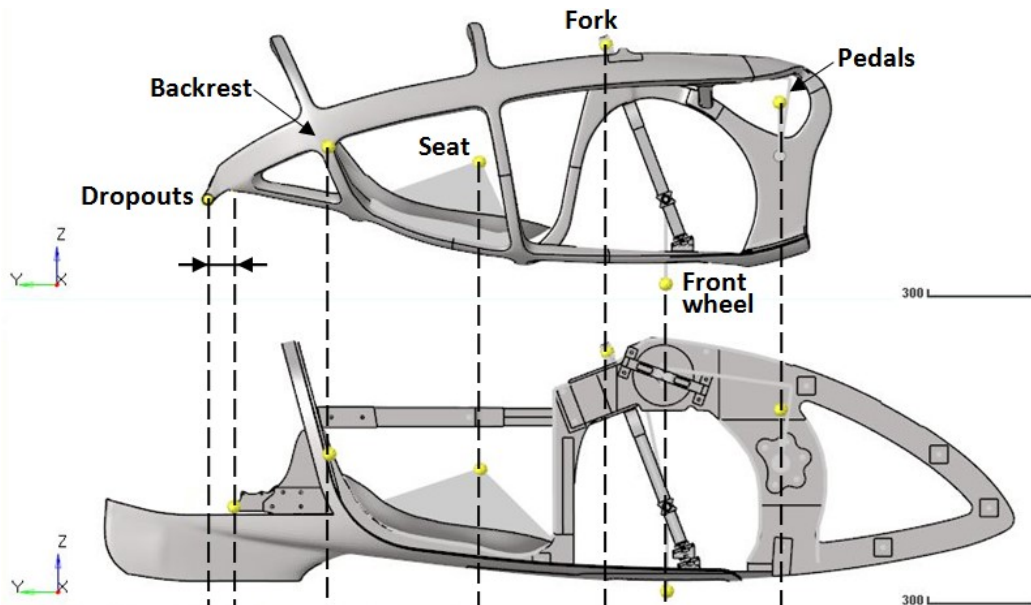


**Figure 4.1**: Comparing the loaded and constrained nodes of the new frame with those of the Taurus frame.

There will follow a first part dedicated to the pre-processing phase, which is valid for all the static subcases, and then a dedicated post-processing phase per each subcase.

*Pre-Processing*

Compared to those in Taurus, the applied forces and the global constraints are unchanged, but we have to use the frame obtained at the end of the shuffle optimization. In order to calculate the correct failure

indexes, we need to define the laminate through one STACK card, as done until the end of the size optimization. A shuffle optimization changes only the stacking sequence of the plies, therefore we have used the FE model obtained at the end of the size optimization and reorganized the plies as indicated by the results of the shuffle optimization. The FE model that was obtained from these modifications is contained in the include 'INC_TELAIO_AleB .fem'. The input file used to run the three static subcases recalls the includes 'INC_TELAIO_AleB .fem' and 'INC_TRASMISSIONE_SIMULACRO_PLUS.fem '. The latter contains the transmission that was described in Section 3.2.3.

*Post-Processing*

In the post-processing phase, as done for the Taurus frame, for each subcase we will evaluate:

- the reaction forces,
- the interacting forces inside the transmission,
- the displacements due to deformations, and the stiffness,
- the stress, strain and failure index distributions.

The results obtained for each subcase are shown below.

### 4.1.1 Subcase 1

*Constraint reactions and global equilibrium check*

| | Node id | SUBCASE 1: Applied forces (in global system) | | |
| --- | --- | --- | --- | --- |
| | | Fx [N] | Fy [N] | Fz [N] |
| **Right pedal** | 2 | 0,0 | 0,0 | 0,0 |
| **Left pedal** | 3 | 0,0 | 0,0 | 0,0 |
| **Seat** | 9 | 0,0 | 0,0 | -687,0 |
| **Backrest** | 10 | 0,0 | 0,0 | 0,0 |
| **TOT** | | 0,0 | 0,0 | -687,0 |

**Table 4.1**: Applied forces in global system for Subcase 1.

| | Node id | SUBCASE 1: Reaction forces (in global system) | | | | | |
| --- | --- | --- | --- | --- | --- | --- | --- |
| | | RFx [N] | RFy [N] | RFz [N] | RMx [Nm] | RMy [Nm] | RMz [Nm] |
| **Front wheel** | 1 | 0,0 | 0,0 | 407,3 | 0,0 | 0,0 | 0,0 |
| **Fork** | 4 | 0,0 | 0,0 | 0,0 | 0,0 | 0,0 | 0,0 |
| **Left bike dropout** | 20059 | 54,3 | -2,2 | 140,6 | 0,0 | -1,1 | 1,2 |
| **Right bike dropout** | 20060 | -54,3 | 2,2 | 139,1 | 0,0 | 1,2 | -1,0 |
| **TOT** | | 0,0 | 0,0 | 687,0 | 0,0 | 0,1 | 0,2 |

**Table 4.2**: Reaction forces in global system for Subcase 1.

The global equilibrium along X, Y and Z-axes is verified since the constraint reactions are equal and opposite to the applied forces in every direction. The equilibrium of the moments is verified by Equations 2.1, 2.2, and 2.3. The constraint reactions on the fork are null as no force is applied on the pedals.

*Transmission forces*

In this subcase there are no applied forces on the pedals, so there are no internal forces in the transmission.

*Deformations*

In this subcase the frame bends downwards and rotates around the rear bike dropouts (*C* in Fig. 4.2), while the fork bends moving forward (*D* in Fig. 4.2). As a first approach, the following image shows the plotel elements in red for the initial condition, and in blue for the final condition, with deformation view amplified by 100 times so as to see the global behavior.
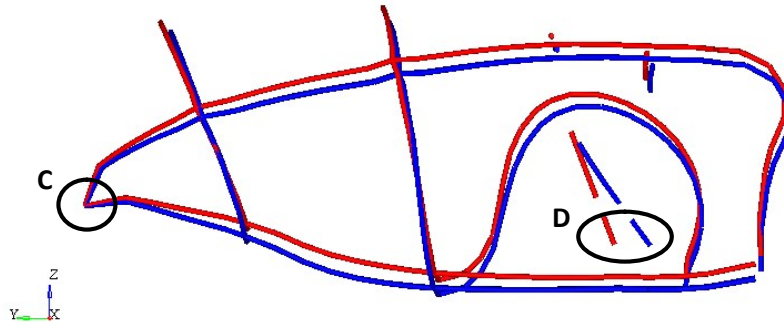


**Figure 4.2**: Plotel elements before (red) and after (blue) load application for Subcase 1.

The deformation of the frame is manly symmetrical between the left and the right side, but the asymmetry of the fork and the fork-guide induces a slight asymmetry in the global deformations. This observation is made clearer by the graphs in Figure 4.7 and 4.8, which show the Z-displacements of the nodes belonging to the plotel elements (Fig. 4.5 and 4.6). The plotel elements and their relative graph have the same color to simplify viewing, and each node ID is listed in the key (Fig. 4.5 to Fig. 4.8).
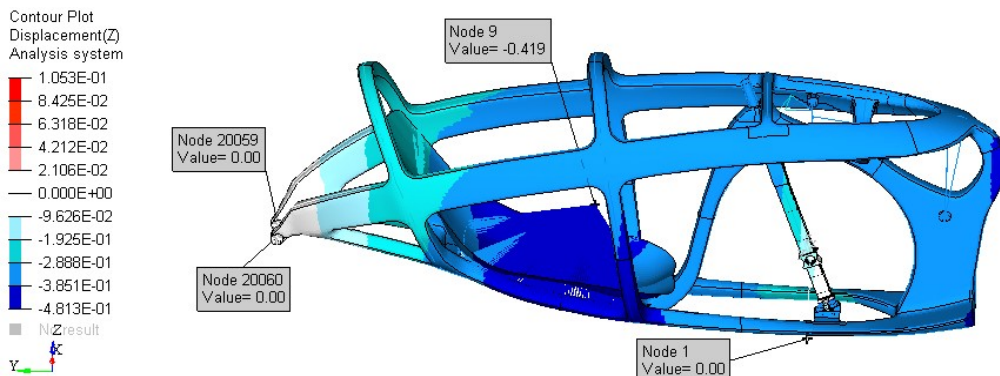


**Figure 4.3**: Z-displacements in global system for Subcase 1. Right view. Scale in mm.
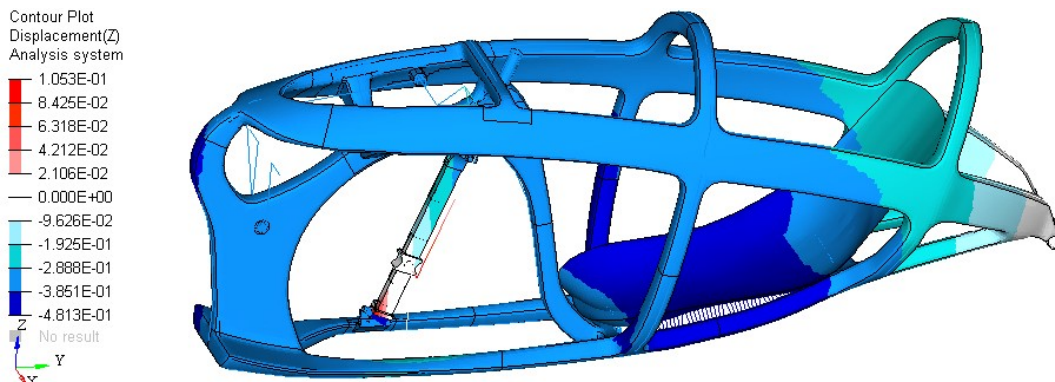


**Figure 4.4**: Z-displacements in global system for Subcase 1. Left view. Scale in mm.
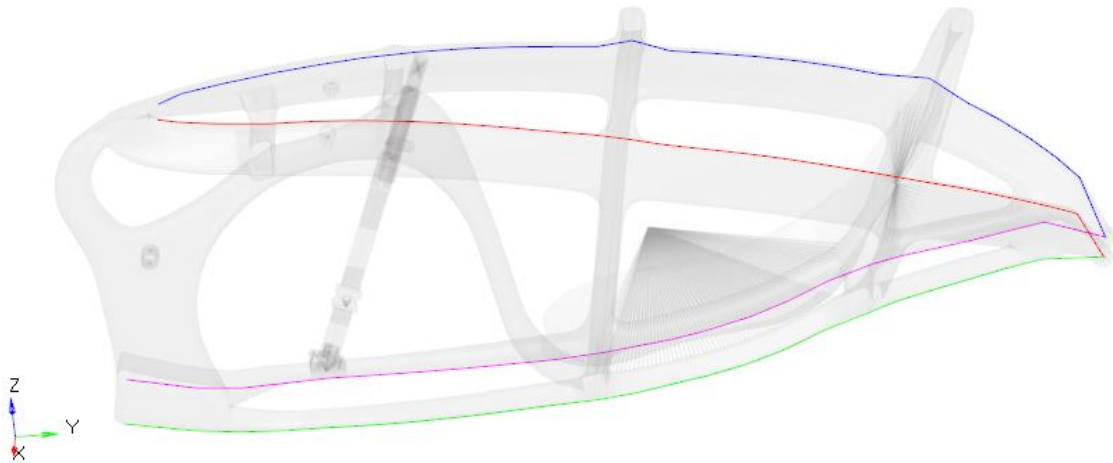
**Figure 4.5**: Position of the plotel elements on the frame.
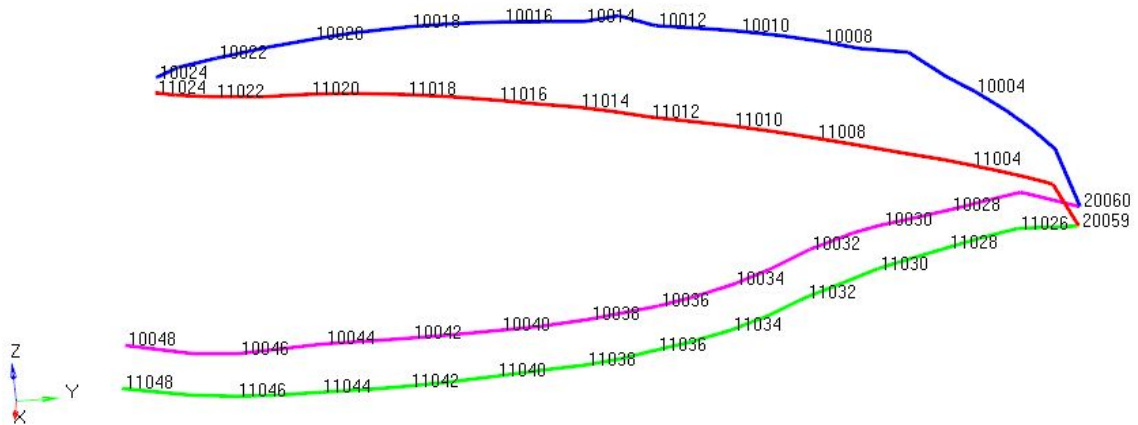


**Figure 4.6**: Plotel elements. Only the ID of some nodes of the series are shown.
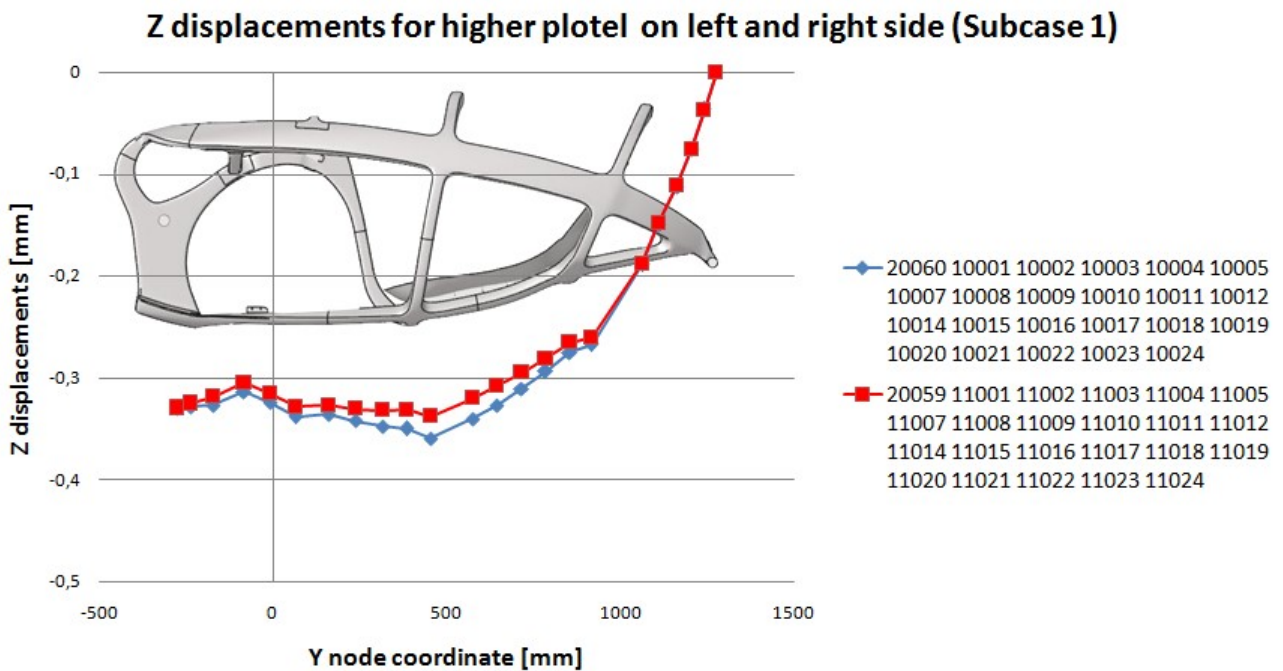


**Figure 4.7**: Z-displacements in global system of plotel nodes for Subcase 1.
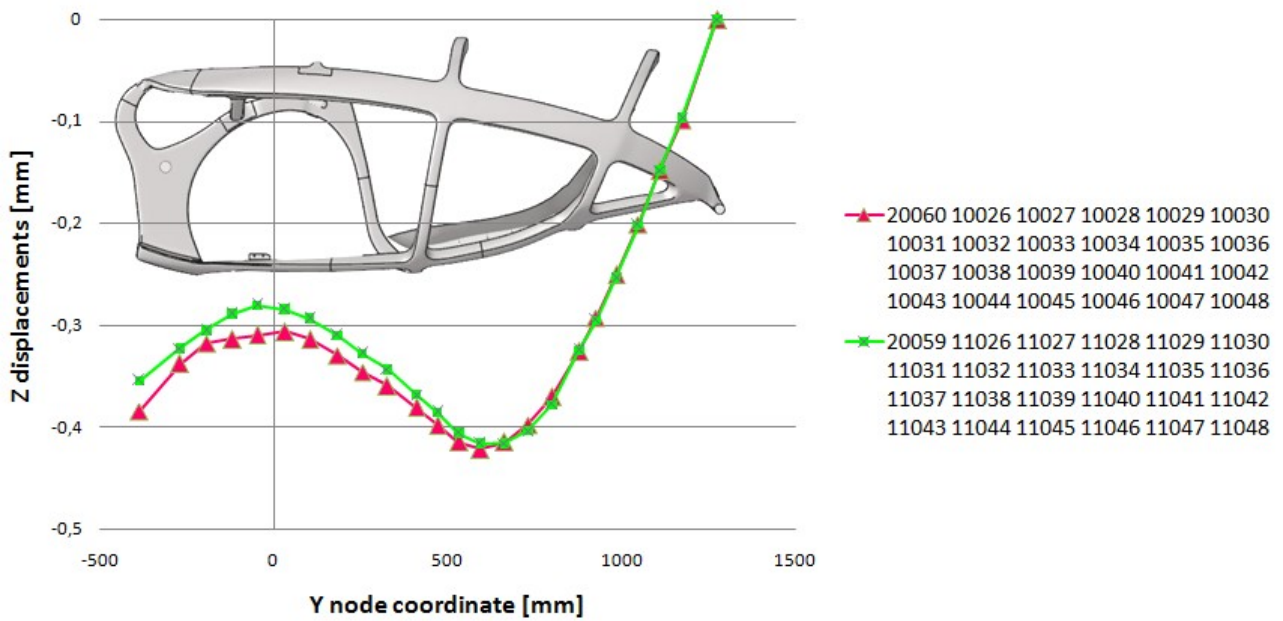
**Figure 4.8**: Z-displacements in global system of plotel nodes for Subcase 1.

This slightly asymmetrical condition between the left and right side causes a rotation around the Y-axis. The rotation around the Y-axis is visible from the deformation in the X-direction, in which the upper part has negative values (blue in Fig. 4.9 and 4.10) and the bottom part and the seat have values almost equal to zero (white in Fig. 4.9 and 4.10).
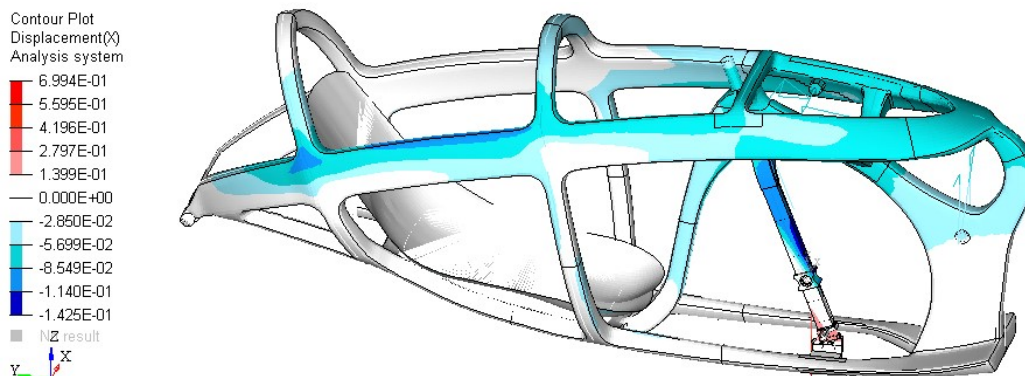


**Figure 4.9**: X-displacements in global system for Subcase 1. Right view. Scale in mm.
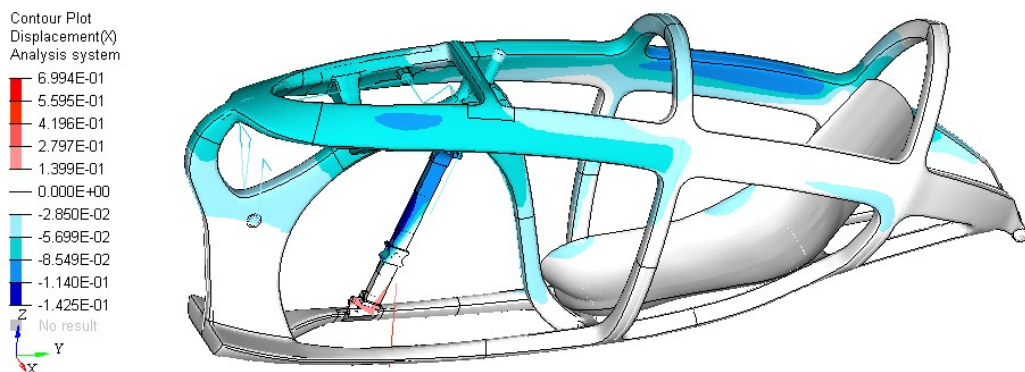


**Figure 4.10**: X-displacements in global system for Subcase 1. Left view. Scale in mm.

From the Y-displacements we can notice that the fork bends moving forward (blue in Fig. 4.11 and 4.12) and that the frame, which rotates around the rear dropouts, does not show relevant displacements along Y-axis (white in Fig. 4.11 and 4.12).
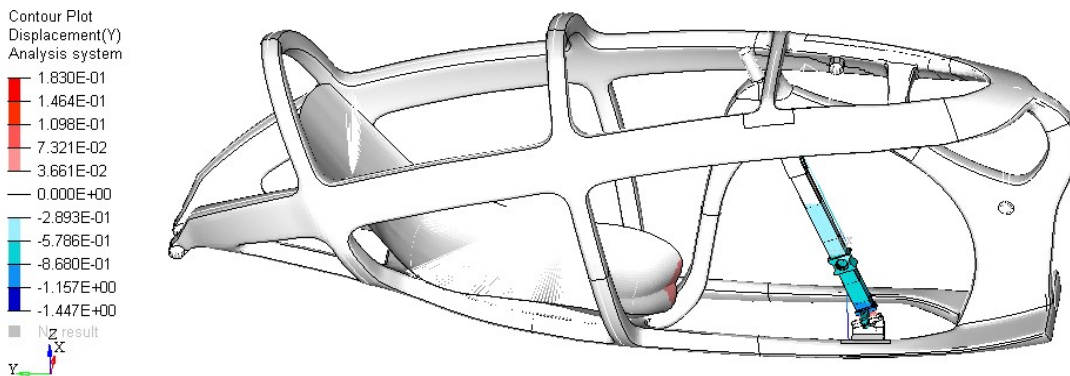


**Figure 4.11**: Y-displacements in global system for Subcase 1. Right view. Scale in mm.
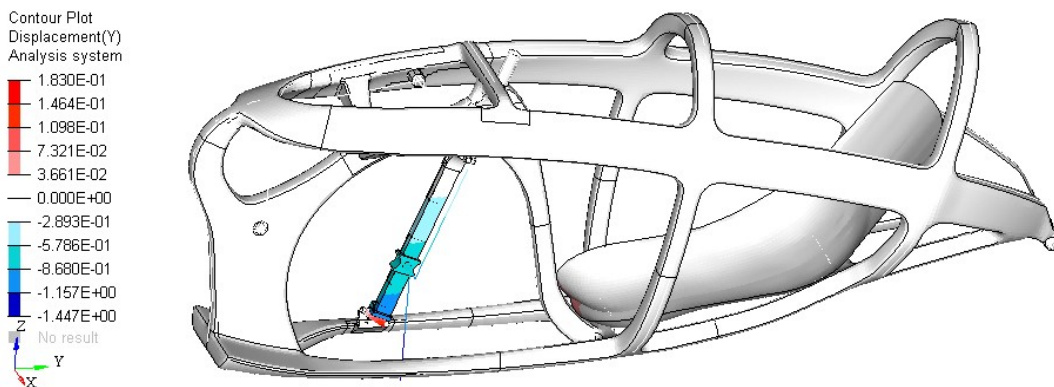


**Figure 4.12**: Y-displacements in global system for Subcase 1. Left view. Scale in mm.

The relative displacements between the bottom of the fork and the frame are so small that the guide bearings of the fork do not leave the rail that is attached to the frame (Fig. 4.13). In Figure 4.13 there is no view amplification factor and the red lines represent the condition of the unloaded frame.
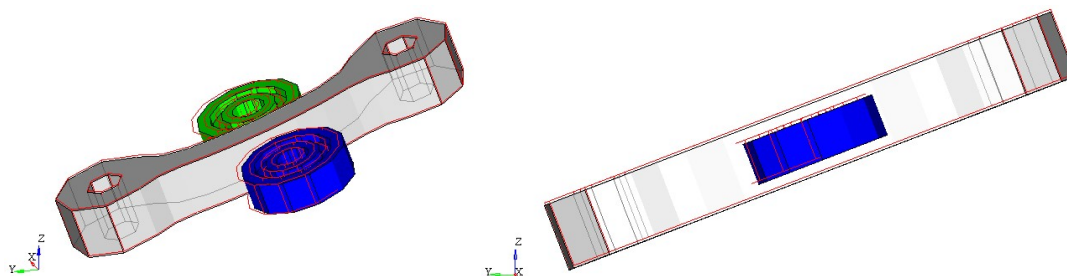


**Figure 4.13**: Guide bearings and rail of the fork during load application for Subcase 1. The red lines are for when unloaded.

*Stiffness and displacement of seat loading point*

In the loading point there is a displacement of -0.419 mm in Z (Fig. 4.3) and the loading force is -687 N in Z (Tab. 4.1), so the local static stiffness of the loading point is:

$$K_{z,9} = \frac{F_{z,9}}{displ_{z,9}} = 1640 \; N/mm$$

*Stress, strain e failure index*

The contour plots in Figure 4.14 and 4.15 show the maximum stress and strain values in the laminate. We can notice that the bottom-bracket zone is not stressed because no load is applied on the pedals. Since these contour plots cannot show us where the material could break, Figure 4.16 shows the maximum failure indexes of the laminate, and Figure 4.17 shows the ply in which these maximum failure indexes are present by means of the ply ID number. The highest composite failure index is on the frame (ply ID = 6213100) and it is equal to 0.025.
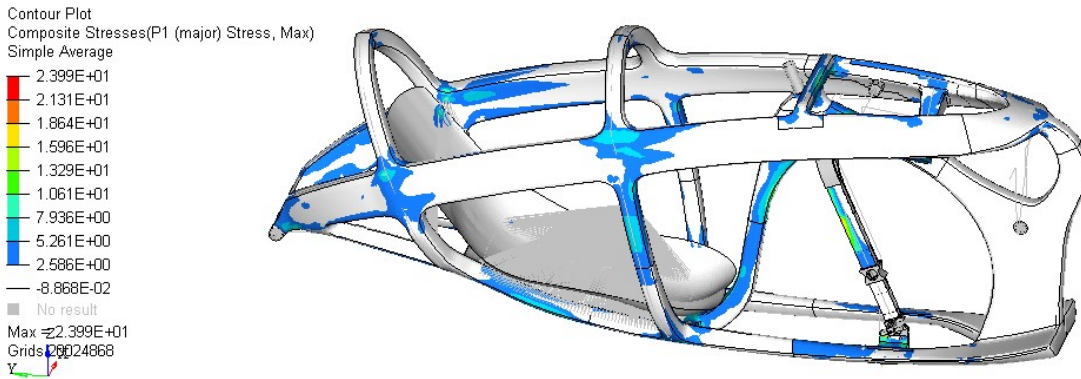


**Figure 4.14**: P1 max stresses for Subcase 1. Scale in MPa.
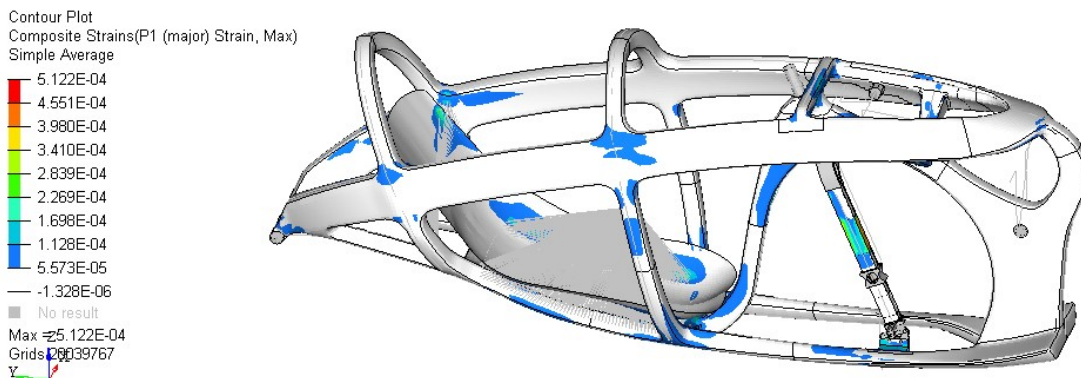


**Figure 4.15**: P1 max strains for Subcase 1. Scale in MPa.
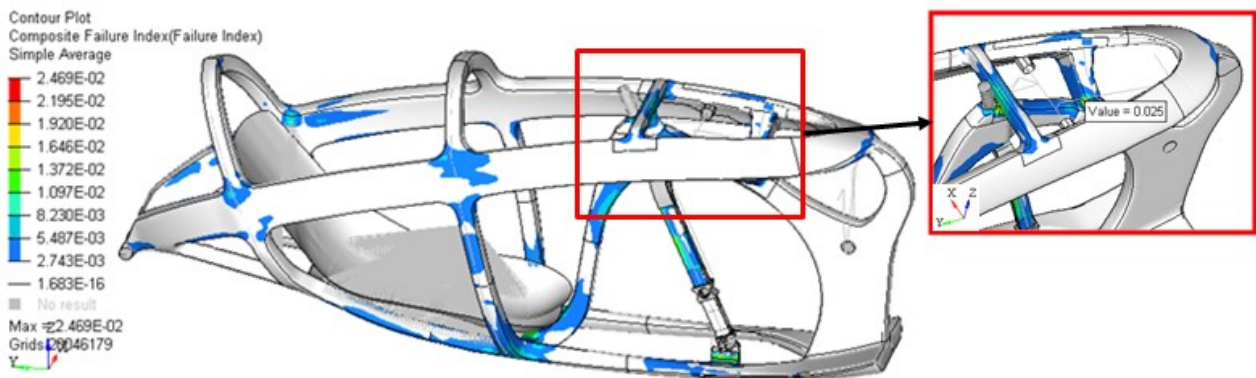


**Figure 4.16**: Maximum composite failure indexes for Subcase 1.
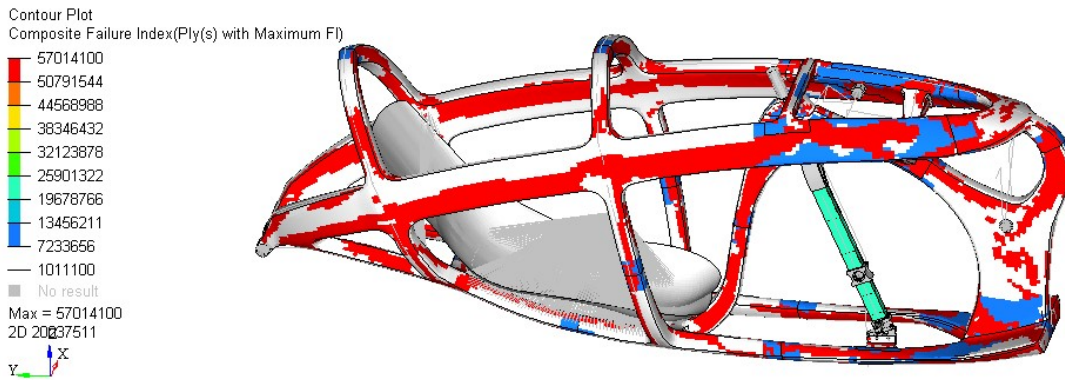
**Figure 4.17**: Ply ID in which there is the maximum failure index for Subcase 1.

## 4.1.2 Subcase 2

*Constraint reactions and global equilibrium check*

| | Node id | SUBCASE 2: Applied forces (in global system) | | |
|---|---|---|---|---|
| | | Fx [N] | Fy [N] | Fz [N] |
| **Right pedal** | 2 | -55,2 | -694,4 | 68,7 |
| **Left pedal** | 3 | 0,0 | 0,0 | 0,0 |
| **Seat** | 9 | 0,0 | 0,0 | -687,0 |
| **Backrest** | 10 | 55,2 | 694,4 | -68,7 |
| **TOT** | | 0,0 | 0,0 | -687,0 |

**Table 4.3**: Applied forces in global system for Subcase 2.

| | Node id | SUBCASE 2: Reaction forces (in global system) | | | | | |
|---|---|---|---|---|---|---|---|
| | | RFx [N] | RFy [N] | RFz [N] | RMx [Nm] | RMy [Nm] | RMz [Nm] |
| **Front wheel** | 1 | 0,0 | 0,0 | 407,3 | 0,0 | 0,0 | 0,0 |
| **Fork** | 4 | 0,0 | 0,0 | 0,0 | 0,0 | 0,0 | 0,0 |
| **Left bike dropout** | 20059 | 60,1 | 7,4 | 171,0 | 0,0 | 0,9 | 0,5 |
| **Right bike dropout** | 20060 | -60,1 | -7,4 | 108,8 | 0,0 | 1,5 | -1,1 |
| **TOT** | | 0,0 | 0,0 | 687,0 | 0,0 | 2,4 | -0,6 |

**Table 4.4**: Reaction forces in global system for Subcase 2.

The global equilibrium along X, Y and Z-axes is verified since the constraint reactions are equal and opposite to the applied forces in every direction. The equilibrium of the moments is verified by Equations 2.1, 2.2 and 2.3. The constraint reactions on the fork are null because the chain – and as a consequence also the force $F_{5009}$ – is parallel to the fork-axis with enough precision to make the reaction-moment around the fork-axis irrelevant (Fig. 4.19.b). This result proves that the added sprocket fulfilled its function.

*Transmission forces*

In Subcase 2 we apply a force on the right pedal (node ID=2), so we have forces inside the transmission. In Figure 4.18 and 4.19.a there is the free-body diagram of some parts of the transmission, and in Table 4.5 their numerical values.

| SUBCASE 2 | | | |
|---|---|---|---|
| Node Id | Fx [N] | Fy [N] | Fz [N] |
| 2 | -55,19 | -694,40 | 68,67 |
| 3 | 0,00 | 0,00 | 0,00 |
| 5001 | -0,02 | -53,22 | -138,60 |
| 5002 | 0,53 | 472,60 | 65,56 |
| 5003 | 0,02 | -83,79 | 123,20 |
| 5005 | -0,53 | -472,60 | -65,56 |
| 5009 | 0,02 | 53,22 | 138,60 |
| 5011 | -0,02 | 83,79 | -123,20 |
| 5014 | 25,86 | 1059,00 | -92,99 |
| 5015 | 28,80 | -836,70 | -41,24 |
| 5019 | 8,79 | 94,93 | 105,10 |
| 5020 | 0,01 | 137,00 | 15,40 |
| 5021 | -8,24 | 293,90 | 83,71 |

Table 4.5: Forces inside the transmission for Subcase 2.
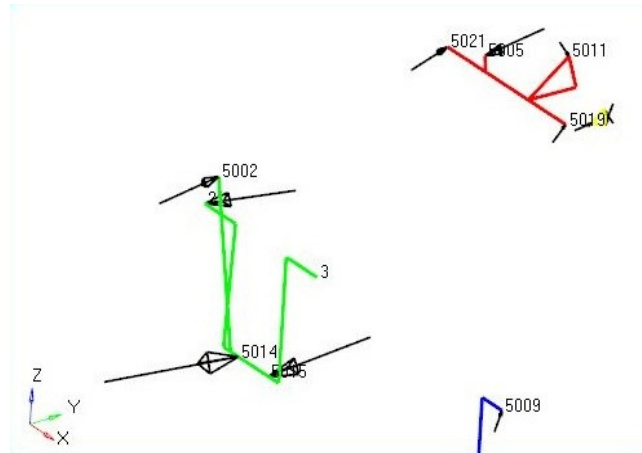


Figure 4.18: Free-body diagram of the transmission elements for Subcase 2.
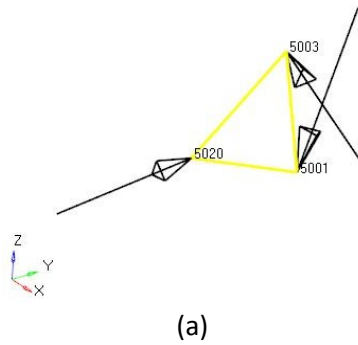


(a)
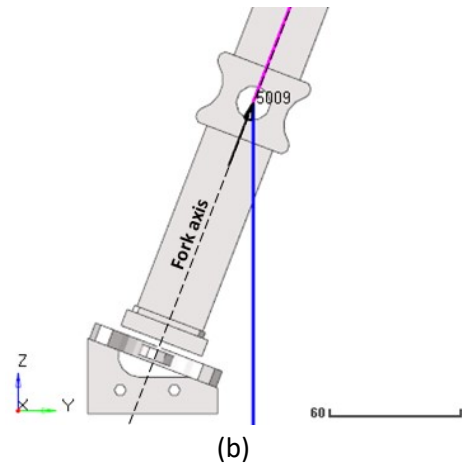


(b)

Figure 4.19: (a) Zoom on the free-body diagram of the added sprocket. (b) Details about the direction of the force F$_{5009}$ in relation to the fork axis.

Compared to those in Taurus, the ID numbers of the nodes of the pedals and of the first chainring (green in Fig. 4.18) are unchanged, therefore we used Equation 2.4 to check the forces equilibrium, and Equations 2.6, 2.8, 2.10 to check the moments equilibrium. The sprocket-set nodes have been re-numbered, therefore we used Equation 4.1 to check the forces equilibrium, and Equations 4.3, 4.5, 4.7 to check the moments equilibrium. The added sprocket is connected to the frame through a Rigid Node-Node that follows the Type-1 modeling and that has the locked DOF 1, 2, 3, 5, 6, in order to allow only the rotation around its axis. For this reason, the values of $RM_y$ and $RM_z$ in Nodes 5020 and 20061 are different from zero, even if they are very low. The other rigid elements that have been used to connect the transmission to the frame are unchanged and have the DOF 1, 2, 3, locked (see Section 2.2.2). The global equilibrium of the added sprocket has been checked by Equation 4.2 for the forces, and by Equations 4.4, 4.6, 4.8 for the moments.

$$F_{5005} + F_{5011} + F_{5019} + F_{5021} = 0 \ N \tag{4.1}$$

$$F_{5001} + F_{5003} + F_{5020} = 0 \ N \tag{4.2}$$

Equilibrium check of moments around X-axis passing through Node 1:

$$\sum_{k\in\{5005,5011,5019,5021\}} \left(-F_{y,k} \cdot coord_{z,k} + F_{z,k} \cdot coord_{y,k}\right) = 0 \; Nm \tag{4.3}$$

$$\sum_{k\in\{5001,5003,5020\}} \left(-F_{y,k} \cdot coord_{z,k} + F_{z,k} \cdot coord_{y,k}\right) = 0 \; Nm \tag{4.4}$$

Equilibrium check of moments around Y-axis passing through Node 1:

$$\sum_{k\in\{5005,5011,5019,5021\}} \left(F_{x,k} \cdot coord_{z,k} - F_{z,k} \cdot coord_{x,k}\right) = 0 \; Nm \tag{4.5}$$

$$\sum_{k\in\{5001,5003,5020\}} \left(F_{x,k} \cdot coord_{z,k} - F_{z,k} \cdot coord_{x,k} + RM_{y,k}\right) = 0 \; Nm \tag{4.6}$$

Equilibrium check of moments around Z-axis passing through Node 1:

$$\sum_{k\in\{5005,5011,5019,5021\}} \left(-F_{x,k} \cdot coord_{y,k} + F_{y,k} \cdot coord_{x,k}\right) = 0 \; Nm \tag{4.7}$$

$$\sum_{k\in\{5001,5003,5020\}} \left(-F_{x,k} \cdot coord_{y,k} + F_{y,k} \cdot coord_{x,k} + RM_{z,k}\right) = 0 \; Nm \tag{4.8}$$

In the current substitute transmission, there are three tie rods that replace the two chains of the real transmission. Node 5002 is linked to Node 5005 with the first tie rod, Node 5003 is linked to Node 5011 with the second tie rod, and Node 5001 is linked to Node 5009 with the third tie rod. For this reason, we have:

$$F_{5002} = -F_{5005} \tag{4.9}$$

$$F_{5003} = -F_{5011} \tag{4.10}$$

$$F_{5001} = -F_{5009} \tag{4.11}$$

Forces acting on the tie rod are opposite to $F_{5002}$, $F_{5005}$, $F_{5003}$, $F_{5011}$, $F_{5001}$, $F_{5009}$ so the tie rods are in traction just as the real chain. In Figure 4.20 we can see the forces transmitted from the transmission to the frame, so we observe forces at the nodes of the frame. As described previously, the connections between the frame and the transmission are made by special rigid elements. For this reason we have that:

$$F_{5014} = -F_{20000} \tag{4.12}$$

$$F_{5015} = -F_{20001} \tag{4.13}$$

$$F_{5019} = -F_{20056} \tag{4.14}$$

$$F_{5020} = -F_{20061} \tag{4.15}$$

$$RM_{y,5020} = -RM_{y,20061} \tag{4.16}$$

$$RM_{z,5020} = -RM_{z,20061} \tag{4.17}$$

$$F_{5021} = -F_{20058} \tag{4.18}$$
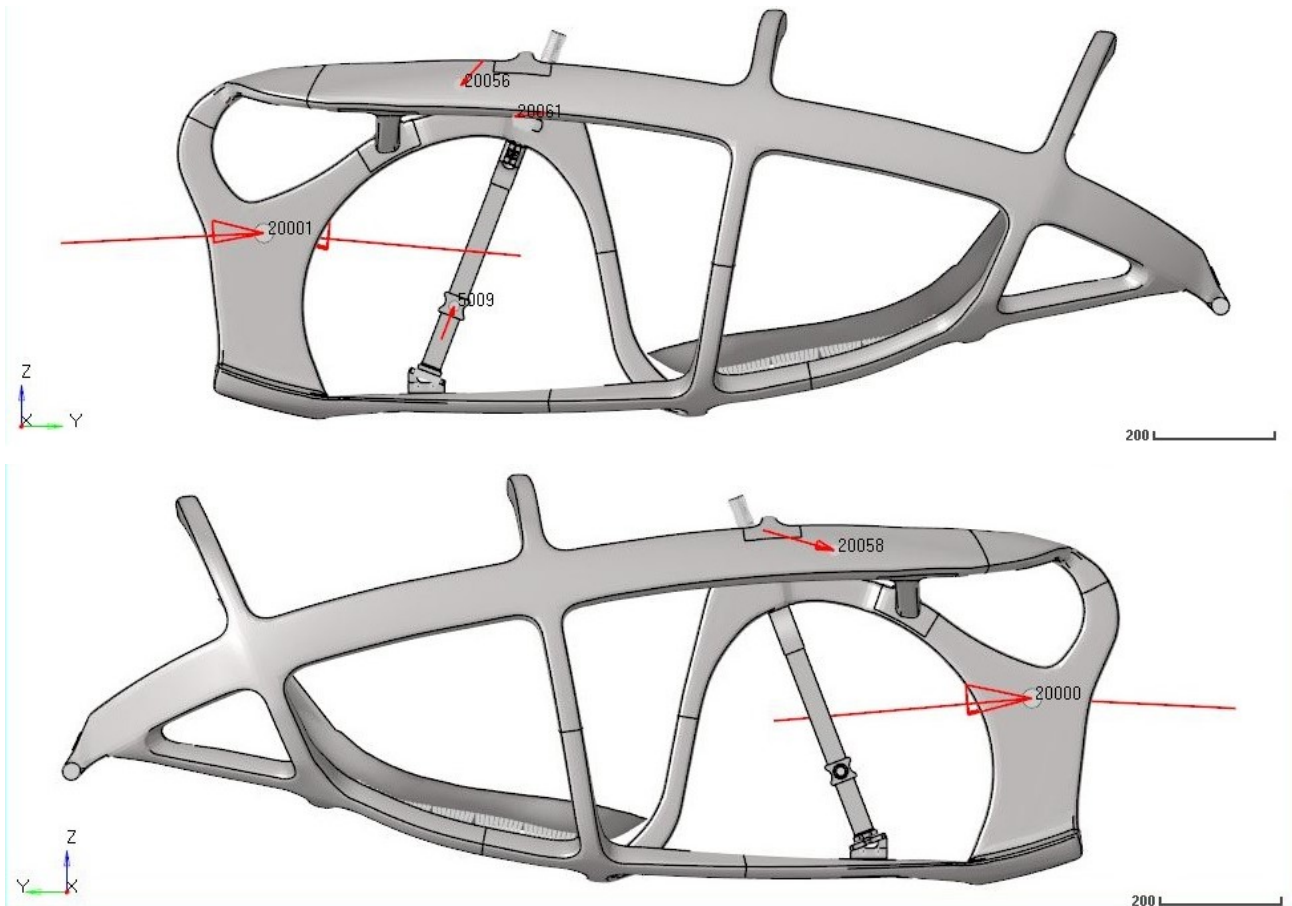
**Figure 4.20**: Forces transmitted from the transmission to the frame for Subcase 2. (above) Left view, (below) right view.

As we have seen in the Taurus frame, the forces at the attaching points of the bottom bracket (Nodes 20000 and 20001) and of the sprocket-set-shaft bearings (Nodes 20056 and 20058) induce a torque on the frame. To evaluate their value we use the Equations 2.18 and 2.19.

$$M_{z,bottom\ bracket} = 50.2\ Nm$$

$$M_{z,sprocket\text{-}set\ shaft} = 22.0\ Nm$$

To be thorough, we evaluate also the torque on the frame, around the Z-axis, due to the added sprocket. Its value is computed by Equation 4.19 and although it is very low, it completes the previous evaluations.

$$M_{z,added\ sprocket} = -F_{x,20061} \cdot coord_{y,20061} + F_{y,20061} \cdot coord_{x,20061} + RM_{z,20061} \tag{4.19}$$

$$M_{z,\ added\ sprocket} = -4.86 \cdot 10^{-3}\ Nm$$

Where:

$RM_{y,20061} = 8.7 \cdot 10^{-3}$ Nm

$RM_{z,20061} = -3.4 \cdot 10^{-3}$ Nm

*Deformations*

Subcase-2 loading forces are equal to those in Subcase 1, plus a force on the right pedal and a force on the backrest. Therefore, the frame bends downwards as in Subcase 1; it also bends with negative sign around

Y-axis, and the upper part of the frame bends rightwards. As a first approach, Figure 4.21 shows the plotel elements in red for the initial condition, and in blue for the final condition, with deformation view amplified by 100 times so as to see the global behavior.
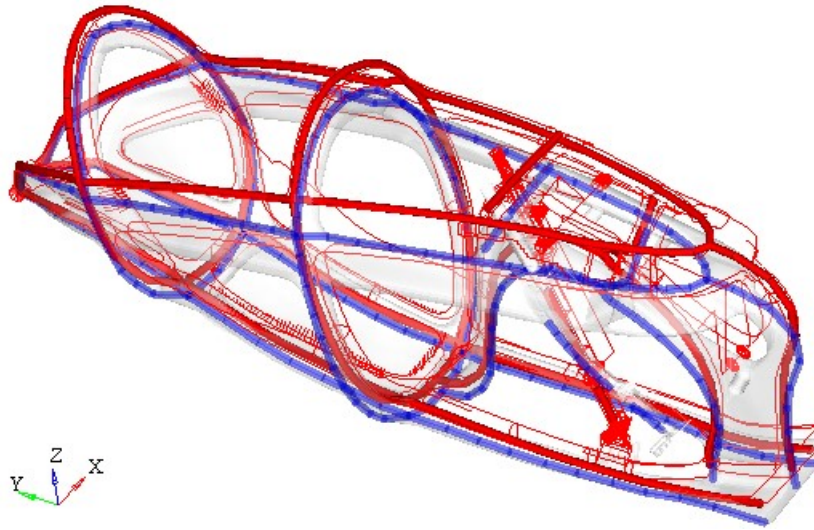


**Figure 4.21**: Plotel elements before (red) and after (blue) load application for Subcase 2.

The frame rotates around the rear dropouts and bends downwards due to the cyclist's weight and due to force $F_{5009}$, which bends the fork as in the Taurus frame. The applied forces on the right pedal and on the backrest increase their distance, and the bottom bracket tends to rotate with positive sign around its Z-axis, as in the Taurus frame. In this case, even if the boundary conditions are the same and the reaction forces at the bottom bracket are similar to those of Taurus, they produce a different result because the structure of the frame and its stiffness distribution are very different. The result is a complex deformed shape, which is described more in detail in the following images.

The highest Y-displacements in absolute value are at the lower extremity of the fork (Fig. 4.22). If we exclude the fork and the transmission from the contour plot of the Y-displacements, we can observe that the upper-right part stretches more that the left-upper part (Fig. 4.23 and 4.24). This is due to the force applied on the right pedal and to the positive moments around the Z-axis from both the bottom bracket and the sprocket-set-shaft bearings to the frame.
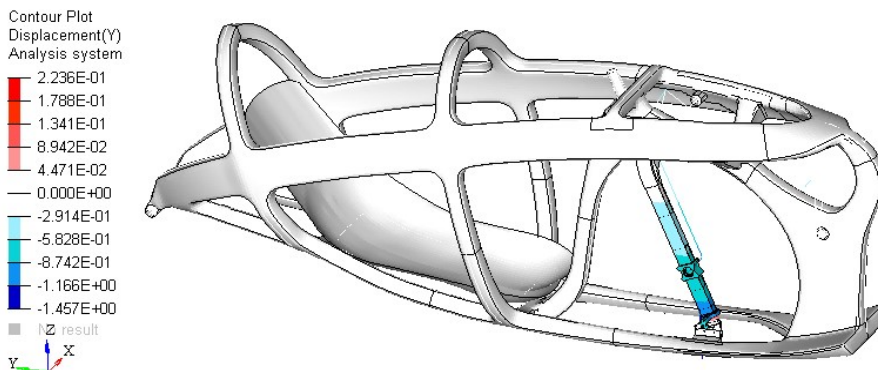


**Figure 4.22**: Y-displacements in global system for Subcase 2. Scale in mm.
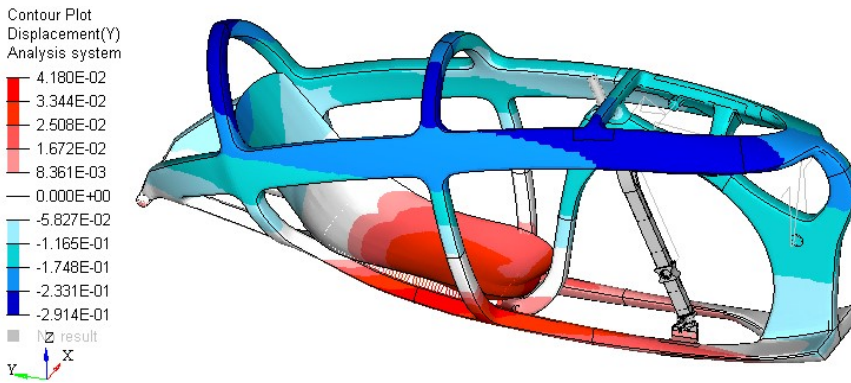
**Figure 4.23**: Y-displacements in global system for Subcase 2. The displacements of the fork and of the transmission are excluded to highlight the displacements of the frame. Right view. Scale in mm.
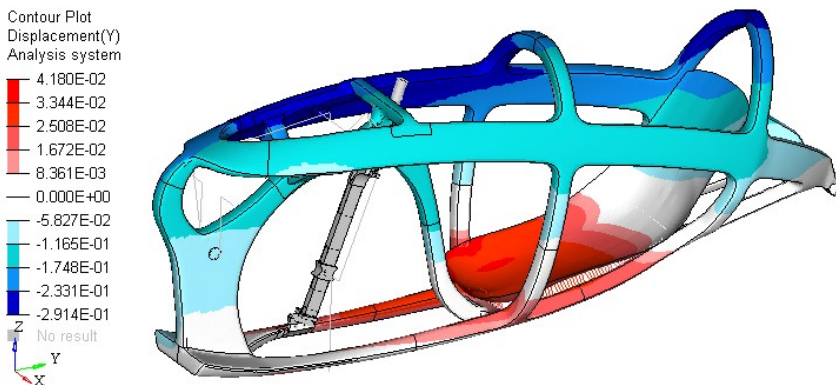


**Figure 4.24**: Y-displacements in global system for Subcase 2. The displacements of the fork and of the transmission are excluded to highlight the displacements of the frame. Left view. Scale in mm.

The main differences in terms of deformations between the new frame proposal and the Taurus frame are visible from the X-displacements (Fig. 4.25). The new frame bends rightwards, while the Taurus frame bends leftwards. This also influences the rotation around the Y-axis (Fig. 4.26). To allow for an accurate evaluation, we have plotted the X-displacements of the nodes belonging to the plotel elements placed in the upper part of the frame (Fig. 4.27). The observation of the X-displacements explains the deformed shape of the new frame. If we consider only the X-displacements, the weakest areas of the new frame are limited to the sprocket-set-shaft-bearing zones, while in Taurus these are at the attaching points of the front panels. In any case, comparing the graph in Figure 4.27 with the graph in Figure 2.40, it results that the new frame is stiffer.



**Figure 4.25**: X-displacements in global system for Subcase 2. Scale in mm.
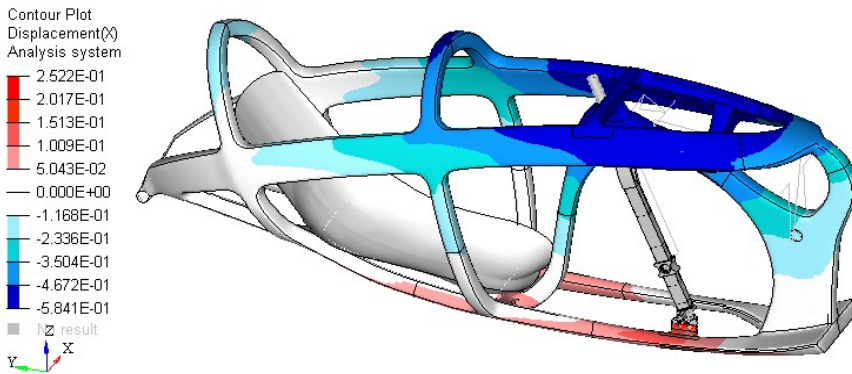
**Figure 4.26**: X-displacements in global system for Subcase 2. The displacements of the fork and of the transmission are excluded to highlight the displacements of the frame. Scale in mm.
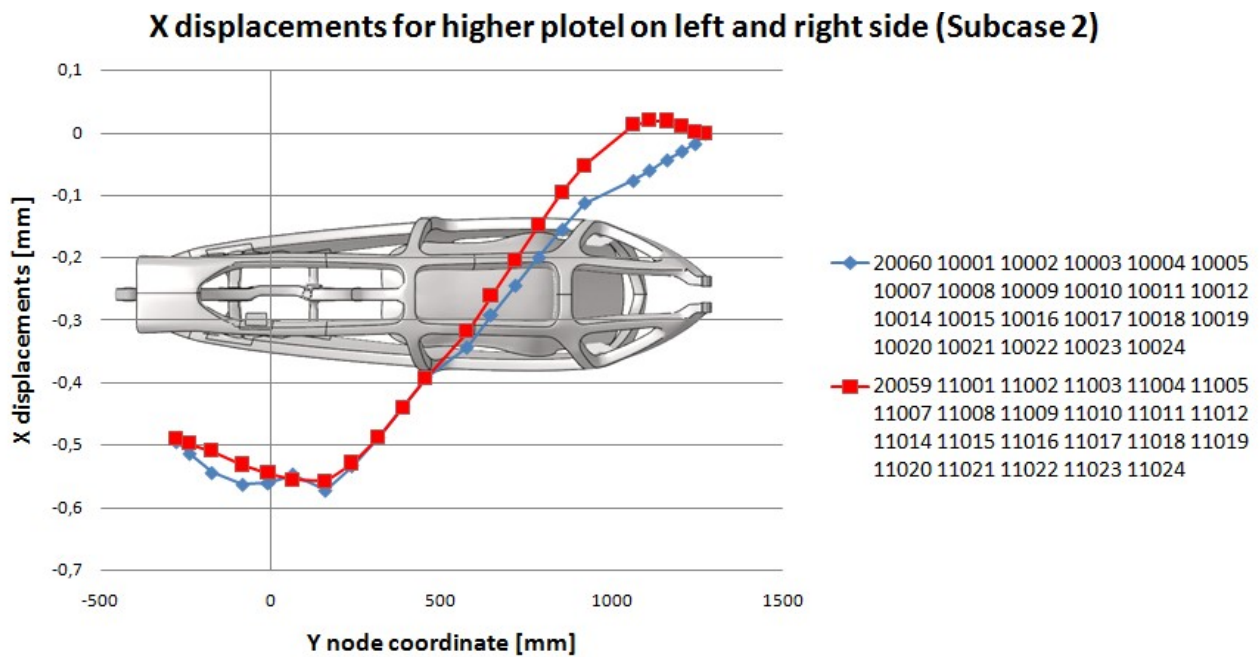


**Figure 4.27**: X-displacements in global system of plotel nodes for Subcase 2.

Z-displacements are equal to zero in the constrained points of the rear dropouts and of the front wheel due to the global constraints. Z-displacements are mainly negative due to the downward bending induced by the cyclist's weight force. Looking more accurately, the right part of the frame has higher displacements in absolute value compared to the left part (Fig. 4.28) due to the rotation around Y-axis.
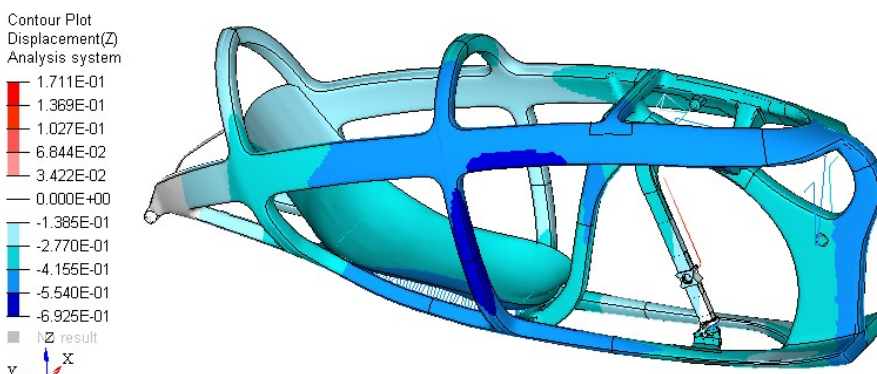


**Figure 4.28**: Z-displacements in global system for Subcase 2. Right view. Scale in mm.
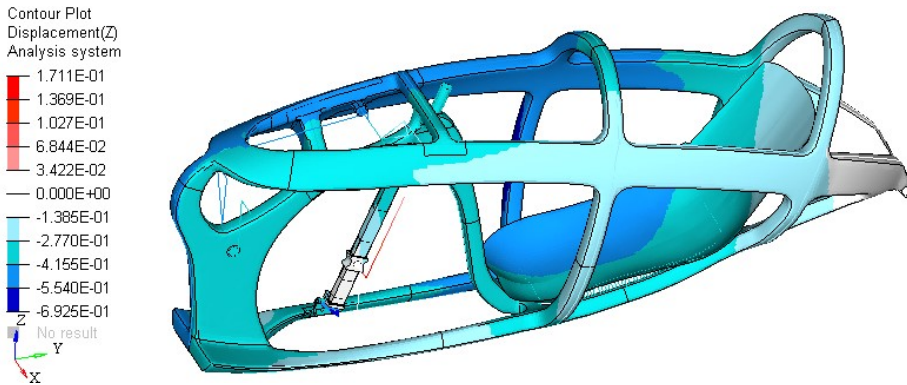
**Figure 4.29**: Z-displacements in global system for Subcase 2. Left view. Scale in mm.

In the following figure we can check that, in Subcase 2, the bearings that guide the fork do not leave the rail. In Figure 4.30 there is no view amplification factor and the red lines represent the condition of the unloaded frame.



**Figure 4.30**: Guide bearings and rail of the fork during load application for Subcase 2. The red lines are for when unloaded.

*Stiffness and displacement between right pedal and backrest*

The relative displacement between Node 2 and Node 10 is:

- 0.003 mm at the end of Subcase 1,
- 0.249 mm at the end of Subcase 2.

Therefore, the total deformation between Node 2 and Node 10 is $d_{2,10}$ = 0.246 mm. Recalling the applied force of *F*=700 N we have a local stiffness of:

$$K_{2,10} = \frac{F}{d_{2,10}} = 2846 \, N/mm$$

*Stress, strain e failure index*

The contour plots from Figure 4.31 to 4.34 show the maximum stress and strain values in the laminate. In this subcase, contrary to the previous one, the bottom-bracket zone is stressed because we apply a force on the right pedal. For the same reason, we can notice that Part 40 is more stressed than Part 41 (Fig. 4.31 and 3.33). Figures 4.35 and 4.36 show the maximum failure indexes of the laminate, and Figures 4.37 and 4.38 show the ply in which these maximum failure indexes are present, by means of the ply ID number. The highest composite failure index is on the attaching point of the fork guide (ply ID = 7013100) and it is equal to 0.037.

**Figure 4.31**: P1 max stress for Subcase 2. Scale in MPa. Right view.



**Figure 4.32**: P1 max stress for Subcase 2. Scale in MPa. Left view.



**Figure 4.33**: P1 max strains for Subcase 2. Scale in MPa. Right view.



**Figure 4.34**: P1 max strains for Subcase 2. Scale in MPa. Left view.

**Figure 4.35**: Maximum composite failure indexes for Subcase 2. Right view.



**Figure 4.36**: maximum composite failure indexes for Subcase 2. Left view.



**Figure 4.37**: Ply ID in which there is the maximum failure index for Subcase 2. Right view.



**Figure 4.38**: Ply ID in which there is the maximum failure index for Subcase 2. Left view.

### 4.1.3 Subcase 3

*Constraint reactions and global equilibrium check*

| | Node id | SUBCASE 3: Applied forces (in global system) | | |
|---|---|---|---|---|
| | | Fx [N] | Fy [N] | Fz [N] |
| Right pedal | 2 | 0,0 | 0,0 | 0,0 |
| Left pedal | 3 | 55,2 | -694,4 | 68,7 |
| Seat | 9 | 0,0 | 0,0 | -687,0 |
| Backrest | 10 | -55,2 | 694,4 | -68,7 |
| TOT | | 0,0 | 0,0 | -687,0 |

**Table 4.6**: Applied forces in global system for Subcase 3.

| | Node id | SUBCASE 3: Reaction forces (in global system) | | | | | |
|---|---|---|---|---|---|---|---|
| | | RFx [N] | RFy [N] | RFz [N] | RMx [Nm] | RMy [Nm] | RMz [Nm] |
| Front wheel | 1 | 0,0 | 0,0 | 407,3 | 0,0 | 0,0 | 0,0 |
| Fork | 4 | 0,0 | 0,0 | 0,0 | 0,0 | 0,0 | 0,0 |
| Left bike dropout | 20059 | 60,6 | -2,8 | 122,1 | 0,0 | -1,2 | 0,9 |
| Right bike dropout | 20060 | -60,6 | 2,8 | 157,7 | 0,0 | -0,2 | -0,7 |
| TOT | | 0,0 | 0,0 | 687,0 | 0,0 | -1,4 | 0,2 |

**Table 4.7**: Reaction forces in global system for Subcase 3.

The global equilibrium along X, Y and Z-axes is verified since the constraint reactions are equal and opposite to the applied forces in every direction. The equilibrium of the moments is verified by Equations 2.1, 2.2 and 2.3. The torque reaction at Node 4 (due to fork rotation constraint) is equal to that of Subcase 2 because it depends on the forces transmitted by the third tie rod, which do not change magnitude and direction.

*Transmission forces*

In Subcase 3 we apply a force on the left pedal (node ID=3) so we have forces inside the transmission. Figures 4.39 and 4.40.a show the free-body diagram of some parts of the transmission, and Table 4.8 their numerical values.

| SUBCASE 3 | | | |
|---|---|---|---|
| Node Id | Fx [N] | Fy [N] | Fz [N] |
| 2 | 0,00 | 0,00 | 0,00 |
| 3 | 55,19 | -694,40 | 68,67 |
| 5001 | -0,02 | -53,22 | -138,60 |
| 5002 | 0,53 | 472,60 | 65,56 |
| 5003 | 0,02 | -83,79 | 123,20 |
| 5005 | -0,53 | -472,60 | -65,56 |
| 5009 | 0,02 | 53,22 | 138,60 |
| 5011 | -0,02 | 83,79 | -123,20 |
| 5014 | -28,10 | -1562,00 | -146,30 |
| 5015 | -27,62 | 1784,00 | 12,03 |
| 5019 | 7,94 | 94,93 | 105,10 |
| 5020 | 0,01 | 137,00 | 15,40 |
| 5021 | -7,40 | 293,90 | 83,71 |

**Table 4.8**: Forces inside the transmission for Subcase 3.
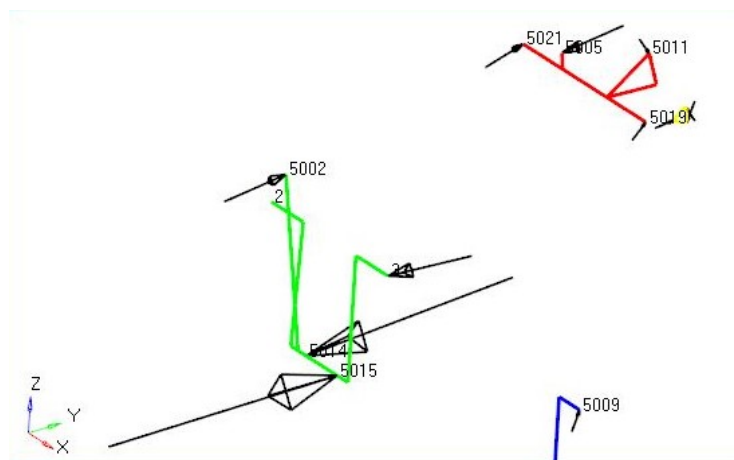


**Figure 4.39**: Free-body diagram of transmission elements for Subcase 3.
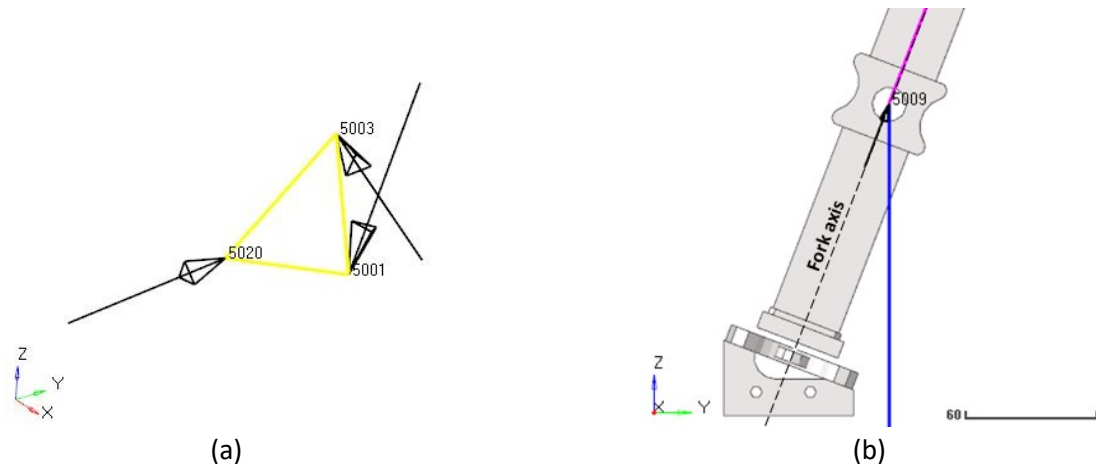
**Figure 4.40**: (a) Zoom on the free-body diagram of the added sprocket.(b) Details about the direction of the force $F_{5009}$ in relation to the fork axis.

Using the same equations presented for the previous subcase, we have verified the global equilibrium of the components of the transmission, and that the tie rods are in traction condition. The drive torque produced by the left pedal does not change compared to the previous subcase. Indeed, forces at the tie rod extremities (Nodes 5001, 5002, 5003, 5005, 5009 and 5011) do not change. We notice that the distance between Node 3 and Node 5002 is greater than the distance between Node 2 and Node 5002 (Fig. 4.39). Therefore, to satisfy the equilibrium of the green parts (Fig. 4.39), the forces at the bottom bracket (Nodes 5014 and 5015) have to increase, causing a higher reaction torque on the frame.
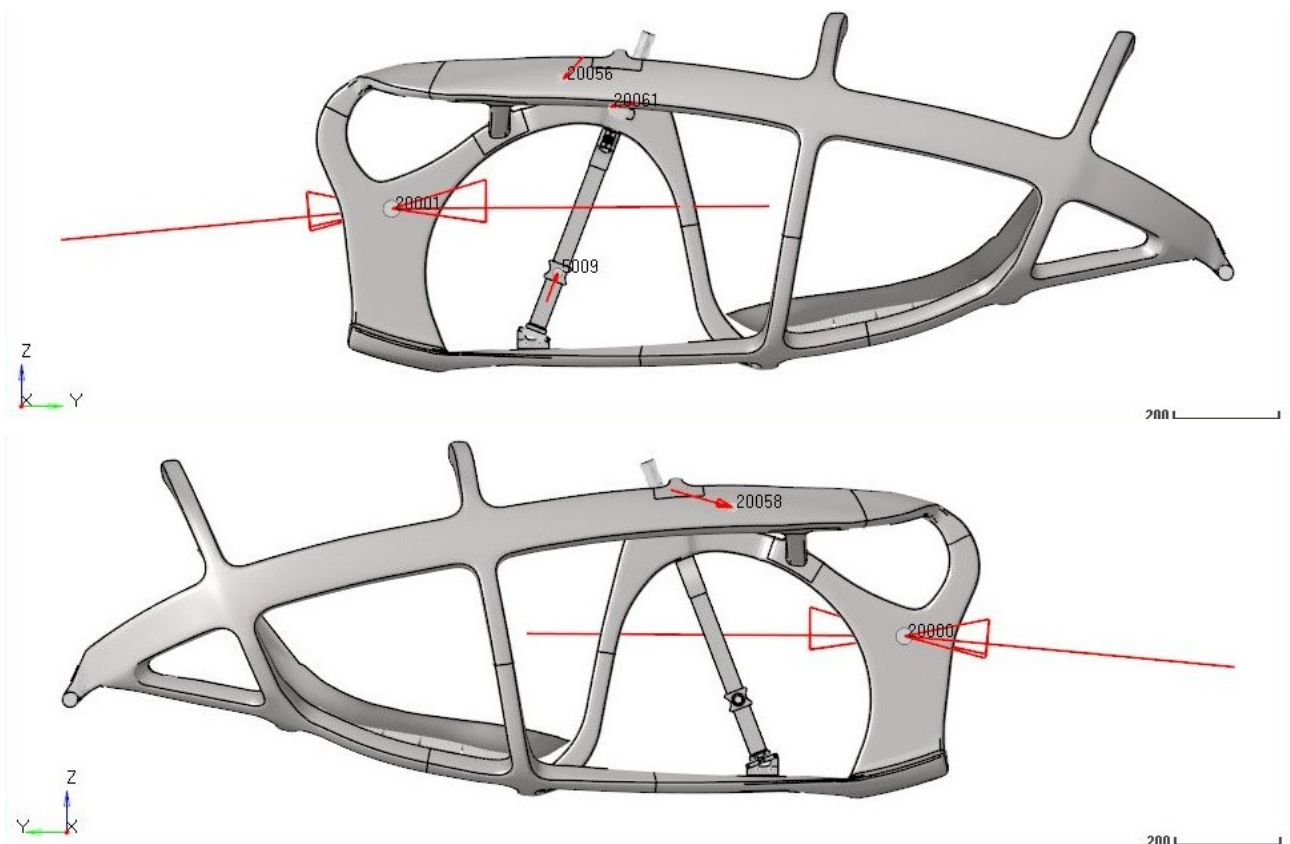


**Figure 4.41**: Forces transmitted from the transmission to the frame for Subcase 3. (above) Left view, (below) right view.

Moreover, the forces at Nodes 5014 and 5015 have an opposite sign compared to those in Subcase 2. The torque transmitted from the bottom bracket to the frame is:

$$M_{z,bottom\ bracket} = -88.7\ Nm$$

The reaction torques on the frame due to the sprocket-set-shaft bearings and due to the added sprocket remain unchanged compared to the previous subcase.

$$M_{z,sprocket\text{-}set\ shaft} = 22.0\ Nm$$

$$M_{z,\ added\ sprocket} = -4.86 \cdot 10^{-3}\ Nm$$

The $M_{z,bottom\ bracket}$ and $M_{z,sprocket\text{-}set\text{-}shaft}$ have opposite direction to each other and this produces different deformations on the frame.

*Deformations*

Subcase-3 loading forces are equal to those in Subcase 1, plus a force on the left pedal and a force on the backrest. Except for the fact that we load the opposite pedal, the loading forces are equal to those in Subcase 2. Therefore, the frame bends downwards as in Subcase 1, and it also bends with positive sign around Y-axis; the upper part of the frame bends leftwards. As a first approach, Figure 4.42 shows the plotel elements in red for the initial condition, and in blue for the final condition, with deformation view amplified by 100 times so as to see the global behavior.
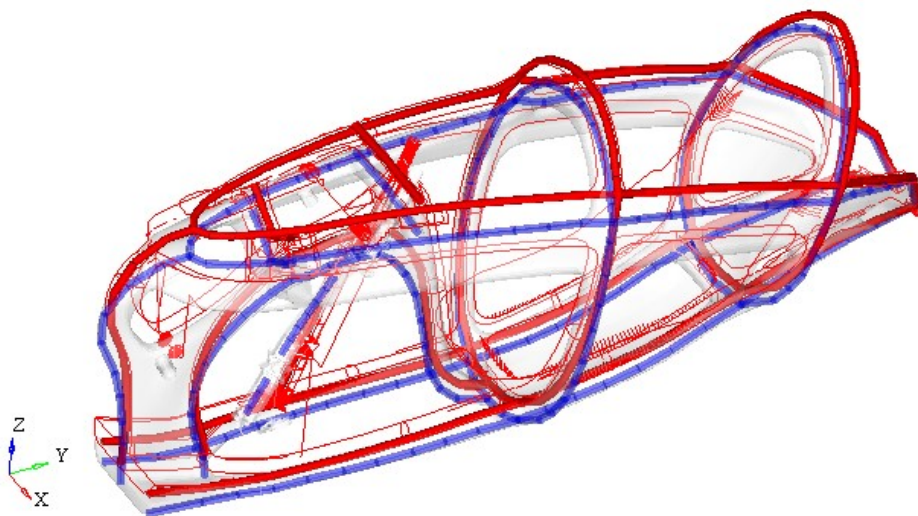


**Figure 4.42**: Plotel elements before (red) and after (blue) load application for Subcase 3.

All the observations made for the Subcase 2 are valid for the current one, except that the deformations that we previously had on the right are now on the left, and vice versa. The frame rotates around the rear dropouts and bends downwards due to the cyclist's weight and due to force $F_{5009}$, which bends the fork. The applied forces on the left pedal and on the backrest increase their distance, and the bottom bracket tends to rotate with negative sign around its Z-axis. The result of the deformed shape is described more in detail in the following images.

The highest Y-displacements in absolute value are at the lower extremity of the fork (Fig. 4.43). If we exclude the fork and the transmission from the contour plot of the Y-displacements, we can observe that the upper-left part stretches more that the upper-right part (Fig. 4.44 and 4.45), as opposed to what happens in Subcase 2.
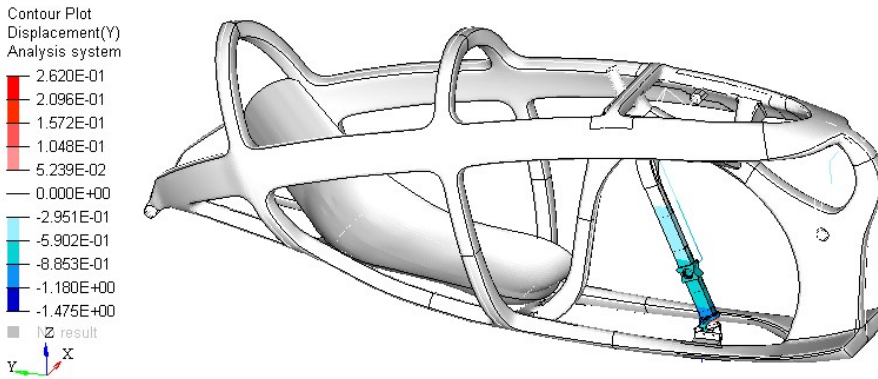


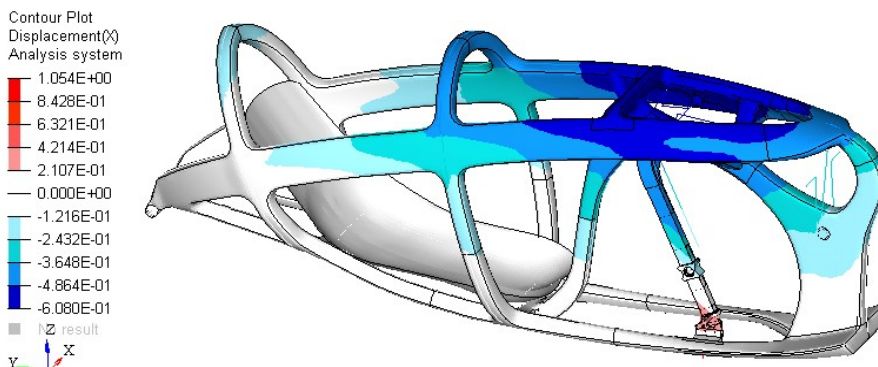**Figure 4.43**: Y-displacements in global system for Subcase 3. Scale in mm.
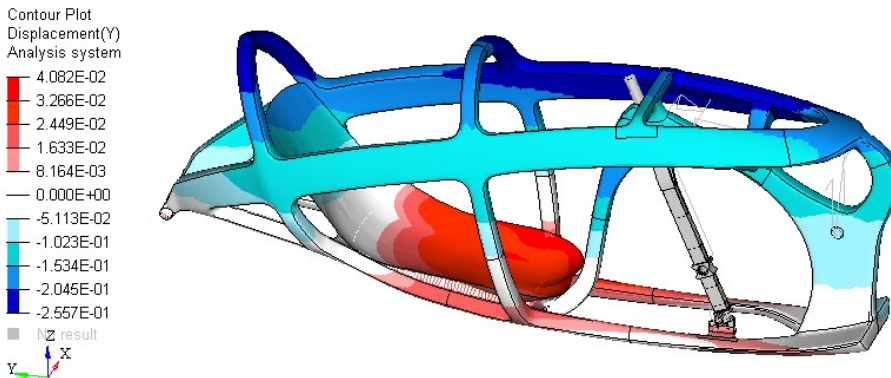


**Figure 4.44**: Y-displacements in global system for Subcase 3. The displacements of the fork and of the transmission are excluded to highlight the displacements of the frame. Right view. Scale in mm.
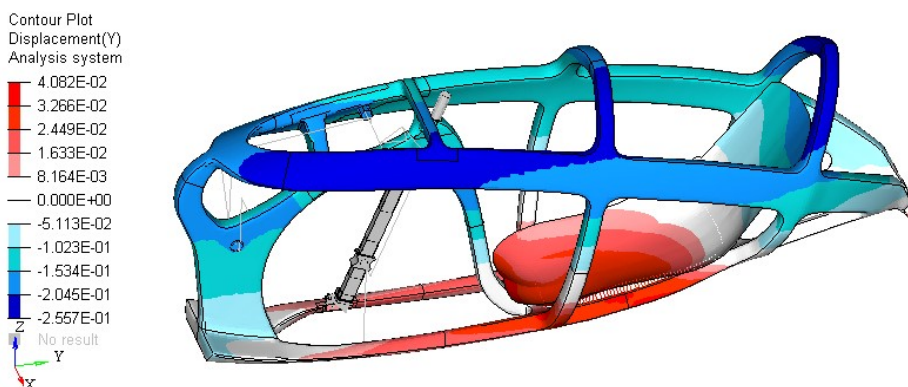


**Figure 4.45**: Y-displacements in global system for Subcase 3. The displacements of the fork and the transmission are excluded to highlight the displacements of the frame. Left view. Scale in mm.

The X-displacements show that the upper part of the frame bends leftwards. That is the opposite of what happens in Subcase 2 because we load the opposite pedal. The lateral displacements in Subcase 3 are lower than those in Subcase 2 because the torques transmitted from the bottom bracket and from the sprocket-set shaft have opposite sign to each other (Fig. 4.47).

116
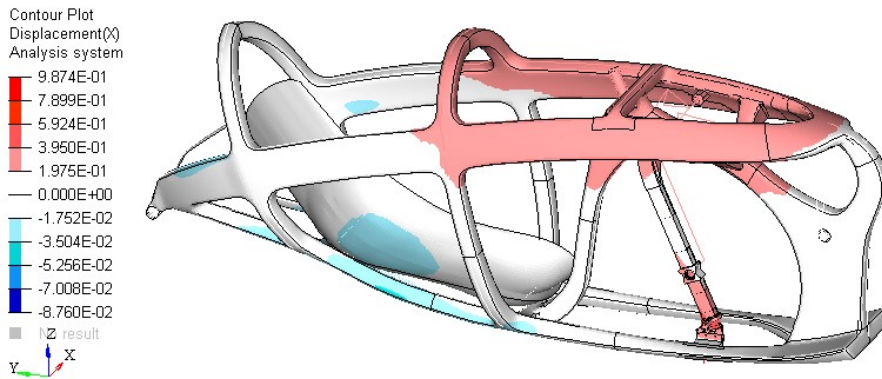
**Figure 4.46**: X-displacements in global system for Subcase 3. Scale in mm.
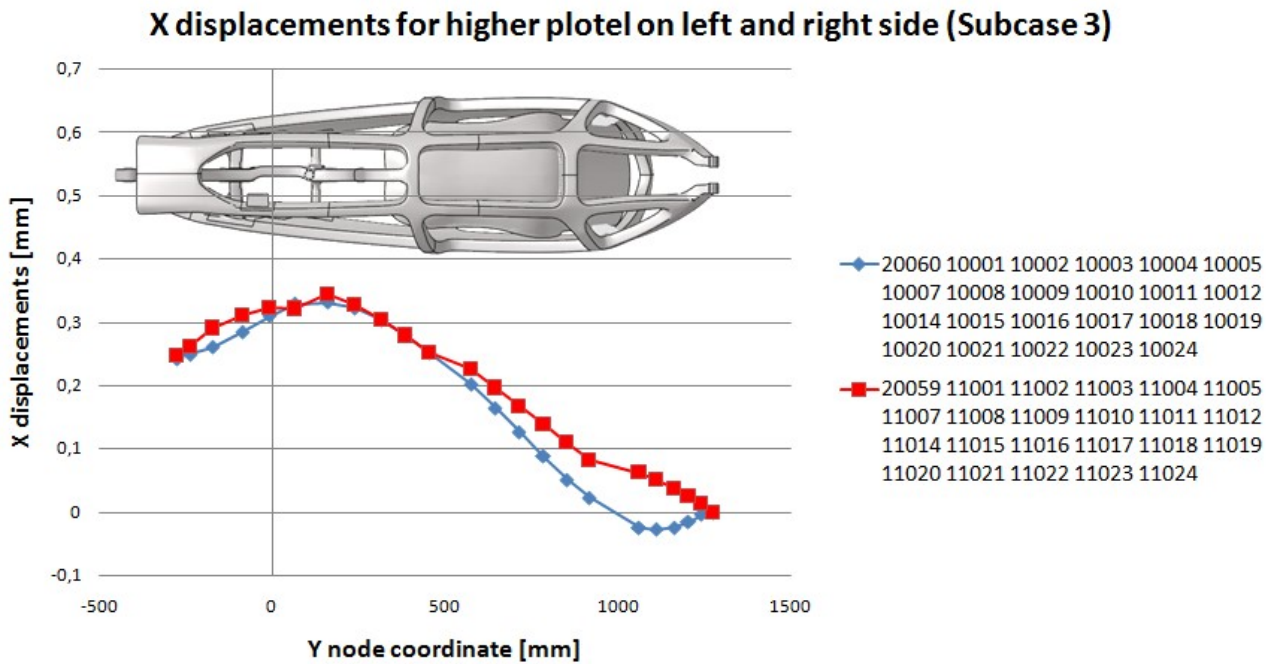


**Figure 4.47**: X-displacements in global system of plotel nodes for Subcase 3.

The Z-displacements are mainly negative due to the downward bending induced by the cyclist's weight force. Looking more accurately, the left part of the frame has higher displacements in absolute value compared to the right part (Fig. 4.48 and 4.49) due to the rotation around Y-axis.
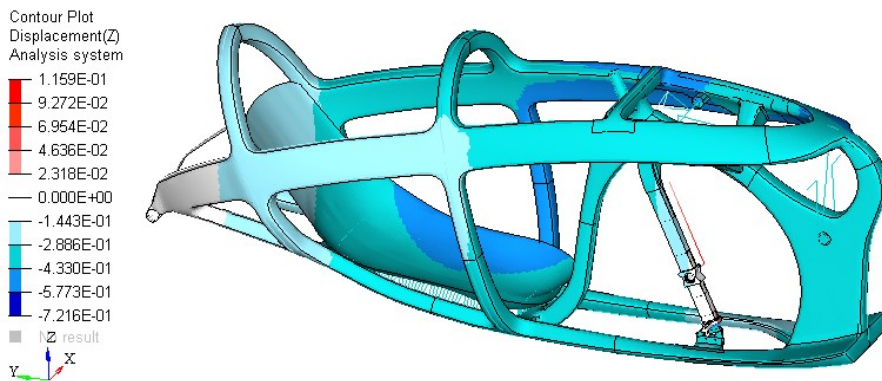


**Figure 4.48**: Z-displacements in global system for Subcase 3. Right view. Scale in mm.
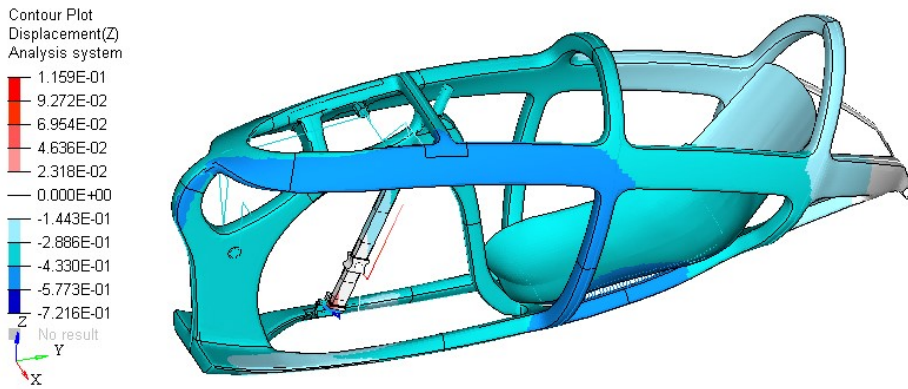
**Figure 4.49**: Z-displacements in global system for Subcase 3. Left view. Scale in mm.

In the following image we can check that also in Subcase 3 the bearings that guide the fork do not leave the rail. In Fig. 4.50 there is no view amplification factor and the red lines represent the condition of the unloaded frame.
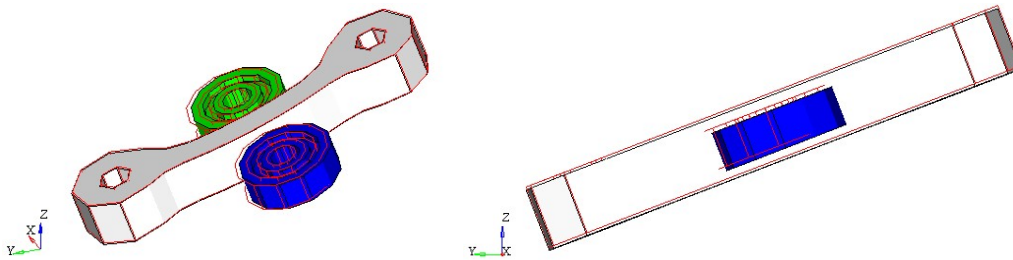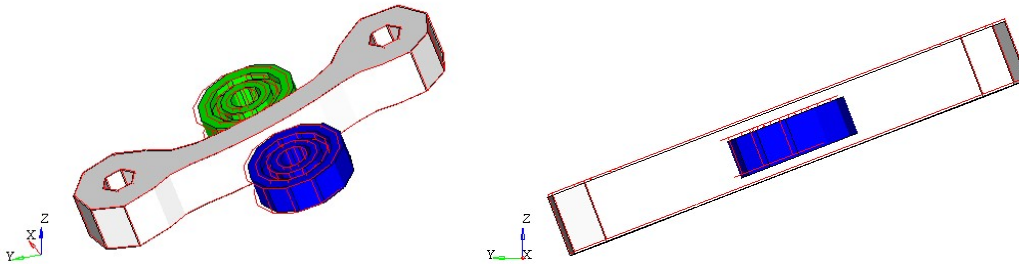


**Figure 4.50**: Guide bearings and rail of the fork during load application for Subcase 3. The red lines are for when unloaded.

*Stiffness and displacement between left pedal and backrest*

The relative displacement between Node 3 and Node 10 is:

- -0.008 mm at the end of Subcase 1,
- 0.347 mm at the end of Subcase 3.

The total deformation between Node 3 and Node 10 is $d_{3,10}$ = 0.355 mm. Recalling the applied force of F=700 N we have a local stiffness of:

$$K_{3,10} = \frac{F}{d_{3,10}} = 1972 \; N/mm$$

*Stress, strain e failure index*

The contour plots from Figure 4.51 to 4.54 show the maximum stress and strain values in the laminate. We can notice that Part 41 is more stressed than Part 40 (Fig. 4.51 and 3.33). Figures 4.55 and 4.56 show the maximum failure indexes of the laminate, and Figures 4.57 and 4.58 show the ply in which these maximum failure indexes are present, by means of the ply ID number. The highest composite failure index is on the attaching point of the fork guide (ply ID = 7013100) and it is equal to 0.043.
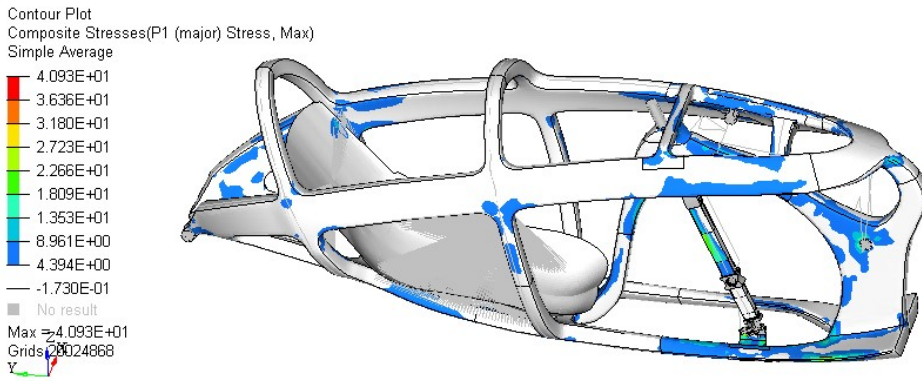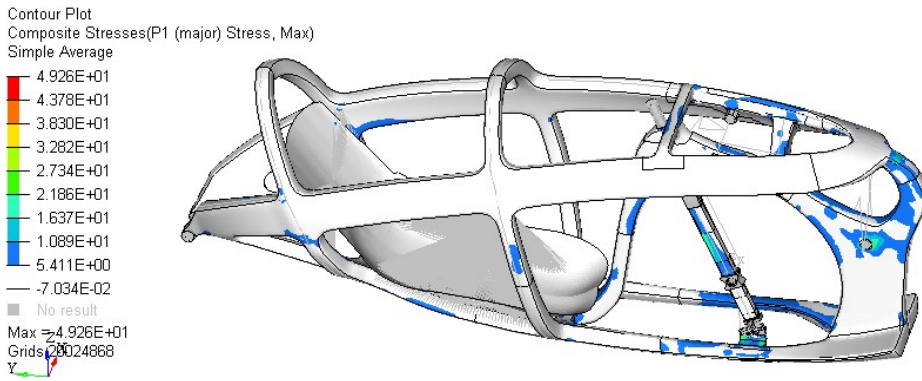
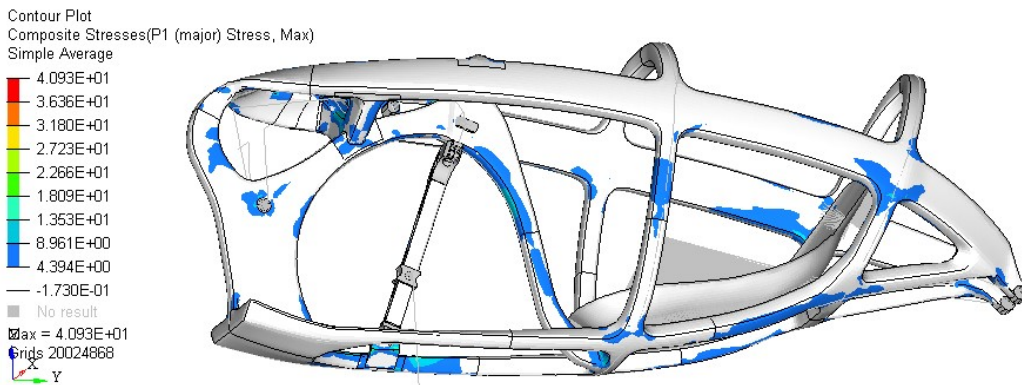**Figure 4.51**: P1 max stress for Subcase 3. Scale in MPa. Right view.
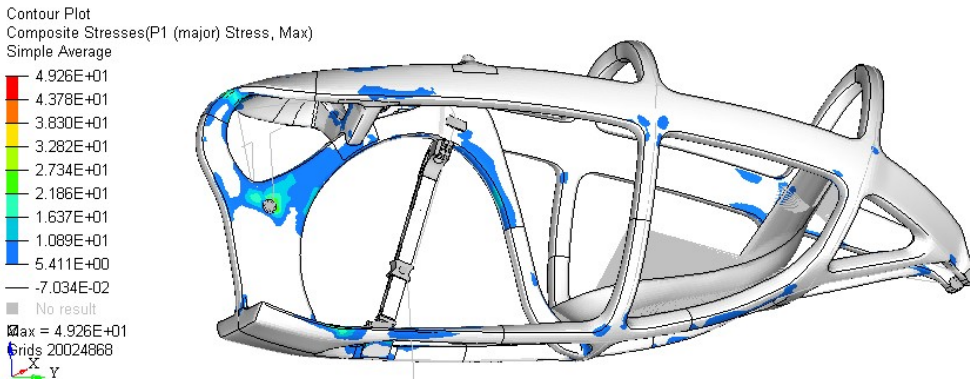


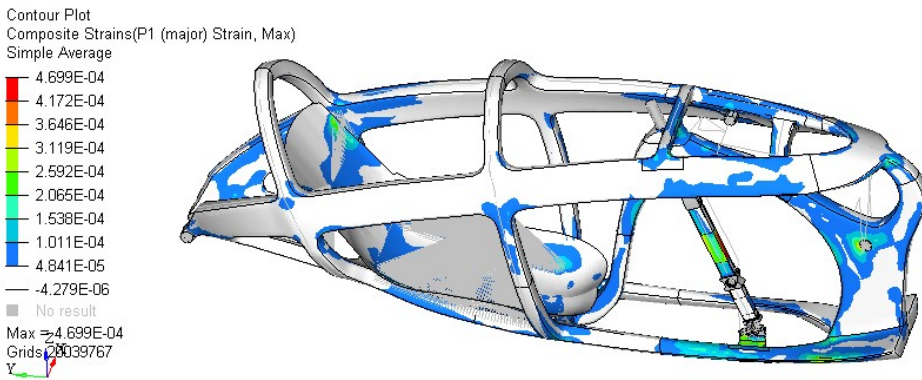**Figure 4.52**: P1 max stress for Subcase 3. Scale in MPa. Left view.
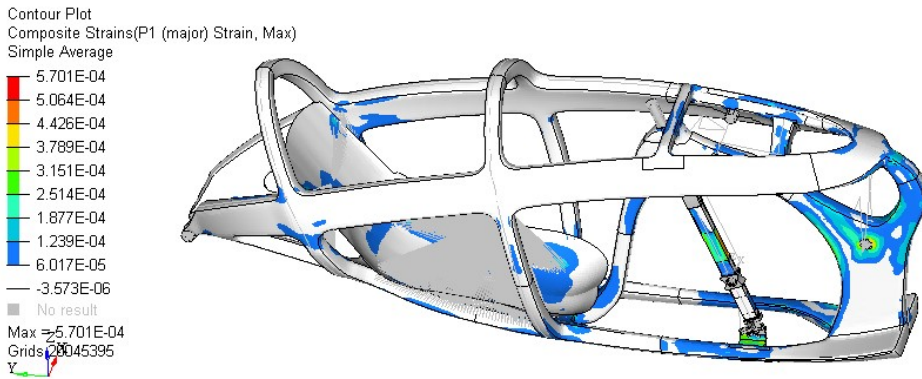


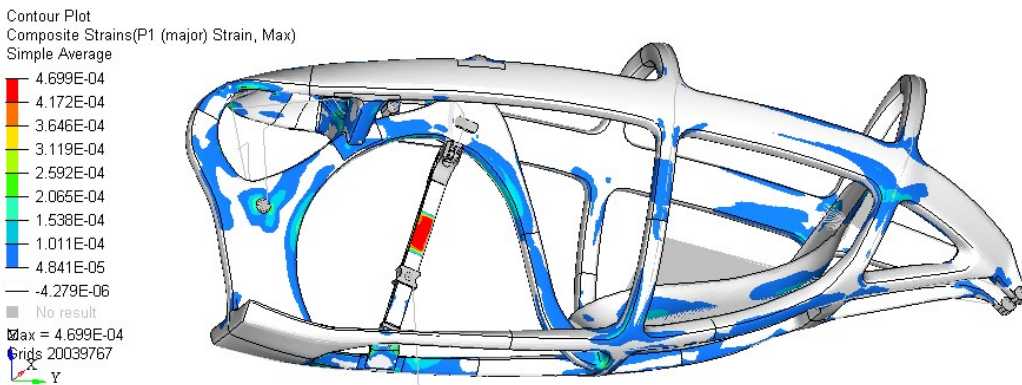**Figure 4.53**: P1 max strains for Subcase 3. Right view.
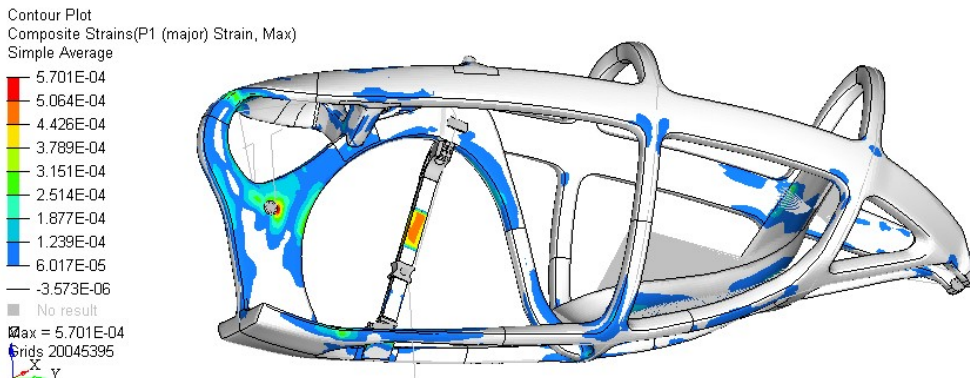


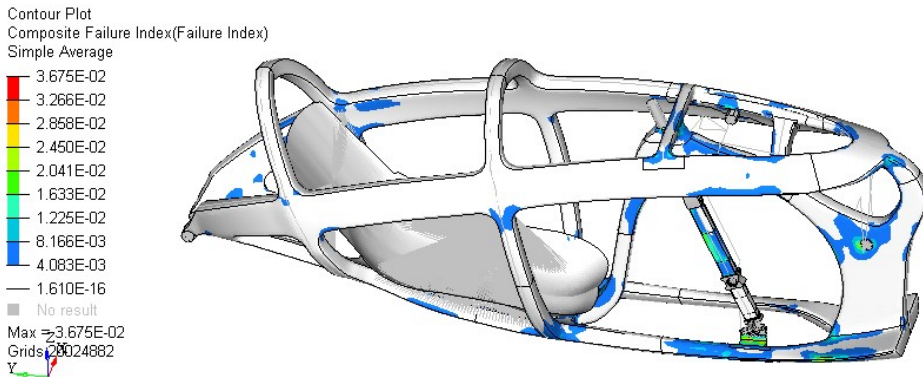**Figure 4.54**: P1 max strains for Subcase 3. Left view.
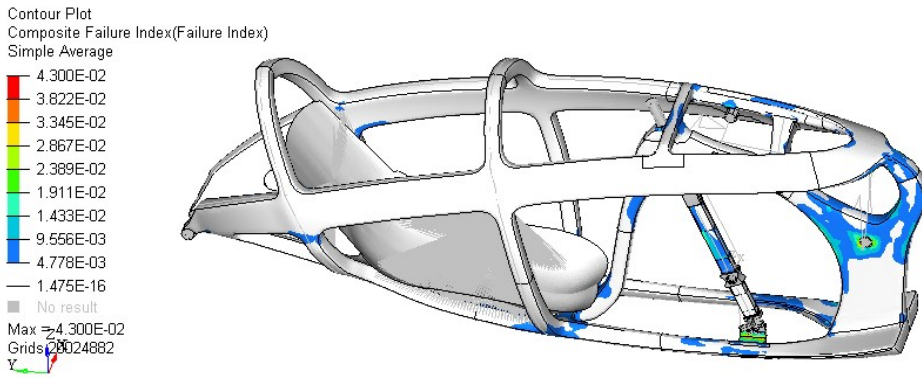
**Figure 4.55**: Maximum composite failure indexes for Subcase 3. Right view.
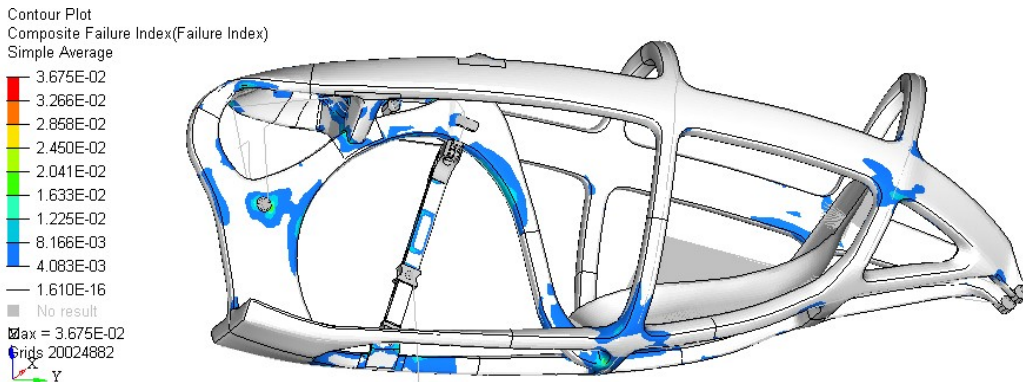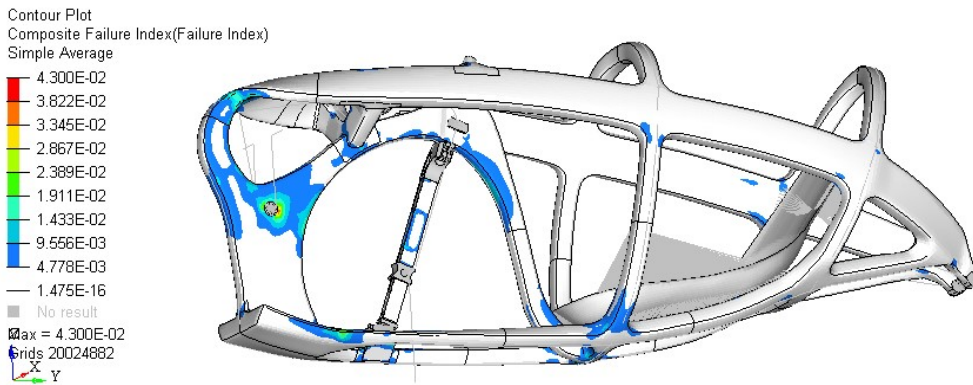


**Figure 4.56**: Maximum composite failure indexes for Subcase 3. Left view.
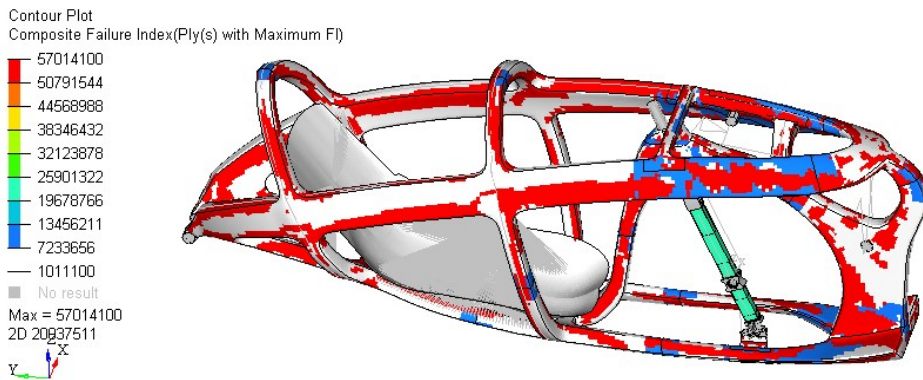


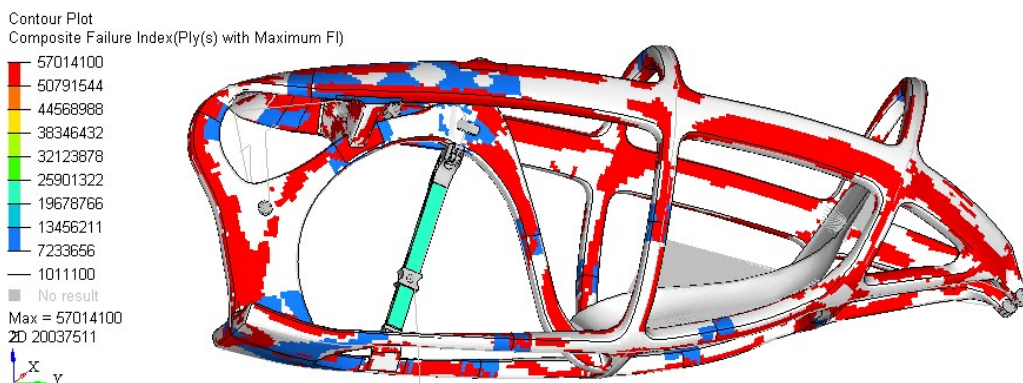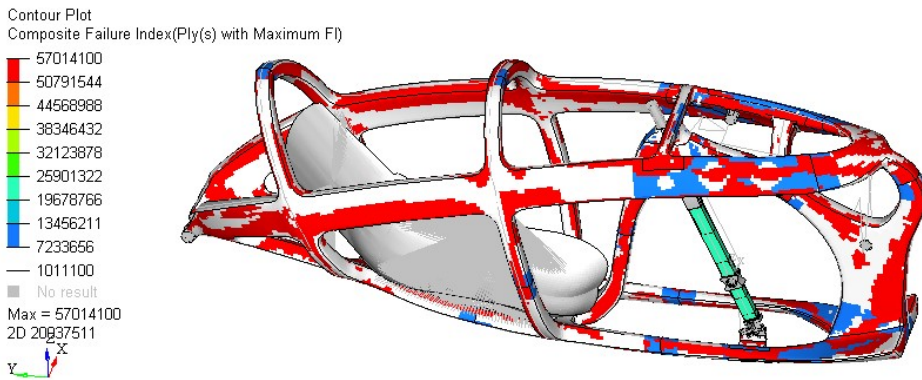**Figure 4.57**: Ply ID in which there is the maximum failure index for Subcase 3. Right view.
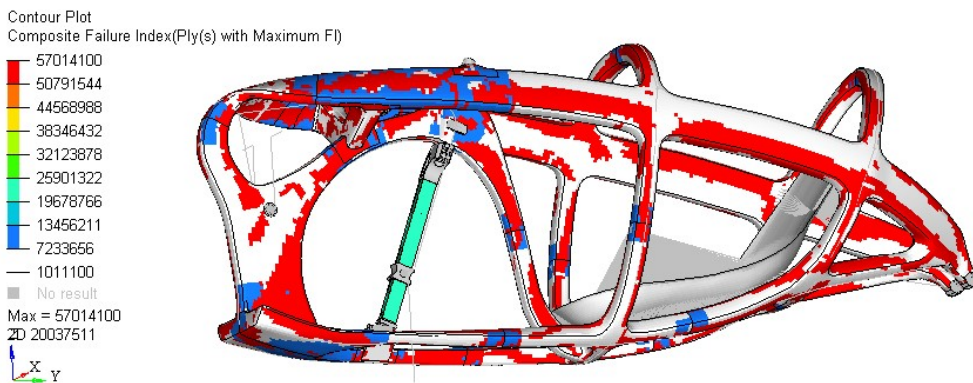


**Figure 4.58**: Ply ID in which there is the maximum failure index for Subcase 3. Left view.

## 4.2 Modal analyses

The modal analyses are the last ones that we perform on the new frame proposal. The modal analyses are performed with two different models. The first model is composed of the frame and cyclist mass, whereas the second one is composed of the frame, cyclist mass and aerodynamic fairing. The new fairing and the dedicated attaching points will be described in this subchapter. The aim of these analyses has been explained in Section 2.5, so we will evaluate only the natural frequencies of the first global modes.



**Figure 4.59**: (left) Model composed of frame and cyclist lumped mass. (Right) model composed of frame, aerodynamic fairing and cyclist lumped mass.

### 4.2.1 Modal analysis of the model with frame and cyclist mass

The following images show the seven rigid modes for the first model - the one with the frame and the lumped mass of the cyclist. The red lines indicate the non-deformed condition.
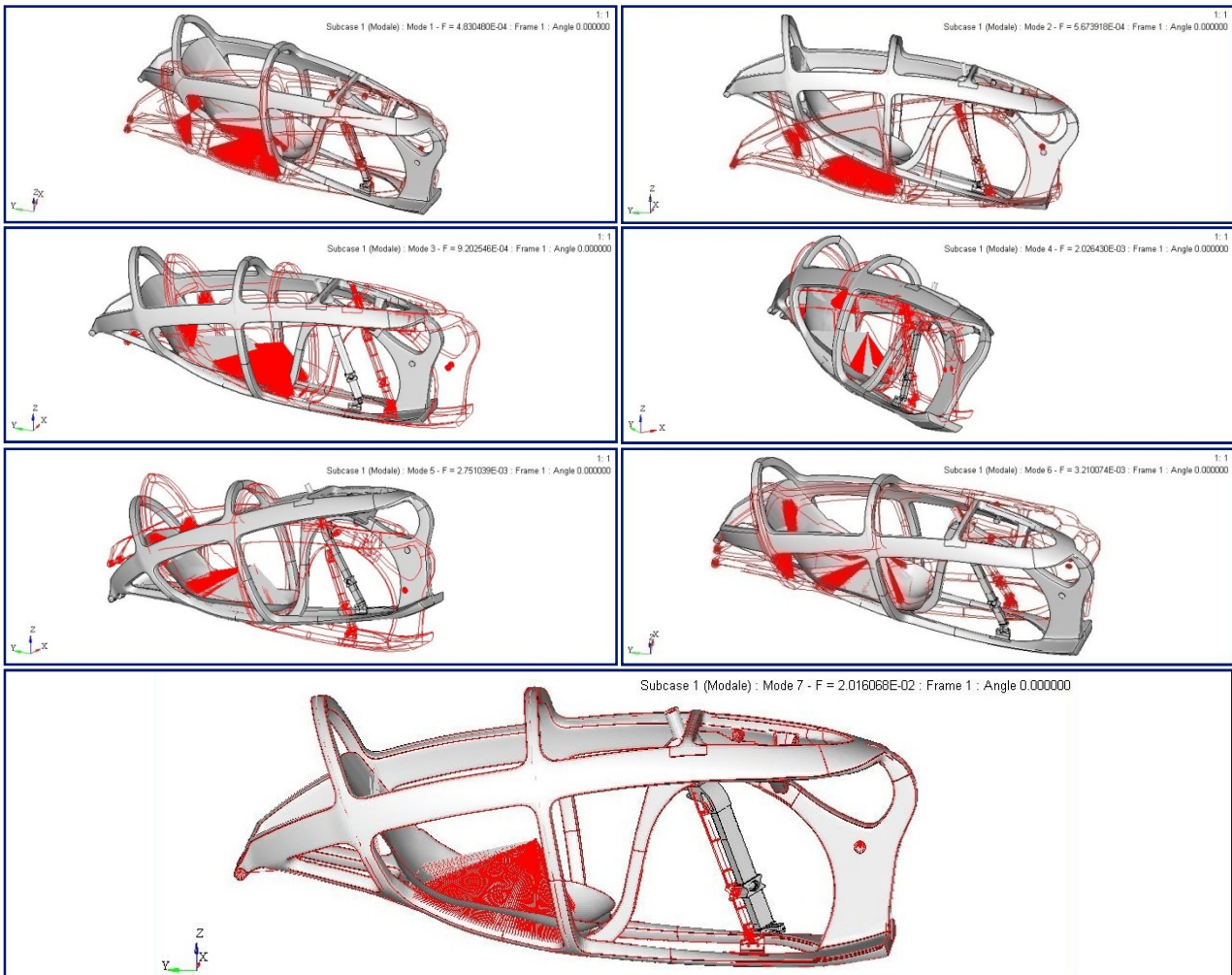


**Figure 4.60**: Modes 1 to 6 are the rigid modes of the frame. Mode 7 is the rigid mode due to the rotation of the fork around its axis.

The first bending mode around Z-axis is at 71.7 Hz (Fig. 4.61).
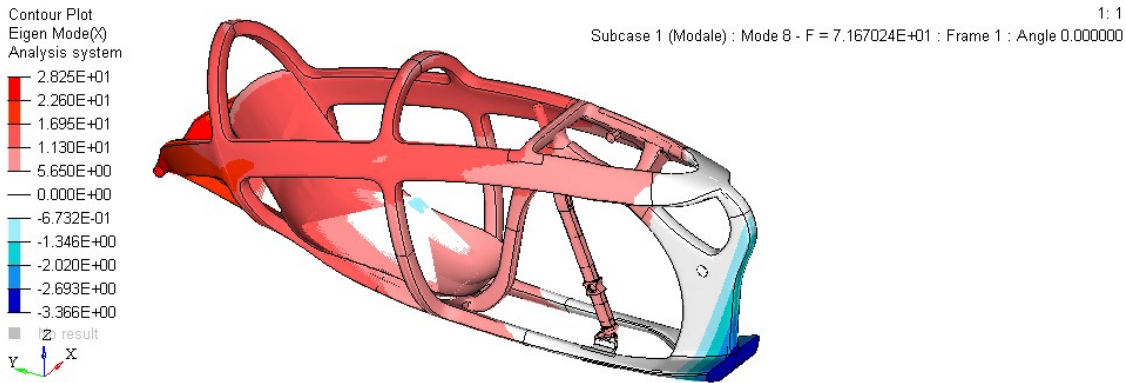


**Figure 4.61**: (Mode 8) First bending mode around Z-axis.

The first bending mode around X-axis is at 95.0 Hz (Fig. 4.62).
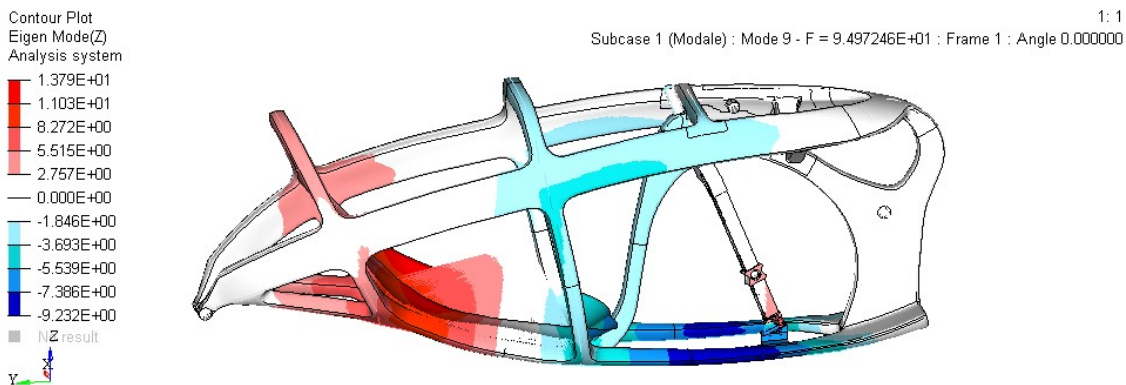


**Figure 4.62**: (Mode 9) First bending mode around X-axis.

The first torsion mode around Y-axis is at 138.5 Hz (Fig. 4.63).
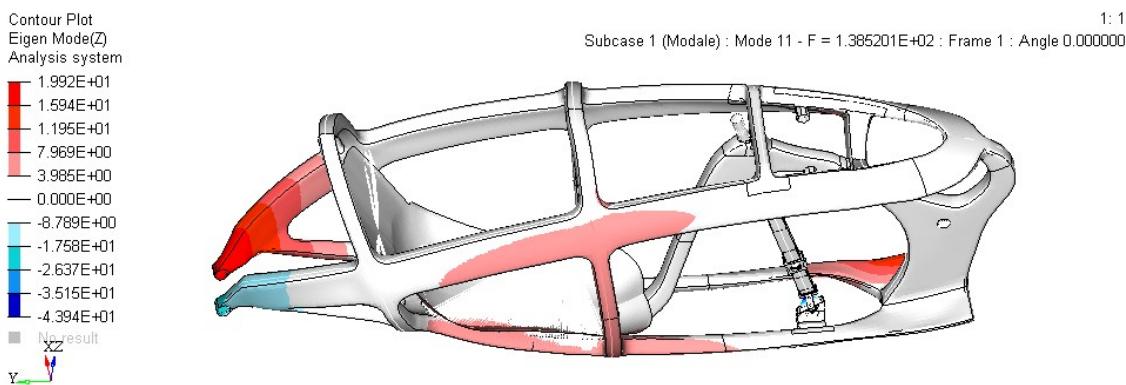


**Figure 4.63**: (Mode 11) First bending mode around Y-axis.

The first bending mode is at 71.7 Hz, which is higher than the cadence frequency and the RPS (round per second) of the wheel.

### 4.2.2 Description of the new aerodynamic fairing

The fairing has an important role in the modal analysis of the complete model. The mass and the stiffness of the fairing, and also the connections between the fairing and the frame, have an important influence on

the modes and frequencies of the complete model. For this reason, it follows the complete description of the removable and fixed faring and of its connecting elements.



| | |
|---|---|
| | Green, red and yellow: |
| | Carbon-fiber fabric, 180 g/m$^2$ *(external layer)* |
| | PVC, 3 mm |
| | Kevlar-fiber fabric, 115 g/m$^2$ *(internal layer)* |
| | Cyan: |
| | Carbon-fiber fabric, 180 g/m$^2$ *(external lyr)* |
| | Neomex honeycomb, 3 mm |
| | Kevlar-fiber fabric, 115 g/m$^2$ *(internal lyr)* |
| | Blue: |
| | Carbon-fiber fabric (junction), 180 g/m$^2$ *(external lyr)* |
| | Carbon-fiber fabric, 180 g/m$^2$ |
| | Neomex honeycomb, 3 mm |
| | Kevlar-fiber fabric, 115 g/m$^2$ |
| | Kevlar-fiber fabric (junction), 115 g/m$^2$ *(internal lyr)* |
| | Fuchsia: |
| | Carbon-fiber fabric (junction), 180 g/m$^2$ *(external lyr)* |
| | Carbon-fiber fabric, 180 g/m$^2$ |
| | PVC, 3 mm |
| | Kevlar-fiber fabric, 115 g/m$^2$ |
| | Kevlar-fiber fabric (junction), 115 g/m$^2$ *(internal lyr)* |

**Table 4.9**: Ply book of the removable fairing (green, red, cyan, blue, fuchsia) and of the fixed fairing (yellow).

A new set of attaching elements have been developed to mount the existing removable fairing on the new frame proposal. The attaching elements consist of seven hooks that allow the displacements along the Y-axis so as to make the detachment of the removable fairing possible (Fig. 4.64). The details about the attaching phase are shown in Figures 4.65-4.68.
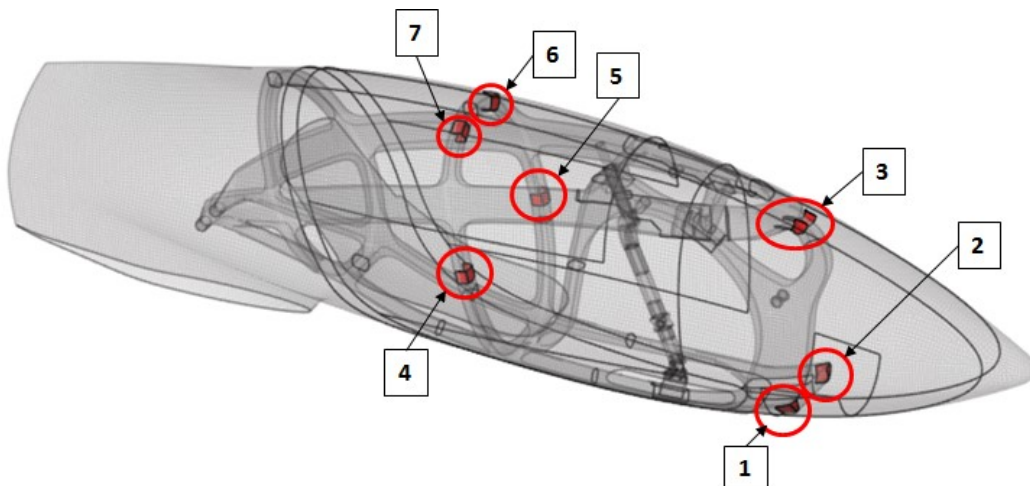


**Figure 4.64**: The seven hooks specially designed to mount the existing fairing on the new frame proposal.
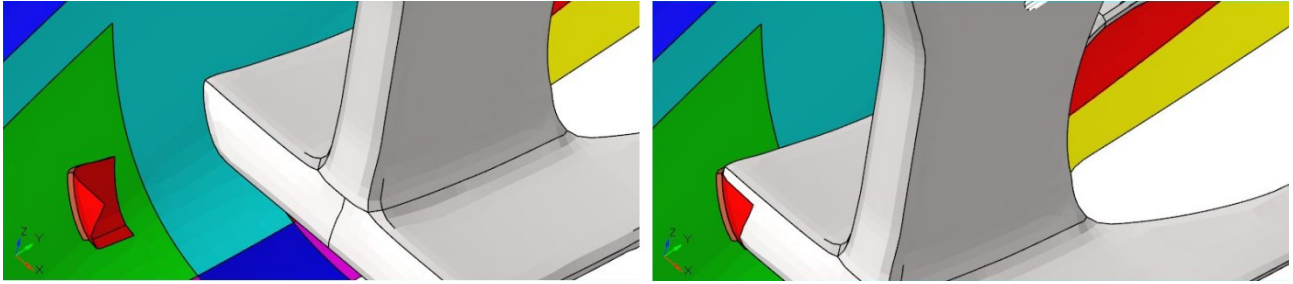
**Figure 4.65**: Hook 1 during the mounting of the removable fairing.
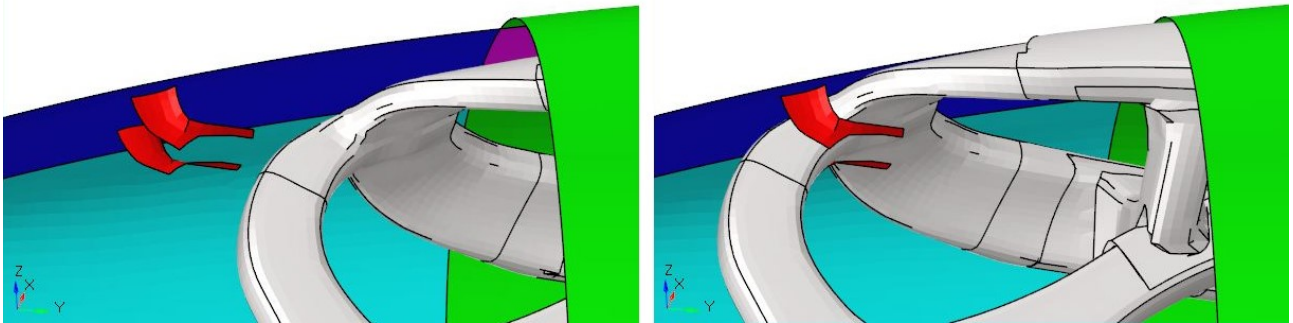


**Figure 4.66**: Hook 3 during the mounting of the removable fairing.
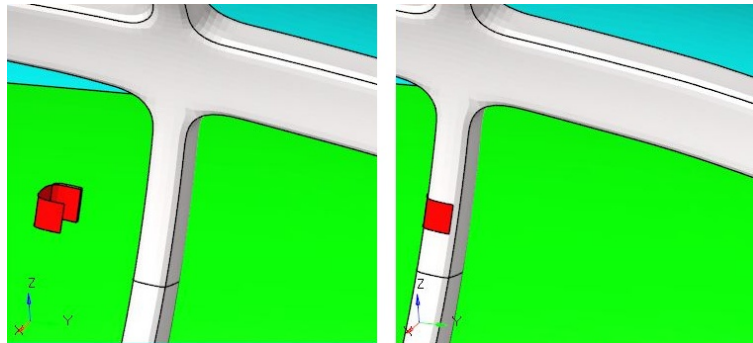


**Figure 4.67**: Hook 4 during the mounting of the removable fairing.
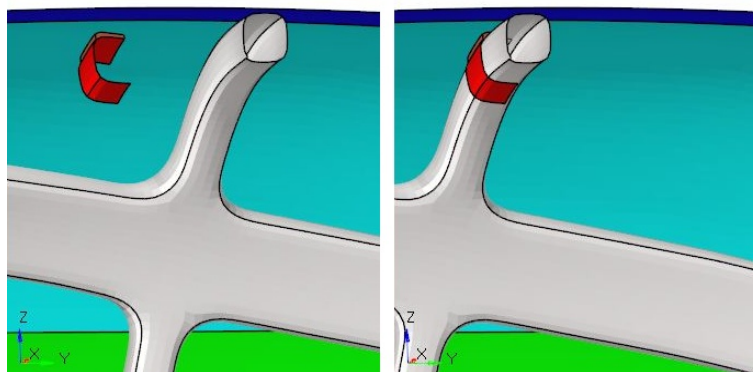


**Figure 4.68**: Hook 7 during the mounting of the removable fairing.

The hooks are linked to the frame by rigid elements that follow the Type-1 modeling with locked DOF 1, 3, 4, 5, 6. The removable fairing is attached to the fixed fairing using the same method as for Taurus.

### 4.2.3 Modal analysis of the model with frame, cyclist mass and removable aerodynamic fairing

The following images show the seven rigid modes for the second model - the one with the frame, aerodynamic fairing and lumped mass of the cyclist. The red lines indicate the non-deformed condition.
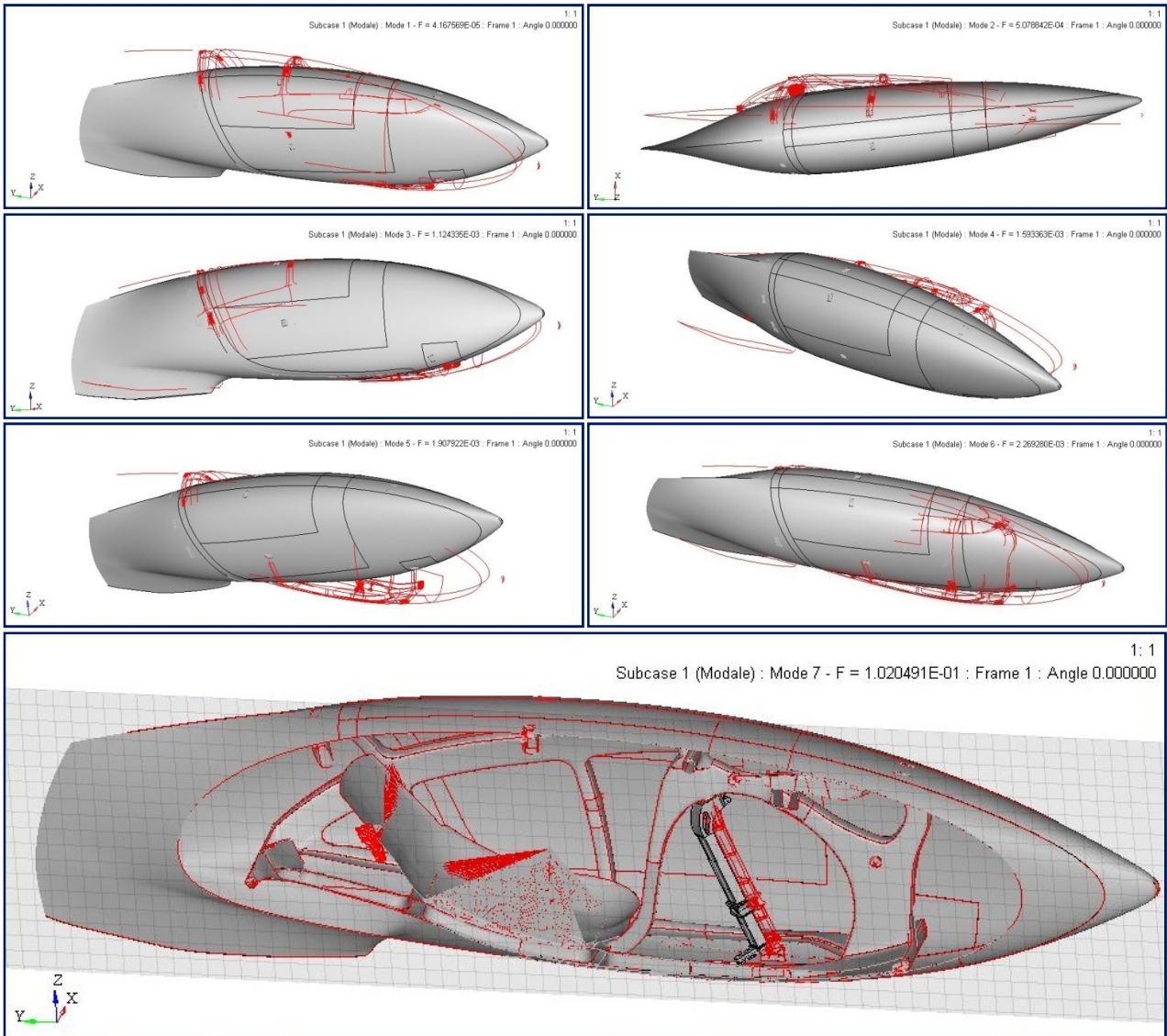


**Figure 4.69**: Modes 1 to 6 are the rigid modes of the frame and of the fairing. Mode 7 is the rigid mode due to the rotation of the fork around its axis (section cut to visualize the fork).

The first bending mode around Z-axis is at 55.6 Hz (Fig. 4.70).
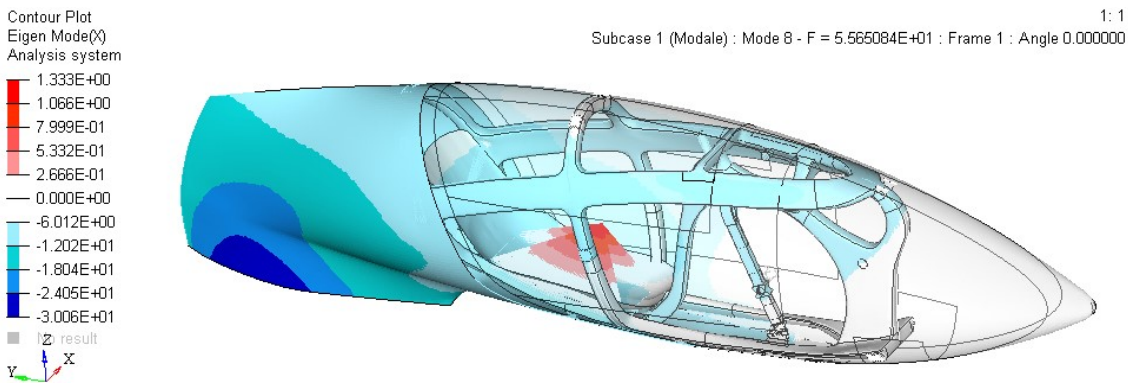


**Figure 4.70**: (Mode 8) First bending mode around Z-axis.

The first bending mode around X-axis is at 91.0 Hz (Fig. 4.71).
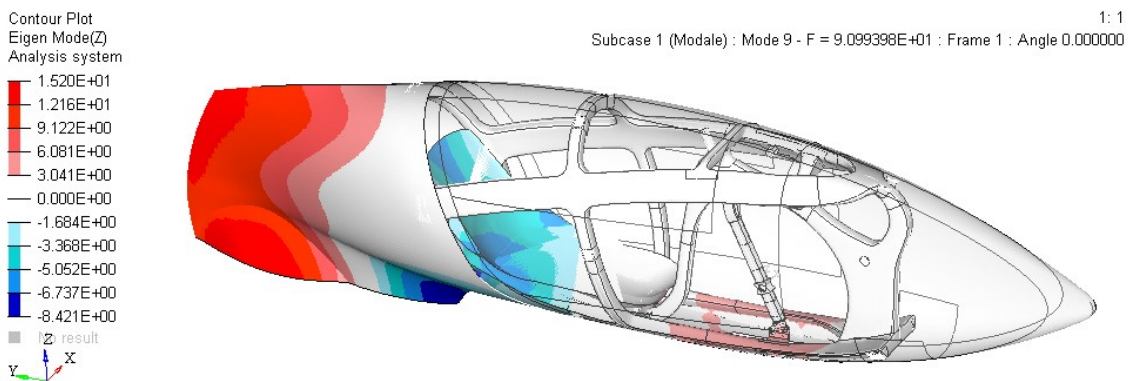


**Figure 4.71**: (Mode 9) First bending mode around X-axis.

The global natural frequencies of the complete model are higher than the cadence and the RPS of the wheel.

## 4.3 Summary of the results and comparison with Taurus

At the end of the final tests, we can summarize the results of the new frame proposal and the results of the Taurus frame (Tab. 4.10). Through the comparison we can check whether the objectives have been achieved. The objectives that had been set were halving the mass and increasing the stiffness in comparison to the Taurus frame.
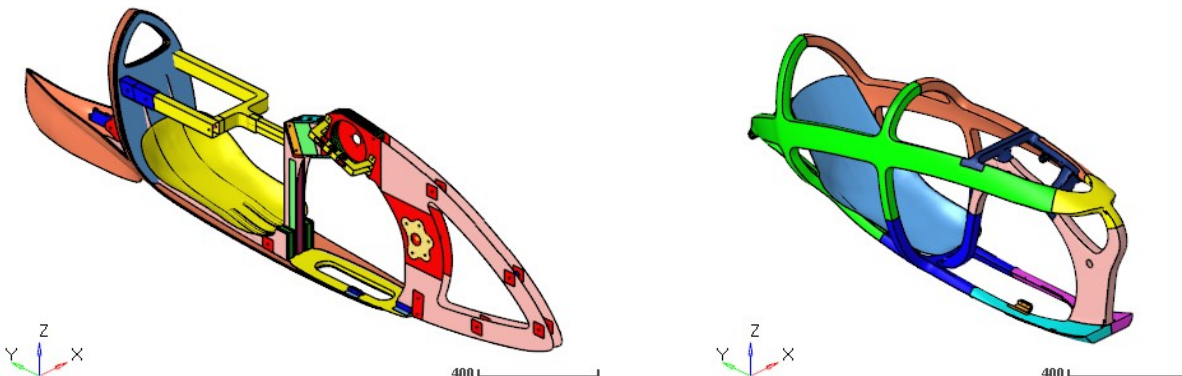


**Figure 4.72**: Components used to compute the mass of the Taurus frame (left) and the mass of the new proposal frame (right).

126

| | Taurus | New frame proposal | Δ between the new frame and Taurus |
|---|---|---|---|
| **Mass of the frame** [kg] | 12 | 6 | -6 _(-50%)_ |
| **K$_{z,9}$ in Subcase 1** [N/mm] | 1399 | 1640 | 241 _(+17%)_ |
| **K$_{2,10}$ in Subcase 2** [N/mm] | 1115 | 2846 | 1731 _(+155%)_ |
| **K$_{3,10}$ in Subcase 3** [N/mm] | 706 | 1972 | 1266 _(+179%)_ |
| **Frequency of the first global mode without fairing** | Bending mode around Z-axis at 27.2 Hz | Bending mode around Z-axis at 71.7 Hz | +44.5 Hz |
| **Frequency of the first global mode with fairing** | Bending mode around Z-axis at 40.2 Hz | Bending mode around Z-axis at 55.6 Hz | +15.4 Hz |

**Table 4.10**: Final comparison between the results of the Taurus frame and of the new frame proposal.

The data in the Table 4.10 show that the new frame proposal weighs half and is stiffer. As a consequence, also the frequencies of the first global modes increase, further avoiding the resonances with the excitation frequencies due to the pedaling and the rotation of the wheels. To further verify the higher stiffness of the new frame in comparison to the Taurus frame, we can observe that the new proposed frame is capable of developing higher reaction torques in absolute value at the bottom-bracket attaching points and at the sprocket-set-shaft attaching points (Tab. 4.11).

| | | Taurus | New frame proposal |
|---|---|---|---|
| **SUBCASE 2** | **M$_{Z,bottom\ bracket}$** [Nm] | 32.9 | 50.2 |
| | **M$_{Z,sprocket-set-shaft}$** [Nm] | 18.0 | 22.0 |
| **SUBCASE 3** | **M$_{Z,bottom\ bracket}$** [Nm] | -71.0 | -88.7 |
| | **M$_{Z,sprocket-set-shaft}$** [Nm] | 18.0 | 22.0 |

**Table 4.11**: Comparison between the reaction torques of the two frames at the bottom bracket attaching points and at the sprocket-set-shaft attaching points.

The better results of the new frame are justified by the more complex geometry; as a matter of fact, the technical data of the materials are equal. The new frame is made with carbon fibers having the same elastic modulus and the same strength, and the carbon fiber volume fraction of the composite material is unchanged. Of course, a more elaborate geometry requires a more complex mould and more working hours. The mould of the Taurus frame is obtained from two flat plates, while the new frame requires many dedicated moulds and a longer phase of junction since it is made up of 10 components and 13 junctions. Another positive result of the new project is represented by the upgrade done to the transmission, which allows to eliminate the steering torque on the fork that occurs during pedaling.

# CONCLUSIONS

The project proposed in this paper meets the objectives that had been set: the new frame is stiffer and weighs half of that of the Taurus prototype. Moreover, the new project considers the practical aspects related to its manufacturing. In fact, the decision to build the frame with several separate tubes and to join them with interlocking sections and bond joints represents a more accessible solution from a construction point of view. In addition, the design used only carbon-fiber fabrics available on the market and the same fiber volume fraction as that obtained in previous prototypes. A further positive aspect is represented by the proposed transmission upgrade, which favors driving stability.

The software HyperMesh, HyperView, HyperGraph and the solver Optistruct are powerful tools but at the same time they have required in-depth study; without it, complete control of the models and of the analyses would not have been achieved. The study and modeling of long-fiber composite materials represented another important aspect for carrying out the analyses.

In future, this work could be used as a basis for new studies. It might be possible to develop many optimized solutions, each by setting a different mass target and then observing changes in stiffness.

In this way, the cyclist may be able to choose the best personal compromise between mass and stiffness for the WHPSC race. If the variation in the type of fiber or in the volume fraction of resin were also taken into consideration, the possible solutions to analyze would be endless.

# APPENDIX A: INPUT FILES TO RUN THE ANALYSES OF THE TAURUS PROTOTYPE

This appendix is dedicated to the input files used to run the analyses of the Taurus prototype. The include files are not provided due to their large dimension.

## Input file to run the static analysis of the Taurus prototype

```
STRAIN(H3D) = ALL
STRESS(H3D) = ALL
DISPLACEMENT(H3D) = ALL
$$
DISPLACEMENT(OPTI) = 10000
GPFORCE(OPTI) = 1000
SPCFORCE(OPTI) = ALL
$$
CFAILURE(H3D,NDIV=1) = ALL
CSTRAIN(H3D,NDIV=1) = ALL
CSTRESS(H3D,NDIV=1) = ALL
$
SUBCASE         1
  LABEL Forza peso ciclista
ANALYSIS STATICS
  SPC =         3
  LOAD =         4
$
$
SUBCASE         2
  LABEL Pedalata DX
ANALYSIS STATICS
  SPC =         3
  LOAD =         7
$
$
SUBCASE         3
  LABEL Pedalata SX
ANALYSIS STATICS
  SPC =         3
  LOAD =         8
$$
$$
BEGIN BULK
$$
INCLUDE 'include/INC_TELAIO_TAURUS.fem'
INCLUDE 'include/INC_TRASMISSIONE_SIMULACRO.fem'
$
$$  SPCADD cards
$$
$ Combination of the constraints on the rear dropouts, on the substitute of the front
$ wheel and on the fork
SPCADD          3         1         2
$
$$
$$  SPC Data
$$
$$ Constraints on the rear dropouts
SPC             1    20059    12356     0.0
SPC             1    20060    12356     0.0
$$ Constraint on the substitute of the front wheel
SPC             1        1        3     0.0
$$ Constraint on the rotation of the fork around its axis
SPC             2        4        6     0.0
$
$$
$$  LOADADD cards
$$
$ Combination of the cyclist weight force and the forces due to the right pedaling phase
LOADADD         7      1.0      1.0         4      1.0         5
$ Combination of the cyclist weight force and the forces due to the left pedaling phase
```

```
LOADADD         8     1.0     1.0         4     1.0         6
$$
$$  FORCE Data
$$
$ Cyclist weight force on the seat
FORCE           4     9     01.0     0.0     0.0     -687.0
$
$ Force on backrest during the right pedaling phase (magnitude = 700N)
FORCE           5    10     01.0     55.188     0.0     0.0
FORCE           5    10     01.0     0.0 694.435     0.0
FORCE           5    10     01.0     0.0     0.0 -68.665
$ Force on backrest during the left pedaling phase (magnitude = 700N)
FORCE           6    10     01.0     -55.186     0.0     0.0
FORCE           6    10     01.0     0.0 694.435     0.0
FORCE           6    10     01.0     0.0     0.0 -68.665
$
$ Force on right pedal during the right pedaling phase (magnitude = 700N)
FORCE           5     2     01.0     -55.188     0.0     0.0
FORCE           5     2     01.0     0.0-694.435     0.0
FORCE           5     2     01.0     0.0     0.0  68.665
$
$ Force on left pedal during the left pedaling phase (magnitude = 700N)
FORCE           6     3     01.0     55.186     0.0     0.0
FORCE           6     3     01.0     0.0-694.435     0.0
FORCE           6     3     01.0     0.0     0.0  68.665
$
$
ENDDATA
$$
```

## Input file to run the modal analysis of the Taurus model with frame and cyclist mass

```
$
SUBCASE         1
  LABEL Modale
ANALYSIS MODES
  METHOD(STRUCTURE) =       100
  DISPLACEMENT = ALL
$
BEGIN BULK
$
INCLUDE 'include/INC_TELAIO_TAURUS.fem'
INCLUDE 'include/INC_MASSA_CICLISTA.fem'
$
PARAM,G,0.06
PARAM,EFFMAS,YES
$$
EIGRA        100     0.0   200.0
$$
ENDDATA
```

## Input file to run the modal analysis of the Taurus model with frame, cyclist mass and removable

## aerodynamic faring

```
$
SUBCASE         1
  LABEL Modale
ANALYSIS MODES
  METHOD(STRUCTURE) =       100
  DISPLACEMENT = ALL
$
BEGIN BULK
$
INCLUDE 'include/INC_TELAIO_TAURUS.fem'
INCLUDE 'include/INC_CARENA_TAURUS.fem'
INCLUDE 'include/INC_TIE_TELAIO_CARENA.fem'
INCLUDE 'include/INC_MASSA_CICLISTA.fem'
$
PARAM,G,0.06
PARAM,EFFMAS,YES
$$
EIGRA        100     0.0   200.0
$$
ENDDATA
```

# APPENDIX B: INPUT FILES TO RUN THE OPTIMIZATION ANALYSES OF THE NEW FRAME PROPOSAL

This appendix is dedicated to the input files used to run the optimization analyses of the new frame proposal. The include files are not provided due to their large dimension. However, for the size and shuffle optimizations, some parts of the include files have been reported as they contain cards related to the optimization settings.

**Input file to run the topology analysis of the new frame proposal**

```
STRAIN(H3D) = ALL
STRESS(H3D) = ALL
DISPLACEMENT(H3D) = ALL
$$
DISPLACEMENT(OPTI) = 10000
GPFORCE(OPTI) = 1000
SPCFORCE(OPTI) = ALL
$$
CFAILURE(H3D,NDIV=1) = ALL
CSTRAIN(H3D,NDIV=1) = ALL
CSTRESS(H3D,NDIV=1) = ALL
$
$$
$$   OBJECTIVES Data
$$
$
$HMNAME OBJECTIVES        1objective
$$$$ Objective function of the optimization
DESOBJ(MIN)=2
$
$$$$ Global constraint function of the optimization
DESGLB         2
$
$
SUBCASE        1
  LABEL Forza peso ciclista
ANALYSIS STATICS
  SPC =          3
  LOAD =         4
  WEIGHT = 0.5
$
$
SUBCASE        2
  LABEL Pedalata DX
ANALYSIS STATICS
  SPC =          3
  LOAD =         5
  WEIGHT = 1.0
$
$
SUBCASE        3
  LABEL Pedalata SX
ANALYSIS STATICS
  SPC =          3
  LOAD =         6
  WEIGHT = 1.0
$$
$$
BEGIN BULK
$$
INCLUDE 'include/Modello_Vol_Boolean_Tetra_20mm_20220627.fem'
INCLUDE 'include/INC_TRASMISSIONE_SIMULACRO_PLUS.fem'
$
$$$$ DTPL card defines the design variable of the topology optimization
$$
$
$HMNAME OPTICONTROLS        1"optistruct_opticontrol" 1
```

```
$
DOPTPRM DESMAX  30       MINDENS 0.002

$HMNAME DESVARS         1design_prop
DTPL    1       PSOLID  2000000720000008
+       MEMBSIZ 50.0
$$
$$  OPTIRESPONSES Data
$$
$$$$ DRESP1 card defines the response function
$$
DRESP1  1       mass_r  MASS
DRESP1  2       w_compl_WCOMP
$$
$$  OPTICONSTRAINTS Data
$$
$
$HMNAME OPTICONSTRAINTS         1mass_constr
$
$$$$ DCONSTR card defines the constraint function
DCONSTR         1       1       0.006

DCONADD         2       1
$$
$$$$ DCONADD creates a combination of many DCONSTR cards
$
$
$$  SPCADD cards
$$
$ Combination of the constraints on the rear dropouts, on the substitute of the front
$ wheel and on the fork
SPCADD          3       1       2
$
$$
$$  SPC Data
$$
$$ Constraints on the rear dropouts
SPC             1   20059   12356       0.0
SPC             1   20060   12356       0.0
$$ Constraint on the substitute of the front wheel
SPC             1       1       3       0.0
$$ Constraint on the rotation of the fork around its axis
SPC             2       4       6       0.0
$
$$
$$  LOADADD cards
$$
$ Combination of the cyclist weight force and the forces due to the right pedaling phase
LOADADD         7   1.0     1.0         4   1.0         5
$ Combination of the cyclist weight force and the forces due to the left pedaling phase
LOADADD         8   1.0     1.0         4   1.0         6
$$
$$  FORCE Data
$$
$ Cyclist weight force on the seat
FORCE           4       9       01.0    0.0     0.0     -687.0
$
$ Force on backrest during the right pedaling phase (magnitude = 700N)
FORCE           5       10      01.0        58.153 692.862 -81.301
$ Force on backrest during the left pedaling phase (magnitude = 700N)
FORCE           6       10      01.0        -58.153 692.862 -81.301
$
$ Force on right pedal during the right pedaling phase (magnitude = 700N)
FORCE           5       2       01.0        -58.153-692.862  81.301
$
$ Force on left pedal during the left pedaling phase (magnitude = 700N)
FORCE           6       3       01.0        58.153-692.862  81.301
$
$
ENDDATA
$$
```

## Input file to run the free-size analysis of the new frame proposal

```
OUTPUT,FSTOSZ,YES
$
STRAIN(H3D) = ALL
```

```
STRESS(H3D) = ALL
DISPLACEMENT(H3D) = ALL
$$
DISPLACEMENT(OPTI) = 10000
GPFORCE(OPTI) = 1000
SPCFORCE(OPTI) = ALL
$$
CFAILURE(H3D,NDIV=1) = ALL
CSTRAIN(H3D,NDIV=1) = ALL
CSTRESS(H3D,NDIV=1) = ALL
$
$$
$$   OBJECTIVES Data
$$
$
$
DESOBJ(MIN)=50001
$
$
DESGLB    50004
$
$
SUBCASE        1
  LABEL Forza peso ciclista
ANALYSIS STATICS
  SPC =         3
  LOAD =        4
  WEIGHT = 0.5
$
$
SUBCASE        2
  LABEL Pedalata DX
ANALYSIS STATICS
  SPC =         3
  LOAD =        7
  WEIGHT = 1.0
$
$
SUBCASE        3
  LABEL Pedalata SX
ANALYSIS STATICS
  SPC =         3
  LOAD =        8
  WEIGHT = 1.0
$$
$$
BEGIN BULK
$$
INCLUDE 'include/INC_TELAIO_for_FREESIZE.fem'
INCLUDE 'include/INC_TRASMISSIONE_SIMULACRO_PLUS.fem'
$
$HMSET    10000         1 "NSET_for_disp_values"
$HMSETTYPE     10000 "regular"
SET    10000   GRID    LIST
+        2       3       4       9       10      20000   20001   20056
+        20057   20058   20059   20060
$
$
$$
$$$$ DSIZE card defines the design variables of the free-size optimization
$$
$HMNAME DESVARS      50000desvar_stack
DSIZE   50000   STACK   20000000
+       MEMBSIZ 50.0
+       COMP    LAMTHK  0.5     2.5
+       COMP    PLYTHK  ALL     0.01
+       COMP    BALANCE 45.0    -45.0                   BYANG
+       COMP    PLYDRP  ALL                     1.25
$$
$$   OPTIRESPONSES Data
$$
DRESP1  50001   wcompl_rWCOMP
DRESP1  50002   mass    MASS    MAT                             SUM20000000
+       2000000120000004100000002000000220000003
$$
$$   OPTICONSTRAINTS Data
$$
$
```

```
$HMNAME OPTICONSTRAINTS    50003constr_M
$
DCONSTR     50003   50002        0.005

DCONADD     50004   50003
$$
$
$$  SPCADD cards
$$
$ Combination of the constraints on the rear dropouts, on the substitute of the front
$ wheel and on the fork
SPCADD          3       1       2
$
$$
$$  SPC Data
$$
$$ Constraints on the rear dropouts
SPC             1   20059   12356     0.0
SPC             1   20060   12356     0.0
$$ Constraint on the substitute of the front wheel
SPC             1       1       3     0.0
$$ Constraint on the rotation of the fork around its axis
SPC             2       4       6     0.0
$
$$
$$  LOADADD cards
$$
$ Combination of the cyclist weight force and the forces due to the right pedaling phase
LOADADD         7     1.0     1.0       4     1.0       5
$ Combination of the cyclist weight force and the forces due to the left pedaling phase
LOADADD         8     1.0     1.0       4     1.0       6
$$
$$  FORCE Data
$$
$ Cyclist weight force on the seat
FORCE           4       9    01.0     0.0     0.0    -687.0
$
$ Force on backrest during the right pedaling phase (magnitude = 700N)
FORCE           5      10    01.0    55.188    0.0     0.0
FORCE           5      10    01.0     0.0  694.435     0.0
FORCE           5      10    01.0     0.0     0.0  -68.665
$ Force on backrest during the left pedaling phase (magnitude = 700N)
FORCE           6      10    01.0   -55.186    0.0     0.0
FORCE           6      10    01.0     0.0  694.435     0.0
FORCE           6      10    01.0     0.0     0.0  -68.665
$
$ Force on right pedal during the right pedaling phase (magnitude = 700N)
FORCE           5       2    01.0   -55.188    0.0     0.0
FORCE           5       2    01.0     0.0-694.435     0.0
FORCE           5       2    01.0     0.0     0.0  68.665
$
$ Force on left pedal during the left pedaling phase (magnitude = 700N)
FORCE           6       3    01.0    55.186    0.0     0.0
FORCE           6       3    01.0     0.0-694.435     0.0
FORCE           6       3    01.0     0.0     0.0  68.665
$
$
ENDDATA
$$
```

## Input file to run the size analysis of the new frame proposal

```
OUTPUT,SZTOSH,YES
OUTPUT,DESIGN,ALL
$
STRAIN(H3D) = ALL
STRESS(H3D) = ALL
DISPLACEMENT(H3D) = ALL
$$
DISPLACEMENT(OPTI) = 10000
SPCFORCE(OPTI) = ALL
$$
CFAILURE(H3D,NDIV=1) = ALL
CSTRAIN(H3D,NDIV=1) = ALL
CSTRESS(H3D,NDIV=1) = ALL
$
$$
```

```
$$   OBJECTIVES Data
$$
$
$
DESOBJ(MIN)=50001
$
$
DESGLB    50004
$
$
SUBCASE        1
  LABEL Forza peso ciclista
ANALYSIS STATICS
  SPC =         3
  LOAD =         4
  WEIGHT = 1.0
$
$
SUBCASE        2
  LABEL Pedalata DX
ANALYSIS STATICS
  SPC =         3
  LOAD =         7
  WEIGHT = 1.0
$
$
SUBCASE        3
  LABEL Pedalata SX
ANALYSIS STATICS
  SPC =         3
  LOAD =         8
  WEIGHT = 1.0
$$
$$
BEGIN BULK
$$
INCLUDE 'include/INC_TELAIO_for_SIZE.fem'
INCLUDE 'include/INC_TRASMISSIONE_SIMULACRO_PLUS.fem'
$
$HMSET    10000         1 "NSET_for_disp_values"
$HMSETTYPE    10000 "regular"
SET     10000   GRID    LIST
+        2        3        4        9       10    20000    20001    20056
+       20057    20058    20059    20060
$
$
$$
$$   OPTIRESPONSES Data
$$
DRESP1   50001   wcompl_rWCOMP
DRESP1   50002   mass    MASS
$$
$$   OPTICONSTRAINTS Data
$$
$
$HMNAME OPTICONSTRAINTS    50003constr_M
$
DCONSTR    50003    50002         0.0071

DCONADD    50004    50003
$$
$
$$   SPCADD cards
$$
$ Combination of the constraints on the rear dropouts, on the substitute of the front
$ wheel and on the fork
SPCADD         3        1        2
$
$$
$$   SPC Data
$$
$$ Constraints on the rear dropouts
SPC            1    20059    12356     0.0
SPC            1    20060    12356     0.0
$$ Constraint on the substitute of the front wheel
SPC            1        1        3     0.0
$$ Constraint on the rotation of the fork around its axis
SPC            2        4        6     0.0
```

135

```
$
$$
$$  LOADADD cards
$$
$ Combination of the cyclist weight force and the forces due to the right pedaling phase
LOADADD        7     1.0     1.0         4     1.0         5
$ Combination of the cyclist weight force and the forces due to the left pedaling phase
LOADADD        8     1.0     1.0         4     1.0         6
$$
$$  FORCE Data
$$
$ Cyclist weight force on the seat
FORCE          4       9     01.0      0.0     0.0       -687.0
$
$ Force on backrest during the right pedaling phase (magnitude = 700N)
FORCE          5      10     01.0     55.188    0.0      0.0
FORCE          5      10     01.0      0.0 694.435      0.0
FORCE          5      10     01.0      0.0     0.0 -68.665
$ Force on backrest during the left pedaling phase (magnitude = 700N)
FORCE          6      10     01.0     -55.186    0.0     0.0
FORCE          6      10     01.0      0.0 694.435      0.0
FORCE          6      10     01.0      0.0     0.0 -68.665
$
$ Force on right pedal during the right pedaling phase (magnitude = 700N)
FORCE          5       2     01.0     -55.188    0.0     0.0
FORCE          5       2     01.0      0.0-694.435      0.0
FORCE          5       2     01.0      0.0     0.0  68.665
$
$ Force on left pedal during the left pedaling phase (magnitude = 700N)
FORCE          6       3     01.0     55.186    0.0      0.0
FORCE          6       3     01.0      0.0-694.435      0.0
FORCE          6       3     01.0      0.0     0.0  68.665
$
$
ENDDATA
$$
```

## Definition of the design variables for the size optimization

In the size optimization we have many design variables and design-variable-to-property relationship cards

and for this reason it was more convenient to include them in the include 'INC_TELAIO_for_SIZE.fem'.

```
$$
$$   Discrete Design Variable Data
$$
$HMNAME DDVAL                  1"DDVAL_GIUNZ"
DDVAL   1       0.035   0.07    0.088   0.105   0.14    0.176   0.211
+       0.281   0.421
$
$HMNAME DDVAL                  2"DDVAL_TUBI"
DDVAL   2       0.07    0.14    0.176   0.211   0.281   0.351   0.421
+       0.562   0.843
$
$HMNAME DDVAL                  3"DDVAL_CORE"
DDVAL   3       3.0     6.0     10.0
$
$HMNAME DESVARS  2000001f2000001
DESVAR   2000001f20000010.02    0.02    1.0                     2
$HMNAME DESVARS  2000002f2000002
DESVAR   2000002f20000020.02    0.02    1.0                     2
$HMNAME DESVARS  2000003f2000003
DESVAR   2000003f20000031.0     1.0     11.0                    3
$HMNAME DESVARS  1011100f1011100
DESVAR   1011100f10111000.02    0.02    1.0                     2
$HMNAME DESVARS  1111100f1111100
DESVAR   1111100f11111000.02    0.02    1.0                     2
$HMNAME DESVARS  2211100f2211100
DESVAR   2211100f22111000.02    0.02    1.0                     2
$HMNAME DESVARS  3211100f3211100
DESVAR   3211100f32111000.02    0.02    1.0                     2
$HMNAME DESVARS  4011100f4011100
DESVAR   4011100f40111000.02    0.02    1.0                     2
$HMNAME DESVARS  4111100f4111100
DESVAR   4111100f41111000.02    0.02    1.0                     2
$HMNAME DESVARS  5211100f5211100
DESVAR   5211100f52111000.02    0.02    1.0                     2
```

```
$HMNAME DESVARS  6211100f6211100
DESVAR   6211100f62111000.02    0.02    1.0                        2
$HMNAME DESVARS  7011100f7011100
DESVAR   7011100f70111000.02    0.02    1.0                        2
$HMNAME DESVARS  1012100f1012100
DESVAR   1012100f10121000.02    0.02    1.0                        2
$HMNAME DESVARS  1112100f1112100
DESVAR   1112100f11121000.02    0.02    1.0                        2
$HMNAME DESVARS  2212100f2212100
DESVAR   2212100f22121000.02    0.02    1.0                        2
$HMNAME DESVARS  3212100f3212100
DESVAR   3212100f32121000.02    0.02    1.0                        2
$HMNAME DESVARS  4012100f4012100
DESVAR   4012100f40121000.02    0.02    1.0                        2
$HMNAME DESVARS  4112100f4112100
DESVAR   4112100f41121000.02    0.02    1.0                        2
$HMNAME DESVARS  5212100f5212100
DESVAR   5212100f52121000.02    0.02    1.0                        2
$HMNAME DESVARS  6212100f6212100
DESVAR   6212100f62121000.02    0.02    1.0                        2
$HMNAME DESVARS  7012100f7012100
DESVAR   7012100f70121000.02    0.02    1.0                        2
$HMNAME DESVARS  1013100f1013100
DESVAR   1013100f10131000.02    0.02    1.0                        2
$HMNAME DESVARS  1113100f1113100
DESVAR   1113100f11131000.02    0.02    1.0                        2
$HMNAME DESVARS  2213100f2213100
DESVAR   2213100f22131000.02    0.02    1.0                        2
$HMNAME DESVARS  3213100f3213100
DESVAR   3213100f32131000.02    0.02    1.0                        2
$HMNAME DESVARS  4013100f4013100
DESVAR   4013100f40131000.02    0.02    1.0                        2
$HMNAME DESVARS  4113100f4113100
DESVAR   4113100f41131000.02    0.02    1.0                        2
$HMNAME DESVARS  5213100f5213100
DESVAR   5213100f52131000.02    0.02    1.0                        2
$HMNAME DESVARS  6213100f6213100
DESVAR   6213100f62131000.02    0.02    1.0                        2
$HMNAME DESVARS  7013100f7013100
DESVAR   7013100f70131000.02    0.02    1.0                        2
$HMNAME DESVARS  1014100f1014100
DESVAR   1014100f10141000.02    0.02    1.0                        2
$HMNAME DESVARS  1114100f1114100
DESVAR   1114100f11141000.02    0.02    1.0                        2
$HMNAME DESVARS  2214100f2214100
DESVAR   2214100f22141000.02    0.02    1.0                        2
$HMNAME DESVARS  3214100f3214100
DESVAR   3214100f32141000.02    0.02    1.0                        2
$HMNAME DESVARS  4014100f4014100
DESVAR   4014100f40141000.02    0.02    1.0                        2
$HMNAME DESVARS  4114100f4114100
DESVAR   4114100f41141000.02    0.02    1.0                        2
$HMNAME DESVARS  5214100f5214100
DESVAR   5214100f52141000.02    0.02    1.0                        2
$HMNAME DESVARS  6214100f6214100
DESVAR   6214100f62141000.02    0.02    1.0                        2
$HMNAME DESVARS  7014100f7014100
DESVAR   7014100f70141000.02    0.02    1.0                        2
$HMNAME DESVARS  1011200f1011200
DESVAR   1011200f10112000.02    0.02    1.0                        2
$HMNAME DESVARS  1111200f1111200
DESVAR   1111200f11112000.02    0.02    1.0                        2
$HMNAME DESVARS  3212300f3212300
DESVAR   3212300f32123000.02    0.02    1.0                        2
$HMNAME DESVARS  3213300f3213300
DESVAR   3213300f32133000.02    0.02    1.0                        2
$HMNAME DESVARS  1012200f1012200
DESVAR   1012200f10122000.02    0.02    1.0                        2
$HMNAME DESVARS  1013200f1013200
DESVAR   1013200f10132000.02    0.02    1.0                        2
$HMNAME DESVARS  1112200f1112200
DESVAR   1112200f11122000.02    0.02    1.0                        2
$HMNAME DESVARS  1113200f1113200
DESVAR   1113200f11132000.02    0.02    1.0                        2
$HMNAME DESVARS  1014200f1014200
DESVAR   1014200f10142000.02    0.02    1.0                        2
$HMNAME DESVARS  1114200f1114200
DESVAR   1114200f11142000.02    0.02    1.0                        2
```

137

```
$HMNAME DESVARS  2211200f2211200
DESVAR   2211200f22112000.02     0.02     1.0                          2
$HMNAME DESVARS  2212200f2212200
DESVAR   2212200f22122000.02     0.02     1.0                          2
$HMNAME DESVARS  2213200f2213200
DESVAR   2213200f22132000.02     0.02     1.0                          2
$HMNAME DESVARS  2214200f2214200
DESVAR   2214200f22142000.02     0.02     1.0                          2
$HMNAME DESVARS  3214200f3214200
DESVAR   3214200f32142000.02     0.02     1.0                          2
$HMNAME DESVARS  3214300f3214300
DESVAR   3214300f32143000.02     0.02     1.0                          2
$HMNAME DESVARS  5211200f5211200
DESVAR   5211200f52112000.02     0.02     1.0                          2
$HMNAME DESVARS  3211200f3211200
DESVAR   3211200f32112000.02     0.02     1.0                          2
$HMNAME DESVARS  3211300f3211300
DESVAR   3211300f32113000.02     0.02     1.0                          2
$HMNAME DESVARS  9111100f9111100
DESVAR   9111100f91111000.02     0.02     1.0                          1
$HMNAME DESVARS  9211100f9211100
DESVAR   9211100f92111000.02     0.02     1.0                          1
$HMNAME DESVARS  9311100f9311100
DESVAR   9311100f93111000.02     0.02     1.0                          1
$HMNAME DESVARS  9411100f9411100
DESVAR   9411100f94111000.02     0.02     1.0                          1
$HMNAME DESVARS  9511100f9511100
DESVAR   9511100f95111000.02     0.02     1.0                          1
$HMNAME DESVARS  9611100f9611100
DESVAR   9611100f96111000.02     0.02     1.0                          1
$HMNAME DESVARS  9711100f9711100
DESVAR   9711100f97111000.02     0.02     1.0                          1
$HMNAME DESVARS  9811100f9811100
DESVAR   9811100f98111000.02     0.02     1.0                          1
$HMNAME DESVARS  9911100f9911100
DESVAR   9911100f99111000.02     0.02     1.0                          1
$HMNAME DESVARS  9101110f9101110
DESVAR   9101110f91011100.02     0.02     1.0                          1
$HMNAME DESVARS  9111110f9111110
DESVAR   9111110f91111100.02     0.02     1.0                          1
$HMNAME DESVARS  9121110f9121110
DESVAR   9121110f91211100.02     0.02     1.0                          1
$HMNAME DESVARS  9131110f9131110
DESVAR   9131110f91311100.02     0.02     1.0                          1
$HMNAME DESVARS  9111200f9111200
DESVAR   9111200f91112000.02     0.02     1.0                          1
$HMNAME DESVARS  9111300f9111300
DESVAR   9111300f91113000.02     0.02     1.0                          1
$HMNAME DESVARS  9111400f9111400
DESVAR   9111400f91114000.02     0.02     1.0                          1
$HMNAME DESVARS  9212100f9212100
DESVAR   9212100f92121000.02     0.02     1.0                          1
$HMNAME DESVARS  9213100f9213100
DESVAR   9213100f92131000.02     0.02     1.0                          1
$HMNAME DESVARS  9214100f9214100
DESVAR   9214100f92141000.02     0.02     1.0                          1
$HMNAME DESVARS  9312100f9312100
DESVAR   9312100f93121000.02     0.02     1.0                          1
$HMNAME DESVARS  9313100f9313100
DESVAR   9313100f93131000.02     0.02     1.0                          1
$HMNAME DESVARS  9314100f9314100
DESVAR   9314100f93141000.02     0.02     1.0                          1
$HMNAME DESVARS  9412100f9412100
DESVAR   9412100f94121000.02     0.02     1.0                          1
$HMNAME DESVARS  9413100f9413100
DESVAR   9413100f94131000.02     0.02     1.0                          1
$HMNAME DESVARS  9414100f9414100
DESVAR   9414100f94141000.02     0.02     1.0                          1
$HMNAME DESVARS  9512100f9512100
DESVAR   9512100f95121000.02     0.02     1.0                          1
$HMNAME DESVARS  9513100f9513100
DESVAR   9513100f95131000.02     0.02     1.0                          1
$HMNAME DESVARS  9514100f9514100
DESVAR   9514100f95141000.02     0.02     1.0                          1
$HMNAME DESVARS  9612100f9612100
DESVAR   9612100f96121000.02     0.02     1.0                          1
$HMNAME DESVARS  9613100f9613100
DESVAR   9613100f96131000.02     0.02     1.0                          1
```

```
$HMNAME DESVARS  9614100f9614100
DESVAR   9614100f96141000.02    0.02    1.0                        1
$HMNAME DESVARS  9712100f9712100
DESVAR   9712100f97121000.02    0.02    1.0                        1
$HMNAME DESVARS  9713100f9713100
DESVAR   9713100f97131000.02    0.02    1.0                        1
$HMNAME DESVARS  9714100f9714100
DESVAR   9714100f97141000.02    0.02    1.0                        1
$HMNAME DESVARS  9812100f9812100
DESVAR   9812100f98121000.02    0.02    1.0                        1
$HMNAME DESVARS  9813100f9813100
DESVAR   9813100f98131000.02    0.02    1.0                        1
$HMNAME DESVARS  9814100f9814100
DESVAR   9814100f98141000.02    0.02    1.0                        1
$HMNAME DESVARS  9912100f9912100
DESVAR   9912100f99121000.02    0.02    1.0                        1
$HMNAME DESVARS  9913100f9913100
DESVAR   9913100f99131000.02    0.02    1.0                        1
$HMNAME DESVARS  9914100f9914100
DESVAR   9914100f99141000.02    0.02    1.0                        1
$HMNAME DESVARS  9101210f9101210
DESVAR   9101210f91012100.02    0.02    1.0                        1
$HMNAME DESVARS  9101310f9101310
DESVAR   9101310f91013100.02    0.02    1.0                        1
$HMNAME DESVARS  9101410f9101410
DESVAR   9101410f91014100.02    0.02    1.0                        1
$HMNAME DESVARS  9111210f9111210
DESVAR   9111210f91112100.02    0.02    1.0                        1
$HMNAME DESVARS  9111310f9111310
DESVAR   9111310f91113100.02    0.02    1.0                        1
$HMNAME DESVARS  9111410f9111410
DESVAR   9111410f91114100.02    0.02    1.0                        1
$HMNAME DESVARS  9121210f9121210
DESVAR   9121210f91212100.02    0.02    1.0                        1
$HMNAME DESVARS  9121310f9121310
DESVAR   9121310f91213100.02    0.02    1.0                        1
$HMNAME DESVARS  9121410f9121410
DESVAR   9121410f91214100.02    0.02    1.0                        1
$HMNAME DESVARS  9131210f9131210
DESVAR   9131210f91312100.02    0.02    1.0                        1
$HMNAME DESVARS  9131310f9131310
DESVAR   9131310f91313100.02    0.02    1.0                        1
$HMNAME DESVARS  9131410f9131410
DESVAR   9131410f91314100.02    0.02    1.0                        1
$HMNAME DESVARS  1011300f1011300
DESVAR   1011300f10113000.02    0.02    1.0                        2
$HMNAME DESVARS  1014300f1014300
DESVAR   1014300f10143000.02    0.02    1.0                        2
$HMNAME DESVARS  1114300f1114300
DESVAR   1114300f11143000.02    0.02    1.0                        2
$HMNAME DESVARS  1111300f1111300
DESVAR   1111300f11113000.02    0.02    1.0                        2
$HMNAME DESVARS  1012300f1012300
DESVAR   1012300f10123000.02    0.02    1.0                        2
$HMNAME DESVARS  1013300f1013300
DESVAR   1013300f10133000.02    0.02    1.0                        2
$HMNAME DESVARS  1112300f1112300
DESVAR   1112300f11123000.02    0.02    1.0                        2
$HMNAME DESVARS  1113300f1113300
DESVAR   1113300f11133000.02    0.02    1.0                        2
$HMNAME DESVARS  1012400f1012400
DESVAR   1012400f10124000.02    0.02    1.0                        2
$HMNAME DESVARS  1013400f1013400
DESVAR   1013400f10134000.02    0.02    1.0                        2
$HMNAME DESVARS  1112400f1112400
DESVAR   1112400f11124000.02    0.02    1.0                        2
$HMNAME DESVARS  1113400f1113400
DESVAR   1113400f11134000.02    0.02    1.0                        2
$HMNAME DESVARS  9914101DCOMP
DCOMP    9914101 STACK   20000003
+        BALANCE 45.0    -45.0              BYANG
+        PLYDRP  ALL     TOTDRP  1.25
$HMNAME DVPRELS 2000001 DVPREL1_2000001
DVPREL1 2000001 PLY      2000001       T              0.0
+        2000001 1.0
$HMNAME DVPRELS 2000002 DVPREL1_2000002
DVPREL1 2000002 PLY      2000002       T              0.0
+        2000002 1.0
```

```
$HMNAME DVPRELS 2000003 DVPREL1_2000003
DVPREL1 2000003 PLY      2000003      T              0.0
+       2000003 1.0
$HMNAME DVPRELS 1011100 DVPREL1_1011100
DVPREL1 1011100 PLY      1011100      T              0.0
+       1011100 1.0
$HMNAME DVPRELS 1111100 DVPREL1_1111100
DVPREL1 1111100 PLY      1111100      T              0.0
+       1111100 1.0
$HMNAME DVPRELS 2211100 DVPREL1_2211100
DVPREL1 2211100 PLY      2211100      T              0.0
+       2211100 1.0
$HMNAME DVPRELS 3211100 DVPREL1_3211100
DVPREL1 3211100 PLY      3211100      T              0.0
+       3211100 1.0
$HMNAME DVPRELS 4011100 DVPREL1_4011100
DVPREL1 4011100 PLY      4011100      T              0.0
+       4011100 1.0
$HMNAME DVPRELS 4111100 DVPREL1_4111100
DVPREL1 4111100 PLY      4111100      T              0.0
+       4111100 1.0
$HMNAME DVPRELS 5211100 DVPREL1_5211100
DVPREL1 5211100 PLY      5211100      T              0.0
+       5211100 1.0
$HMNAME DVPRELS 6211100 DVPREL1_6211100
DVPREL1 6211100 PLY      6211100      T              0.0
+       6211100 1.0
$HMNAME DVPRELS 7011100 DVPREL1_7011100
DVPREL1 7011100 PLY      7011100      T              0.0
+       7011100 1.0
$HMNAME DVPRELS 1012100 DVPREL1_1012100
DVPREL1 1012100 PLY      1012100      T              0.0
+       1012100 1.0
$HMNAME DVPRELS 1112100 DVPREL1_1112100
DVPREL1 1112100 PLY      1112100      T              0.0
+       1112100 1.0
$HMNAME DVPRELS 2212100 DVPREL1_2212100
DVPREL1 2212100 PLY      2212100      T              0.0
+       2212100 1.0
$HMNAME DVPRELS 3212100 DVPREL1_3212100
DVPREL1 3212100 PLY      3212100      T              0.0
+       3212100 1.0
$HMNAME DVPRELS 4012100 DVPREL1_4012100
DVPREL1 4012100 PLY      4012100      T              0.0
+       4012100 1.0
$HMNAME DVPRELS 4112100 DVPREL1_4112100
DVPREL1 4112100 PLY      4112100      T              0.0
+       4112100 1.0
$HMNAME DVPRELS 5212100 DVPREL1_5212100
DVPREL1 5212100 PLY      5212100      T              0.0
+       5212100 1.0
$HMNAME DVPRELS 6212100 DVPREL1_6212100
DVPREL1 6212100 PLY      6212100      T              0.0
+       6212100 1.0
$HMNAME DVPRELS 7012100 DVPREL1_7012100
DVPREL1 7012100 PLY      7012100      T              0.0
+       7012100 1.0
$HMNAME DVPRELS 1013100 DVPREL1_1013100
DVPREL1 1013100 PLY      1013100      T              0.0
+       1013100 1.0
$HMNAME DVPRELS 1113100 DVPREL1_1113100
DVPREL1 1113100 PLY      1113100      T              0.0
+       1113100 1.0
$HMNAME DVPRELS 2213100 DVPREL1_2213100
DVPREL1 2213100 PLY      2213100      T              0.0
+       2213100 1.0
$HMNAME DVPRELS 3213100 DVPREL1_3213100
DVPREL1 3213100 PLY      3213100      T              0.0
+       3213100 1.0
$HMNAME DVPRELS 4013100 DVPREL1_4013100
DVPREL1 4013100 PLY      4013100      T              0.0
+       4013100 1.0
$HMNAME DVPRELS 4113100 DVPREL1_4113100
DVPREL1 4113100 PLY      4113100      T              0.0
+       4113100 1.0
$HMNAME DVPRELS 5213100 DVPREL1_5213100
DVPREL1 5213100 PLY      5213100      T              0.0
+       5213100 1.0
```

```
$HMNAME DVPRELS 6213100 DVPREL1_6213100
DVPREL1 6213100 PLY      6213100      T              0.0
+       6213100 1.0
$HMNAME DVPRELS 7013100 DVPREL1_7013100
DVPREL1 7013100 PLY      7013100      T              0.0
+       7013100 1.0
$HMNAME DVPRELS 1014100 DVPREL1_1014100
DVPREL1 1014100 PLY      1014100      T              0.0
+       1014100 1.0
$HMNAME DVPRELS 1114100 DVPREL1_1114100
DVPREL1 1114100 PLY      1114100      T              0.0
+       1114100 1.0
$HMNAME DVPRELS 2214100 DVPREL1_2214100
DVPREL1 2214100 PLY      2214100      T              0.0
+       2214100 1.0
$HMNAME DVPRELS 3214100 DVPREL1_3214100
DVPREL1 3214100 PLY      3214100      T              0.0
+       3214100 1.0
$HMNAME DVPRELS 4014100 DVPREL1_4014100
DVPREL1 4014100 PLY      4014100      T              0.0
+       4014100 1.0
$HMNAME DVPRELS 4114100 DVPREL1_4114100
DVPREL1 4114100 PLY      4114100      T              0.0
+       4114100 1.0
$HMNAME DVPRELS 5214100 DVPREL1_5214100
DVPREL1 5214100 PLY      5214100      T              0.0
+       5214100 1.0
$HMNAME DVPRELS 6214100 DVPREL1_6214100
DVPREL1 6214100 PLY      6214100      T              0.0
+       6214100 1.0
$HMNAME DVPRELS 7014100 DVPREL1_7014100
DVPREL1 7014100 PLY      7014100      T              0.0
+       7014100 1.0
$HMNAME DVPRELS 1011200 DVPREL1_1011200
DVPREL1 1011200 PLY      1011200      T              0.0
+       1011200 1.0
$HMNAME DVPRELS 1111200 DVPREL1_1111200
DVPREL1 1111200 PLY      1111200      T              0.0
+       1111200 1.0
$HMNAME DVPRELS 3212300 DVPREL1_3212300
DVPREL1 3212300 PLY      3212300      T              0.0
+       3212300 1.0
$HMNAME DVPRELS 3213300 DVPREL1_3213300
DVPREL1 3213300 PLY      3213300      T              0.0
+       3213300 1.0
$HMNAME DVPRELS 1012200 DVPREL1_1012200
DVPREL1 1012200 PLY      1012200      T              0.0
+       1012200 1.0
$HMNAME DVPRELS 1013200 DVPREL1_1013200
DVPREL1 1013200 PLY      1013200      T              0.0
+       1013200 1.0
$HMNAME DVPRELS 1112200 DVPREL1_1112200
DVPREL1 1112200 PLY      1112200      T              0.0
+       1112200 1.0
$HMNAME DVPRELS 1113200 DVPREL1_1113200
DVPREL1 1113200 PLY      1113200      T              0.0
+       1113200 1.0
$HMNAME DVPRELS 1014200 DVPREL1_1014200
DVPREL1 1014200 PLY      1014200      T              0.0
+       1014200 1.0
$HMNAME DVPRELS 1114200 DVPREL1_1114200
DVPREL1 1114200 PLY      1114200      T              0.0
+       1114200 1.0
$HMNAME DVPRELS 2211200 DVPREL1_2211200
DVPREL1 2211200 PLY      2211200      T              0.0
+       2211200 1.0
$HMNAME DVPRELS 2212200 DVPREL1_2212200
DVPREL1 2212200 PLY      2212200      T              0.0
+       2212200 1.0
$HMNAME DVPRELS 2213200 DVPREL1_2213200
DVPREL1 2213200 PLY      2213200      T              0.0
+       2213200 1.0
$HMNAME DVPRELS 2214200 DVPREL1_2214200
DVPREL1 2214200 PLY      2214200      T              0.0
+       2214200 1.0
$HMNAME DVPRELS 3214200 DVPREL1_3214200
DVPREL1 3214200 PLY      3214200      T              0.0
+       3214200 1.0
```

```
$HMNAME DVPRELS 3214300 DVPREL1_3214300
DVPREL1 3214300 PLY       3214300       T               0.0
+       3214300 1.0
$HMNAME DVPRELS 5211200 DVPREL1_5211200
DVPREL1 5211200 PLY       5211200       T               0.0
+       5211200 1.0
$HMNAME DVPRELS 3211200 DVPREL1_3211200
DVPREL1 3211200 PLY       3211200       T               0.0
+       3211200 1.0
$HMNAME DVPRELS 3211300 DVPREL1_3211300
DVPREL1 3211300 PLY       3211300       T               0.0
+       3211300 1.0
$HMNAME DVPRELS 9111100 DVPREL1_9111100
DVPREL1 9111100 PLY       9111100       T               0.0
+       9111100 1.0
$HMNAME DVPRELS 9211100 DVPREL1_9211100
DVPREL1 9211100 PLY       9211100       T               0.0
+       9211100 1.0
$HMNAME DVPRELS 9311100 DVPREL1_9311100
DVPREL1 9311100 PLY       9311100       T               0.0
+       9311100 1.0
$HMNAME DVPRELS 9411100 DVPREL1_9411100
DVPREL1 9411100 PLY       9411100       T               0.0
+       9411100 1.0
$HMNAME DVPRELS 9511100 DVPREL1_9511100
DVPREL1 9511100 PLY       9511100       T               0.0
+       9511100 1.0
$HMNAME DVPRELS 9611100 DVPREL1_9611100
DVPREL1 9611100 PLY       9611100       T               0.0
+       9611100 1.0
$HMNAME DVPRELS 9711100 DVPREL1_9711100
DVPREL1 9711100 PLY       9711100       T               0.0
+       9711100 1.0
$HMNAME DVPRELS 9811100 DVPREL1_9811100
DVPREL1 9811100 PLY       9811100       T               0.0
+       9811100 1.0
$HMNAME DVPRELS 9911100 DVPREL1_9911100
DVPREL1 9911100 PLY       9911100       T               0.0
+       9911100 1.0
$HMNAME DVPRELS 9101110 DVPREL1_9101110
DVPREL1 9101110 PLY       9101110       T               0.0
+       9101110 1.0
$HMNAME DVPRELS 9111110 DVPREL1_9111110
DVPREL1 9111110 PLY       9111110       T               0.0
+       9111110 1.0
$HMNAME DVPRELS 9121110 DVPREL1_9121110
DVPREL1 9121110 PLY       9121110       T               0.0
+       9121110 1.0
$HMNAME DVPRELS 9131110 DVPREL1_9131110
DVPREL1 9131110 PLY       9131110       T               0.0
+       9131110 1.0
$HMNAME DVPRELS 9111200 DVPREL1_9111200
DVPREL1 9111200 PLY       9111200       T               0.0
+       9111200 1.0
$HMNAME DVPRELS 9111300 DVPREL1_9111300
DVPREL1 9111300 PLY       9111300       T               0.0
+       9111300 1.0
$HMNAME DVPRELS 9111400 DVPREL1_9111400
DVPREL1 9111400 PLY       9111400       T               0.0
+       9111400 1.0
$HMNAME DVPRELS 9212100 DVPREL1_9212100
DVPREL1 9212100 PLY       9212100       T               0.0
+       9212100 1.0
$HMNAME DVPRELS 9213100 DVPREL1_9213100
DVPREL1 9213100 PLY       9213100       T               0.0
+       9213100 1.0
$HMNAME DVPRELS 9214100 DVPREL1_9214100
DVPREL1 9214100 PLY       9214100       T               0.0
+       9214100 1.0
$HMNAME DVPRELS 9312100 DVPREL1_9312100
DVPREL1 9312100 PLY       9312100       T               0.0
+       9312100 1.0
$HMNAME DVPRELS 9313100 DVPREL1_9313100
DVPREL1 9313100 PLY       9313100       T               0.0
+       9313100 1.0
$HMNAME DVPRELS 9314100 DVPREL1_9314100
DVPREL1 9314100 PLY       9314100       T               0.0
+       9314100 1.0
```

```
$HMNAME DVPRELS 9412100 DVPREL1_9412100
DVPREL1 9412100 PLY      9412100     T              0.0
+       9412100 1.0
$HMNAME DVPRELS 9413100 DVPREL1_9413100
DVPREL1 9413100 PLY      9413100     T              0.0
+       9413100 1.0
$HMNAME DVPRELS 9414100 DVPREL1_9414100
DVPREL1 9414100 PLY      9414100     T              0.0
+       9414100 1.0
$HMNAME DVPRELS 9512100 DVPREL1_9512100
DVPREL1 9512100 PLY      9512100     T              0.0
+       9512100 1.0
$HMNAME DVPRELS 9513100 DVPREL1_9513100
DVPREL1 9513100 PLY      9513100     T              0.0
+       9513100 1.0
$HMNAME DVPRELS 9514100 DVPREL1_9514100
DVPREL1 9514100 PLY      9514100     T              0.0
+       9514100 1.0
$HMNAME DVPRELS 9612100 DVPREL1_9612100
DVPREL1 9612100 PLY      9612100     T              0.0
+       9612100 1.0
$HMNAME DVPRELS 9613100 DVPREL1_9613100
DVPREL1 9613100 PLY      9613100     T              0.0
+       9613100 1.0
$HMNAME DVPRELS 9614100 DVPREL1_9614100
DVPREL1 9614100 PLY      9614100     T              0.0
+       9614100 1.0
$HMNAME DVPRELS 9712100 DVPREL1_9712100
DVPREL1 9712100 PLY      9712100     T              0.0
+       9712100 1.0
$HMNAME DVPRELS 9713100 DVPREL1_9713100
DVPREL1 9713100 PLY      9713100     T              0.0
+       9713100 1.0
$HMNAME DVPRELS 9714100 DVPREL1_9714100
DVPREL1 9714100 PLY      9714100     T              0.0
+       9714100 1.0
$HMNAME DVPRELS 9812100 DVPREL1_9812100
DVPREL1 9812100 PLY      9812100     T              0.0
+       9812100 1.0
$HMNAME DVPRELS 9813100 DVPREL1_9813100
DVPREL1 9813100 PLY      9813100     T              0.0
+       9813100 1.0
$HMNAME DVPRELS 9814100 DVPREL1_9814100
DVPREL1 9814100 PLY      9814100     T              0.0
+       9814100 1.0
$HMNAME DVPRELS 9912100 DVPREL1_9912100
DVPREL1 9912100 PLY      9912100     T              0.0
+       9912100 1.0
$HMNAME DVPRELS 9913100 DVPREL1_9913100
DVPREL1 9913100 PLY      9913100     T              0.0
+       9913100 1.0
$HMNAME DVPRELS 9914100 DVPREL1_9914100
DVPREL1 9914100 PLY      9914100     T              0.0
+       9914100 1.0
$HMNAME DVPRELS 9101210 DVPREL1_9101210
DVPREL1 9101210 PLY      9101210     T              0.0
+       9101210 1.0
$HMNAME DVPRELS 9101310 DVPREL1_9101310
DVPREL1 9101310 PLY      9101310     T              0.0
+       9101310 1.0
$HMNAME DVPRELS 9101410 DVPREL1_9101410
DVPREL1 9101410 PLY      9101410     T              0.0
+       9101410 1.0
$HMNAME DVPRELS 9111210 DVPREL1_9111210
DVPREL1 9111210 PLY      9111210     T              0.0
+       9111210 1.0
$HMNAME DVPRELS 9111310 DVPREL1_9111310
DVPREL1 9111310 PLY      9111310     T              0.0
+       9111310 1.0
$HMNAME DVPRELS 9111410 DVPREL1_9111410
DVPREL1 9111410 PLY      9111410     T              0.0
+       9111410 1.0
$HMNAME DVPRELS 9121210 DVPREL1_9121210
DVPREL1 9121210 PLY      9121210     T              0.0
+       9121210 1.0
$HMNAME DVPRELS 9121310 DVPREL1_9121310
DVPREL1 9121310 PLY      9121310     T              0.0
+       9121310 1.0
```

```
$HMNAME DVPRELS 9121410 DVPREL1_9121410
DVPREL1 9121410 PLY        9121410      T                    0.0
+       9121410 1.0
$HMNAME DVPRELS 9131210 DVPREL1_9131210
DVPREL1 9131210 PLY        9131210      T                    0.0
+       9131210 1.0
$HMNAME DVPRELS 9131310 DVPREL1_9131310
DVPREL1 9131310 PLY        9131310      T                    0.0
+       9131310 1.0
$HMNAME DVPRELS 9131410 DVPREL1_9131410
DVPREL1 9131410 PLY        9131410      T                    0.0
+       9131410 1.0
$HMNAME DVPRELS 1011300 DVPREL1_1011300
DVPREL1 1011300 PLY        1011300      T                    0.0
+       1011300 1.0
$HMNAME DVPRELS 1014300 DVPREL1_1014300
DVPREL1 1014300 PLY        1014300      T                    0.0
+       1014300 1.0
$HMNAME DVPRELS 9914103 DVPREL1_1114300
DVPREL1 9914103 PLY        1114300      T                    0.0
+       1114300 1.0
$HMNAME DVPRELS 9914104 DVPREL1_1111300
DVPREL1 9914104 PLY        1111300      T                    0.0
+       1111300 1.0
$HMNAME DVPRELS 1012300 DVPREL1_1012300
DVPREL1 1012300 PLY        1012300      T                    0.0
+       1012300 1.0
$HMNAME DVPRELS 1013300 DVPREL1_1013300
DVPREL1 1013300 PLY        1013300      T                    0.0
+       1013300 1.0
$HMNAME DVPRELS 1112300 DVPREL1_1112300
DVPREL1 1112300 PLY        1112300      T                    0.0
+       1112300 1.0
$HMNAME DVPRELS 1113300 DVPREL1_1113300
DVPREL1 1113300 PLY        1113300      T                    0.0
+       1113300 1.0
$HMNAME DVPRELS 1012400 DVPREL1_1012400
DVPREL1 1012400 PLY        1012400      T                    0.0
+       1012400 1.0
$HMNAME DVPRELS 1013400 DVPREL1_1013400
DVPREL1 1013400 PLY        1013400      T                    0.0
+       1013400 1.0
$HMNAME DVPRELS 1112400 DVPREL1_1112400
DVPREL1 1112400 PLY        1112400      T                    0.0
+       1112400 1.0
$HMNAME DVPRELS 1113400 DVPREL1_1113400
DVPREL1 1113400 PLY        1113400      T                    0.0
+       1113400 1.0
```

## Input file to run the shuffle analysis of the new frame proposal

```
OUTPUT,DESIGN,ALL
$
STRAIN(H3D) = ALL
STRESS(H3D) = ALL
DISPLACEMENT(H3D) = ALL
$$
DISPLACEMENT(OPTI) = 10000
SPCFORCE(OPTI) = ALL
$$
CFAILURE(H3D,NDIV=1) = ALL
CSTRAIN(H3D,NDIV=1) = ALL
CSTRESS(H3D,NDIV=1) = ALL
$
$$
$$  OBJECTIVES Data
$$
$
$
DESOBJ(MIN)=50001
$
$
DESGLB    50004
$
$
SUBCASE        1
  LABEL Forza peso ciclista
```

```
ANALYSIS STATICS
  SPC =        3
  LOAD =        4
  WEIGHT = 1.0
$
$
SUBCASE        2
  LABEL Pedalata DX
ANALYSIS STATICS
  SPC =        3
  LOAD =        7
  WEIGHT = 1.0
$
$
SUBCASE        3
  LABEL Pedalata SX
ANALYSIS STATICS
  SPC =        3
  LOAD =        8
  WEIGHT = 1.0
$$
$$
BEGIN BULK
$$
INCLUDE 'include/INC_TELAIO_AleB_for_shuffle.fem'
INCLUDE 'include/INC_TRASMISSIONE_SIMULACRO_PLUS.fem'
$
$HMSET    11000        1 "NSET_for_disp_values"
$HMSETTYPE     11000 "regular"
SET    11000    GRID    LIST
+        2        3        4        9        10     20000    20001    20056
+     20057    20058    20059    20060
$
$
$$
$$   OPTIRESPONSES Data
$$
DRESP1  50001    wcompl_rWCOMP
DRESP1  50002    mass    MASS
$$
$$   OPTICONSTRAINTS Data
$$
$
$HMNAME OPTICONSTRAINTS    50003constr_M
$
DCONSTR    50003    50002        0.0071

DCONADD    50004    50003
$$
$
$$   SPCADD cards
$$
$ Combination of the constraints on the rear dropouts, on the substitute of the front
$ wheel and on the fork
SPCADD        3        1        2
$
$$
$$   SPC Data
$$
$$ Constraints on the rear dropouts
SPC            1    20059    12356     0.0
SPC            1    20060    12356     0.0
$$ Constraint on the substitute of the front wheel
SPC            1        1        3     0.0
$$ Constraint on the rotation of the fork around its axis
SPC            2        4        6     0.0
$
$$
$$   LOADADD cards
$$
$ Combination of the cyclist weight force and the forces due to the right pedaling phase
LOADADD        7     1.0     1.0        4     1.0        5
$ Combination of the cyclist weight force and the forces due to the left pedaling phase
LOADADD        8     1.0     1.0        4     1.0        6
$$
$$   FORCE Data
$$
$ Cyclist weight force on the seat
```

```
FORCE            4        9        01.0      0.0      0.0      -687.0
$
$ Force on backrest during the right pedaling phase (magnitude = 700N)
FORCE            5       10        01.0     55.188     0.0      0.0
FORCE            5       10        01.0      0.0 694.435      0.0
FORCE            5       10        01.0      0.0      0.0 -68.665
$ Force on backrest during the left pedaling phase (magnitude = 700N)
FORCE            6       10        01.0    -55.186     0.0      0.0
FORCE            6       10        01.0      0.0 694.435      0.0
FORCE            6       10        01.0      0.0      0.0 -68.665
$
$ Force on right pedal during the right pedaling phase (magnitude = 700N)
FORCE            5        2        01.0    -55.188     0.0      0.0
FORCE            5        2        01.0      0.0-694.435      0.0
FORCE            5        2        01.0      0.0      0.0  68.665
$
$ Force on left pedal during the left pedaling phase (magnitude = 700N)
FORCE            6        3        01.0     55.186     0.0      0.0
FORCE            6        3        01.0      0.0-694.435      0.0
FORCE            6        3        01.0      0.0      0.0  68.665
$
$
ENDDATA
$$
```

## Design variables for the shuffle optimization

These design variables are in the include 'INC_TELAIO_AleB_for_shuffle.fem'.

```
$HMNAME DESVARS           1DSHUF_T10
DSHUFFLE         1   STACK20000006
+        MAXSUCC      ALL        4
+          COVER        1      0.0     45.0     90.0    -45.0
$HMNAME DESVARS           2DSHUF_T11
DSHUFFLE         2   STACK20000007
+        MAXSUCC      ALL        4
+          COVER        1      0.0     45.0     90.0    -45.0
```

# APPENDIX C: INPUT FILES TO RUN THE FINAL ANALYSES OF THE NEW FRAME PROPOSAL

This appendix is dedicated to the input files used to run the final analyses of the new frame proposal. The include files are not provided due to their large dimension.

**Input file to run the static analysis of the new frame proposal**

```
STRAIN(H3D) = ALL
STRESS(H3D) = ALL
DISPLACEMENT(H3D) = ALL
$$
DISPLACEMENT(OPTI) = 10000
GPFORCE(OPTI) = 1000
SPCFORCE(OPTI) = ALL
$$
CFAILURE(H3D,NDIV=1) = ALL
CSTRAIN(H3D,NDIV=1) = ALL
CSTRESS(H3D,NDIV=1) = ALL
$
SUBCASE          1
  LABEL Forza peso ciclista
ANALYSIS STATICS
  SPC =          3
  LOAD =          4
$
$
SUBCASE          2
  LABEL Pedalata DX
ANALYSIS STATICS
  SPC =          3
  LOAD =          7
$
$
SUBCASE          3
  LABEL Pedalata SX
ANALYSIS STATICS
  SPC =          3
  LOAD =          8
$$
$$
BEGIN BULK
$$
INCLUDE 'include/INC_TELAIO_AleB.fem'
INCLUDE 'include/INC_TRASMISSIONE_SIMULACRO_PLUS.fem'
$
$$  SPCADD cards
$$
$ Combination of the constraints on the rear dropouts, on the substitute of the front
$ wheel and on the fork
SPCADD          3          1          2
$
$$
$$  SPC Data
$$
$$ Constraints on the rear dropouts
SPC          1   20059   12356      0.0
SPC          1   20060   12356      0.0
$$ Constraint on the substitute of the front wheel
SPC          1          1          3      0.0
$$ Constraint on the rotation of the fork around its axis
SPC          2          4          6      0.0
$
$$
$$  LOADADD cards
$$
$ Combination of the cyclist weight force and the forces due to the right pedaling phase
LOADADD          7      1.0      1.0          4      1.0          5
$ Combination of the cyclist weight force and the forces due to the left pedaling phase
```

```
LOADADD         8      1.0     1.0      4      1.0      6
$$
$$  FORCE Data
$$
$ Cyclist weight force on the seat
FORCE           4      9      01.0     0.0     0.0     -687.0
$
$ Force on backrest during the right pedaling phase (magnitude = 700N)
FORCE           5      10     01.0    55.188   0.0     0.0
FORCE           5      10     01.0     0.0  694.435    0.0
FORCE           5      10     01.0     0.0    0.0  -68.665
$ Force on backrest during the left pedaling phase (magnitude = 700N)
FORCE           6      10     01.0   -55.186   0.0     0.0
FORCE           6      10     01.0     0.0  694.435    0.0
FORCE           6      10     01.0     0.0    0.0  -68.665
$
$ Force on right pedal during the right pedaling phase (magnitude = 700N)
FORCE           5      2      01.0   -55.188   0.0     0.0
FORCE           5      2      01.0     0.0-694.435     0.0
FORCE           5      2      01.0     0.0    0.0   68.665
$
$ Force on left pedal during the left pedaling phase (magnitude = 700N)
FORCE           6      3      01.0    55.186   0.0     0.0
FORCE           6      3      01.0     0.0-694.435     0.0
FORCE           6      3      01.0     0.0    0.0   68.665
$
$
ENDDATA
$$
```

**Input file to run the modal analysis of the new proposed model, with frame and cyclist mass**

```
$
SUBCASE        1
  LABEL Modale
ANALYSIS MODES
  METHOD(STRUCTURE) =      100
  DISPLACEMENT = ALL
$
BEGIN BULK
$
INCLUDE 'include/INC_TELAIO_AleB.fem'
INCLUDE 'include/INC_MASSA_CICLISTA.fem'
$
PARAM,G,0.06
PARAM,EFFMAS,YES
$$
EIGRA       100    0.0   200.0
$$
ENDDATA
```

**Input file to run the modal analysis of the new proposed model, with frame, cyclist mass and removable aerodynamic faring**

```
$
SUBCASE        1
  LABEL Modale
ANALYSIS MODES
  METHOD(STRUCTURE) =      100
  DISPLACEMENT = ALL
$
BEGIN BULK
$
INCLUDE 'include/INC_TELAIO_AleB.fem'
INCLUDE 'include/INC_CARENA_PHONEIX.fem'
INCLUDE 'include/INC_MASSA_CICLISTA.fem'
INCLUDE 'include/INC_GANCI_CARENA_PHONEIX_TELAIO_AleB.fem'
$
PARAM,G,0.06
PARAM,EFFMAS,YES
$$
EIGRA       100    0.0   200.0
$$
ENDDATA
```

# BIBLIOGRAPHY

[1]     World Human Powered Speed Challenge. At: *http://ihpva.org/whpsc/*, (Accessed on 01.12.2022)

[2]     Team Policumbent. At: *https://www.policumbent.it/it/prototypes/taurus/*, (Accessed on 01.12.2019)

[3]     Bathe K.J., *Finite Element Procedures*, Upper Saddle River, Prentice Hall Inc., 1996

[4]     Optistruct Reference Guide, *Optistruct Overview*. At:
        *https://2017.help.altair.com/2017/hm/hwsolvers.htm?os_features.htm*, (Accessed on 06.06.2021)

[5]     Optistruct Reference Guide, *Input file structure*. At:
        *https://2017.help.altair.com/2017/hm/hwsolvers.htm?input_file.htm*, (Accessed on 06.06.2021)

[6]     Liu G.R., Quek S.S., *The finite element method a practical course*, Oxford, Butterworth-Heinemann,
        2003

[7]     Optistruct Reference Guide, *Bulk Data Section*. At:
        *https://2017.help.altair.com/2017/hm/hwsolvers.htm?bulk_data_section.htm*, (Accessed on
        06.06.2021)

[8]     Wollschlager J.A., *Introduction to practical aspects of composites with Altair Optistruct*, Altair
        Engineering Inc., 2021

[9]     Hull D., *An Introduction to composite materials*, Cambridge, Cambridge University Press, 1995

[10]    Gay D., Hoa S.V., *Composite materials design and applications*, Boca Raton, CRC Press, 2007

[11]    Alessandro Crea, *Un innovativo cambio ciclistico progettato dal team Policumbent* (26 Maggio 2020).
        At:
        *https://poliflash.polito.it/ricerca_e_innovazione/un_innovativo_cambio_ciclistico_progettato_dal_te
        am_policumbent*, (Accessed on 30.05.2020)

[12]    British Standards Institute (2005), *EN14781:2005 Racing bicycles – Safety requirements and test
        methods*. At: *https://bsol-bsigroup-
        com.ezproxy.biblio.polito.it/PdfViewer/Viewer?pid=000000000030030396*, (Accessed on 16.05.2021)

[13]    Gordon W. and Schmidt T., *Bicycling Science*, Cambridge, The MIT Press, 2020

[14]    Genta G. and Morello L., *The Automotive Chassis Volume 1: Components Design*, Springer, 2009

[15]   Genta G. and Morello L., *The Automotive Chassis Volume 2: System Design*, Springer, 2009

[16]   *Structural Opimization using Optistruct - Concepts, Analysis, and Optimization for General Structures*, Altair Engineering Inc.

[17]   *Practical Aspects of Structural Optimization - A Study Guide*, Altair University, 2018

[18]   Singiresu S. Rao., *Engineering Optimization - Theory and Practice*, John Wiley & Sons, 1996

[19]   Prasanna Kurhatkar, *Learn Optimization Fundamentals with OptiStruct*, Altair University, 2019. At: *https://certification.altairuniversity.com/course/view.php?id=159* (Accessed on 20.05.2021)

[20]   Di Stefano Aglianò, *MotoGP TECNICA - Il tiro catena ed i suoi effetti sulla dinamica di guida* (20.04.2020). At: *https://www.gpone.com/it/2020/04/20/motogp/tecnica-il-tiro-catena-ed-i-suoi-effetti-sulla-dinamica-di-guida.html?amp=1* (Accessed on 21.05.2021)

[21]   All-City site, *Sliding dropouts*. At: *https://allcitycycles.com/parts/small_parts/master_dropout* (Accessed on 21.05.2021)

[22]   Prasanna Kurhatkar, *Learn Topology Optimization with OptiStruct*, Altair University, 2019. At: *https://certification.altairuniversity.com/course/view.php?id=162* (Accessed on 16.05.2021)

[23]   IFToMM Dictionary. At: *https://iftomm-terminology.antonkb.nl/2057/frames.html* (Accessed on 21.05.2021)

[24]   Prasanna Kurhatkar, *Learn Composite Optimization with OptiStruct*, Altair University, 2020. At: *https://certification.altairuniversity.com/course/view.php?id=173* (Accessed on 10.04.2021)

[25]   Barbero E.J., *Introduction to Composite Materials Design*, Boca Raton, CRC Press, 2011

[26]   Raphael Olabanji Ogunleye, Sona Rusnakova, Milan Zaludek and Samuel Emebu, *The Influence of Ply Stacking Sequence on Mechanical Properties of Carbon/Epoxy Composite Laminates* (19.12.2022). At: *https://www.mdpi.com/2073-4360/14/24/5566* (Accessed on 09.01.2023)

[27]   Gong-Dong Wang, Jun Wang EMAIL logo, Sayed K.M. Hossain and Hao Chen, *Research on design rules for composite laminate, Journal Science and Engineering of Composite Materials*, published by De Gruyter on 22.01.2014. At: *https://www.degruyter.com/document/doi/10.1515/secm-2013-0251/html#fig10_w2aab3b7d164b1b6b1ab1b3b7b4Aa* (Accessed on 23.05.2021)

[28]   Institute of Space Technology, *Design Guidelines*. At: *https://www.ist.edu.pk/* (Accessed on 23.05.2021)